UNIVERSITÉ PARIS SUD

Comprendre le monde, construire l'avenir®

UNIVERSITE PARIS-SUD

ÉCOLE DOCTORALE : STITS
Laboratoire de signaux et système

DISCIPLINE : Physique

THÈSE DE DOCTORAT SUR TRAVAUX

soutenue le 06/04/2012

par

Alessio FRANCI

Pathological synchronization in neuronal populations : a control theoretic perspective

-

Vision Automatique de la synchronisation neuronale pathologique

Composition du jury :

Directeur de thèse :	Françoise LAMNABHI-LAGARRIGUE	Directeur de recherche CNRS (Laboratoire des signaux et systèmes)
Président du jury :	Constance HAMMOND	Directeur de recherche INSERM (INMED)
Encadrants :	Antoine CHAILLET William PASILLAS-LEPINE	Maître de conférences (Univ. Paris Sud) Chargé de recherche CNRS (Laboratoire des signaux et systèmes)
Rapporteurs :	Dirk AEYELS Jamal DAAFOUZ	Professeur (Univ. Gent) Professeur (Institut National Polytechnique de Lorraine)
Examinateurs :	Rodolphe SEPULCHRE	Professeur (Univ. Liège)

Pe'lla mi' mamma e'l mi' babbo

Acknowledgments

I sincerely thank Profs. Aeyels and Daafouz for giving me the honor of reviewing this document, and the examiners of my committee, Profs. Hammond and Sepulchre, for having accepted to participate in the evaluation of this work.

I will never be thankful enough to my supervisors Dr. Chaillet, Dr. Pasillas-Lépine, and Dr. Lamnabhi-Lagarrigue, for their invaluable guide throughout these years, for their enthusiasm in transmitting their knowledge, and for all the funny and relaxed moments we shared.

I also thanks all the people with whom I had the privilege and the pleasure to work during these years: Prof. Scardovi at TUM (Munich), Prof. Sepulchre at ULg (Liège) and his PhD student G. Drion, and Dr. Panteley at L2S (Paris). These collaborations have been of great importance for my PhD work and have largely broaden my knowledge and my interests.

Abstract

Motivated by the development of deep brain stimulation for Parkinson's disease, in the first part of this thesis we consider the problem of reducing the synchrony of a neuronal population via a closed-loop electrical stimulation under the constraints that only the mean membrane voltage of the ensemble is measured and that only one stimulation signal is available (*mean-field feedback*). In order to derive analytical results, we model the periodic behavior of a regularly firing neuronal population subject to a closed-loop electrical stimulation as a network of diffusively coupled Landau-Stuart oscillators controlled via a linear single-input single-output feedback device. Under standard assumptions, the obtained system reduces to a modified version of the Kuramoto model.

We start by showing that non-zero mean-field feedback prevents the existence of oscillating phase-locked solutions for a generic interconnection topology and feedback gain. In order to justify the persistence of perturbed phase-locked states under a too small proportional mean-field feedback, we show some robustness properties (namely total stability) of phase-locking in the Kuramoto system to time-varying inputs and for a general symmetric coupling topology. As a corollary of these results we derive necessary conditions for an effectively desynchronizing mean-field feedback.

We further show that, when the feedback gain is sufficiently large, its effect is to inhibit the global oscillation (neuronal inhibition). All the phases converge in this case to a constant value, corresponding to a fixed point of the closed-loop system, which is shown to be almost globally asymptotically stable in the fictitious case of zero natural frequencies and all-to-all coupling. In the case of an odd number of oscillators, this property is shown to be robust to small natural frequencies and uncertainties in the coupling and feedback topologies.

We finally introduce two notions of desynchronization for interconnected phase oscillators by requiring that phases drift away from one another either at all times or in average, and provide a characterization of these two concepts in terms of a classical notion of instability valid in Euclidean spaces. An illustration is provided on the Kuramoto system, which is shown to be desynchronizable by proportional mean-field feedback.

We conclude the first part of the thesis with some extensions to more general coupling and feedback schemes.

In the second part, we explore two possible ways to analyze related problems on more biologically sound models.

The first contribution is to analyze neuronal synchronization with the input-output approach recently developed by L. Scardovi and co-workers. Neurons are modeled as an input-output interconnection of nonlinear operators acting on a signal space. Coupling between the neurons is described via tools from graph theory. A strength of this approach is that it does not require a detailed knowledge of the underlying dynamics, and it permits to cast disturbances and uncertainties in a natural way. We illustrate this method on the Hindmarsh-Rose neuron model.

The second contribution is motivated by the need of gaining a deeper mathematical insight on experimental and numerical observations obtained on dopaminergic neurons. It consists in reducing a detailed physiological model to a simple two dimensional one. The chief property of the detailed model is the simultaneous activation of positive and negative ionic currents, which has important consequences for neuronal excitability. Based on normal form reduction, we propose a novel reduced model to capture this antisynergistic cooperation. Beside dopaminergic neurons, the proposed model explains the dynamics behavior of a large class of neurons, which are not captured by other existing reduced models.

Résumé

Motivé par le développement de la stimulation cérébrale profonde comme traitement des symptômes moteurs de la maladie de Parkinson, nous considérons le problème de réduire la synchronie d'une population neuronale par l'intermédiaire d'une stimulation électrique en boucle fermée, sous les contraintes que seule la tension de membrane moyenne de l'ensemble est mesuré et qu'un seul signal de stimulation est disponible (rétroaction du champ moyen). Afin d'obtenir des résultats analytiques, nous modélisons le comportement périodique d'une population neuronale soumise à une stimulation électrique en boucle fermée comme un réseau d'oscillateurs de Landau-Stuart couplés de façon diffusive et contrôlés via un dispositif de rétroaction linéaire mono-entrée mono-sortie. Sous des hypothèses standards, le système obtenu se réduit à une version modifiée du modèle de Kuramoto.
Nous commençons par montrer qu'une rétroaction non nulle du champ moyen empêche l'existence des solutions à verrouillage de phase pour une topologie d'interconnexion et un de gain de rétroaction génériques. Afin de justifier la persistance de solutions à verrouillage de phase perturbés pour un gain de rétroaction trop petit, nous montrons quelques propriétés de robustesse du verrouillage de phase dans le système de Kuramoto par rapport à des entrée variantes dans le temps et pour une topologie d'interconnexion symétrique quelconque. Comme corollaire de ces résultats, nous dérivons les conditions nécessaires pour une désynchronisation efficace par rétroaction du champ moyen.
En outre, nous montrons que, lorsque le gain de rétroaction est suffisamment grand, son effet est d'inhiber l'oscillation globale (inhibition neuronale). Dans ce cas, toutes les phases convergent à une valeur constante, correspondant à un point fixe du système en boucle fermée, que nous montrons être presque globalement asymptotiquement stable dans le cas fictif où toutes les fréquences naturelles sont nulles et le couplage est du type tous-à-tous. Dans le cas d'un nombre impair d'oscillateurs, cette propriété se révèle robuste aux petites fréquences naturelles et aux incertitudes dans les topologies de couplage et de rétroaction.
Nous proposons enfin deux notions de désynchronisation pour des oscillateurs de phase interconnectés, en exigeant que les phases s'éloignent les unes des autres, soit à chaque instant, soit en moyenne. Nous fournissons également une caractérisation de ces deux concepts en termes d'une notion classique d'instabilité valable dans les espaces euclidiens. Une illustration est fournie pour le système de Kuramoto, qui se révèle être desynchronizable par rétroaction du champ moyen.
Nous concluons la première partie de la thèse avec quelques extensions à des schémas de couplage et de rétroaction plus généraux.

Dans la deuxième partie, nous explorons deux voies possibles pour l'analyse des problèmes similaires dans des modèles biologiquement plus plausibles.
La première contribution est l'analyse de la synchronisation neuronale par l'approche entrée-sortie récemment développé par L. Scardovi et collègues. Les neurones sont modélisés comme une interconnexion entrée-sortie d'opérateurs non linéaires agissants sur un espace de signaux. Le couplage entre les neurones est décrit via des outils de la théorie des graphes. Un des points forts de cette approche est qu'elle ne nécessite pas de connaissance détaillée de la dynamique, et elle permet de considérer perturbations et incertitudes d'une manière naturelle. Nous illustrons cette méthode sur le modèle de neurone de Hindmarsh-Rose.
La deuxième contribution a été motivée par la nécessité d'une connaissance mathématique plus profond sur des observations expérimentales et numériques obtenues sur les neurones dopaminergiques. Il s'agit de la réduction d' un modèle physiologique détaillé à un modèle simple à deux dimensions. La propriété principale du modèle détaillé est l'activation simultanée de courants ioniques positifs et négatifs, ce qui a des conséquences importantes sur l'excitabilité neuronale. Basé sur une réduction du type forme normale, nous proposons un nouveau modèle réduit qui capture cette coopération antisynergique. A côté des neurones dopaminergiques, le modèle proposé explique le comportement dynamique d'une grande classe de neurones, qui ne sont pas capturés par d'autres modèles réduits existants.

Contents

"*There are things known and there are things unknown, and in between are the doors of perception.*"

Aldous Huxley

Chapter 1

Introduction

Brains are an aggregate of units that communicate with each other to achieve a common goal. Neurons are the elementary units, and both electrical and chemical messages constitute the support through which neurons communicate. Through these electrical and chemical messages, neurons are able to achieve a coherent oscillatory activity, or neuronal synchronization, among large and sometimes distant populations.

On the one hand, neuronal oscillations are at the basis of fundamental brain functions like memory (Rutishauser et al., 2010), cognition (Fries, 2001) and movement path generation (Sanes and Donoghue, 1993). On the other hand, a too strong neuronal synchronization can lead to pathological states. Prominent synchronous oscillations in the motor cortex are linked to essential tremors (Hellwig et al., 2003), while in the hippocampus they are at the basis of epileptic seizures (Traub and Wong, 1982). Another synchronization related neural pathology is Parkinson's disease (PD), which constitutes the main motivation for this thesis.

Parkinsonian patients exhibit an intense oscillatory synchronous activity in some deep brain areas (Volkmann et al., 1996) that is tightly correlated to PD physical symptoms (Hammond et al., 2007; Boraud et al., 2005) and is mainly due to the scarcity of a neurotransmitter: dopamine. In the first phase of the illness, pharmacological therapies are able to efficiently compensate for the deficiency of physiological dopamine and reduce PD pathological synchronization, but in a second phase their efficiency rapidly decreases. At this stage, some patients find an alternative in deep brain stimulation (DBS), a symptomatic treatment of PD and some other synchronization related neurological diseases, such as chronic pain, essential tremor, and dystonia (Kringelbach et al., 2007). DBS consists in the electrical stimulation of deep brain areas through implanted electrodes (Benabid et al., 1991). Although DBS is a successful treatment, it still suffers from considerable limitations.

In its present form, DBS is based on heuristics or experimental deductions, and does not use any cerebral measurement (open-loop stimulation). Consequently, a neurologist must run a day-long empirical tuning of the stimulator's parameters, and this tuning is not guaranteed to work (Rodriguez-Oroz et al., 2005). In addition, several studies observed a number of side effects due, for example, to the excessive current injected in the brain tissues (Kumar et al., 2003). Finally, an intense debate is still open about the exact functioning of DBS and its relations with neuronal synchronization (Hammond et al., 2008; Kringelbach et al., 2007).

The research community is well aware of the limitations of the present open-loop approach. In (Vitek, 2005), feedback control systems were identified as one of the major challenges confronting the DBS development in years ahead. After almost six years this challenge has not been won yet. We believe that a deeper theoretical understanding of neuronal synchronization

and its control via electrical stimulation will both help developing a closed-loop DBS technology and gain a deeper knowledge of the mechanisms involved.

The main goal of this thesis is thus to contribute to the development of principles and methodologies for the analysis and control of neuronal synchronization. We take inspiration from medical problems to derive mathematically treatable models and analyze them rigorously, using control theoretical tools, with the twofold goal of understanding complex phenomena and suggesting experimental directions.

Part I of this manuscript is dedicated to the derivation of a simple model of an interconnected neuronal population under the effects of a closed loop electrical stimulation and to the analytical study of the observed synchronization phenomena. Part II presents some recent works aiming at extending the analysis contained in Part I to more realistic models.

Introduction to Part I - Neurons as oscillators

We start by providing an introductory picture of the electrophysiology behind Parkinson's disease. The link between PD physical symptoms and neuronal synchronization is highlighted. After, we present the available clinical treatments, including present DBS, and their limitations. Based on these problematics, we define concisely the main objective of Part I, and provide a review of existing related works. Finally, we outline in some details the content of Part I and its contributions.

1.1 The problem: Parkinson's disease and neuronal synchronization

1.1.1 Electrophysiology and clinical treatment of Parkinson's disease

As briefly recalled above, the parkinsonian neuronal state is characterized by intense synchronous oscillation in a deep brain network: the basal ganglia (BG). Such pathological synchronization is mainly the byproduct of the degeneration and death of dopaminergic neurons (Vernier et al., 2004), and the consequent deficiency of this neurotransmitter in the brain. Roughly speaking, the BG network acts as a filter on cortical inputs encoding voluntary movements. An illustration of the anatomy and electrophysiology behind this filtering does not enter in the scope of this dissertation, but the interested reader can find some information in (Parent and Hazrati, 1993; Bolam et al., 2000). Local field potential (LFP) recordings in two of the basal ganglia, namely the subthalamic nucleus (STN), and the globus pallidus internum (GPi), reveal in PD patients a synchronized oscillatory activity in the band 13Hz-32Hz (beta band). See (Brown et al., 2001; Williams et al., 2002, 2003; Brown and Williams, 2005; Weinberger et al., 2006; Priori et al., 2004). Correlations in neurons electrical activity underlying these oscillations are found locally, *i.e.* between neurons belonging to the same nucleus (Brown et al., 2001; Williams et al., 2002, 2003; Priori et al., 2004, 2002; Silberstein et al., 2003), among neurons belonging to different ganglia (Brown et al., 2001), and between BG neurons and cortical activity (Marsden et al., 2001; Williams et al., 2002). Thus, synchronous beta band oscillations in STN and GPi are a hallmark of PD basal ganglia electrical activity. Conversely, they are absent, or small, under healthy conditions (Courtemanche et al., 2003; Sochurkova and Rektor, 2003).

While its origins are still object of debate, the implication of BG synchronous oscillations in PD physical symptoms is confirmed by experimental evidences. The reduction of the intensity of

the BG synchronized oscillatory activity at the beta band is roughly proportional to the clinical improvement in bradikinesia, the slowness in the execution of movements, and akinesia, the inability to initiate movements (Kühn et al., 2006; Brown et al., 2004). Furthermore, under healthy conditions, beta band oscillations are suppressed prior and during voluntary movements (Williams et al., 2003; Priori et al., 2002; Cassidy et al., 2002; Doyle et al., 2005).

Despite these experimental evidences, however, the mechanisms through which STN/GPi synchronous oscillations lead to PD physical symptoms are still unclear. We just mention two explicative hypothesis. In (Bar-Gad et al., 2003) the authors suggest that the movement-related desynchronization is associated to a dimensionality reduction in the representation of cortical inputs. Eliminating correlations, a small group of STN neurons can efficiently encode the information originally contained in a large coherently oscillating cortical population. In (Rubin and Terman, 2004) the authors consider how PD synchronous oscillations transform the BG network output, and the effects of these changes on the target neurons. Computational evidences suggest, in particular, that beta band synchronized inhibitory inputs from the GPi to the thalamus compromise the ability of thalamic relay neurons to correctly respond to cortical inputs. Interestingly, if the synchronization frequency and pattern are changed through electrical stimulation of the STN, the same pathological effect is not observed. Beyond these intriguing hypothesis, as a matter of fact, a healthy basal ganglia network exhibits a desynchronized STN/GPi activity (Courtemanche et al., 2003; Sochurkova and Rektor, 2003).

A first-line treatment of PD is the administration of *L*-dopa, a dopamine promoter drug. This pharmacological therapy efficiently compensates for the lack of physiological dopamine, at least in the first few years of the illness (Cotzias et al., 1969). In this period, *L*-dopa has been shown to efficiently suppress the pathological synchronization (Priori et al., 2002; Sydow, 2008; Doyle et al., 2005). Afterwards, its efficiency rapidly decreases with the diminishing number of dopaminergic cells that can benefit from this chemical boost (Muenter and Tyce, 1971). Moreover, a series of sever side effects come over with time, in particular the generation of involuntary movements, or dyskinesia (Barbeau, 1974). At this stage pharmacological therapies are no longer sufficient.

A predecessor and an alternative to drug therapies, used since the early sixties, is the lesioning of some BG areas. This surgical ablation is effective in reducing PD tremors in drug resistant patients (Jankovic et al., 1995). The physiological mechanism behind the therapeutic effects of BG lesioning, and in particular STN lesion, are not clear. There are anyhow some evidences that BG ablation suppresses the pathological synchronous oscillation at the lesion site (Trošt et al., 2003). At the same time the surgical complication of this invasive and non-reversible procedure can be severe (Schuurman et al., 2008).

In the early nineties the medical research group of Benabid noticed that the chronic stimulation of the STN, via a pair of implanted electrodes, drastically reduces tremors and akinesia in Parkinson's disease (Benabid et al., 1991). Comparative studies show that this type of deep brain stimulation (DBS) is as effective as BG lesioning in reducing PD symptoms, but with less severe side effects (Schuurman et al., 2008) and, more important, in a reversible way. Since then, DBS has become an alternative to the pharmaceutical and ablative treatments of synchronization-related parkinsonian motor symptoms, yet, far from being optimized for the scope.

1.1.2 Open-loop DBS: Its limitations and preliminary generalizations

Nowadays DBS is an open-loop stimulation. The signal injected is similar to that of a standard cardiac pacemaker (Benabid et al., 1991), that is a train of current pulses of adjustable amplitude and frequency, on which neurologists must run a day-long empirical tuning in order

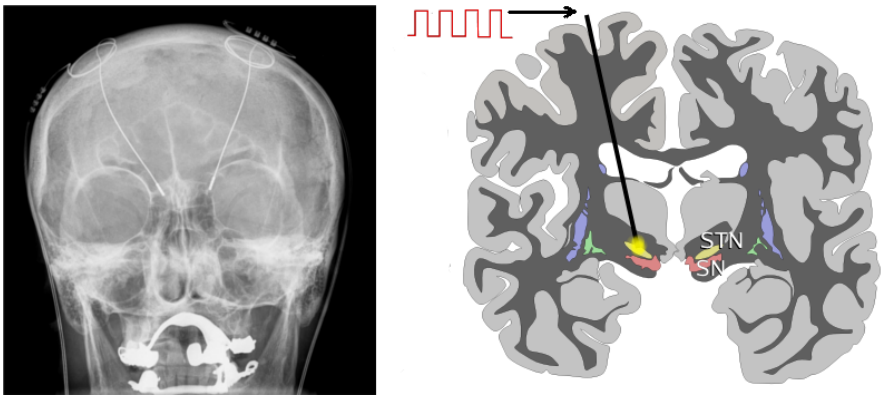

FIGURE 1.1: Present DBS: a pair of electrodes are surgically implanted in central nervous system. The electrode is guided until its head touches the STN, or, alternatively, the GPi (not shown in the picture). The injected input is a train of voltage pulses of frequency $\gtrsim 130Hz$ and amplitude $\sim 5V$. Adapted from (Wikipedia, 2011).

to optimize the patient response to the therapy. Indeed, no automatic optimization algorithm has yet been developed. The only "feedback" between the stimulation pattern and the patient response is provided by the physicians during the parameters regulation stage. Once the DBS apparel is installed, no physiological measurements are exploited to track the therapy efficiency and to adapt to possible variations, suggesting that the stimulation pattern might not be optimized either for the scope. As a consequence, the present stimulation strategy has different repercussions (Kumar et al., 2003). Firstly, due to the continuous current injection, the stimulator batteries discharge faster than needed, requiring additional surgical operations to replace them. Secondly, the permanent electrical stimulation of the BG can have sever psychological and physiological side effects, such as memory decline, psychiatric disturbances, depression, speech disturbances, and dysequilibrium (Kumar et al., 2003). Finally, roughly a half of the patients find no symptomatic benefit in DBS (Rodriguez-Oroz et al., 2005).

The electrical measurements obtained with the help of the implanted electrode gives an opportunity to track the neuronal state and adapt the therapy on-line. Due to the size of the electrode with respect to the neuronal scale, the measurement is given by the mean electrical activity of the neuronal population near the electrode head, or local field potential. In the following we refer at this population measurement as mean-field.

A first practical attempt to exploit mean-field measurement in DBS optimization has already been worked out by the group of Prof. Tass (Tass, 1999, 2003b,a; Tass and Majtanik, 2006). See also the USPTO patent (Tass, 2011). In their approach, whenever the pathological synchronous state is detected, the DBS stimulator is turned on automatically and the standard pulsed DBS signal is injected in a spatially coordinated way to desynchronize the ensemble. This strategy helps to extend batteries life and to reduce side effects by reducing the amount of injected current, but it does not optimize the stimulation pattern, which consists of large voltage pulses, still sent in an open loop fashion.

1.1.3 Closing the loop: Control theory and DBS

In this section, we reformulate as precise control objectives (for a closed-loop DBS) the problematics discussed in Sections 1.1.1 and 1.1.2. More precisely, we will introduce two distinct control strategies: neuronal desynchronization and neuronal inhibition.

In most control applications, synchronization is a goal to achieve: for instance, formations of autonomous vehicles (Sepulchre et al., 2007, 2008), consensus protocols (Scardovi et al., 2007; Olfati-Saber and Murray, 2004; Sarlette, 2009) and master-slave control of mechanical systems

(Spong, 1996; Nijmeijer and Rodriguez-Angeles, 2003) can all be formulated as a synchronization objective. DBS for PD has exactly the opposite goal: given an originally synchronized ensemble, find a control signal to induce it in a disordered desynchronized behavior.

Beside desynchronization, another interesting control strategy is to use the DBS signal to inhibit the neuronal oscillations, that is to block completely the pathological spiking activity of the population. This solution mimics the effects of a BG lesion, which can be seen as a drastic and irreversible inhibition. Conversely, a DBS-induced neuronal inhibition is reversible and could be activated only on demand. Apart from PD (McIntyre et al., 2004; Benazzouz et al., 2000; Olanow, 2001), the possibility of inhibiting the global synchronous activity of a group of neurons in a reversible and controlled way may also find applications in the treatment of other synchronization-related neurological diseases, like the block of fast oscillation associated to epileptic seizures (Traub, 2003; Traub and Wong, 1982).

The originality of the DBS control problem that we address here stands also in the practical input-output constraints. As already noted above, the only available measurement consist in the neuron population mean-field. For the same reason, all the neurons receive basically the same input signal. The resulting control setup consists of an extremely large number of units, the neurons, whose collective behavior has to be regulated relying only on a scalar output, the mean-field, and a scalar input, the injected current (see Figure 1.2). This is in opposition with classic synchronization (Sepulchre et al., 2007, 2008; Scardovi et al., 2007; Olfati-Saber and Murray, 2004; Sarlette, 2009) and desynchronization (Angeli and Kountouriotis, 2011) problems, where each agent is endowed with a controller that can access local information through a communication graph.

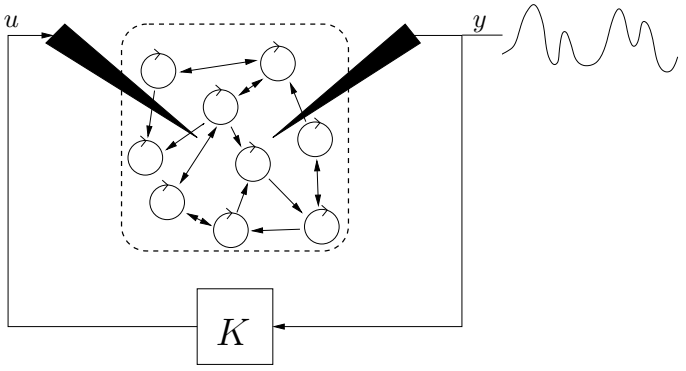

FIGURE 1.2: Proposed proportional mean-field feedback DBS control scheme. The mean electrical activity of a population of neurons, each modeled for simplicity as an oscillator, is recorder via a DBS electrode. This output is multiplied by a feedback gain and injected back in the neuronal population.

In order to keep the proposed control scheme simple, we close the loop between the patient and the DBS controller with a proportional (linear) feedback scheme. In other words, the injected input is proportional to the measured output (Ogata, 2001, Chapter 5). The resulting *proportional mean-field feedback* control scheme is summarized in Figure 1.2. The analysis of the resulting closed-loop system guides the tuning of the feedback gain. Apart from its simple nature, which ensures mathematical treatability and an easy practical implementation, the proportional feedback approach is particularly tempting for DBS for energetic concerns. Energy efficiency is a crucial issue in DBS. As mentioned above, a too strong injected current has the twofold drawback of letting the stimulator batteries discharge too fast and of inducing severe side effects. Since the population mean electrical activity is small in both the desynchronized and inhibited states, a proportional feedback approach ensures, at least for small feedback

gains, a small DBS signal, and thus energy efficiency and side-effects reduction. In a nutshell, we abstract the control strategy for a closed-loop DBS proposed in Part I as follows:

Objective of Part I: Given a neuronal population exhibiting a highly regular synchronous activity, explore how it can be brought to either a healthy irregular desynchronized state or to a silent inhibited state, via proportional mean-field feedback.

1.2 State of the art: Eliminating synchronization by control

In recent years, several works have appeared facing the problem of controlling the synchronization behavior of an interconnected neuronal population through mean-field feedback, proportional or not (Rosenblum and Pikovsky, 2004b,a; Rosenblum et al., 2006; Hauptmann et al., 2005a,b,c; Popovych et al., 2006b, 2005, 2006a; Popovych and Tass, 2010; Luo et al., 2009). We share with all these works the same modeling principle, that is to consider periodically spiking neurons and to model them as simple nonlinear or phase oscillators. Other approaches, different in philosophy from the work presented in this manuscript, employ optimal control techniques for the computation of open-loop desynchronizing signals (Danzl et al., 2009) or for the tuning of open-loop DBS parameters (Schiff, 2010). Finally, some works investigate the oscillation inhibition, or oscillators death, phenomenon in coupled oscillators population (Ermentrout, 1990; Ermentrout and Kopell, 1990). In what follows, we describe those references in some detail. The aimed extensions are summarized in Section 1.2.5.

1.2.1 Desynchronization via delayed feedback

In (Rosenblum and Pikovsky, 2004b,a; Rosenblum et al., 2006) the authors consider a linear single-site delayed feedback. That is, they consider a group of neurons stimulated and recorded with one electrode. The injected signal is taken proportional to the delayed mean-field of the ensemble. Analytical investigations on simplified oscillators and phase models reveal that, depending on the feedback gain and delay, this closed-loop control can enhance or suppress neural synchrony. In the latter case the stimulation is vanishing when effective desynchronization is achieved, which ensures energy efficiency and stimulation on demand. Numerical simulation on detailed neuron models verify this analysis.

The main idea behind the approach proposed in (Hauptmann et al., 2005a,b,c) is to use multiple stimulation sites and inject in each of them the delayed mean-field of the stimulated ensemble with different delays. This stimulation leads to cluster of neurons, each of them oscillating synchronously with the delayed mean-field of the ensemble for a particular delay value. When the delays are chosen following a suitable law, the different clusters oscillate out of phase and a global synchronization index is minimized. This control scheme is tested both on simplified phase models and on detailed microscopic models.

A natural extension to linear delayed feedback is to consider nonlinear delayed feedback, as proposed in (Popovych et al., 2006b, 2005, 2006a). The authors show numerically on detailed models and analytically on phase models, that such a closed-loop stimulation can have a twofold effect. If the ensemble is originally strongly interconnected, then the stimulation effectively desynchronizes it for a broad range of feedback gains and delays. If the ensemble is originally weakly interconnected, some parameter ranges appear in which synchronization is enhanced. The case of two interacting populations with different internal connectivity degrees is considered in (Popovych and Tass, 2010). The important finding is that, by applying a nonlinear delayed

feedback only to the weakly coupled population, it is possible to find parameter ranges for which the strongly coupled population becomes effectively desynchronized via the indirect control mediated by the populations interaction.

1.2.2 Desynchronization via non-delayed feedback

Proportional-integro-differential (PID) feedback is at the basis of the approach proposed in (Pyragas et al., 2008). The authors assume the existence of a recorded and a stimulated populations, in which the stimulated population is subject to a PID feedback derived from the mean behavior of the recorded population. This approach is particularly important in an experimental framework where practical constraints may forbid the simultaneous recording and stimulation of the whole network. The authors compute, in the limit of an infinite number of oscillators, the gain threshold ensuring the effective desynchronization of both populations. Numerical examples support these theoretical predictions.

In (Tukhlina et al., 2007) the authors exploit the interesting idea that a synchronized neuronal population can, in first approximation, be modeled as a single active oscillator. Then a possible solution to contrast global oscillations, leading to a desynchronized ensemble, is by dissipating their energy. This can be achieved by interconnection with a passive oscillator. The obtained results suggest that this feedback scheme can effectively block the global synchronous oscillation, and thus desynchronize the ensemble, with vanishing stimulation. The last point ensures stimulation on demand and an energy efficient policy. Numerical examples validate these results on realistic neuron models. A more recent work from the same authors (Tukhlina and Rosenblum, 2008) aims at extending this approach to the case of two interacting populations. One population is recorded, the other is stimulated. This generalization further increases the practical soundness of this stimulation scheme.

A similar idea to the one proposed in (Tukhlina et al., 2007) is explored in (Luo et al., 2009). In this latter reference, instead of a passive oscillator, the authors consider the use of a traditional washout filter (or washout circuit), a stable high-pass filter, which is able to block the Andronov-Hopf bifurcation exhibited by the mean-field at the synchronization transition. The authors prove the efficiency of this control scheme through numerical examples.

1.2.3 Optimal control and open-loop stimulation strategies

In (Danzl et al., 2009) the authors rely on a detailed computational model of neurons and employ optimal control techniques to compute the waveform ensuring convergence toward a small ball centered around an unstable fixed point in minimum time. Since all the isochrons[1] converge in this zone, reflecting the fact that the unstable fixed point is phase-less, the asymptotic phase of the controlled system is very sensitive to tiny amounts of perturbations, resulting in phase-randomization. When applied at the population level, this technique works to transiently desynchronize an ensemble of identical oscillators in an original perfectly synchronized state. Nonetheless, the use of optimal control techniques requires a perfect knowledge of the underlying dynamics and leaves no space to parametric uncertainties and heterogeneities, making this approach difficult to apply in an experimental framework.

Apart from desynchronization via closed-loop stimulation, other approaches have been explored in literature. Notably, the control of DBS through model-based approaches aim at exploiting

[1] Given a system with an almost globally asymptotically stable limit cycle, isochrons are hypersurfaces made of all the points with the same phase (Guckenheimer, 1975). Unstable fixed points, in particular, are phase-less and do not belong to any isochron.

computational models of sufficient complexity to emulate the behavior of different brain structures with enough fidelity. Optimization algorithms can then be used in real-time to tune a limited number of parameters by comparison with experimental data. The resulting tuned computational model is used to generate an open-loop control signal. We refer the reader to the recent review of the subject (Schiff, 2010) for more details and a complete list of references. We stress that this approach is quite different in philosophy to the one explored in Part I of this thesis. We will, however, come back to it in Part II.

1.2.4 Neuronal inhibiton

The possibility of inhibiting the pathological STN oscillations by blocking the neuronal spiking is also considered in Part I. A similar oscillation inhibition phenomenon has already been studied in the literature, even though not with a control objective. In (Ermentrout, 1990) the author analyzes a population of all-to-all interconnected complex oscillators, of the same type of the one used in Chapter 2 as a simple representation of periodically spiking neurons. He shows that if the coupling between the oscillators is strong compared to the attractiveness of the limit cycle, and the natural frequencies are sufficiently sparse, then diffusive coupling can stabilize the origin of the interconnected system. This phenomenon corresponds to the disappearance of the oscillation's amplitude and frequency, and is often referred to as oscillators death. The mechanism underlying this analysis are thus quite different, if not opposite, to the one analyzed in Part I of this manuscript, which relies on the assumption that the coupling is sufficiently weak so to ensure the persistence of the limit cycle (cf. Assumption 1 in Chapter 2).

The analysis presented in our work is nearer in spirit to the one in (Ermentrout and Kopell, 1990). There, the authors show that, under suitable assumptions on the coupling functions, oscillation inhibition arises in two identical coupled phase oscillators as a supercritical fold bifurcation on the synchronization line with the coupling strength as the bifurcation parameter. A further non-degeneracy condition ensures that the stable node born in this bifurcation corresponds to a stable solution of the full system. A similar result is proved with the help of numerical simulations for couples of general nonlinear oscillators. In the case of a larger number of oscillators the authors restrict their attention to the chain topology, and focus on a suitable subclass of coupling functions to prove a similar stability result.

1.2.5 Aimed extensions

Neuronal desynchronization. All the works reviewed in Section 1.2.1 and 1.2.2 consider only very simple interconnection topologies between the neurons, and do not account for the possibility that different neurons contribute to the recorded mean-field and receive the injected signal with different intensity. Furthermore, in (Rosenblum and Pikovsky, 2004b,a; Rosenblum et al., 2006; Hauptmann et al., 2005a,b,c; Popovych et al., 2006b, 2005, 2006a; Pyragas et al., 2008; Popovych and Tass, 2010) the output and the input of the system are complex, which does not reflect the electrical single-input-single-output nature of an experimental DBS control scheme. Finally, no rigorous definition of desynchronization are provided. The analysis in Part I aims at relaxing these constraints and at providing a more rigorous framework for the analytical study of desynchronization.

Neuronal inhibition. The analysis (Ermentrout and Kopell, 1990) suggest that oscillation inhibition is possible, at least for some interconnection topologies and coupling functions. Inspired by this work, we analyze in Part I whether the coupling induced by a proportional mean-field feedback can obtain the same result.

1.3 Contributions: Coupled oscillators under mean-field feedback

1.3.1 Model derivation

As introduced in Section 1.1, our goal being to derive analytical results on the control of synchronization in an interconnected neuronal population via a scalar input that is function of the population mean-field only, we start by deriving a mathematically treatable model.

The main idea guiding our model derivation is to focus on *periodically spiking neurons*. The form of the dynamics associated to such a periodic behavior can be quite complicated for physiological models, hampering the mathematical treatability, in particular for large interconnected networks. We thus look for a simple alternative representation of the associated limit cycle. We refer the reader to (Ermentrout and Terman, 2010, Chapter 8) and (Izhikevich, 2007, Chapter 10), and the exhaustive list of references therein, for an introduction to the dynamics of periodically spiking neurons and their synchronization properties.

In the spirit of (Rosenblum and Pikovsky, 2004b; Popovych et al., 2006b, 2005, 2006a; Pyragas et al., 2008), we represent each neuron as a complex Landau-Stuart oscillator. As detailed in Sections 2.1 and 2.2, we associate the real part of the oscillations to the membrane voltage and its imaginary part to a recovery variable that represents the effects of other physiological variables. This distinction is crucial to define a biologically meaningful output. More precisely, as opposed to (Rosenblum and Pikovsky, 2004b,a; Rosenblum et al., 2006; Hauptmann et al., 2005a,b,c; Popovych et al., 2006b, 2005, 2006a; Pyragas et al., 2008; Popovych and Tass, 2010), given an oscillators population, we assume that the only available measurement is the mean real part of the oscillation, corresponding to the mean membrane voltage of the neuronal ensemble, or local-field potential. This measurement is standard in the medical practice (Legatt et al., 1980), and is imposed by the size of the electrode head, much larger than the neuron scale. Similarly, the injected input is a scalar that models the injected current and affects only the real part of the oscillation. The obtained model, while not accounting for the dynamical details of physiological models, still exhibits some important features of periodically spiking neurons, and maintains a meaningful link with their input-output variables.

Furthermore, in order to account for the heterogeneous and unknown distance of each neuron from the electrode head, we also assume that the weight with which each oscillator contributes to the recorded mean-field is heterogeneous and unknown. The same experimental constraint imposes that each oscillator receives the same scalar input, modulo an unknown gain that is related to its distance from the electrode head. We stress that these modeling assumptions relax the ones used in all the works reviewed in Section 1.2, where the authors consider only simple interconnection topologies and registration-stimulation setups.

While neuronal coupling relies on different mechanisms, in our study we consider exclusively diffusive coupling between the oscillators. Even though this assumption may be too simplistic, it ensures the mathematical treatability of the resulting model. Some extensions are considered in Appendix A and in Part II. As for the measurement-stimulation setup, we assume the interconnection topology between the neurons to be arbitrary. Our working choice is to close the loop between the oscillator population and the DBS controller via a proportional (linear) mean-field feedback. As already said in Section 1.1, its simple nature guarantees both mathematical treatability and an easy practical implementation.

The obtained model is presented in Section 2.2. Preliminary numerical observations, reported in Figures 2.4, 2.5, and 2.6 on page 38), highlight a series of interesting synchronization/desynchronization phenomena. For a generic choice of the interconnection topology and feedback

gain, the system does not exhibit phase-locked solutions with a non-zero frequency of oscillation. At the same time, if the feedback gain is small compared to both the natural frequencies and coupling strength, the oscillators remain practically phase-locked, meaning that they exhibit small oscillations around a perfectly phase-locked solution. Conversely, if the feedback gain is sufficiently large, mean-field feedback can block the oscillations, that is the oscillators phases converge to a constant value (oscillation inhibition). Finally, for a certain range of feedback gains, mean-field feedback is able to desynchronize some pairs of oscillators, while others remains practically synchronized in small clusters. This type of partial phase-locking, or partial entrainment, is also studied in (Aeyels and Rogge, 2004; De Smet and Aeyels, 2009; Aeyels and De Smet, 2010). Part I of this manuscript is devoted to an analytical understanding of these phenomena.

We informally derive at the end of Section 2.2 the phase model associated to the ensemble of Landau-Stuart oscillators under mean-field feedback. A rigorous derivation is provided in Section A.2. The resulting system is the following:

$$\dot{\theta}_i = \overbrace{\omega_i + \sum_{j=1}^{N} k_{ij} \sin(\theta_j - \theta_i)}^{\text{Kuramoto phase dynamics}} \overbrace{- \sum_{j=1}^{N} \gamma_{ij} \big(\sin(\theta_j + \theta_i) - \sin(\theta_j - \theta_i) \big)}^{\text{Mean-field feedback contribution}} .$$

The scalar θ_i is the phase of the oscillator i, and describes the evolution of the neuron i along the periodically spiking limit cycle. The entries of the vector $\omega := [\omega_i]_{i=1,\dots,N} \in \mathbb{R}^N$ are the natural frequency of the oscillators and are associated to the endogenous rate of spiking of the neurons. The matrix $k = [k_{ij}]_{i,j=1,\dots,N} \in \mathbb{R}^{N \times N}$ is the coupling matrix and contains information about the interconnection topology between the neurons. The matrix $\gamma = [\gamma_{ij}]_{i,j=1,\dots,N} \in \mathbb{R}^{N \times N}$ is the feedback gains and can be computed from the registration-stimulation setup. This model basically consists of two parts. The first one is the standard Kuramoto dynamics (Kuramoto, 1984), corresponding to diffusive coupling between the oscillators. The second one, corresponding to the proportional mean-field feedback, is original. On one side, depending on the feedback gain, it reduces or enhances the strength of the effective diffusive coupling. On the other, it introduces a sinusoidal additive coupling $\sin(\theta_i + \theta_j)$ between couples of oscillators. These two distinct effects are at the basis of all the phenomena observed in simulations on both simplified (see Section 2.4.1) and more physiologically sound (see Section A.7) models, as we are going to briefly and informally explain in this introduction.

In Section A.1, we consider some generalization of the studied closed-loop dynamics, permitting to extend the class of modeled neuron networks. We also provide in Section A.2 an analytical derivation of the associated phase dynamics. We deduce, in particular, an explicit bound on the coupling and feedback strengths (the *small coupling condition*) for which the proposed phase dynamics is a good (first order) approximation of the full closed-loop dynamics. This technical part can however be skipped in a first reading[2].

1.3.2 Definition and existence of oscillating phase-locked solutions

After having derived the model equations in Sections 2.1 and 2.2, we define in Section 2.3 its pathological states in a rigorous manner. We can think of the pathological neuronal activity affecting Parkinson's disease patients as a highly ordered synchronous state, in which a group of neurons discharge spike trains at the same frequency. In our model, such a behavior is described by *oscillating phase-locked solutions*. See, *e.g*, (Kuramoto, 1984; Strogatz, 2000; Kopell

[2]Appendix A was inspired by the comments of Prof. G. B. Ermentrout and Prof. D. Aeyels on the first version of this thesis.

and Ermentrout, 2002; Aeyels and Rogge, 2004; Fradkov, 2007). Such solutions, rigorously presented in Definition 2.1, are characterized by all the oscillators evolving with constant phase differences, and thus the same frequency, and exhibiting a global oscillation, that is a non-zero collective frequency. If the last condition is removed, we simply speak of phase-locked solution. It is interesting to consider this distinction since phase-locked solution with zero natural frequency correspond to a silent (inhibited) neuronal ensemble (see Chapter 4).

A first positive result supporting closed-loop DBS is contained in Theorem 2.2. It states that for a generic interconnection topology between the neurons, with both inhibitory and excitatory links, the existence of any oscillating phase-locked solution is not compatible with the presence of a non-zero mean-field feedback. This result is independent of the weights with which each neuron contributes to the recorded mean-field and of the gains with which it receives the injected signal. The adjective "generic" should be understood here in the sense of the Lebesgue measure associated to the space of the interconnection topology and feedback gain matrices, and natural frequencies vectors. Numerical simulations illustrate this theoretical result. The same existence result is proved in Section A.3 for the generalized closed-loop dynamics considered in Section A.1.

We stress that the disappearance of the perfectly oscillating phase-locked solutions may or may not have a therapeutic interest. The resulting state might indeed correspond to an effectively desynchronized ensemble, but also to an almost (practically) phase-locked oscillator population. In the latter case, the neurons discharge at approximately the same natural frequency, which would still correspond to a pathological behavior. Alternatively, the system may converge to a non-oscillating (inhibited) phase-locked solution. Effective desynchronization, practical phase-locking, and neuronal inhibition will all be analyzed in Chapters 3, 4, and 5.

The proof of Theorem 2.2 relies on two points, presented as Lemma 2.3 and Lemma 2.4 in Section 2.4.2. Lemma 2.3 provides an original characterization of the oscillating phase-locked solutions in term of a fixed point equation. This equation is composed of two subset of equations, corresponding, respectively, to the classic Kuramoto fixed point equation (Aeyels and Rogge, 2004; Jadbabaie et al., 2004) and to the new constraints imposed by the presence of the mean-field feedback. Lemma 2.4 is an invertibility lemma for the Kuramoto fixed point equation. It states that generically, with respect to the natural frequency and the interconnection matrix, the Kuramoto fixed point equation can be locally inverted around any of its solutions in terms of the implicit function theorem.

1.3.3 Robustness of phase-locked solutions

In Chapter 2 we have derived the model equations and analyzed the existence of phase-locked solutions. Chapter 3 has a twofold objective: justify the persistence of robust practically phase-locked solutions for small feedback gains and give explicit bounds on the tolerated disturbances to compute necessary conditions for an effectively desynchronizing DBS. We address this problem by analyzing the robustness of phase-locked solutions in the Kuramoto system with respect to general time-varying inputs, including, as a particular case, the effects of a proportional mean-field feedback DBS.

In Section 3.1 we introduce a generalized version of the Kuramoto model characterized by the presence of time-varying natural frequencies modeling exogenous inputs. A natural mathematical object to study the robustness of phase-locking is the incremental dynamics associated to this system. The *incremental dynamics* rules the evolution of the phase differences, and phase-locking corresponds, in this representation, to a fixed point. As such, standard tools from nonlinear system analysis are available to analyze its robustness properties. More precisely we rely on a Lyapunov-based Input-to-State stability analysis (Sontag, 1989, 2006a).

We start by defining in Section 3.2 the set of *asymptotically stable phase-locked solutions* in terms of the asymptotically stable fixed point of the incremental dynamics, as formalized in Definition 3.1. We show that, for a general symmetric interconnection topology, each asymptotically stable phase-locked solution is also locally input-to-state stable (Sontag and Wang, 1996) with respect to small inputs (Theorem 3.4). Our proof comes with an explicit Lyapunov function for the incremental dynamics and permits to derive *explicit bounds* on the size of the tolerated inputs, the region of attraction, and the convergence rate for a general asymptotically stable phase-locked solution. We specialize this analysis in Section 3.3 to the case of all-to-all coupling (Theorem 3.5), and show how the obtained bounds are in line with recently published results analyzing the case of constant inputs (Chopra and Spong, 2009; Dörfler and Bullo, 2011). The robustness bounds are computed in Corollary 3.6 for the special case of proportional mean-field feedback for a general symmetric interconnection topology, and the *necessary conditions* for an effectively desynchronizing DBS are derived. The robustness analysis of Chapter 3 can be extended to the generalized phase dynamics considered in Section A.1. A sketch of this extension, along with a generalized version of Theorem 3.5 (see Theorem A.7) are the subject of Section A.4.

The results presented in Chapter 3 are supported by a specific mathematical analysis. The variables of the incremental dynamics are linked by algebraic relationship that constrain the evolution of the system on a suitable *invariant submanifold*. Lemmas 3.7 and 3.8 characterize the critical points of the incremental Lyapunov function restricted to this submanifold and relate them to the fixed point of the incremental dynamics. As a general conclusion of this analysis we propose at the end of Section 3.5 a novel characterization of the robust phase-locked states in terms of the isolated local minima of the restricted incremental Lyapunov function.

1.3.4 Neuronal inhibition

While Chapters 2 and 3 mainly deal with the analysis of the closed-loop system, Chapter 4 contains sufficient conditions on how to achieve a precise control goal: *neuronal inhibition*. With this we mean to bring an originally synchronously oscillating population toward a silent state, in which no spikes are emitted. This objective has a practical interest since it eliminates the synchronous oscillatory activity of the STN and may allow a healthier cortical information flow in the BG. This strategy is also supported by the fact that the precursor of DBS was the surgical ablation of the STN, corresponding to a radical neuronal inhibition.

In Section 4.1 we recall the model under analysis. We split the diffusive coupling and the mean-field feedback terms into a homogeneous part, in which the coupling and feedback gains between each pair of oscillators are all given by the mean of the coupling and feedback gains, respectively, and a heterogeneous part, accounting for the dispersion of the gains around their means. The form of the obtained equations suggests that the diffusive coupling term, which is responsible for the pathological synchronous behavior, can be drastically reduced by matching the mean of the feedback gains to the mean of the coupling gains. Apart from the natural frequencies and the heterogeneous parts of the coupling and feedback, the resulting dynamics is ruled by the sinusoidal additive coupling only, which is small provided that the original diffusive coupling is small, thus ensuring the persistence of the oscillators limit cycle attractor (cf. Figure 2.5), provided that the small coupling condition derived in Section A.2 is satisfied.

We start by noticing that the system under analysis can be written as a *gradient system*. The main idea is then to focus on the case of zero natural frequencies and homogeneous gains, and study the corresponding unperturbed potential function. Natural frequencies and gain heterogeneities can then be plugged back in as a perturbation. Section 4.2 provides a complete description, summarized in Lemmas 4.1, 4.2, and 4.3 of the set of critical points of

the unperturbed potential function. We conclude Section 4.2 with a global convergence result, presented as Proposition 4.4, stating that in the ideal case of zero natural frequencies and homogeneous gains almost every solution converges to the set of isolated global minima. The proof is based on the properties of gradient systems (Hirsch and Smale, 1974) and, due to the presence of non-isolated critical points, on some results on normally hyperbolic invariant manifolds (Hirsch et al., 1977).

The convergence results derived in Section 4.2 are at the basis of the oscillation inhibition analysis in the case of non-zero natural frequencies and heterogeneous gains. More precisely, we consider small natural frequencies and gain heterogeneities, and treat them as a perturbations. In this case, the isolated hyperbolic fixed points, as well as the normally hyperbolic invariant manifolds of fixed points, persist along with their stable and unstable manifolds (Hirsch et al., 1977). The main result, presented as Theorem 4.5, then follows from standard results on gradient systems, and ensures that a small intensity proportional mean-field feedback DBS can inhibit a neuronal population, provided that the natural frequencies and the gain heterogeneities are not too large.

An extension of the results of Chapter 4 to the generalized dynamics presented in Section A.1 is provided in Section A.5. More precisely, we relax the assumption that the gain heterogeneities are small, and derive conditions on the extended set of parameters and the associated generalized potential function for which oscillation inhibition is still guaranteed. This extension is formally stated in Theorem A.8.

1.3.5 Effective desynchronization via mean-field feedback

Desynchronization via mean-field feedback is the subject of Chapter 5, concluding the list of numerically observed phenomena in an ensemble of diffusively coupled oscillators under mean-field feedback. We start by examining how desynchronization might be suitably defined for an ensemble of phase-oscillators. Since our mathematical analysis relies on the phase equations associated to the oscillators, we must first answer this question in order to proceed rigorously.

We thus propose in Section 5.1 a short digression on existing concepts of synchronization and derive a natural and simple definition of desynchronization, compactly presented in Definition 5.1 and called *Strong Desynchronization*. It requires the relative drift between two oscillators to be uniformly bounded away from zero. This definition owns the advantage of being locally defined, and thus suitable for a use both on compact spaces like the N-torus, or non-compact spaces like $\mathbb{R}^N$.

The chapter continues with a mathematical characterization of strong desynchronization. This characterization is based on the *grounded variable* associated to the phase dynamics. This variable describes the phase evolution lifted to $\mathbb{R}^N$ in a reference frame moving with the mean drift of the population. We show, in particular, that the proposed definition of desynchronization admits a mathematical characterization in terms of instability concepts on Euclidean spaces that is in perfect opposition to that of synchronization in terms of asymptotic stability, cf. *e.g.* (Aeyels and Rogge, 2004; Jadbabaie et al., 2004; Sepulchre et al., 2007).

Strong desynchronization is generally too harsh a constraint to be satisfied in practical applications, due to its all-time nature. We thus weaken the notion of strong desynchronization in Definition 5.6 by asking the oscillators to be drifting away in average over a suitable time window. Such a requirement is particularly suited for phase oscillators, characterized by a periodic internal dynamics. We call this weaker notion of desynchronization *practical desynchronization* and characterize it mathematically in Section 5.2.2.

After the having posed the theoretical background for the study of desynchronization, we switch in Section 5.3 back to the neuronal desynchronization problem. More precisely, we consider the phase model derived in Chapter 2 with a general interconnection topology and recording-stimulation setup and study the possibility of inducing a desynchronized activity via mean-field feedback. The result of this analysis consists of a *sufficient condition*, given in Theorem 5.10, ensuring that a given pair of oscillators is descynhronized. This condition involves three terms. The first one requires the difference in natural frequency to be large, or at least non-zero. The second imposes the mean natural frequency of the ensemble to be large. Note that this condition complements the results derived in Chapter 4, by which one expects the mean-field feedback to induce oscillation inhibition rather than desynchronization if the natural frequencies are small (cf. Theorem 4.5). The third term guides the feedback gain design, in particular the DBS electrode positioning and the choice of the stimulation intensity, by imposing to minimize the closed-loop diffusive coupling strength. The same desynchronization analysis is extended in Section A.6 to the generalized dynamics introduced in Section A.1.

This result is specialized to the all-to-all Kuramoto model in Corollary 5.11. Interestingly, this result constitutes a complement to the clustering investigation in (Aeyels and Rogge, 2004). The former provides a sufficient condition for a pair of originally phase-locked oscillators to be desynchronized by mean-field feedback, while the latter gives a sufficient condition for a pair of oscillators to form a practically phase-locked cluster in the absence of external inputs.

Introduction to Part II - More realistic neuron models

Motivated by the development of a closed-loop DBS, the mathematical analysis in Part I highlights and rigorously explains the synchronization and desynchronization phenomena observed in a population of interconnected oscillators, under the effect of its mean-field proportional feedback. The objective of the second part of the manuscript is to explore other modeling approaches that might permit to extend this analysis to more biologically sound neuron models.

We start by briefly recalling some essentials on the electrical activity of neurons, and the rich variety of associated dynamical behaviors beyond the periodically spiking one. The role of a precise type of ionic current in the neuron membrane, namely the calcium current, is especially highlighted, in particular in relation to the electrical activity of some PD-related neurons. A review of some recently proposed modeling and analysis approaches beyond oscillator and phase models is then presented. Finally, we provide an outline of the two modeling approaches explored in Part II, and of the obtained results.

1.4 The problem: Modeling and analyzing non-periodically spiking neurons

1.4.1 Ionic basis of spiking

Let us briefly recall some basic physiological facts about the ionic mechanisms underlying the electrical activity of neurons. A more detailed discussion can be found in Section 6.1. All the information presented here, and many more details can be found in (Hille, 1984, Chapters 1-5).

The neuron membrane is permeable to different types of ions, mainly sodium Na^+, potassium K^+, and calcium Ca^{2+} ions. Ions cross the neuron membrane through protein ionic channels, generating in this way ionic membrane currents. The ionic channels permeability to the different ions determines the membrane conductance with respect to a given ionic current.

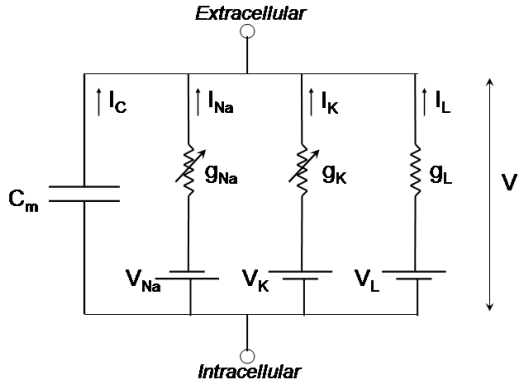

FIGURE 1.3: Electrical circuit equivalent to a model. C_m denotes the neuron membrane capacitance. V_{Na} and V_K are, respectively, the sodium and potassium equilibrium potential. The nonlinear conductances g_{Na} and g_K changes dynamically according to voltage changes. $I_C = C_m dV/dt$ is the current at membrane capacitance. I_{Na} and I_K are the ionic currents generated by, respectively, sodium and potassium ions. The leak current I_L approximates passive properties of the cell. Adapted from (Skinner, 2006), with permission.

At the same time, the difference in ions concentration between the intracellular and extracellular mediums generates a potential difference, or membrane voltage. Finally, the lipid bilayer of the neuron membrane acts as an insulator, or capacitance, between the two charged mediums.

Specific ionic channels properties render the obtained conductive-capacitive circuit, sketched in Figure 1.3, nonlinear. More precisely, the ionic channels permeability to the different ions is dynamically and nonlinearly regulated by voltage changes. Consequently, the membrane conductance too changes dynamically according to voltage dependent nonlinear equations. The nonlinear nature of the resulting electrical circuit is at the basis of the rich behavior of neurons illustrated in the next section.

1.4.2 A rich variety of behaviors

We include in this section a few examples of the different behaviors associated to the intrinsically nonlinear nature of neurons dynamics. The interested reader can find in (Ermentrout and Terman, 2010, Chapters 1-7) and (Izhikevich, 2007, Chapters 5-9) an exhaustive list of electrical phenomena occurring in neurons membrane, along with a complete analysis of the underlying dynamical mechanisms.

Neural excitability (Figure 1.4a) describes the abrupt and large excursion of the membrane voltage (spike) of an originally resting neuron in response to small and brief stimuli (in red in the figure). This nonlinear behavior relies on the interaction of the fast reacting inward (positive) Na^+ current and the slower outward (negative) K^+ current. As the stimulus induces a positive voltage change, the sodium current activates much faster than the potassium current. As a consequence, a net inward current is activated that tends to further increase the membrane voltage (upstroke). This positive feedback continues until the potassium current is large enough. At this point the two currents are equilibrated, and the membrane voltage starts to decrease. Both potassium and sodium currents then decrease as well, and the system relaxes back to rest (downstroke).

Periodic spiking (Figure 1.4b) appears when, due to an injected dc-current (in red in the figure), the stable resting state disappears. In this case, the mechanism is essentially the same

(a) (b)

FIGURE 1.4: Neuronal excitability and periodic spiking

as the one described for neuronal excitability, apart that, after the spike, the injected current triggers again the fast positive feedback mediated by Na^+ currents, and the cycle continues.

Bursting (Figure 1.5a) describes the alternation of resting/excitable spiking and periodic spiking. It is mainly due to the slow adaptation mechanism provided by changes in the intracellular Ca^{2+} concentration (in green in the figure). Indeed, while other ions concentrations barely influence the cell electrical properties, variations in Ca^{2+} concentration can switch the neuron from a resting excitable state to a periodically spiking one, and vice-versa.

After-depolarization potential (Figure 1.5b). While relaxing to rest, after a spike has been generated, the membrane voltage exhibits a second small bump (depolarization). This second depolarization is usually much smaller then a real spike. The ionic mechanism involves Ca^{2+} currents. Together with sodium, Ca^{2+} currents provide a further, but slower, source of depolarizing currents. Consequently, during the spike downstroke, inward Ca^{2+} currents are still active and, if the number of calcium channels is sufficiently large, they can temporarily overcome the hyperpolarizing effects of K^+ currents and generate a small depolarization.

Plateau oscillations (Figure 1.6). If depolarizing calcium currents are sufficiently strong, they might trigger the fast positive feedback mediated by sodium currents and transform the ADP in a real spike. The resulting sustained oscillations lie on a "plateau" above the rest membrane voltage (dashed gray line in the figure). Plateau oscillations continue until the slow modulation from intracellular Ca^{2+} (green in the Figure) ends the burst.

Calcium channels play a fundamental role in some of the spiking behavior described above. Citing (Hille, 1984):

> "...(voltage-regulated) Ca channels are found in almost every excitable cell..."

They directly participate in the spiking pattern by providing, together with sodium channels, an extra source of depolarizing currents. But, as opposite to sodium channels that inactivate very fast, calcium channels contribution last longer, on a similar timescale as potassium channels. As described above, the antagonistic cooperation of the resulting depolarizing calcium currents and hyperpolarizing potassium currents regulates the afterspike cell excitability, and is involved, for instance, in the generation of ADPs (Chen and Yaari, 2008; Brown and Randall, 2009) and plateau oscillation (Rekling and Feldman, 1997; Beurrier et al., 1999).

Intracellular Ca^{2+} variation due to calcium currents have also a slower modulating effect on the global cell properties. Citing (Hille, 1984):

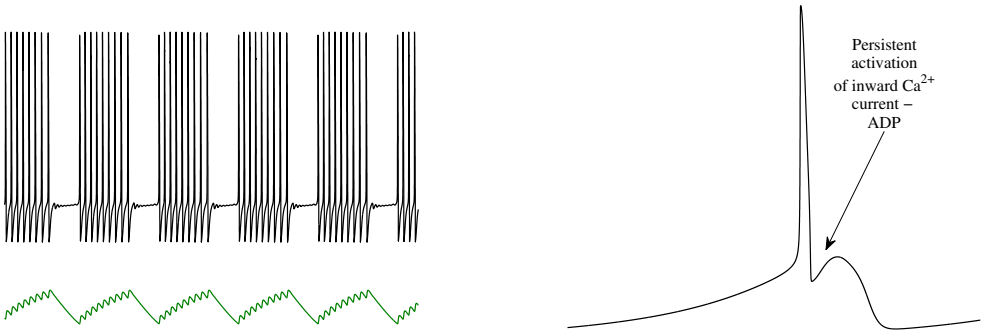

FIGURE 1.5: Bursting and ADP

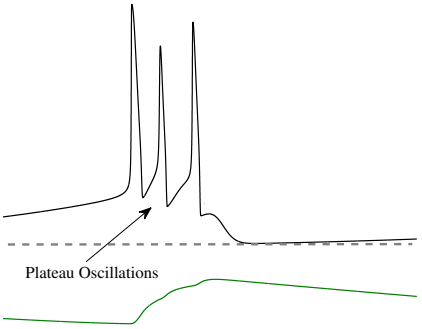

FIGURE 1.6: Plateau oscillations.

> "...excitable cells translate their electricity into action by Ca^{2+} fluxes modulated by voltage-sensitive Ca-permeable channels. Calcium ions are intracellular messenger capable of activating many cell function."

The slow Ca modulation thus permits to shape and adapt the cell activity. In this regard, bursting and plateau oscillations are just examples. Changes in Ca^{2+} ions concentration affect as well neurotransmitters release, and ionic channels permeability (Hille, 1984, Chapter 4).

Calcium channels are important also from a PD/DBS perspective. They abound indeed in STN and dopaminergic neurons cells, where they are believed to participate in the regulation of the neuronal pacemaking, excitability, and bursting. See for instance: STN (Beurrier et al., 1999; Hallworth et al., 2003; Song et al., 2000; Zhu et al., 2004); DA (Amini et al., 1999; Cui et al., 2004; Foehring et al., 2009; Waroux et al., 2005)

1.4.3 Searching simple models of complex dynamics

All the phenomenology presented in Section 1.4.2 is usually described via detailed conductance-based models of the Hodgkin-Huxley type (Hodgkin and Huxley, 1952). The number of variables and parameters of such models rapidly increases with the sought level of realism, with the risk of obscuring the essential firing mechanisms and hampering the mathematical understanding of the observed phenomena, in particular for large networks. It is thus of fundamental

importance to derive simple models able to capture the basic properties of neuronal dynamics. In this regard, the complex oscillator model used in Part I is a simple model for oscillatory dynamics.

In Part II of this manuscript we explore the mathematical abstraction of some neuron dynamics from detailed to simple models, with the aim of combining physiological soundness and mathematical understanding. The objective of this investigation is to extend to more realistic neuron models the synchronization and desynchronization analysis developed in Part I.

Objective of Part II: Given a neuron type exhibiting some electrophysiological properties, find a simple model exhibiting and explaining these properties. Based on the simple model, investigate analytically synchronization and desynchronization phenomena observed in the complex model.

1.5 State of the art: Simple models of complex dynamics

We recall in this section some existing modeling and analysis strategies that allows the simplified modeling of many of the neuronal properties described in Section 1.4.2.

1.5.1 Reduced neuron models

In (FitzHugh, 1961), FitzHugh derives a two-dimensional reduced model of the Hodgkin-Huxley dynamics. His reduction is mainly based on the observation, obtained through analogical electronic simulations, that the system spends most of the time near a two-dimensional submanifold. Even though not rigorously derived, his simple model, later known as the FitzHugh-Nagumo equation, captures all the qualitative properties of the Hodgkin-Huxley dynamics, in the sense that they possess the same bifurcation diagram. The bifurcation diagram describes how the limit sets (in the past and in future) of a dynamical system change as a given parameter, or set of parameters, changes.

The interest of Fitz-Hugh reduction is that it permits to visualize and understand complex physiological behaviors through a planar phase-portrait analysis, that FitzHugh called the "physiological state diagram". The same phenomena are obscured in the Hodgkin-Huxley model by the four dimensions of the underlying dynamics.

The principle of FitzHugh reduction have been extended and formalized in (Kepler et al., 1992). The authors develop an algorithm to replace variables having similar timescales and similar effects on the membrane voltage dynamics by their weighted mean. Thus, for instance, in the Hodgkin-Huxley model the variables describing the inactivation of the inward Na^+ current and the activation of the outward K^+ current, both providing a negative feedback on membrane voltage variations and evolving on similar time scales, can be embedded in a single variable still providing a negative feedback on membrane voltage variations. Heuristically, FitzHugh performed the same reduction, obtaining the famous "recovery variable" of the FitzHugh-Nagumo model. The algorithm in (Kepler et al., 1992) fails, however, to embed variables with opposite effects, called in that paper "antisynergistic". An example is provided by the activation of the calcium (inward) and potassium (outward) currents on a similar time scale, whose antisynergistic cooperation is responsible for the generation of ADPs and plateau oscillations, as described in Section 1.4.2.

1.5.2 Hybrid neuron models

Recent works, in particular (Izhikevich, 2010) and (Izhikevich, 2007, Chapter 8), have revived the interest for reduced hybrid models that are amenable to a comprehensive mathematical analysis and yet offer sufficient fidelity to the quantitative model to allow for effective large-scale simulations. The hybrid[3] nature of the Izhikevich model adequately captures the fast (almost discontinuous) behavior of spiking neurons. Hybrid quantitative modeling can also find applications in the DBS computational model-based approach (Schiff, 2010) discussed in Section 1.2, where computational efficiency and quantitative fidelity are essential.

Izhikevich's reduction relies on the fundamental observation that the (fast) voltage dynamics of many reduced models, including the aforementioned FitzHugh-Nagumo, exhibit, near the resting state, a fold bifurcation, while the (slow) dynamics of the recovery variable is essentially linear. By picking a normal form of the fold bifurcation for the voltage dynamics, a linear equation for the recovery variable, and a reset mechanism for the spike down-stroke, Izhikevich model is able to reproduce the qualitative and quantitative behavior of a large class of neurons (Izhikevich, 2003). The resulting phase-portrait is characterized by a quadratic voltage nullcline and a linear recovery variable nullcline, and its rich phase-portrait permits to explain a number of physiological phenomena.

1.5.3 Incremental passivity and convergent/contracting dynamics

In recent years, control theorists have shown a growing interest in the analysis and control of interconnected nonlinear oscillators, in particular in relation to neuronal oscillators. In this framework, ideas derived from standard stability analysis are adapted to the study of synchronization, and the related control tools thoroughly exploited.

A first approach relies on passivity techniques. More precisely, in (Stan and Sepulchre, 2007; Hamadeh et al., 2008; Stan et al., 2007; Oud and Tyukin, 2004) the authors investigate passivity (Van der Schaft, 1999; Byrnes et al., 1991; Ortega, 1991), semi-passivity (Pogromsky and Nijmeijer, 2001), and their incremental counterparts of neuronal and other biological oscillators. Roughly speaking, a system is (strictly output) passive if it dissipates the perturbations' energy, which ensures asymptotic stability in the absence of perturbations and robustness if exogenous inputs are present (Van der Schaft, 1999). Clearly, an oscillator can not be passive, or it would rather converge to some fixed point. It turns out, however, that many oscillators are semi-passive, that is they are passive only out of the region of oscillation. By diffusive interconnection, it can also be shown that the semi-passivity property extends to the incremental dynamics (incremental semi-passivity), ruling states differences between the oscillators. Moreover, diffusive coupling tends to shrink the region of the incremental state space where strict incremental output passivity does not hold, and, for sufficiently large coupling strength, diffusive coupling makes the incremental dynamics strictly output passive, which ensures synchronization. In conclusion, passivity and its generalization have proved to be a valid tool for the analysis of diffusively interconnected neural and nonlinear oscillators.

A second approach for the analysis of synchronization relies on convergent dynamics and contraction theory (Demidovich, 1967; Pavlov et al., 2004, 2006; Spong, 1996; Wang and Slotine, 2004; Pham and Slotine, 2007; Lohmiller and Slotine, 1998). Both concepts deal with incremental stability, that is the stability of motion of one trajectory with respect to an other. Roughly speaking a system is called convergent, or its dynamics contractive, if locally trajectories approach each other exponentially. The application to synchronization is thus straightforward

[3] A system is said to be hybrid if its dynamics is ruled by both continuous differential equations and discrete upgrades (Van der Schaft, 2000; Lygeros et al., 2003; Goebel et al., 2009).

by comparing the trajectories of different subsystems. We point out, however, that these requirements, originally formulated for the control of robot manipulators, might be too strong for biological oscillators.

Works that combine both approaches are (Pogromsky and Nijmeijer, 2001) and (Steur et al., 2009). In (Steur et al., 2009) the authors show that many neuron models, including physiological models like the Hodgkin-Huxley dynamics, can be decomposed in a scalar dynamics, receiving external inputs, and a convergent dynamics, associated to membrane conductances. Based on the results in (Pogromsky and Nijmeijer, 2001), they are able to provide sufficient conditions for synchronization in networks of diffusively coupled neuronal oscillators.

1.6 Contributions: A preliminary exploration of two new modeling approaches

Most of the results collected in Part I come from preliminary unpublished works. They stem from two collaborations undertaken during the last year of this PhD thesis. The results contained in Chapter 6 were obtained under the supervision of Prof. R. Sepulchre at the University of Liège, Belgium. The results contained in Chapter 7 were obtained under the supervision of Prof. L. Scardovi at the Technische Universität München, Germany. Further details about the available research fundings can be found in the relative chapters.

1.6.1 Reduced and hybrid modeling of calcium gated neurons

Recent results (Drion et al., 2011a,b) have highlighted the importance of voltage-regulated calcium currents and calcium-regulated potassium channels in the pacemaking, excitability, and synchronization properties of midbrain dopaminergic neurons. More precisely, these currents have been shown to participate in the generation of the endogenous neuron rhythm (Drion et al., 2011a) and in the regulation of the synchronizability of neurons with an external input (Drion et al., 2011b), as shown in Figure 1.7. This latter property might have an importance also for DBS. One of the conjectures behind the functioning of present DBS is that indeed STN neurons synchronize with the DBS signal to a high non-pathological frequency (Hammond et al., 2008). While STN and dopaminergic neurons do not exhibit exactly the same families of ionic channels, in both types of neurons voltage-regulated calcium currents and calcium-regulated potassium channels play a significant role (see page 1.4.2). Motivated by these experimental and numerical evidences, we proceed further with the mathematical reduction of a dopaminergic (DA) neuron model, mimicking the reduction of the (four-state) Hodgkin-Huxley (HH) model to the (two-state) FitzHugh-Nagumo model, and the recent work by Izhikevich on spiking neurons to reduced HH-type models with a calcium dynamics to a two-state hybrid model. Even though we do not treat the DBS computational model-based approach (Schiff, 2010) in this thesis, the potentiality of a quantitative, computationally efficient, hybrid modeling of the neurons involved in PD/DBS might be relevant also in that framework.

As recalled in Section 1.5.2, the Izhikevich model (Izhikevich, 2010) is a hybrid model of neurons that permits to reproduce with fidelity the spiking pattern of a vast family of neurons. The parameters of the Izhikevich model can also be tuned to reproduce with fidelity the spiking pattern of dopaminergic neurons, that is a slow periodic spiking (pacemaking) with ADPs. Interestingly, however, when some external inputs are applied, the behavior of the obtained hybrid dynamics is extremely sensitive, and even tiny amounts of current, which barely influence the behavior of detailed computational models of dopaminergic neurons, completely disrupt

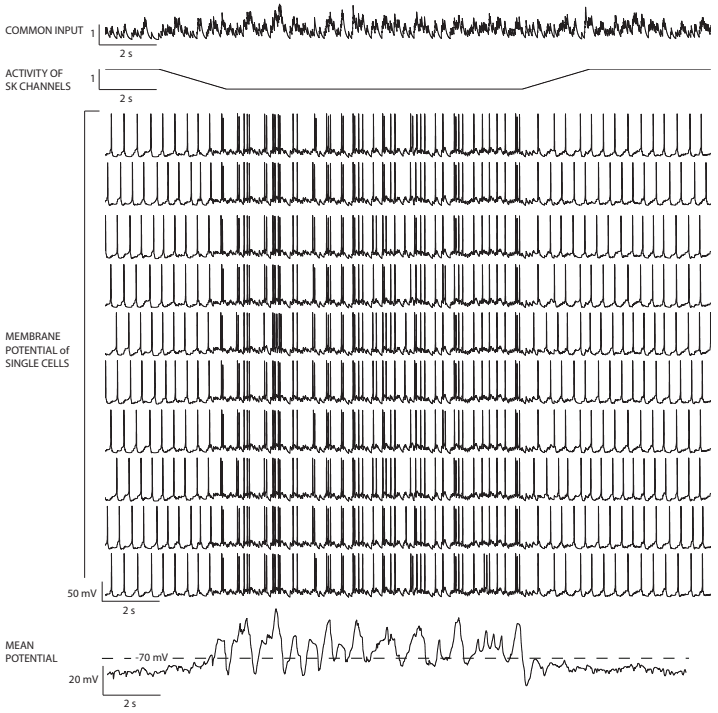

FIGURE 1.7: Response of an ensemble of heterogeneous dopaminergic neurons to a common noisy input. SK channels inhibit the calcium-regulated excitability, letting the neurons insensitive to the injected synaptic current and the ensemble desynchronized. When SK channels are downregulated, the ensemble is entrained by the exogenous current, resulting in a synchronous behavior. Adapted from (Drion et al., 2011b).

its regular spiking activity. This behavior is not satisfactory in biologically meaningful conditions and makes the obtained dynamics not suitable for the analysis of the neuron response to external inputs. See Figure 6.13 on page 153.

In Chapter 6 we show that this deficiency is due to the absence, in the Izhikevich model, of a specific type of bifurcation exhibited by calcium-gated and, in particular, dopaminergic neurons. Furthermore, we propose an alternative reduced model embedding this bifurcation, and exhibiting robust pacemaking and ADPs. More precisely, after a brief recall of the ionic basis of neuron dynamics (Section 6.1), we present in Section 6.2 a modified version of the Hodgkin-Huxley model, including a voltage-regulated calcium current and exhibiting the typical behavior of calcium-gated neurons. The obtain model can be reduced in a standard way to a planar dynamics, exhibiting the same behavior. Phase portrait and numerical bifurcation analysis are then exploited in Sections 6.2.2 and 6.2.3 to investigate the dynamics of calcium-gated neurons and some typical physiological phenomena.

A deeper phase portrait investigation reveals that the voltage nullcline[4] has a self intersection for a particular value of the input current. We explain in Section 6.3.1 how this self-intersection is associated to a singular *transcritical bifurcation* of the fast voltage dynamics. This bifurcation is absent in other existing simple models of neurons, including Izhikevich, and might be identified as a mathematical signature of calcium-gated neurons. Furthermore, we show analytically in Section 6.3.3 through normal forms and geometrical singular perturbations (Jones, 1995; Krupa and Szmolyan, 2001b) that this singular transcritical bifurcation is closely related to the saddle homoclinic bifurcation highlighted by the numerical bifurcation analysis.

[4] Given a planar dynamics $\dot{x} = f(x, y)$ and $\dot{y} = g(x, y)$, the x-nullcline is defined as the set $\{(x, y) \in \mathbb{R}^2 : \dot{x} = 0\}$ and, similarly, the y-nullcline as $\{(x, y) \in \mathbb{R}^2 : \dot{y} = 0\}$.

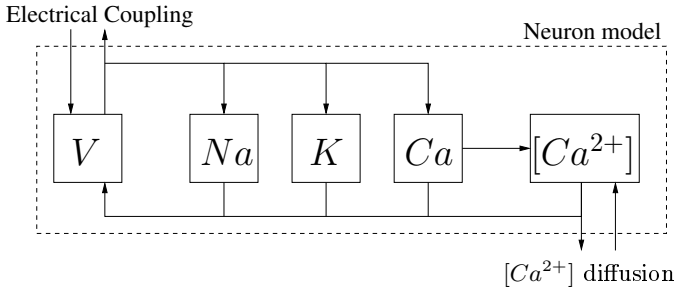

FIGURE 1.8: Input-output model of the neuron memebrane. The membrane voltage interacts with the different ionic currents via parallel feedback loops. In turn, calcium currents change the intracellular Ca^{2+} concentration, providing a further slower feedback on the voltage dynamics (see Section 1.4.2, page 16). The interconnection with other neurons is due to electrical coupling and to the diffusion of Ca^{2+} ions in the extracellular medium. Other forms of internal and external interaction can similarly be modeled.

Apart from the mathematical interest of this phenomenon, which appears to be new in neurons modeling, the computed normal form is used to derive in Section 6.4 a *novel reduced hybrid model* of neurons. The parameters of this model can be chosen in order to reproduce the behavior of a dopaminergic neuron. We finish with a comparison of the detailed computational model of dopaminergic neurons, the novel reduced model, and the Izhikevich model. We rely on the mathematical analysis developed in the rest of the chapter to show that the transcritical bifurcation discussed above is crucial in generating robust pacemaking and ADPs, and that its absence is at the basis of the non-robust behavior exhibited by the Izhikevich model.

As a conclusion, we propose the novel reduced model as a simple choice for the modeling of dopaminergic neurons, and, more generally, calcium-gated neurons, and the analysis of their response to external stimuli.

1.6.2 An input-output approach to neuronal synchronization

As discussed in Section 1.5, passivity and convergent dynamics techniques proved to be an effective tool to analyze and control synchronization between neurons. At the same time, all the cited works heavily use a state-space formalism, which requires a detailed knowledge of the underlying dynamics, while biological systems are intrinsically affected by uncertainties, variability, and noise.

In (Scardovi et al., 2010), the authors propose a purely input-output approach based on the theory of nonlinear operators to model and analyze robust synchronization between interconnected systems. This approach requires minimal knowledge of the physical laws governing the systems, and is therefore particularly well suited to applications displaying high uncertainties such as biological systems and in particular neuronal populations.

In cellular networks the signaling occurs both internally (through the interaction of electrical, chemical, and other types of species) and externally (through intercellular signaling). In neurons, in particular, the membrane voltage interacts dynamically with the different ionic currents and with intracellular Ca^{2+} variations, as described in Sections 1.4.1 and 1.4.2. See also Section 6.1. This internal type of signaling is at the basis of the neuron endogenous behavior. Meanwhile, interneuronal electrical and chemical signals travel among large populations. Figure 1.8 illustrates how these intracellular and intercellular interactions can naturally be modeled as the interconnection of different units that model electrical, ionic, and chemical species.

In the framework developed in (Scardovi et al., 2010), each species involved in the neuron dynamics is modeled as an input-output operator. The input/output interconnection of these operators forms a compartment that models the whole neuron. The operators associated to each species are then interconnected among different compartments via diffusive coupling, modeling electrical and chemical neuronal interaction (Figure 7.1). The obtained system is naturally suited for the study of open- and closed-loop controls, and in particular DBS, due to the input-output nature of its constituting elements and the rich control theory literature available in this domain. See, for instance, (Vidyasagar, 1981; Moylan and Hill, 1978; Van der Schaft, 1999) and references therein.

Relying on this modeling principle, we provide in Chapter 7 a theoretical extension of the work in (Scardovi et al., 2010) to take into account heterogeneous populations, and accordingly adapt the main result in in that reference. More precisely, we provide in Theorem 7.3 sufficient conditions for a network of heterogeneous interconnected systems to achieve robust synchronization and compute explicitly the bound on the synchronization error, given the strength of disturbances.

Finally, we illustrate these techniques in the neuronal synchronization context. We show that the Hindmarsh-Rose neuron can be naturally modeled as the negative feedback interconnection of two nonlinear operators modeling, respectively, the fast excitable membrane dynamics, and the slow intracellular calcium dynamics. As an application of Theorem 7.3, Proposition 7.9 provides sufficient conditions for the robust synchronization in a network of diffusively coupled Hindmarsh-Rose neurons. This result thus constitutes a first extension of the main result in Chapter 3 to more realistic neuron models. A numerical example is finally considered, in which we model the interaction of two heterogeneous neuronal population with different electrical properties (Section 7.4.3).

List of publications

Journal papers

[J1] A. Franci, A. Chaillet, and W. Pasillas-Lépine. Existence and robustness of phase-locking in coupled Kuramoto oscillators under mean-field feedback. *Automatica - Special Issue on Biology Systems*, 47(6):1193–1202, 2010. Regular paper.

[J2] A. Franci, A. Chaillet, E. Panteley, and F. Lamnabhi-Lagarrigue. Desynchronization and inhibition of all-to-all interconnected Kuramoto oscillators by scalar mean-field feedback. *Math. Control Signals Syst. - Special Issue on Large-Scale Nonlinear Systems*, 24:169-217, 2011. Regular paper.

[J3] G. Drion†, A. Franci†, and R. Sepulchre. A Novel Phase Portrait for Neuronal Excitability, 2012. Submitted to: *PLoS Computational Biology.* †Double first author.

[J4] A. Franci†, G. Drion†, and R. Sepulchre. A model of neuronal excitability organized by a degenerate pitchfork bifurcation, 2012. In preparation. To be submitted to: *SIAM Journal on Applied Dynamical Systems.* †Double first author.

[J5] A. Franci†, G. Drion†, and R. Sepulchre. A balance equation determines neuronal excitability in conductance-based models, 2012. In preparation. To be submitted to: *J. Neuroscience.* †Double first author.

[J6]* A. Franci and A. Chaillet. Quantised control of nonlinear systems: analysis of robustness to parameter uncertainty, measurement errors, and exogenous disturbances. *International Journal of Control*, 83(12):2453–2462, 2010.

Conference papers

[IC1] A. Franci, A. Chaillet, and W. Pasillas-Lépine. Le modèle de Kuramoto sous retour du champ moyen réel n'admet pas de solutions à phases verrouillées. In *Proc. Conférence Internationale Francophone d'Automatique*, Nancy, France, 2010.

[IC2] A. Franci, A. Chaillet, and W. Pasillas-Lépine. Robustness of phase-locking between Kuramoto oscillators to time-varying inputs. In *Proc. 49th. IEEE Conf. Decision Contr.*, pages 1587–1595, Atlanta, GA, USA, December 2010.

[IC3] A. Franci, W. Pasillas-Lépine, and A. Chaillet. Existence of phase-locking in coupled Kuramoto oscillators under real mean-field feedback with applications to Deep Brain Stimulation. In *Proc. 18th. IFAC World Congress*, pages 5419–5424, Milano, Italy, August 2011.

[IC4] A. Franci, A. Chaillet, and S. Bezzaoucha. Toward oscillations inhibition by mean-field feedback in Kuramoto oscillators. In *Proc. 18th. IFAC World Congress*, pages 2511–2516, Milan, Italy, August 2011.

[IC5] A. Franci, L. Scardovi, and A. Chaillet. An input-output approach to the robust synchronization of dynamical systems with an application to the Hindmarsh-Rose neuronal model. In *Proc. 50th. IEEE Conf. Decision Contr.*, Orlando, FL, USA, December 2011.

[IC6] A. Franci, E. Panteley, A. Chaillet, and F. Lamnabhi-Lagarrigue. Desynchronization of coupled phase oscillators, with application to the Kuramoto system under mean-field feedback. In *Proc. 50th. IEEE Conf. Decision Contr.*, Orlando, FL, USA, December 2011.

[IC7] A. Franci, W. Pasillas-Lépine, and A. Chaillet. Validity of the phase approximation for coupled nonlinear oscillators: a case study, 2012. Submitted to: *Proc. 51th. IEEE Conf. Decision Contr.*

[IC8]* A. Franci and A. Chaillet. Quantised control of nonlinear systems: analysis of robustness to parameter uncertainty, measurement errors, and exogenous disturbances. *Proc. 7th Conf. on Informatics in Control, Automation and Robotics*, Funchal, Madeira, Portugal, June 2010

*These publications were also produced in the course of this PhD thesis. For homogeneity reasons, its contribution is not included in this manuscript.

Notation

We respectively denote by $\mathbb{Z}$, $\mathbb{N}$ and $\mathbb{R}$ the sets of all integers, all nonnonegative integers, and all real numbers. If $A \in \mathbb{N}$ or $A \in \mathbb{R}$, and $a \in A$, $A_{\geq a}$ denotes the set $\{x \in A : x \geq a\}$. Given $N \in \mathbb{N}_{\geq 1}$, we let $\mathbb{N}_N^{\neq} := \{(i,j) \in \{1,\dots,N\}^2 : i \neq j\}$. If $\mathcal{I} \subset \mathbb{Z}$, $\#\mathcal{I}$ denotes the number of its elements.

Given $n \in \mathbb{N}_{\geq 1}$, T^n denotes the n-dimensional torus, or simply n-torus.

Given a set $A \subset \mathbb{R}^n$ (resp. $A \subset T^n$), ∂A denotes its boundary.

Given tow sets X, Y, a function $f : X \to Y$, and $A \subset X$, we denote by $f|_A : A \to Y$ the restriction of f to A, which is defined by $f_A(x) = f(x)$, for all $x \in A$.

We denote by $\mathbf{1}_{n\times m} \in \mathbb{R}^{n\times m}$ the $n \times m$ matrix with all unitary entries, and $\mathbf{1}_n := \mathbf{1}_{n\times 1}$. I_n denotes the identity matrix in dimension n. Given any square matrix A, $\mathrm{spect}(A)$ denotes the set of its eigenvalues.

Given $i \in \{1,\dots,N\}$, $e_i \in \mathbb{R}^N$ is the vector with only zero entries, except the i-th which is equal to 1. Given $x \in \mathbb{R}^N$, $x^\perp := \left\{z \in \mathbb{R}^N : x^\top z = 0\right\}$.

For all $x \in \mathbb{R}^n$, the Euclidean norm of x is denoted by $|x|_2 := \sqrt{\sum_{i=1}^n x_i^2}$ and its infinity norm by $|x|_\infty := \max_{i=1,\dots,N} |x_i|$. When clear from the context, we simply denote the Euclidean norm as $|x|$. For $\mathcal{A} \subset \mathbb{R}^n$ and $x \in \mathbb{R}^n$, the Euclidean point-to-set distance is denoted by $|x|_{\mathcal{A}} := \inf_{y\in\mathcal{A}} |y - x|$. Given $A, B \subset \mathbb{R}^N$ the Euclidean set-to-set distance is denoted by $|A|_B := \inf_{x\in A, y\in B} |x - y|$. For $A \subset \mathbb{R}^n$ and $r \geq 0$, $\mathcal{B}(A, r)$ denotes the closed ball centered at A of radius r in the Euclidean norm, that is $\mathcal{B}(A, r) := \{x \in \mathbb{R}^n : \ |x|_A \leq r\}$.

If $u : \mathbb{R}_{\geq 0} \to \mathbb{R}^n$ denotes a measurable signal, locally essentially bounded, its essential supremum norm is denoted by $\|u\| := \text{ess sup}_{t\geq 0}|u(t)|$.

We denote by ∇_x the vector of partial derivatives (gradient) with respect to x, *i.e.* $\nabla_x = \left(\frac{\partial}{\partial x_1}, \dots, \frac{\partial}{\partial x_n}\right)$.

For all $x, y \in \mathbb{R}$, $z = x \bmod y$ if $z = x + ky$ for some $k \in \mathbb{Z}$. Given $x \in \mathbb{R}^n$ and $a \in \mathbb{R}$, $(x \bmod a) := [x_i \mod a]_{i=1,\dots,n} \subset \mathbb{R}^n$.

A continuous function $\alpha : \mathbb{R}_{\geq 0} \to \mathbb{R}_{\geq 0}$ is said to be of class $\mathcal{K}$ if it is increasing and $\alpha(0) = 0$. It is said to be of class $\mathcal{K}_\infty$ if it is of class $\mathcal{K}$ and $\alpha(s) \to \infty$ as $s \to \infty$. A function $\beta : \mathbb{R}_{\geq 0} \times \mathbb{R}_{\geq 0} \to \mathbb{R}_{\geq 0}$ is said to be of class $\mathcal{KL}$ if $\beta(\cdot, t) \in \mathcal{K}$ for any fixed $t \geq 0$ and$\beta(s, \cdot)$ is continuous decreasing and tends to zero at infinity for any fixed $s \geq 0$.

We denote by μ^n the Lebesgue measure on $\mathbb{R}^n$ (resp. T^n), and *for almost all* ($\forall a.a.$) denotes the equivalence operation with respect to this measure. When no confusion can arise, we simply denote the Lebesgue measure as μ.

The solution of a system $\dot{x} = f(x, t)$ starting at $x_0 \in \mathbb{R}^n$ at time $t_0 \in \mathbb{R}$ is denoted by $x(\cdot; t_0, x_0)$ everywhere it exists. In the autonomous case, the solution of a system $\dot{x} = f(x)$ starting at $x_0 \in \mathbb{R}^n$ at $t = 0$ is denoted as $x(\cdot, x_0)$ everywhere it exists. Given a set $U \subset \mathbb{R}^n$, $x(t; t_0, U) := \{x(t; t_0, x_0) : x_0 \in U\}$. Given a set $A \subset \mathbb{R}^n$, we define its stable (resp. unstable) set with respect to a given dynamics $\dot{x} = f(x)$ as $A^s := \{x_0 \in \mathbb{R}^n : \lim_{t\to\infty} |x(t; x_0)|_A = 0\}$ (resp. $A^u := \{x_0 \in \mathbb{R}^n : \lim_{t\to-\infty} |x(t; x_0)|_A = 0\}$).

Let L_{2e}^m denotes the extended L_2 space Van der Schaft (1999) of signals $w : \mathbb{R}_{\geq 0} \to \mathbb{R}^m$, such that the truncation $w_T := w|_{[0,T]}$ is in $L_2^m([0, T])$, for all $T \geq 0$. In other words, L_{2e}^m is made of all signals that are square-integrable on any finite interval. Given any $T \geq 0$, for all $w, v \in L_{2e}^m$, the scalar product of w_T and v_T is denoted by $\langle w, v\rangle_T$. We write $\|w\|_T$ for the L_2^m norm of $w|_T$.

Part I

Neurons as oscillators

Chapter 2

Model derivation and phase-locking under mean-field feedback

With the aim of approaching the closed-loop DBS control problem described in Section 1.1 in an analytical way, we derive in this chapter a simplified model of an interconnected neuronal population under the effect of a closed-loop electrical stimulation. Some useful definitions and a preliminary analysis of this system are then provided.

Let us briefly recall the problem under analysis. A more complete discussion and more references can be found in Section 1.1. Under healthy conditions the subthalamic nucleus (STN) neurons fire in an uncorrelated (*i.e.*, desynchronized) manner (Nini et al., 1995; Sarma et al., 2010). In PD patients, STN neurons form a cluster of synchronous periodic activity that leads to the PD's physical symptoms (Volkmann et al., 1996; Hammond et al., 2007). In order to overcome tolerance to pharmaceutical therapies, many patients undergo Deep Brain Stimulation (DBS). Through a pair of implanted electrodes, a low voltage "high"-frequency (>100 Hz) electrical input is permanently injected in the STN. This leads to a drastic reduction of the physical symptoms (Benabid et al., 1991). At present this electrical signal is periodic and generated by a standard artificial pacemaker (open-loop control) and is consequently not optimized for the purpose. For each patient an empirical parameter tuning is needed, which may take up to several days and which is not guaranteed to be effective (Rodriguez-Oroz et al., 2005). Moreover patients can develop side effects or tolerance to DBS (Kumar et al., 2003) along the treatment. Also, the permanent electrical stimulation leads to a fast discharge of the pacemaker batteries and, consequently, to further surgical operations to change them.

In order to both provide theoretical justifications to DBS and to overpass the above limitations by exploiting cerebral measurements, we develop a rigorous analysis based on a simplified model. More precisely, we analyze a network of Landau-Stuart oscillators, modeling the neuron population, subject to a scalar input, modeling the effect of DBS. The DBS signal is taken proportional to the mean-field of the neuronal population (*mean-field feedback*).

Due to heterogeneities in the medium, the contribution of each neuron to the mean-field is seen as an unknown parameter. In the same way, the influence of the DBS signal on each neuron is modeled as an unknown gain. The coupling topology is also taken to be arbitrary, allowing for a general time-invariant synaptic interconnection. This approach thus allows to represent any recording-stimulation setup as well as any coupling topology. Nonetheless, we point out that it does not detail the neuronal dynamics, nor the electrode setup.

Under standard assumptions, our model reduces to a modified version of Kuramoto coupled oscillators. This model, originally developed in the seminal work (Kuramoto, 1984), has been already extensively exploited to analyze synchronization phenomena in networks of oscillators

(Pyragas et al., 2008; Daniels, 2005; Acebrón et al., 2005; Kuramoto, 1984; Brown et al., 2003; Cumin and Unsworth, 2007; Maistrenko et al., 2005; Chopra and Spong, 2009; Van Hemmen and Wreszinski, 1993; Jadbabaie et al., 2004; Dörfler and Bullo, 2011). Only recently the interest of the scientific community has focused on desynchronization phenomena, in particular in relation with neurological pathologies (Maistrenko et al., 2005; Pyragas et al., 2008; Tukhlina et al., 2007; Tass, 2003b).

Motivated by the same problem, we introduce in Section 2.1 the Landau-Stuart oscillator as a simple representation of the limit cycle associated to periodically spiking neurons. Relying on this mathematically treatable abstraction of the neuronal rhythm, in Section 2.2 we derive an original model of interconnected oscillators under mean-field feedback. After having formally defined different types of phase-locked solutions (Section 2.3), we show that, for a generic class of interconnections between the oscillators, the existence of perfectly phase-locked oscillating solutions is not compatible with any non-zero mean-field proportional feedback (Section 2.4.1). This analytical result, illustrated through simulations, confirms the expectations of a closed-loop DBS desynchronizing strategy. We present the lemmas needed for the proof of the main result in Section 2.4.2. The proofs of major results are given in Section 2.5, while technical proofs are provided in Section 2.6

2.1 A simple representation of the periodic spiking limit cycle

As anticipated in Section 1.3, in Part I we focus on periodically spiking neurons, that is neurons generating an infinite regular train of action potentials. Even though a rich variety of behaviors exist beside this, periodic neurons are commonly considered for the analysis of neuronal synchronization. See for instance (Ermentrout and Terman, 2010, Chapter 8) and (Izhikevich, 2007, Chapter 10), and references therein. As a first step in exploring the control of neuronal synchronization, we thus start by focusing on this particular type of neurons, and postpone possible extensions to more realistic neuron models in Part II.

The dynamics underlying periodic spiking behavior can be extremely complicated. Even basic physiological models, such as the Hodgkin-Huxley model (Hodgkin and Huxley, 1952) depicted in Figure 2.1, consist of four coupled nonlinear differential equations. If the mathematical analysis of some isolated physiological neuron models, or small networks of them, is still feasible[1], the only realistic analysis of large networks is through numerical simulation. With the aim of establishing analytical results on networks with an arbitrary number of neurons controlled via electrical stimulation, we look for a simpler model still exhibiting some of the peculiarities of its complex counterparts.

A hallmark of periodically spiking neurons is the existence of a (locally) exponentially stable limit cycle attractor, as it is evident in the two dimensional $I_{Na,p} + I_K$ (persistent sodium plus potassium) neuron model depicted in Figure 2.2. One could look for a simple representation of the periodically spiking limit cycle relying on analytical tools, like center manifolds reduction and topological equivalence arguments. See (Guckenheimer and Holmes, 2002, Sections 1.7, 1.8, and 1.9, and Chapter 3) and (Guckenheimer, 1995), and references therein for an introduction to these techniques. Such a rigorous derivation would go beyond the motivation and the goal of this modeling section. Our goal is to find a mathematically treatable representation of a locally exponentially stable limit cycle attractor.

Apart from exhibiting a stable oscillation, we require the simple model to exhibit another basic property, dictated by control theoretical needs. All the physiological models possess an electrical variable associated to the neuron membrane voltage, while the rest of the variables

[1] See for instance Part II of the book (Coombes and Bressloff, 2005), and references therein.

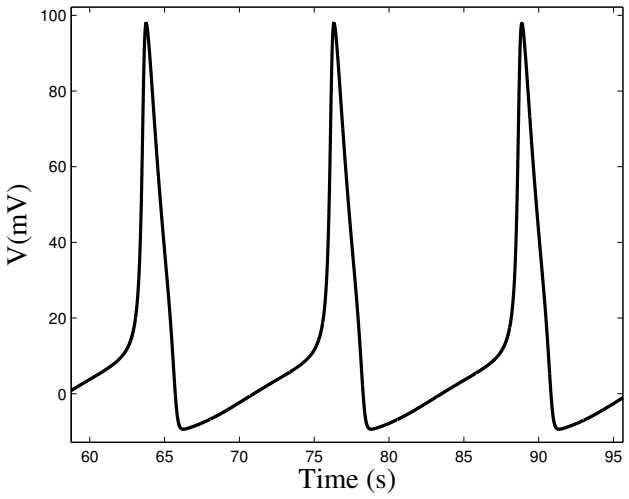

FIGURE 2.1: Periodic spiking in the Hodgkin-Huxley model. Equations and parameters as in (Hodgkin and Huxley, 1952).

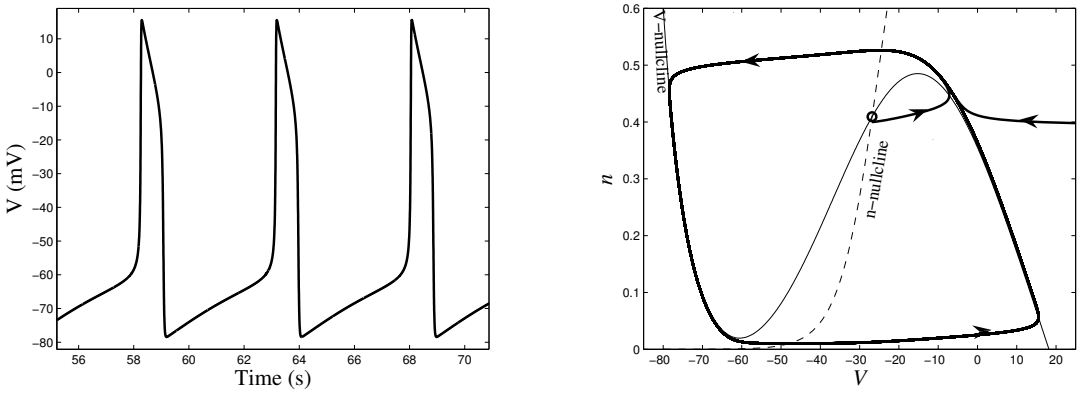

FIGURE 2.2: Periodic spiking and associated limit cycle in the $I_{Na,p} + I_K$ model. Equations and parameters as in (Izhikevich, 2007, Figure 4.1)

describe the membrane permeability to the different ions involved in the spiking generation mechanism. This distinction is crucial when we have to define a meaningful output. In the DBS practice, indeed, only electrical measurements are available. We thus require the simple model to possess at least two variables. So, one can be associated to the membrane voltage, and constitutes the model output, while the other is associated to the other variables of physiological models.

Consider, the following complex oscillator, known as Landau-Stuart oscillator,

$$\dot{z} = (\mathrm{i}\omega_\circ + \rho^2 - |z|^2)z, \quad z \in \mathbb{C}, \tag{2.1}$$

where $\omega_\circ \in \mathbb{R}$ and $\rho > 0$. In its simple form this model captures the two aforementioned basic properties of periodically spiking neurons. First, it exhibits an exponentially stable oscillation of radius ρ and frequency $\omega_\circ$ (Guckenheimer and Holmes, 2002, Theorem 3.4.2). More precisely, the local convergence rate, which measures the limit cycle attractivity, is $2\rho^2$ (see the proof of Proposition A.1, in Chapter A). Thus, the radius, the frequency, and the attractivity of the oscillation can easily be tuned by changing $\omega_\circ$ and ρ. Secondly, we can associate its real

part to the membrane voltage, representing the measured output, and its imaginary part to a recovery variable, embedding the effects of the other variables of physiological neuron models. A similar simplification of the neural rhythm has been extensively used in the synchronization and desynchronization literature. See for instance (Kuramoto, 1984; Ermentrout, 1990; Winfree, 1980; Rosenblum et al., 2006; Hauptmann et al., 2005a; Popovych et al., 2006b; Pyragas et al., 2008), just to name a few references. Figure 2.3 summarizes this modeling approach. However, (2.1) constitutes a simplification of more complex models under different aspects. For instance, its phase phase-dynamics is invariant with respect to natural radius re-scaling. This fact is reflected in the model's radial "isochrons" (Guckenheimer, 1975), which leads to consistent simplifications in the form of the coupled phase dynamics. More complex limit cycle oscillators do not share the same simple structure, and the consequence of this difference on the form of the phase coupling can be important, see e.g. (Ermentrout and Terman, 2010, Sections 8.1.3 and 8.1.4, and references therein).

We stress that, throughout Part I, we use (2.1) in the strong attractivity regime, that is for sufficiently large natural radius ρ. Other works, e.g. Aronson et al. (1990), study the dynamics of coupled Landau-Stuart oscillators (2.1) as a normal form of coupled oscillators near a supercritical Hopf bifurcation, corresponding to small natural radius, when the limit cycle attractivity is small. The behavior in the two regime is rather different, as we further discuss in Sections A.1 and A.3.4.

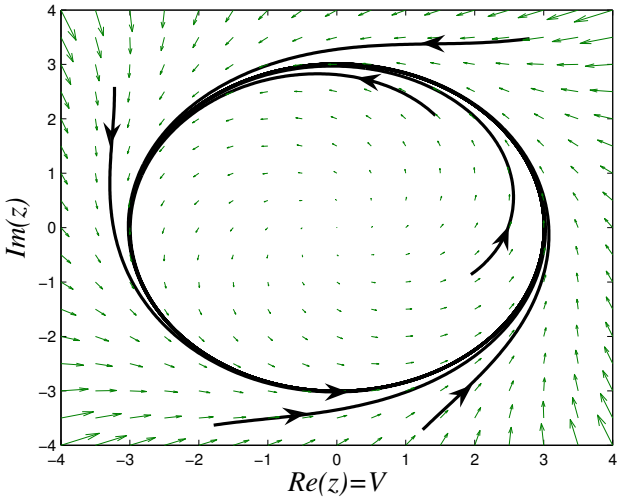

FIGURE 2.3: Limit cycle in the Landau-Stuart oscillator

2.2 Coupled oscillators under mean-field feedback

Relying on the simple representation (2.1) of periodically spiking neurons, in this section we derive a phase model describing a neuronal population under the effect of mean-field feedback.

While the coupling between real neurons can rely on different physical mechanisms (electrical diffusive coupling or gap-junction, impulsive coupling, synaptic coupling, chemical coupling, *etc.*), we assume diffusive coupling between the oscillators, in order to derive a mathematically treatable model. The same approach has been exploited, for instance, in (Maistrenko et al., 2005; Pyragas et al., 2008; Tukhlina et al., 2007; Tass, 2003b). The model for $N \in \mathbb{N}_{\geq 1}$ coupled

oscillators is then given by

$$\dot{z}_i = (\mathrm{i}\omega_i + \rho_i^2 - |z_i|^2)z_i + \sum_{j=1}^{N} \kappa_{ij}(z_j - z_i), \quad \forall i = 1, \ldots, N,$$

where κ_{ij}, $i, j = 1, \ldots, N$, denotes the coupling gain from oscillator j to oscillator i. We denote $\omega := [\omega_i]_{i=1,\ldots,N} \in \mathbb{R}^N$ as the vector of natural frequencies. As in practice the neuronal interconnection is poorly known, we allow κ_{ij}, $i, j = 1, \ldots, N$, to be arbitrary in our study. The possibility of considering any interconnection topology is an interesting particularity of the approach presented here. Furthermore, the presence of a limited number of electrodes and their large size with respect to the neuronal scale, makes the mean-field (*i.e.* the mean neurons membrane voltages) the only realistic measurement for DBS. In the same way, the unknown distances from the neurons to the electrodes and the unknown conductivity of nearby tissues make the contribution of each neuron to the overall recording both heterogeneous and unknown. Consequently the only measurement assumed to be available for DBS is the weighted sum of the neuron membrane voltages. Associating the real part of (2.1) to the voltage, the output of our system is therefore

$$y := \sum_{j=1}^{N} \alpha_j \mathrm{Re}(z_j), \tag{2.2}$$

which is referred to as the *mean-field* of the ensemble, where $\alpha := [\alpha_j]_{j=1,\ldots,N} \in \mathbb{R}^N_{\geq 0}$ describes the influence of each neuron on the electrode's recording. Similarly, we define $\beta := [\beta_j]_{j=1,\ldots,N} \in \mathbb{R}^N$, as the gain of the electrical input on each neuron. It is assumed to be unknown. The pair (α, β) thus defines the stimulation-registration setup. The dynamics of N coupled oscillators under mean-field feedback then reads:

$$\dot{z}_i = (\mathrm{i}\omega_i + \rho_i^2 - |z_i|^2)z_i + \sum_{j=1}^{N} \kappa_{ij}(z_j - z_i) + \beta_i \sum_{j=1}^{N} \alpha_j \mathrm{Re}(z_j), \tag{2.3}$$

for all $i = 1, \ldots, N$. Let us briefly compare the above model to existing ones. A complete review of other related works can be found in Section 1.2. In (Rosenblum and Pikovsky, 2004a; Tukhlina et al., 2007) the global dynamics of the network is modeled as a single Landau-Stuart oscillator, exploiting the fact that oscillators are synchronized. Hence that model is valid only near the synchronous state. On the contrary (2.3) is valid for both synchronized and desynchronized behaviors. In (Popovych et al., 2006b) the authors use a population approach with all-to-all coupling that makes the results valid only for large number of oscillators with an homogeneous interconnection topology. Our paper allows for general coupling topology and number of agents. Finally, we consider a real output as opposed to the complex output assumed in (Popovych et al., 2006b).

In order to simplify the analysis, we make the assumption that each oscillator evolves with constant radius.

Assumption 1. *For all $i = 1, \ldots, N$ there exists a constant $r_i > 0$ such that the solution of (2.3) satisfies $|z_i(t)| = r_i$, for all $t \geq 0$.*

This assumption is equivalent to neglecting the radius dynamics. It is commonly made in synchronization studies (Acebrón et al., 2005; Aeyels and Rogge, 2004; Jadbabaie et al., 2004; Van Hemmen and Wreszinski, 1993; Brown et al., 2003; Kuramoto, 1984; Ermentrout and Kopell, 1990), and is justified by the normal hyperbolicity of the stable limit cycle of (2.1) that let the oscillation persist under sufficiently small external perturbations (cf. *e.g.* (Hoppensteadt and Izhikevich, 1997, Chapter 4.3)). More precisely, as we rigorously show in Section A.2,

given $\rho_i > 0$, $i = 1, \ldots, N$, it is possible to find an upper bound $\delta_h(\rho) > 0$ on the coupling and feedback strength, such that, if

$$|(\kappa, \beta, \alpha)| < \delta_h, \tag{2.4}$$

where $\kappa := [\kappa_{ij}]_{ij=1,\ldots,N}$, then the oscillator radius variations around their natural radius are bounded by

$$|r(t) - \rho| < C_h |(\kappa, \beta, \alpha)|, \quad \forall t \geq 0, \tag{2.5}$$

for some positive constant $C_h = C_h(\rho)$. Thus, Assumption 1 can be verified with an arbitrary precision, provided that the coupling and the feedback gains are sufficiently small. Note that the small coupling condition (2.4) and the radius variation bound (2.5) solely depend on the natural radius ρ. In particular they are independent of the oscillator natural frequencies.
By relying on Assumption 1 we can derive the phase dynamics of (2.3). A more rigorous derivation can be found in Section A.2. By letting $z_i = r_i e^{\mathrm{i}\theta_i}$, which defines the phase $\theta_i \in T^1$ of each oscillator, we get from Assumption 1 that $\dot{z}_i = \dot{r}_i e^{\mathrm{i}\theta_i} + \mathrm{i} r_i \dot{\theta}_i e^{\mathrm{i}\theta_i} = \mathrm{i} r_i \dot{\theta}_i e^{\mathrm{i}\theta_i}$. Dividing each side of this equation by $r_i e^{\mathrm{i}\theta_i}$, and extracting the imaginary part of both sides, we get from (2.3) that

$$\dot{\theta}_i = \omega_i + \sum_{j=1}^{N} \kappa_{ij} \frac{r_j}{r_i} \sin(\theta_j - \theta_i) - \beta_i \sin(\theta_i) \sum_{j=1}^{N} \alpha_j \frac{r_j}{r_i} \cos(\theta_j).$$

We can now use the trigonometric identity $\sin\theta_i \cos\theta_j = \frac{1}{2}\sin(\theta_j + \theta_i) - \frac{1}{2}\sin(\theta_j - \theta_i)$ to derive

$$\dot{\theta}_i = \omega_i + \sum_{j=1}^{N} (k_{ij} + \gamma_{ij}) \sin(\theta_j - \theta_i) - \sum_{j=1}^{N} \gamma_{ij} \sin(\theta_j + \theta_i), \tag{2.6}$$

for all $i = 1, \ldots, N$, where

$$k = [k_{ij}]_{i,j=1,\ldots,N} := \left[\kappa_{ij} \frac{r_j}{r_i}\right]_{i,j=1,\ldots,N} \in \mathbb{R}^{N \times N} \tag{2.7}$$

is referred to as the *coupling matrix*, and

$$\gamma = [\gamma_{ij}]_{i,j=1,\ldots,N} := \left[\frac{\beta_i}{2} \frac{\alpha_j r_j}{r_i}\right]_{i,j=1,\ldots,N} \in \mathbb{R}^{N \times N} \tag{2.8}$$

defines the *feedback gain*. We also define the *modified coupling matrix*, $\Gamma \in \mathbb{R}^{N \times N}$, as

$$\Gamma := [\Gamma_{ij}]_{i,j=1,\ldots,N} = [k_{ij} + \gamma_{ij}]_{i,j=1,\ldots,N} \ . \tag{2.9}$$

Our study is based on the *incremental dynamics* of (2.6), defined, for all $i, j = 1, \ldots, N$, by

$$\dot{\theta}_i - \dot{\theta}_j = \omega_i - \omega_j - \sum_{n=1}^{N} \big(\gamma_{in} \sin(\theta_j + \theta_i) + \gamma_{jn} \sin(\theta_n + \theta_i)\big) + \sum_{n=1}^{N} \big(\Gamma_{in} \sin(\theta_n - \theta_i) - \Gamma_{jn} \sin(\theta_n - \theta_j)\big). \tag{2.10}$$

The model (2.6) appears to be new in the literature and allows, by properly choosing α, β and κ, to encompass all kinds of interconnection topologies and recording-stimulation setups. We stress that the use of a nonzero feedback gains γ breaks the T^1 (*i.e* global phase shift (Sepulchre et al., 2007, Eq. (8))) symmetry of the original Kuramoto system. As it will be clearer in the sequel, this complicates the analysis, but allows for new desynchronization and inhibition expectations.

2.3 Different types of phase-locked solutions

In this section we formally define the concept of phase-locking. From a modeling point of view, phase-locking describes the pathological STN synchronous activity. Roughly speaking, a phase-locked solution can be interpreted as a fixed point of the incremental dynamics (2.10). We distinguish solutions that exhibit collective oscillations (pathological case for DBS) from non-oscillating ones, corresponding to a neuronal inhibition.

Definition 2.1. A solution $\{\theta_i^*\}_{i=1,\dots,N}$ of (2.6) is said to be *phase-locked* if it satisfies

$$\dot{\theta}_j^*(t) - \dot{\theta}_i^*(t) = 0, \quad \forall\ i,j = 1,\dots,N,\ \forall t \geq 0. \tag{2.11}$$

A phase-locked solution is *oscillating* if, in addition, $\dot{\theta}_i^*(t) \neq 0$, for almost all $t \geq 0$ and all $i = 1,\dots,N$.

In other words, for oscillating phase-locked solutions, the discharge rhythm is the same for each neuron, which corresponds to a synchronous (pathological) activity, while in the non oscillating case the neurons are in a quiescent (non pathological) state. The above definition of phase-locking corresponds to that of "Frequency (Huygens) Synchronization" (Fradkov, 2007, Definition 5.1 and Example 5.1), which is the most widely studied in the analysis of synchronization between coupled oscillators (Kopell and Ermentrout, 2002; Scardovi et al., 2007; Chopra and Spong, 2009; Acebrón et al., 2005; Aeyels and Rogge, 2004; Jadbabaie et al., 2004; Van Hemmen and Wreszinski, 1993; Brown et al., 2003; Assisi et al., 2005; Sepulchre et al., 2007; Sarlette, 2009; Fradkov, 2007; Pikovsky et al., 2001; Dörfler and Bullo, 2011; Ko and Ermentrout, 2009). It is trivially equivalent to the existence of a matrix $\Delta := [\Delta_{ij}]_{i,j=1,\dots,N}$, such that

$$\theta_j^*(t) - \theta_i^*(t) = \Delta_{ij}, \quad \forall\ i,j = 1,\dots,N,\ \forall t \geq 0, \tag{2.12}$$

or to the existence of a measurable function $\Omega : \mathbb{R}_{\geq 0} \to \mathbb{R}$ such that, for each $i = 1,\dots,N$,

$$\theta_i^*(t) = \int_0^t \Omega(s)ds + \theta_i^*(0), \quad \forall t \geq 0, \tag{2.13}$$

where Ω is the instantaneous *collective frequency of oscillation*, that is $\dot{\theta}_i^*(t) = \Omega(t)$ for all $i = 1,\dots,N$. In case of oscillating phase-locking, $\Omega(t) \neq 0$ for almost all $t \geq 0$.

In the original Kuramoto system, *i.e.* without mean-field feedback, the oscillating and non-oscillating cases are equivalent due to the T^1 symmetry, which guarantees invariance to a common phase drift such as a nonzero mean natural frequency. More precisely, if $\nu \in \mathbb{R}$ is the synchronization frequency of a Kuramoto phase-locked solution, one can introduce a new variable $\theta_\nu(t)$, defined by $\theta_i = (\theta_\nu)_i(t) + \nu t$, for all $t \geq 0$, which corresponds to switching to a rotating reference frame. Due to the invariance of the Kuramoto system with respect to a global phase-shift, it is easy to verify that θ_ν is ruled by an autonomous dynamics and that it converges to a non-oscillating phase-locked solution. See also (Jadbabaie et al., 2004; Sepulchre et al., 2007) for the Kuramoto model and (Ermentrout, 1990) for a similar discussion in diffusively coupled complex Landau-Stuart oscillators. Conversely, the sinusoidal additive term brought by the mean-field feedback breaks the T^1 invariance, and oscillating and non-oscillating phase-locked solutions become physically and mathematically distinct objects. This distinction is crucial for the achievement of oscillation inhibition (Chapter 4) and desynchronization (Chapter 5) via mean-field feedback. In both cases indeed, the magnitude of the oscillators natural frequencies plays a fundamental role.

Example 2.1. *Consider the following system*[2] *of two oscillators:*

$$\begin{aligned}\dot{\theta}_1 &= 1+\sin(\theta_1+\theta_2)+\sin(2\theta_1)\\ \dot{\theta}_2 &= 2+2\sin(\theta_1+\theta_2)+2\sin(2\theta_2),\end{aligned}$$

that is, with the above notations, $\omega_1=1$, $\omega_2=2$, $\Gamma=0$, $\gamma_{11}=\gamma_{12}=1$, $\gamma_{21}=\gamma_{22}=2$. *For* $\theta_1(0)=\theta_2(0)=\pi/12$, *it can be seen that* $\dot{\theta}_1(t)=\dot{\theta}_2(t)=0$, *for all* $t\geq 0$. *This corresponds to a non-oscillating (inhibited) phase-locked solution.*

We note that a simple sufficient condition to avoid non-oscillating phase-locking is given by

$$\max_{i=1,\dots,N}|\omega_i| > \max_{i=1,\dots,N}\sum_{j=1,j\neq i}^{N}|k_{ij}+\gamma_{ij}| + \max_{i=1,\dots,N}\sum_{j=1}^{N}|\gamma_{ij}|,$$

meaning that at least one natural frequency is sufficiently large with respect to the coupling and feedback gain. This condition ensures that the phase dynamics (2.6) does not have fixed points.

2.4 Phase-locked solutions under mean-field feedback

2.4.1 Existence of oscillating phase-locking

We now present a general result on phase-locking under mean-field feedback.

Theorem 2.2. *For almost all natural frequencies* $\omega\in\mathbb{R}^N$, *for almost all interconnection matrices* $k\in\mathbb{R}^{N\times N}$, *and for almost all feedback gains* $\gamma\in\mathbb{R}^{N\times N}$, *system (2.6) admits no oscillating phase-locked solution.*

Theorem 2.2, whose proof can be found in Section 2.5.3, states that, for a generic neuronal interconnection, the use of a proportional mean-field feedback prevents the oscillators to all evolve at the exact same frequency. Generically, under mean-field feedback, only two situations may thus occur: either no phase-locking or no oscillations. This result therefore constitutes a promising feature of mean-field feedback DBS. We stress that the result of Theorem 2.2 is meaningful for the full dynamics (2.3) only if the small coupling condition (2.4) is satisfied, which ensures that the phase dynamics (2.6) is a good approximation of (2.3). More precisely, the result of Theorem 2.2 extend to (2.3) only if k and γ are sufficiently small, independently of the natural frequencies ω.

On the one hand, the strength of Theorem 2.2 stands in the generality of its assumptions: it holds for generic interconnections between neurons, including negative weights (inhibitory synapses), and does not require any knowledge neither on the contribution α_j of each neuron on the overall measurement nor on the intensity β_j of the stimulation on each neuron. On the other hand, the disappearance of the phase-locked states does not prevent a pathological behavior. Indeed, while Theorem 2.2 states that the perfectly synchronized behavior is not compatible with mean-field feedback, it does not exclude the possibility of some kind of "practical" phase-locking, such as solutions whose mean behavior is near to that of a phase-locked one, but with small oscillations around it. For instance, they may correspond to phase differences which, while not remaining constant, stay bounded at all time. From a medical point of view, such a behavior for the neurons in the STN would anyway lead to tremor. We address this

[2]This example was suggested by an anonymous reviewer of the CDC 2010 conference version of the result presented in this chapter. We are very thankful to him for this suggestion.

problem in Chapter 3. Moreover, as illustrated in Example 2.1, and discussed in details in Chapter 4, if the feedback gain is too large with respect to the natural frequencies, mean-field feedback may leads to non-oscillating phase-locked solution, corresponding to neuronal inhibition. Conversely, when the natural frequencies are sufficiently large there exists a range of feedback gains for which mean-field feedback can induce full desynchronization. We provide in Chapter 5 a sufficient condition to ensure full desynchronization in the Kuramoto system under mean-field feedback for a general interconnection topology and feedback setup.

Numerical simulations illustrate these features. We simulate an ensemble of N=20 coupled Landau-Stuart oscillators (2.3). Their natural radius is $\rho_i = 10$ for all $i = 1, \ldots, N$. Defining $rand_{n\times m} \subset \mathbb{R}^{n\times m}$ as the ensemble of matrices whose elements are randomly chosen on the interval $[0, 1]$ according to a uniform distribution, the interconnection matrix is chosen as $k = \frac{1}{2}K_0 R$, where $K_0 \in \mathbb{R}$ is the coupling strength and $R \in rand_{N\times N}$. In the simulation K_0 is chosen sufficiently large to yield the existence of an asymptotically stable phase-locked solution in the absence of an external stimulation. The weight of each neuron on the measured mean-field (2.2) is chosen as $\alpha = rand_{N\times 1}$. The influence of the input on each neuron (see (2.3)) is chosen as $\beta = \tilde{\beta}B$, with $B \in rand_{N\times 1}$, where $\tilde{\beta} \in \mathbb{R}$ denotes the feedback gain. This choice for α and β defines a generic and imprecise recording and stimulation setup. In order to have a heterogeneous ensemble, the natural frequencies are randomly chosen on the interval $[\omega_{min}, \omega_{min} + 3\pi]$ according to the uniform distribution, where ω_{min} is either 0.2π or 2π.
We quantify the synchronization of the system, by defining the collective radius r_∞ (Kuramoto, 1984) and the mean phase ψ of the network as

$$r_\infty(t)e^{\mathrm{i}\psi(t)} := \frac{1}{N}\sum_{i=1}^{N} e^{\mathrm{i}\theta_i(t)}, \quad \forall t \geq 0. \tag{2.14}$$

The mean-field feedback is switched on at $t = 3$.

As shown in Figure 2.4(a), for a sufficiently large negative feedback gain $\tilde{\beta} = -K_0$ and if the natural frequencies are large, *i.e.* $\omega_{min} = 2\pi$, mean-field feedback induces full-desynchronization. Indeed, by noting that $\theta_i - \theta_j = \theta_i - \psi - (\theta_j - \psi)$, for all $i, j = 1, \ldots, N$, the plot in Figure 2.4(b) shows that the phase differences between most pairs of oscillators, at the exception of small clusters (Aeyels and Rogge, 2004; Aeyels and De Smet, 2010; De Smet and Aeyels, 2009), tend to grow indefinitely and with uniformly non-zero drift, at least in average, which corresponds to a fully desynchronized behavior[3] (cf. Definitions 5.1 and 5.6 in Chapter 5). As shown in the inset of Figure 2.4(b), the disordered behavior of the collective radius r_∞ is also similar to that of an uncoupled ensemble.
Conversely, if the natural frequencies are small, *i.e.* $\omega_{min} = 0.2\pi$, the mean-field feedback blocks the oscillations, as shown in Figure 2.5(a). We stress that this type of oscillation inhibition does not correspond to an oscillator death, as the one discussed in (Ermentrout, 1990), when also the oscillation amplitude goes to zero. Indeed, as imposed by Assumption 1, and confirmed by Figure 2.5(b), in the case under analysis here only the frequency of oscillation goes to zero, while the oscillation radius remains practically unchanged during the oscillators evolution. A similar oscillation inhibition is considered in (Ermentrout and Kopell, 1990).
The system remains however practically phase-locked if a too small feedback gain $\tilde{\beta} = -0.5K_0$ is used (cf. Figure 2.6), that is the oscillators exhibit small oscillations around a perfectly phase-locked state. We stress that also in this case, as stated by Theorem 2.2, the oscillating phase-locked solution disappears as soon as we activate the mean-field feedback. Indeed, from

[3] For the sake of clarity, these plots are given with the phases evolving in $\mathbb{R}$ rather than in T^1

Definition 2.1, and Equation (2.12), if the system is phase-locked we have

$$r_\infty(t) := \left| \frac{1}{N} \sum_{i=1}^{N} e^{\mathrm{i}\theta_i(t)} \right| = \left| \frac{1}{N} e^{\mathrm{i}\theta_1(t)} \left(1 + \sum_{i=2}^{N} e^{\Delta_{i1}} \right) \right| \equiv \left| 1 + \sum_{i=2}^{N} e^{\Delta_{i1}} \right|, \tag{2.15}$$

that is r_∞ has to be constant, which is the case for neither small (Figure 2.6(b)) nor large (Figure 2.4(b)) feedback gain.

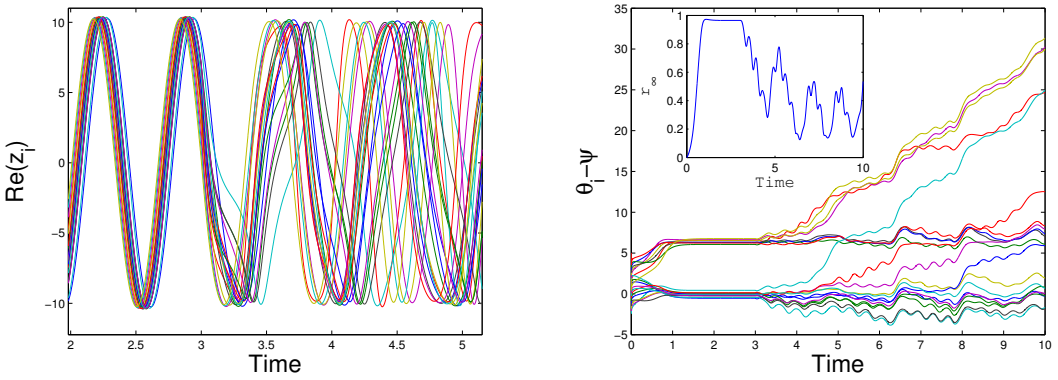

(a) (b)

FIGURE 2.4: Large feedback gain and natural frequencies: full desynchronization.

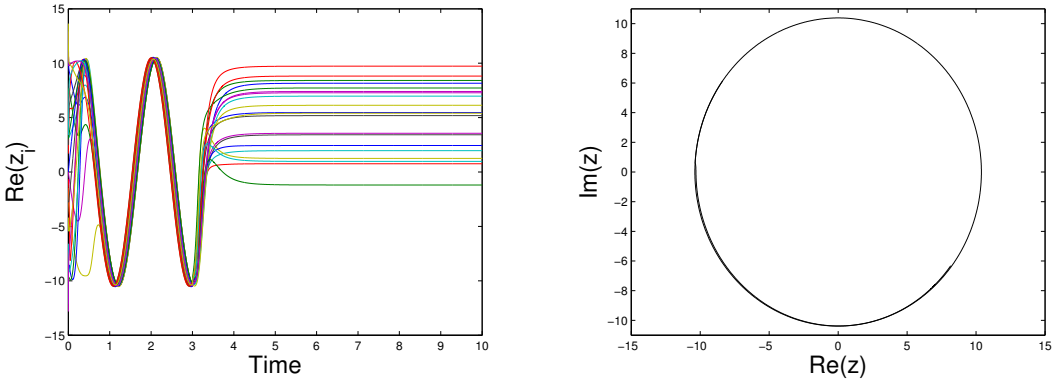

(a) (b)

FIGURE 2.5: Large feedback gain and small natural frequencies: neuronal inhibition.

2.4.2 Characterizations

The proof of Theorem 2.2 is based on two main steps, which are presented here as Lemmas 2.3 and 2.4. Their interest goes beyond the technical aspects of the proof, as they underline some intrinsic properties of the Kuramoto system under mean-field feedback, and permit to give a characterization of its phase-locked solutions in terms of an associated fixed point equation. Lemma 2.3 states that the problem of finding a phase-locked solution can be reduced to solving a set of nonlinear algebraic equations in terms of the phase differences Δ and the collective frequency of oscillation Ω. Its proof is provided in Section 2.5.1.

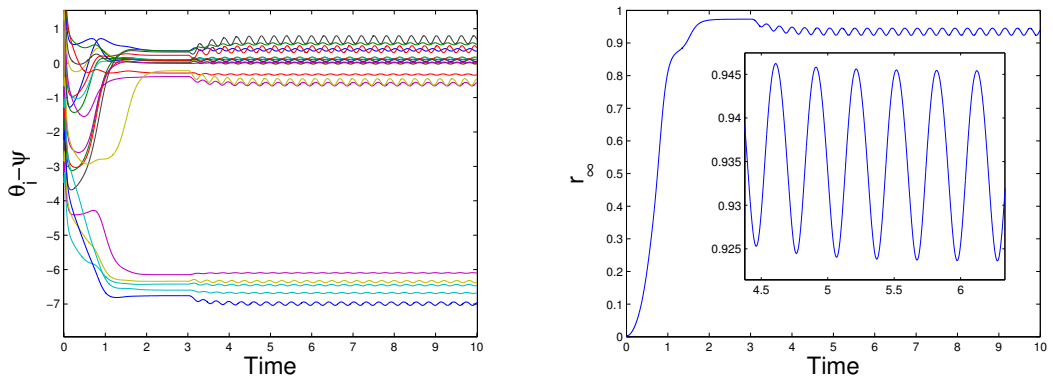

FIGURE 2.6: Small feedback gain: practical phase-locking.

Lemma 2.3. *For all initial conditions $\theta^*(0) \in T^N$, all natural frequencies $\omega \in \mathbb{R}^N$, all coupling matrices $k \in \mathbb{R}^{N\times N}$, and all feedback gains $\gamma \in \mathbb{R}^{N\times N}$, if system (2.6) admits an oscillating phase-locked solution starting in $\theta^*(0)$ with phase differences Δ and collective frequency of oscillation Ω satisfying (2.12)-(2.13), then, for all $1 \le i < j \le N$, it holds that*

$$\omega_j - \omega_i + \sum_{h=1}^{N} \left[(k_{jh} + \gamma_{jh}) \sin(\Delta_{jh}) - (k_{ih} + \gamma_{ih}) \sin(\Delta_{ih}) \right] = 0, \quad (2.16a)$$

$$\sum_{h=1}^{N} \left[\gamma_{jh} \sin\left(2\int_0^t \Omega(s)ds + \Delta_{jh} + 2\theta_j^*(0) \right) - \gamma_{ih} \sin\left(2\int_0^t \Omega(s)ds + \Delta_{ih} + 2\theta_i^*(0) \right) \right] = 0. \quad (2.16b)$$

While this fact is trivial for the Kuramoto system without inputs (*i.e.* $\gamma = 0$), its generalization to the presence of mean-field feedback is not straightforward. The first set of equations (2.16a) can be seen as the classical fixed point equation for a Kuramoto system with natural frequencies ω and coupling matrix $\Gamma = k + \gamma$. It may or may not lead to the existence of a phase-locked solution (see (Jadbabaie et al., 2004) for necessary and sufficient conditions). The second set of equations (2.16b) is linked to the action of the mean-field feedback. It trivially holds if the feedback gain γ is zero. Intuitively, we can expect that if the frequency of the collective oscillation Ω is not zero then (2.16b) admits no solution for any $\gamma \neq 0$. This fact becomes evident in the following example involving only two neurons.

Example 2.2. *For N=2,Equation (2.16b) boils down to a single condition. Consider $\omega_1 \neq \omega_2$, $\gamma_{ij} = 1$ and $k_{ij} = 2$ for all $i, j \in \{1, 2\}$. In view of (2.12), condition (2.16b) reads*

$$\sin\left(2\int_0^t \Omega(s)ds + 2\theta_2^*(0) \right) - \sin\left(2\int_0^t \Omega(s)ds + 2\theta_2^*(0) + 2\Delta_{21} \right) = 0,$$

or, by invoking the trigonometric identity $\sin a - \sin b = 2\cos\left(\frac{a+b}{2}\right)\sin\left(\frac{a-b}{2}\right)$,

$$2\cos\left(2\int_0^t \Omega(s)ds + 2\theta_2^*(0) + \Delta_{21} \right) \sin(\Delta_{12}) = 0,$$

for all $t \ge 0$. In addition, (2.12) imposes that $\Delta_{21} = -\Delta_{12}$. Consequently (2.16a) reads $\omega_1 - \omega_2 = 2\sin(\Delta_{21})$. Since $\omega_1 \neq \omega_2$, it also holds that $\Delta_{21} \notin \{0, \pi\}$. We conclude that (2.16b) admits no solution for any Ω which is not zero almost everywhere and thus, in particular, (2.6) admits no oscillating phase-locked solutions.

The second main step in the proof of Theorem 2.2 confirms that indeed, if (2.16) admits a solution (Δ, Ω), then Δ is fully determined by the "standard" part (2.16a) of this fixed point equation and is thus independent of the collective oscillation frequency Ω. In particular the following lemma states that, around almost any solution of (2.16a), the phase differences that define a phase-locked configuration Δ can be locally expressed as a smooth function of the natural frequencies ω and of the interconnection matrix Γ. The proof of this lemma, mostly relying on the implicit function theorem (Lee, 2006) and elementary measure theory (Billingsley, 1995), is provided in Section 2.5.2.

Lemma 2.4. *There exists a set $\mathcal{N} \subset \mathbb{R}^N \times \mathbb{R}^{N\times N}$, and a set $\mathcal{N}_0 \subset \mathcal{N}$ satifying $\mu(\mathcal{N}_0) = 0$, such that (2.16a) with natural frequencies $\omega^* \in \mathbb{R}^N$ and modified interconnection matrix $\Gamma^* := k^* + \gamma^* \in \mathbb{R}^{N\times N}$ admits a solution $\Delta^* \in \mathbb{R}^{N\times N}$ if and only if $(\omega^*, \Gamma^*) \in \mathcal{N}$. Moreover, for all $(\omega^*, \Gamma^*) \in \mathcal{N} \setminus \mathcal{N}_0$, there exists a neighborhood U of (ω^*, Γ^*), a neighborhood W of Δ^*, and a smooth function $f : U \to W$, such that, for all $(\omega, \Gamma) \in U$, $\big(\omega,\ \Gamma,\ \Delta := f(\omega, \Gamma)\big)$ is the unique solution of (2.16a) in $U \times W$.*

In other words, Lemma 2.4 states that the standard, *i.e.* without mean-field feedback, Kuramoto fixed point equation (Aeyels and Rogge, 2004; Jadbabaie et al., 2004) is invertible for a generic choice of natural frequencies and interconnection topology.

We close this section by stressing a limitation of Theorem 2.2, due to its generic nature. Some particular configurations may indeed allow for phase-locking even under a mean-field feedback stimulation. The following counter-example illustrates this fact, by showing that all-to-all homogeneous interconnections preserves phase-locking under mean-field feedback if all the neurons have the same natural frequencies. We stress that the heterogeneity of neurons and the complexity in their coupling make this example irrelevant for practical neural modeling.

Example 2.3. (Oscillating phase-locking despite mean-field feedback) *Consider the system (2.6) with $\omega_i = \omega_j$, $k_{ij} = k$ and $\gamma_{ij} = \gamma \neq -k$ for all $i, j = 1, \dots, N$. This choice corresponds to the all-to-all coupling of identical Kuramoto oscillators, and is well studied in the literature, cf. e.g. (Kuramoto, 1984; Sepulchre et al., 2007; Aeyels and Rogge, 2004; Sarlette, 2009; Brown et al., 2003). The system of equations (2.16a) then reads, for all $1 \leq 1 < j \leq N$,*

$$\sum_{h=1}^{N} (k+\gamma)\Big(\sin(\Delta_{jh}) - \sin(\Delta_{ih})\Big) = 0.$$

A solution to this equation is $\Delta_{ij} = 0$ for all $1 \leq 1 < j \leq N$. In view of (2.12), this is equivalent to the existence of $\theta_0 \in T^1$ such that $\theta_i^*(0) = \theta_0$, for all $i = 1, \dots, N$. The system of equations (2.16b) then reads

$$\gamma \sum_{h=1}^{N} \left[\sin\left(2\int_0^t \Omega(s)ds + \theta_0\right) - \sin\left(2\int_0^t \Omega(s)ds + \theta_0)\right)\right] = 0,$$

which is trivially satisfied for any collective frequency of oscillation Ω. Lemma 2.4 thus ensures that oscillating phase-locking is preserved despite the mean-field stimulation.

2.5 Main proofs

2.5.1 Proof of Lemma 2.3

From (2.12)-(2.13), phase-locked solutions of (2.6) satisfy, for all $t \geq 0$ and all $i, j = 1, \ldots, N$,

$$\begin{aligned} \theta_j^*(t) + \theta_i^*(t) &= \theta_j^*(t) - \theta_i^*(t) + 2\theta_i^*(t) \\ &= 2\Lambda_\Omega(t) + \Delta_{ij} + 2\theta_i^*(0), \end{aligned} \tag{2.17}$$

where $\Lambda_\Omega(t) := \int_0^t \Omega(s)ds$, for all $t \geq 0$. In view of (2.10), (2.12)-(2.13), and noting that the fixed point equation equation is trivial if $i = j$ and that, due to the antisymmetric dependence of (2.16) on i and j, finding a solution for some $i = i^*$ and $j = j^*$ gives a solution also for $i = j^*$ and $j = i^*$, finding a phase-locked solution is equivalent to solving the set of equations

$$\omega_j - \omega_i + \sum_{h=1}^{N} \left[(k_{jh} + \gamma_{jh}) \sin(\Delta_{jh}) - (k_{ih} + \gamma_{ih}) \sin(\Delta_{ih}) \right]$$

$$- \sum_{h=1}^{N} \left[\gamma_{jh} \sin\left(2\Lambda_\Omega(t) + \Delta_{jh} + 2\theta_j^*(0)\right) - \gamma_{ih} \sin\left(2\Lambda_\Omega(t) + \Delta_{ih} + 2\theta_i^*(0)\right) \right] = 0. \tag{2.18}$$

for all $t \geq 0$ and all $1 \leq i < j \leq N$, in terms of Δ and Ω. Note that the first line of the last equation is constant, that is there exist constants $\{c_{ij}\}_{i,j=1,\ldots,N,i<j}$ such that

$$\omega_j - \omega_i + \sum_{h=1}^{N} \left[(k_{jh} + \gamma_{jh}) \sin(\Delta_{jh}) - (k_{ih} + \gamma_{ih}) \sin(\Delta_{ih}) \right] = c_{ij}. \tag{2.19}$$

Equation (2.18) then reads

$$\sum_{h=1}^{N} \left[\gamma_{jh} \sin\left(2\Lambda_\Omega(t) + \Delta_{jh} + 2\theta_j^*(0)\right) - \gamma_{ih} \sin\left(2\Lambda_\Omega(t) + \Delta_{ih} + 2\theta_i^*(0)\right) \right] = c_{ij}, \tag{2.20}$$

for all $t \geq 0$ and all $1 \leq i < j \leq N$. Hence, if a phase-locked solution exists, then there must exist a solution to the set of equations (2.19) and (2.20) in terms of Δ, Ω and $c := \{c_{ij}\}_{i,j=1,\ldots,N,i<j}$. By time-differentiating (2.20), one gets, for all $t \geq 0$ and all $1 \leq i < j \leq N$,

$$2\Omega(t) \sum_{h=1}^{N} \left[\gamma_{jh} \cos\left(2\Lambda_\Omega(t) + \Delta_{jh} + 2\theta_j^*(0)\right) - \gamma_{ih} \cos\left(2\Lambda_\Omega(t) + \Delta_{ih} + 2\theta_i^*(0)\right) \right] = 0. \tag{2.21}$$

Since Ω is a non identically zero continuous function, there exists an open interval $(\underline{t}, \bar{t})$, $0 \leq \underline{t} < \bar{t}$, such that $\Omega(t) \neq 0$ for all $t \in (\underline{t}, \bar{t})$. Hence (2.21) implies that

$$\sum_{h=1}^{N} \left[\gamma_{jh} \cos\left(2\Lambda_\Omega(t) + \Delta_{jh} + 2\theta_j^*(0)\right) - \gamma_{ih} \cos\left(2\Lambda_\Omega(t) + \Delta_{ih} + 2\theta_i^*(0)\right) \right] = 0, \tag{2.22}$$

for all $t \in (\underline{t}, \bar{t})$. By differentiating (2.22) with respect to time and considering once again that $\Omega(t) \neq 0$ for all $t \in (\underline{t}, \bar{t})$, one gets that (2.20) holds true for all $t \in (\underline{t}, \bar{t})$, and for all $1 \leq i < j \leq N$. c_{ij} being a constant this implies that, for all $t \geq 0$, $c_{ij} = 0$, for all $1 \leq i < j \leq N$. □

2.5.2 Proof of Lemma 2.4

For notational purposes, define $y_i := \Delta_{iN}$, $i = 1, \dots, N-1$, and $y := [y_i]_{i=1,\dots,N-1}$. Since it holds that $\Delta_{mn} = y_n - y_m$, for all $m, n = 1, \dots, N$, we can express all the phase differences in (2.16a) in terms of the components of y. Analogously, since $\dot{\theta}_n - \dot{\theta}_m = \dot{\theta}_n - \dot{\theta}_N - (\dot{\theta}_m - \dot{\theta}_N)$, it suffices to find a solution to the set of equation in (2.16a), relative to the pairs of index (i, N), $i = 1, \dots, N-1$. For the vectors y, we use the suffix * when it refers to Δ^*. Define, for $i = 1, \dots, N-1$,

$$F_i(\omega, \Gamma, y) := \omega_N - \omega_i - \sum_{h=1}^{N-1} \left[\Gamma_{ih} \sin(y_h - y_i) - \Gamma_{Nh} \sin y_h\right] - \Gamma_{iN} \sin y_i. \tag{2.23}$$

With this notation, the equations in (2.16a) relative to the pairs of index (i, N), $i = 1, \dots, N-1$, can be written as

$$F(\omega, \Gamma, y) = 0. \tag{2.24}$$

In order to solve (2.24)in the form $y = f(\Gamma, \omega)$ through the implicit function theorem , we have to show that the matrix

$$J(\Gamma, y) := \left[\frac{\partial F_i}{\partial y_j}(\Gamma, y)\right]_{i,j=1,\dots,N-1}, \tag{2.25}$$

has full rank on the solutions of (2.24). Define, for $y \in \mathbb{R}^{N-1}$,

$$S(y) := \{\Gamma \in \mathbb{R}^{N \times N} : \text{ det } J(\Gamma, y) = 0\}. \tag{2.26}$$

Since det $J(\Gamma, y)$ is a non-identically zero analytical function (for example it is non-zero for $y = 0$ and $\Gamma_{ij} = 1$, for all $i, j = 1, \dots, N$), it is zero only on sets of zero measure (Krantz and Parks, 2002, Chapter 4). In particular $\mu(S(y)) = 0$, for all $y \in \mathbb{R}^{N-1}$. Let the sets $\mathcal{N}$ and $\mathcal{N}_0$ be defined as

$$\mathcal{N} := \left\{(\omega, \Gamma) \in \mathbb{R}^N \times \mathbb{R}^{N \times N} : \ \exists y \in \mathbb{R}^{N-1} : F(\omega, \Gamma, y) = 0\right\} \tag{2.27}$$

and

$$\mathcal{N}_0 := \left\{(\omega, \Gamma) \in \mathbb{R}^N \times \mathbb{R}^{N \times N} \ \exists y \in \mathbb{R}^{N-1} : F(\omega, \Gamma, y) = 0, \Gamma \in S(y)\right\}, \tag{2.28}$$

that is $\mathcal{N}$ contains all the natural frequencies and modified interconnection matrices that admit a solution to (2.16a), and $\mathcal{N}_0$ all the natural frequencies and modified interconnection matrices that admit a solution to (2.16a) such that (2.25) is singular. The next claim, proved in Section 2.6.1, shows that $\mathcal{N}_0$ is of zero Lebesgue measure.

Claim 2.5. Let $\mathcal{N}_0$ be defined as in (2.28). Then $\mu(\mathcal{N}_0) = 0$.

The lemma then follows directly from the implicit function theorem. Indeed, given any point $(\omega^*, \Gamma^*) \in \mathcal{N} \setminus \mathcal{N}_0$, since $\Gamma^* \notin S(y^*)$, the matrix $J(\Gamma^*, y^*)$, defined in (2.25), is invertible, and the existence of the neighborhoods U and W, and of the function f with the properties of the statement of the lemma follows directly from the implicit function theorem (Lee, 2006, Theorem 7.9). □

2.5.3 Proof of Theorem 2.2

The proof consists in explicitly constructing a zero Lebesgue measure set of natural frequencies and coupling and feedback gains, out of which the system of equations (2.16) admits no solutions. The theorem then follows from Lemma 2.3.

Since the interconnection matrix k, the modified interconnection matrix Γ, and the feedback gain γ are linked by the linear relation $k = \Gamma - \gamma$, we can independently fix Γ and γ, and set k accordingly. For all $\omega \in \mathbb{R}$, let

$$\mathcal{M}_0(\omega) := \{\Gamma \in \mathbb{R}^{N\times N} : \ (\omega, \Gamma) \in \mathcal{N}_0\} \tag{2.29}$$

where $\mathcal{N}_0 \subset \mathbb{R}^N \times \mathbb{R}^{N\times N}$ is defined in the statement of Lemma 2.4 and has zero Lebesgue measure. Let

$$\mathcal{S}_0 := \{\omega \in \mathbb{R}^N : \ \mu(\mathcal{M}_0(\omega)) > 0\}. \tag{2.30}$$

If $\mu(\mathcal{S}_0) > 0$, then $\mu(\mathcal{N}_0) = \int_{\mathcal{S}_0} \mu(\mathcal{M}_0(\omega))d\omega > 0$, which contradicts Lemma 2.4. Hence $\mu(\mathcal{S}_0) = 0$.
Consider any $\omega \in \mathbb{R}^N \setminus \mathcal{S}_0$ and any $\Gamma \in \mathbb{R}^{N\times N} \setminus \mathcal{M}_0(\omega)$. In view of what precedes, this constitutes a generic choice or ω and Γ and it holds that $(\omega, \Gamma) \notin \mathcal{N}_0$. Suppose that there exists an oscillating phase-locked solution starting in $\theta^*(0)$, with phase differences Δ and collective frequency of oscillation Ω. From Lemma 2.3, a necessary condition for the existence of an oscillating phase locked solution θ^* is that (ω, Γ, Δ) is a solution of (2.16a). From Lemma 2.4, $(\omega, \Gamma) \in \mathcal{N}$. Since $(\omega, \Gamma) \in \mathcal{N} \setminus \mathcal{N}_0$, Lemma 2.4 guarantees that the phase differences Δ of θ^* can locally be uniquely expressed in the form $\Delta = f(\omega, \Gamma)$, for some smooth function $f : \mathbb{R}^N \times \mathbb{R}^{N\times N} \to \mathbb{R}^{N\times N}$. In particular Δ does not depend on the feedback gain γ. Consider now the line of (2.16b) relative to the pair of indices $(1, 2)$:

$$\sum_{i=1}^{N} \left[\gamma_{1i} \sin(\Lambda_\Omega(t) + \Delta_{1i} + 2\theta_1^*(0)) - \gamma_{2i} \sin(\Lambda_\Omega(t) + \Delta_{2i} + 2\theta_2^*(0))\right] = 0, \ \forall t \geq 0, \tag{2.31}$$

where $\Lambda_\Omega(t) := 2\int_0^t \Omega(s)ds$, for all $t \geq 0$. Using the identity $\sin(a + b) = \sin a \cos b + \cos a \sin b$ and defining

$$\begin{aligned} \Sigma_1 &:= \sum_{i=1}^{N} \gamma_{1i} \cos(\Delta_{1i} + 2\theta_1^*(0)) - \gamma_{2i} \cos(\Delta_{2i} + 2\theta_2^*(0)) \\ \Sigma_2 &:= \sum_{i=1}^{N} \gamma_{1i} \sin(\Delta_{1i} + 2\theta_1^*(0)) - \gamma_{2i} \sin(\Delta_{2i} + 2\theta_2^*(0)), \end{aligned}$$

Equation (2.31) reads $\Sigma_1 \sin \Lambda_\Omega(t) - \Sigma_2 \cos \Lambda_\Omega(t) = 0$. Since $\sin \Lambda_\Omega(0) = 0$ and $\cos \Lambda_\Omega(0) = 1$, Σ_2 has to be zero. Moreover, since the phase-locked solution θ^* is oscillating, there exists $t > 0$ such that $\sin \Lambda_\Omega(t) \neq 0$. Hence, $\Sigma_1 = 0$ as well. Define $b_1, b_2 \in \mathbb{R}^{2N}$ as

$$\begin{aligned} b_1(\Delta) : &= \left[[\cos(\Delta_{1i} + 2\theta_1^*(0))]_{i=1,\dots,N}^T, \ -[\cos(\Delta_{2i} + 2\theta_2^*(0))]_{i=1,\dots,N}^T\right]^T, \\ b_2(\Delta) : &= \left[[\sin(\Delta_{1i} + 2\theta_1^*(0))]_{i=1,\dots,N}^T, \ -[\sin(\Delta_{2i} + 2\theta_2^*(0))]_{i=1,\dots,N}^T\right]^T. \end{aligned}$$

Note that b_1 and b_2 depend only on $\Delta = f(\omega, \Gamma)$ and on the initial conditions. They do not depend on γ. Hence, by defining $\tilde{\gamma} := \left([\gamma_{2i}]_{i=1,\dots,N}^T, [\gamma_{1i}]_{i=1,\dots,N}^T\right)^T \in \mathbb{R}^{2N}$, the condition $\Sigma_1 = \Sigma_2 = 0$ can be re-written as $\tilde{\gamma}^T b_1 = \tilde{\gamma}^T b_2 = 0$ or, equivalently,

$$\tilde{\gamma} \in b_1(f(\omega, \Gamma))^\perp \cap b_2(f(\omega, \Gamma))^\perp. \tag{2.32}$$

Let

$$\mathcal{L}_0(\omega, \Gamma) := b_1(f(\omega, \Gamma))^\perp \cap b_2(f(\omega, \Gamma))^\perp \subset \mathbb{R}^{2N}. \tag{2.33}$$

Noticing that b_1, b_2 can not be both zero, $\mu(\mathcal{L}_0(\omega, \Gamma)) = 0$ for all $\omega, \Gamma \in \mathbb{R} \times \mathbb{R}^{N\times N}$. Recalling (2.32), for all $\omega \in \mathbb{R}^N \setminus \mathcal{S}_0$, for all $\Gamma \in \mathbb{R}^{N\times N} \setminus \mathcal{M}_0(\omega)$, and for all $\gamma \in \mathbb{R}^{N\times N} \setminus \mathcal{L}_0(\omega, \Gamma)$,

system (2.6) admits no oscillating phase-locked solution, where $\mathcal{M}_0, \mathcal{S}_0$, and $\mathcal{L}_0$ are defined in (2.29),(2.30), and (2.33), respectively, and are all of zero Lebesgue measure. The theorem is proved by noticing that, given $\omega \in \mathbb{R} \setminus \mathcal{S}_0$, for any $\Gamma \in \mathbb{R}^{N\times N} \setminus \mathcal{M}_0(\omega)$, the set $\{\gamma \in \mathbb{R}^{N\times N} : \gamma = \Gamma - k,\ k \in \mathbb{R}^{N\times N}\} = \mathbb{R}^{N\times N}$, that is, given any $\Gamma \in \mathbb{R}^{N\times N} \setminus \mathcal{M}_0(\omega)$, $\gamma \notin \mathcal{L}_0(\omega, \Gamma)$ for almost all k. □

2.6 Technical proofs

2.6.1 Proof of Claim 2.5

We start by introducing the notation that will be used along the proof. The two sets $\mathcal{E}$ and $\mathcal{G}$ are defined as follows $\mathcal{E} := \mathbb{R}^{N\times N} \times \mathbb{R}^{N-1}$ and $\mathcal{G} := \mathbb{R}^{N-1} \times \mathbb{R}^{N\times N}$. We recall that, if $A \subset \mathbb{R}^n$, $\mu(A)$ denotes the Lebesgue measure of A in $\mathbb{R}^n$.

Given $\omega \in \mathbb{R}^N$, let $\hat{\omega}_i := \omega_i - \omega_N$, $i = 1, \dots, N-1$, and

$$\hat{\omega} := [\hat{\omega}_i]_{i=1,\dots,N-1}. \tag{2.34}$$

The set $\mathcal{N}$ and $\mathcal{N}_0$, defined, respectively, in (2.27) and (2.28), can be characterized in terms of $\hat{\omega}$ as follows. Let, for all $\omega \in \mathbb{R}^N$, all $\Gamma \in \mathbb{R}^{N\times N}$, and all $y \in \mathbb{R}^{N-1}$,

$$\hat{F}_i(\hat{\omega}_i, \Gamma, y) \ := \ \sum_{h=1}^{N-1} [\Gamma_{ih} \sin(y_h - y_i) - \Gamma_{Nh} \sin y_h] - \sin y_i - \hat{\omega}_i, \quad i = 1, \dots, N-1,$$

and define

$$\hat{F}(\hat{\omega}, \Gamma, y) := \left[\hat{F}_i(\hat{\omega}, \Gamma, y)\right]_{i=1,\dots,N}. \tag{2.35}$$

Moreover, let the set of all pairs $(\hat{\omega}, \Gamma)$ that admit a solution y to $\hat{F}(\hat{\omega}, \Gamma, y) = 0$ be denoted as

$$\Sigma := \{(\hat{\omega}, \Gamma) \in \mathcal{G} : \ \exists y \in \mathbb{R}^{N-1} : \ \hat{F}(\hat{\omega}, \Gamma, y) = 0\}, \tag{2.36}$$

and let the subset $\Sigma_0 \subset \Sigma$ be defined as

$$\Sigma_0 := \{(\hat{\omega}, \Gamma) \in \mathcal{G} : \ \exists y \in \mathbb{R}^{N-1} : \hat{F}(\hat{\omega}, \Gamma, y) = 0, \ \Gamma \in S(y)\}, \tag{2.37}$$

where, for each $y \in \mathbb{R}^{N-1}$, the set $S(y)$ is defined in (2.26). We are going to show that the sets Σ and Σ_0 completely characterize, respectively, the sets $\mathcal{N}$ and $\mathcal{N}_0$.

STEP 1:We claim that *the set $\mathcal{N}$ and $\mathcal{N}_0$, defined, respectively, by (2.27) and (2.28), are the images of, respectively, $\Sigma \times \mathbb{R}$ and $\Sigma_0 \times \mathbb{R}$ by a linear map of determinant 1. In particular, if $\mu(\Sigma_0) = 0$, then $\mu(\mathcal{N}_0) = 0$.*

Given $\hat{\omega} \in \mathbb{R}^{N-1}$, let

$$I_{\hat{\omega}} := \{\omega \in \mathbb{R}^N : \omega_i = \hat{\omega}_i + \omega_N.\ i = 1, \dots, N-1, \omega_N \in \mathbb{R}\}. \tag{2.38}$$

Let the linear map $M : \mathbb{R}^N \to \mathbb{R}^N$ be defined as

$$Mx := \left[I_N - \begin{bmatrix} 1_{N-1} \\ 0 \end{bmatrix} [0, \dots, 0, 1]\right] x, \quad \forall x \in \mathbb{R}^N.$$

Note that M has determinant 1. The set $\hat{\omega} \times \mathbb{R}$ is the image of the set $I_{\hat{\omega}}$ through the linear invertible map M, that is

$$\hat{\omega} \times \mathbb{R} = M(I_{\hat{\omega}}). \tag{2.39}$$

By definitions (2.23),(2.34),(2.35),(2.38), it follows that $\hat{F}(\hat{\omega}, \Gamma, y) = F(\omega, \Gamma, y)$, for all $\omega \in I_{\hat{\omega}}$. Hence,

$$F(\omega, \Gamma, y) = 0 \;\Rightarrow\; \hat{F}(\hat{\omega}, \Gamma, y) = 0, \tag{2.40}$$

and

$$\hat{F}(\hat{\omega}, \Gamma, y) = 0 \;\Rightarrow\; F(\omega, \Gamma, y) = 0, \; \forall \omega \in I_{\hat{\omega}}. \tag{2.41}$$

Relation (2.41) implies that, if $\hat{\omega} \in \Sigma$, then $I_{\hat{\omega}} \subset \mathcal{N}$. Since, from (2.39), $I_{\hat{\omega}} = M^{-1}(\hat{\omega} \times \mathbb{R})$ this also implies that, for all $\hat{\omega} \in \Sigma$, $M^{-1}(\hat{\omega} \times \mathbb{R}) \subset \mathcal{N}$, which shows that

$$M^{-1}(\Sigma \times \mathbb{R}) \subset \mathcal{N}.$$

The converse inclusion follows by noticing that, given $\omega \in \mathcal{N}$, (2.40) implies that $\hat{\omega} \in \Sigma$. It follows that, given $\omega \in \mathcal{N}$, $\hat{\omega} \times \mathbb{R} \subset \Sigma \times \mathbb{R}$, that is, from (2.39), $M(I_{\hat{\omega}}) \subset \Sigma \times \mathbb{R}$. Since, by construction, $\omega \in I_{\hat{\omega}}$, we conclude that, for all $\omega \in \mathcal{N}$, $M(\omega) \in \Sigma \times \mathbb{R}$, that is

$$M(\mathcal{N}) \subset \Sigma \times \mathbb{R},$$

which shows the first part of STEP 1 for $\mathcal{N}$. The statement for $\mathcal{N}_0$ follows similarly.

To show that $\mu(\mathcal{N}_0) = 0$ whenever $\mu(\Sigma_0) = 0$, recall that the Lebesgue measure is invariant under linear maps of determinant 1 and note that, given a collection of open intervals $\{I_i\}_{i \in \mathbb{N}}$, such that $\bigcup_{i \in \mathbb{N}} I_i = \mathbb{R}$, $\Sigma_0 \times \mathbb{R}$ can be written as the countable union $\Sigma_0 \times \mathbb{R} = \bigcup_{i \in \mathbb{N}} \Sigma_0 \times I_i$. Thus, since, for all $i \in \mathbb{N}$, $\mu(\Sigma_0 \times I_i) = \mu(\Sigma_0)\mu(I_i)$ (see for instance (Billingsley, 1995, Section 12)), if $\mu(\Sigma_0) = 0$, then $\mu(\Sigma_0 \times I_i) = 0$, for all $i \in \mathbb{N}$. That is, if $\mu(\Sigma_0) = 0$, then $\mathcal{N}_0$ is the image through an invertible linear map of the union of a countable collection of sets of zero Lebesgue measure, and, hence, of zero Lebesgue measure, which shows STEP 1.

Before introducing the second step of the proof we need the following notation. Let $\mathcal{E}_0$ be the set of matrices Γ and phase-differences y such that the Jacobian of F is singular, that is

$$\mathcal{E}_0 := \{(\Gamma, y) \in \mathcal{E} : \; \Gamma \in S(y)\}, \tag{2.42}$$

where, for all $y \in \mathbb{R}^{N-1}$, the set $S(y)$ is defined in (2.26).

Let $\mathcal{F}$, be the set of triplet $(\hat{\omega}, \Gamma, y)$ that are solution to $F = 0$, that is

$$\mathcal{F} := \{(\hat{\omega}, \Gamma, y) \in \mathcal{G} \times \mathbb{R}^{N-1} : \; \hat{F}(\hat{\omega}, \Gamma, y) = 0\}, \tag{2.43}$$

and $\mathcal{F}_0$ the set of triplet $(\hat{\omega}, \Gamma, y)$ that are solution to $F = 0$, and, moreover, such that the Jacobian of F is singular, that is

$$\mathcal{F}_0 := \{(\hat{\omega}, \Gamma, y) \in \mathcal{G} \times \mathbb{R}^{N-1} : \hat{F}(\hat{\omega}, \Gamma, y) = 0, \Gamma \in S(y)\}, \tag{2.44}$$

The next step shows that Σ is the image of $\mathcal{E}$ through a smooth mapping T, and that Σ_0 is the image of $\mathcal{E}_0$ through T. This will allow to study the measure of Σ_0 as a function of the measure of $\mathcal{E}_0$.

STEP 2: *There exists a smooth map $T : \mathcal{E} \to \mathcal{G}$, such that $\Sigma = T(\mathcal{E})$, and $\Sigma_0 = T(\mathcal{E}_0)$.*
Consider the set $\mathcal{F}$ defined in (2.43). Since $\frac{\partial \hat{F}_i}{\partial \hat{\omega}_j} = \delta_{ij}$, where δ_{ij} denotes the Kroenecker symbol, it follows from (Lee, 2006, Theorem 8.8) that $\mathcal{F}$ is an embedded submanifold of codimension

$N-1$. In particular $\mathcal{F}$ can be described as the graph of the smooth function

$$g := -F(0,\cdot,\cdot) : \mathcal{E} \to \mathbb{R}^{N-1},$$

as

$$\mathcal{F} = \{(\hat{\omega}, \Gamma, y) \in \mathcal{G} \times \mathbb{R}^{N-1} : \ \hat{\omega} = g(\Gamma, y)\}.$$

Similarly $\mathcal{F}_0 = \{(\hat{\omega}, \Gamma, y) \in \mathcal{G} \times \mathbb{R}^{N-1} : \ (\Gamma, y) \in \mathcal{E}_0, \ \hat{\omega} = g(\Gamma, y)\}$. Hence, the point of $\mathcal{F}$ are the image of the point of $\mathcal{E}$ through the smooth mapping (*lift*) $L : \mathcal{E} \to \mathcal{G} \times \mathcal{R}^{N-1}$, defined by

$$L(\Gamma, y) := (g(\Gamma, y), \Gamma, y).$$

Moreover, it follows directly from the definition of Σ that $\Sigma = P_{\mathcal{G}}\mathcal{F}$ and $\Sigma_0 = P_{\mathcal{G}}\mathcal{F}_0$, where $P_{\mathcal{G}}$ is the projection of $\mathcal{G} \times \mathbb{R}^{N-1}$ on $\mathcal{G}$, defined by $P_{\mathcal{G}}(\hat{\omega}, \Gamma, y) = (\hat{\omega}, \Gamma)$.
Hence, by defining $T := P_{\mathcal{G}} \circ L : \mathcal{E} \to \mathcal{G}$, as

$$T(\Gamma, y) = (g(\Gamma, y), \ \Gamma), \ \forall (\Gamma, y) \in \mathcal{E}$$

(see also fig. 2.7), we conclude that, $\Sigma = T(\mathcal{E})$, and $\Sigma_0 = T(\mathcal{E}_0)$.

STEP 3: *The Lebesgue measure of* Σ_0 *is zero.*
Since $\mathcal{E}_0$ is given by the zeros of an analytic function, $\mu(\mathcal{E}_0) = 0$. Since Σ_0 is the image through a smooth map $T : \mathcal{E} \to \mathcal{G}$ of a set of zero measure (cf. STEP 2), Σ_0 has zero measure (Lee, 2006, Lemma 10.2).

The statement of the claim follows directly from STEP 1 and STEP 3 □

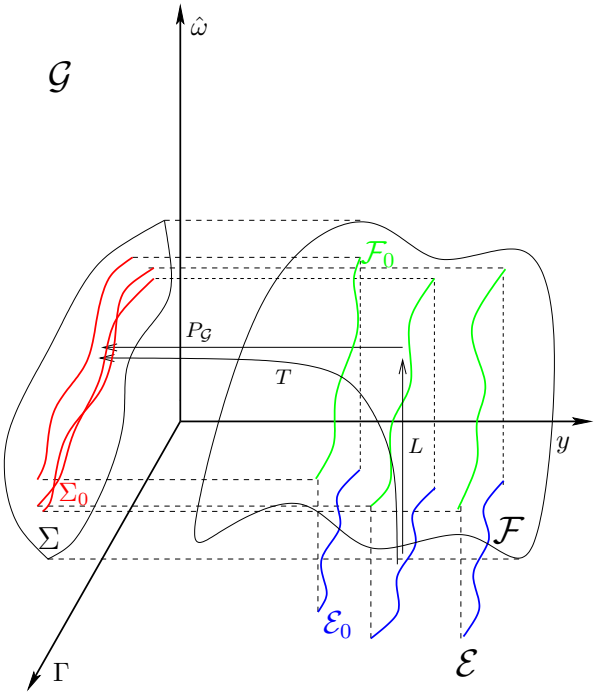

FIGURE 2.7: Construction of the smooth map $T : \mathcal{E} \to \mathcal{G}$.

Chapter 3

Phase-locking robustness and necessary conditions for desynchronization

The main result of Chapter 2 ensures the disappearance of the perfectly phase-locked states under mean-field feedback. This makes closed-loop DBS promising from a therapeutic point of view. However, for small feedback gains, the numerical observations reported in Figure 3.1 (see also Section 2.4.1) highlights the persistence of nearly phase-locked states. Even though not phase-locked, these solutions are not yet desynchronized either. In particular, they are associated to a neuronal ensemble approximately discharging action potential in a synchronous, and thus still pathological, manner.

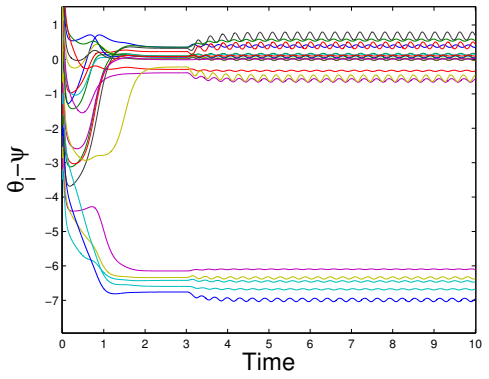

FIGURE 3.1: Practical phase-locking in Equation (2.3).

The evidence of this "practical" phase-locking imposes to compute necessary conditions on the feedback gain which would assure effective desynchronization. This leads us to a robustness analysis of phase-locked solutions in an oscillators population with respect to general time-varying inputs, thus including mean-field feedback as a special case. For this analysis, we rely on the phase model derived in Section 2.2. In the absence of mean-field feedback, this model reduces to the standard Kuramoto system (Kuramoto, 1984).

The robustness of phase-locking in the Kuramoto model has already been partially addressed in the literature both in the case of infinite and finite number of oscillators. On the one hand, the infinite dimensional Kuramoto model allows for an easier analytical treatment of the robustness analysis (see for example (Acebrón et al., 2005) for a complete survey). This

approach has been used to analyze the effect of delayed (Hauptmann et al., 2005a) and multisite (Pyragas et al., 2008) mean-field feedback approaches to desynchronization. In the case of stochastic inputs it allows to find the minimum coupling to guarantee phase-locking in the presence of noise (Daniels, 2005). However, this approach is feasible only in the case of the all-to-all interconnection. On the other hand, the finite dimensional case has been the object of both analytical and numerical studies. In particular, (Cumin and Unsworth, 2007) proposes a complete numerical analysis of robustness to time-varying natural frequencies, time-varying interconnection topologies, and non-sinusoidal coupling. It suggests that phase-locking exhibits some robustness to all these types of perturbations. Analytical studies on the robustness of phase-locking in the finite Kuramoto model have been addressed only for constant natural frequencies (Jadbabaie et al., 2004; Chopra and Spong, 2009; Dörfler and Bullo, 2011). The existence and explicit expression of the fixed points describing stable and unstable phase-locked states is studied in (Aeyels and Rogge, 2004). The Lyapunov approach proposed in (Van Hemmen and Wreszinski, 1993) for an all-to-all coupling suggests that an analytical study of phase-locking robustness can be deepened. To the best of our knowledge the problem of the robustness of phase-locking with respect to time-varying natural frequencies has still not been analytically addressed in the finite Kuramoto model with arbitrary bidirectional interconnection topologies.

In this chapter we establish (Theorem 3.4) that phase-locking is locally input-to-state stable (ISS) with respect to small inputs (Sontag, 1989, 2006a), a property also referred to as total stability (Malkin, 1958). Roughly speaking, a system is ISS if its origin is globally asymptotically stable when no inputs are applied, and the steady-state error in presence of inputs is somewhat proportional to their magnitude. Total stability, or local ISS, imposes this behavior only for small initial conditions and inputs magnitude. The proof of this result, provided in Section 3.6.3, is based on the existence of a local ISS-Lyapunov function for the incremental dynamics of the system. This analysis provides a general methodology to build explicit estimates on the size of the region of convergence, the ISS gain, and the tolerated input bound. It applies to general symmetric interconnection topologies and to any asymptotically stable phase-locked state. In practice, these bounds, together with an approximate knowledge of the interconnection topology between the oscillators and their natural frequencies' distribution, can be used to compute the necessary minimum value of the gain of the mean-field feedback to desynchronize the ensemble (Corollary 3.6). As an illustrative application of the main theorem, we extend in Proposition 3.5 some recent results in (Chopra and Spong, 2009; Dörfler and Bullo, 2011) to the time-varying case. We prove, in particular, the exponential ISS of synchronization in the all-to-all Kuramoto system when all the initial phase differences lie in the interval $[-\frac{\pi}{2}, \frac{\pi}{2}]$, and we give explicit bounds on the convergence rate and the tolerated disturbances magnitude. The size of the region of convergence, the sufficient bound on the coupling strength and the convergence rate are compared to those obtained in (Chopra and Spong, 2009; Dörfler and Bullo, 2011). Furthermore, the Lyapunov function for the incremental dynamics allows for a new characterization of the phase-locked states of the unperturbed system. In particular, when restricted to a suitable invariant manifold, it allows to completely characterize the robust phase-locked states in terms of its isolated local minima, as discussed in Section 3.5 through Lemmas 3.7 and 3.8.

The chapter is structured as follows. In Section 3.1 we extend the simplified neurons population model (2.6) introduced in Chapter 2 in order to include exogenous time-varying inputs. In Section 3.2 we prove local input-to-state stability of the phase-locked states with respect to small inputs (total stability) for general bidirectional interconnection topologies. We specialize this result in Section 3.3 to the case of all-to-all coupling. In Section 3.4 we derive necessary conditions on the mean-field feedback gain assuring effective desynchronization. Section 3.5

introduces the incremental Lyapunov function used in the analysis, and further characterizes the robust phase-locked states. The proofs of the main results are given in Section 3.6.

3.1 Modeling exogenous inputs and uncertainties

We start by slightly generalizing system (2.6) to take into account general time-varying inputs:

$$\dot{\theta}_i(t) = \varpi_i(t) + \sum_{j=1}^{N} \tilde{k}_{ij} \sin(\theta_j(t) - \theta_i(t)), \tag{3.1}$$

for all $t \geq 0$ and all $i = 1, \dots, N$, where $\varpi_i : \mathbb{R} \to \mathbb{R}$ denotes the input of the i-th oscillator, and $\tilde{k} = [\tilde{k}_{ij}]_{i,j=1,\dots,N} \in \mathbb{R}_{\geq 0}^{N \times N}$ is the coupling matrix. We stress that, in this section, only nonnegative interconnection gains are considered; negative gains are assumed minoritary and are trated as perturbations. Beyond the effect of the mean-field feedback, the system (3.1) encompasses the heterogeneity between the oscillators, the presence of exogenous disturbances and the uncertainties in the interconnection topology (time-varying coupling, negative interconnection gains, etc.). To see this clearly, let ω_i denote the (constant) natural frequency of the agent i, let p_i represent its additive external perturbations, and let ε_{ij} denote the uncertainty on each coupling gain $\tilde{k}_{ij}$. We assume that $p_i, \varepsilon_{ij} : \mathbb{R}_{\geq 0} \to \mathbb{R}$ are bounded piecewise continuous functions for each $i, j = 1, \dots, N$. Then the effects of all these disturbances, including mean-field feedback, can be analyzed in a unified manner by (3.1) by letting, for all $t \geq 0$ and all $i = 1, \dots, N$,

$$\varpi_i(t) = \omega_i + p_i(t) + \sum_{j=1}^{N} \varepsilon_{ij}(t) \sin(\theta_j(t) - \theta_i(t)) + \sum_{j=1}^{N} \left[\gamma_{ij} \sin(\theta_j(t) - \theta_i(t)) - \gamma_{ij} \sin(\theta_j(t) + \theta_i(t))\right], \tag{3.2}$$

which is well defined due to the forward completeness of (3.1)[1]. In Definition 2.1, the problem of finding a phase-locked solution has been translated into the search of a fixed point for the incremental dynamics (2.10). In the same spirit, the robustness analysis of phase-locked states is translated into some robustness properties of these fixed points. We define the *common drift* $\overline{\omega}$ of (3.1) as

$$\overline{\omega}(t) = \frac{1}{N} \sum_{j=1}^{N} \varpi_j(t), \quad \forall t \geq 0 \tag{3.3}$$

and the *grounded input* as $\tilde{\omega} := [\tilde{\omega}_i]_{i=1,\dots,N}$, where

$$\tilde{\omega}_i(t) := \varpi_i(t) - \overline{\omega}(t), \quad \forall i = 1, \dots, N, \ \forall t \geq 0. \tag{3.4}$$

Noticing that $\varpi_i - \varpi_j = \tilde{\omega}_i - \tilde{\omega}_j$, the evolution equation of the *incremental dynamics* ruled by (3.1) then reads

$$\dot{\theta}_i(t) - \dot{\theta}_j(t) = \tilde{\omega}_i(t) - \tilde{\omega}_j(t) + \sum_{h=1}^{N} \tilde{k}_{ih} \sin(\theta_h(t) - \theta_i(t)) - \sum_{h=1}^{N} \tilde{k}_{jh} \sin(\theta_h(t) - \theta_j(t)), \tag{3.5}$$

for all $i, j = 1, \dots, N$ and all $t \geq 0$. As expected, the incremental dynamics is invariant to common drifts, which explain why the results of this section hold for all kinds of phase-locking

[1] The forward completeness of (3.1) follows by the fact that (3.1) is a Lipschitz continuous periodic dynamics, and thus bounded and globally Lipschitz, and (Khalil, 2001, Theorem 3.2).

(oscillating or not). In the sequel we use $\tilde{\theta}$ to denote the *incremental variable*

$$\tilde{\theta} := [\theta_i - \theta_j]_{i,j=1,\dots,N,i\neq j} \in T^{(N-1)^2}. \tag{3.6}$$

3.2 Robustness analysis of Kuramoto oscillators

When the same input is applied to the oscillators, *i.e.* $\tilde{\omega} \equiv 0$, we expect the solutions of (3.5) to converge to some asymptotically stable fixed point or, equivalently, the solution of (3.1) to converge to some asymptotically stable phase-locked solution at least for some coupling matrices k. To make this precise, we start by defining the notion of 0-*asymptically stable* (0-AS) *phase-locked solutions*, which are described by asymptotically stable fixed points of the incremental dynamics (3.5) when no incremental inputs are applied.

Definition 3.1. Given a coupling matrix $\tilde{k} \in \mathbb{R}^{N\times N}_{\geq 0}$, let $\mathcal{O}_{\tilde{k}} \subset T^{(N-1)^2}$ denote the set of all asymptotically stable fixed points of the unperturbed (*i.e.* $\tilde{\omega} \equiv 0$) incremental dynamics (3.5). A phase-locked solution θ^* of (3.1) is said to be 0-*asymptotically stable* if and only if the incremental state $\tilde{\theta}^* := \left[\theta^*_i - \theta^*_j\right]_{i,j=1,\dots,N,i\neq j} \in T^{(N-1)^2}$ belongs to $\mathcal{O}_{\tilde{k}}$.

A similar definition of asymptotically stable phase-locked solutions, valid in the case of constant inputs, is provided in (Aeyels and Rogge, 2004). A characterization of 0-AS phase-locked solutions of (3.1) for general interconnection topologies can be found in (Sepulchre et al., 2008) and (Sarlette, 2009). In Section 3.5, we characterize the set $\mathcal{O}_{\tilde{k}}$ in terms of the isolated local minima of a suitable Lyapunov function. The reason for considering only *asymptotically* stable fixed points of the incremental dynamics lies in the fact that only those guarantee the robustness property of local Input-to-State Stability with respect to small inputs (Sontag and Wang, 1996), also referred to as *Total Stability* (Malkin, 1958; Loría and Panteley, 2005). On the contrary, (non 0-AS) stable fixed points may exhibit non-robust phase-locked states, as illustrated by the following example.

Example 3.1. *Consider the case where $N > 2$ and let $\tilde{k}_{12} = \tilde{k}_{21} > 0$, and $\tilde{k}_{ij} = 0$ for all $(i,j) \in \mathbb{N}_{\leq N} \times \mathbb{N}_{\leq N} \setminus \{(1,2),(2,1)\}$, that is oscillators 1 and 2 are mutually coupled with the same positive gain, while all the other interconnection links are absent. When $\tilde{\omega} = 0$, the dynamics (3.5) reads*

$$\dot{\theta}_i - \dot{\theta}_j = 0,$$

for all $(i,j) \in \mathbb{N}_{\leq N} \times \mathbb{N}_{\leq N} \setminus \{(1,2),(2,1)\}$, and

$$\dot{\theta}_1 - \dot{\theta}_2 = -2\tilde{k}_{12}\sin(\theta_1 - \theta_2).$$

In this case, all the solutions of the form $\theta_1(t) - \theta_2(t) = 0$, for all $t \geq 0$, and $\theta_i(t) - \theta_j(t) = \theta_i(0) - \theta_j(0)$, for all $t \geq 0$ and all $(i,j) \in \mathbb{N}_{\leq N} \times \mathbb{N}_{\leq N} \setminus \{(1,2),(2,1)\}$ are phase-locked. They can be shown to be stable, but not asymptotically. By adding any (arbitrarily small) constant inputs $\tilde{\omega}_l \neq 0$ to one of the agent $l \in \mathbb{N}_{\leq N} \setminus \{1,2\}$, the system becomes completely desynchronized, since $\dot{\theta}_l - \dot{\theta}_i \equiv \tilde{\omega}_l$ for all $i = 1,\dots,N, i \neq l$. In particular, the set $\mathcal{O}_{\tilde{k}}$ is empty for this particular case.

Definition 3.2 ((Sontag and Wang, 1996))**.** For a system $\dot{x} = f(x,u)$, a compact set $\mathcal{A} \subset \mathbb{R}^n$ is said to be *locally input-to-state stable (LISS) with respect to small inputs* iff there exist some constants $\delta_x, \delta_u > 0$, a $\mathcal{KL}$ function β and a $\mathcal{K}_\infty$ function ρ, such that, for all $|x_0|_{\mathcal{A}} \leq \delta_x$ and all u satisfying $\|u\| \leq \delta_u$, its solution satisfies

$$|x(t,x_0,u)|_{\mathcal{A}} \leq \beta(|x_0|_{\mathcal{A}}, t) + \rho(\|u\|), \quad \forall t \geq 0.$$

If this holds with $\beta(r,s) = Cre^{-\frac{s}{\tau}}$ for all $r, s \geq 0$, where C, τ are positive constants, then $\mathcal{A}$ is locally *exponentially* Input-to-State Stable with respect to small inputs.

Local input-to-state stability (LISS) of a set $\mathcal{A}$ means that the steady-state distance between the set $\mathcal{A}$ and the trajectories starting in a spheric neighborhood of radius δ_x is smaller than $\rho(\|u\|)$, as dictated by the decreasing term $\beta(|x_0|_{\mathcal{A}}, t)$, provided the input intensity $\|u\|$ is smaller than δ_u. This property is called exponential if the function β can be picked as $\beta(r,s) \leq q_1 re^{-q_2 s}$ for all $r, s \geq 0$, where q_1 and q_2 denote positive constants. In particular, LISS guarantees some system's robustness with respect to the set $\mathcal{A}$, provided the initial state is sufficiently near to $\mathcal{A}$, and the perturbation are sufficiently small.

Remark 3.3. Definition 3.2 is given on $\mathbb{R}^n$, which is not well adapted to the context of this chapter. Its extension to the n-Torus is natural since T^n is locally isometric to $\mathbb{R}^n$ through the identity map $\mathcal{I}$ (*i.e.* $|\theta|_{T^n} := |\mathcal{I}(\theta)| = |\theta|$). In particular this means that the n-Torus can be equipped with the local Euclidean metric and its induced norm. Hence, Definition 3.2 applies locally to the n-Torus.

The next theorem, whose proof is given in Section 3.6.3, states the LISS of $\mathcal{O}_{\tilde{k}}$ with respect to small inputs $\tilde{\omega}$.

Theorem 3.4. *Let $\tilde{k} \in \mathbb{R}^{N\times N}_{\geq 0}$ be a given symmetric interconnection matrix. Suppose that the set $\mathcal{O}_{\tilde{k}}$ of Definition 3.2 is non-empty. Then the the set $\mathcal{O}_{\tilde{k}}$ is LISS with respect to small grounded inputs $\tilde{\omega}$ for (3.5). In other words, there exist $\delta_{\tilde{\theta}}, \delta_\omega > 0$, $\beta \in \mathcal{KL}$ and $\rho \in \mathcal{K}_\infty$, such that, for all $\tilde{\omega} : \mathbb{R}_{\geq 0} \to \mathbb{R}^N$ and all $\tilde{\theta}_0 \in T^{(N-1)^2}$ satisfying $\|\tilde{\omega}\| \leq \delta_\omega$ and $|\theta_0|_{\mathcal{O}_{\tilde{k}}} \leq \delta_{\tilde{\theta}}$,*

$$|\tilde{\theta}(t)|_{\mathcal{O}_{\tilde{k}}} \leq \beta(|\tilde{\theta}_0|_{\mathcal{O}_{\tilde{k}}}, t) + \rho(\|\tilde{\omega}\|), \quad \forall t \geq 0. \tag{3.7}$$

Theorem 3.4 guarantees that, if a given configuration is asymptotically stable for the unperturbed system, then solutions starting sufficiently close to that configuration remain near it at all time, in presence of sufficiently small perturbations $\tilde{\omega}$. Moreover, the steady-state distance of the incremental state $\tilde{\theta}$ from $\mathcal{O}_{\tilde{k}}$ is somewhat "proportional" to the amplitude of $\tilde{\omega}$ with nonlinear gain ρ. This means that the phase-locked states are robust to time-varying natural frequencies, provided that they are not too heterogeneous. In terms of the full dynamics (2.3), Theorem 3.4 applies, provided that the coupling strength $|\kappa|$, where the matrix $\kappa \in \mathbb{R}^{N\times N}$ is defined as in (2.4), is sufficiently small that the open-loop small coupling condition (2.4) is satisfied, that is

$$|\kappa| < \delta_h,$$

where δ_h is defined as in (2.4). See Appendix A for more details.

We stress that, while local ISS with respect to small inputs is a natural consequence of asymptotic stability (Loría and Panteley, 2005), the size of the constants δ_x and δ_u in Definition 3.2, defining the robustness domain in terms of initial conditions and inputs amplitude, are potentially very small. As we show explicitly in the next section in the special case of all-to-all coupling, the Lyapunov analysis used in the proof of Theorem 3.4 (cf. Section 3.6.3) provides a general methodology to build these estimates explicitly. In particular, while the region of attraction depends on the geometric properties of the fixed points of the unperturbed system, the size of admissible inputs can be made arbitrarily large by taking a sufficiently large coupling strength. This is detailed in the sequel. See Equations (3.23), (3.24), (3.28) and (3.29) below.

3.3 Robustness of the synchronized state in the case of all-to-all coupling

In this section we focus the Lyapunov analysis used in the proof of Theorem 3.4 (cf. Section 3.6.3) to the case of all-to-all coupling. In this case, it is known (Sepulchre et al., 2008) that the only asymptotically stable phase-locked solution is the *exact synchronization*

$$\tilde{\theta}(t) = 0, \quad \forall t \geq 0, \tag{3.8}$$

corresponding to a zero phase difference between each pair of oscillators. The following proposition states the local *exponential* input-to-state stability of the synchronized state with respect to small inputs, and provides explicit estimates of the region of convergence, of the size of admissible inputs, of the ISS gain, and of the convergence rate. Its proof can be found in Section 3.6.4.

Proposition 3.5. *Consider the system (3.1) with the all-to-all interconnection topology, i.e.* $\tilde{k}_{ij} = K > 0$ *for all* $i, j = 1, \dots, N$. *Then, for all* $\epsilon \in [0, \frac{\pi}{2}]$, *and all* $\tilde{\omega}$ *satisfying*

$$\|\tilde{\omega}\| \leq \delta_\omega^\epsilon := \frac{K\sqrt{N}}{\pi^2}\left(\frac{\pi}{2} - \epsilon\right), \tag{3.9}$$

the following facts hold:

1. *the set* $\mathcal{D}_\epsilon := \left\{\tilde{\theta} \in T^{(N-1)^2} : \ |\tilde{\theta}|_\infty \leq \frac{\pi}{2} - \epsilon\right\}$ *is forward invariant for the system (3.5);*
2. *for all* $\tilde{\theta}_0 \in \mathcal{D}_0$, *the set* $\mathcal{D}_\epsilon$ *is attractive, and the solution of (3.5) satisfies*

$$|\tilde{\theta}(t)| \leq \frac{\pi}{2}|\tilde{\theta}_0| e^{-\frac{K}{\pi^2}t} + \frac{\pi^2}{K}\|\tilde{\omega}\|, \quad \forall t \geq 0.$$

Proposition 3.5 establishes the exponential ISS of the synchronized state in the all-to-all Kuramoto model with respect to time-varying inputs whose amplitudes are smaller than $\frac{K\sqrt{N}}{2\pi}$. It holds for any initial condition lying in $\mathcal{D}_0$, that is when all the initial phase differences lie in $[-\frac{\pi}{2}, \frac{\pi}{2}]$. Moreover, if the inputs amplitude is bounded by δ_ω^ϵ, for some $0 \leq \epsilon \leq \frac{\pi}{2}$, then the set $\mathcal{D}_\epsilon$ is forward invariant and all the solutions starting in $\mathcal{D}_0$ actually converge to $\mathcal{D}_\epsilon$.

Recently, necessary and sufficient conditions for the exponential synchronization of the Kuramoto system with all-to-all coupling and constant different natural frequencies were given in (Chopra and Spong, 2009; Dörfler and Bullo, 2011). We stress that the estimated region of attraction provided by Proposition 3.5 is strictly larger than the one obtained in (Chopra and Spong, 2009, Theorem 4.1), which does not allow ϵ to be picked as zero. For initial conditions lying in $\mathcal{D}_\epsilon$, with a strictly positive ϵ, it is interesting to compare the convergence rate obtained in Proposition 3.5, $\frac{K}{\pi^2}$, with the one obtained in (Chopra and Spong, 2009, Theorem 3.1), $NK\sin(\epsilon)$. While the convergence rate of Proposition 3.5 is slower than the one obtained in (Chopra and Spong, 2009, Theorem 3.1) for large ϵ, it provides a better estimate for small values of ϵ. Furthermore, for any fixed amplitude $\|\tilde{\omega}\|$, the bound (3.9) allows to find the sufficient coupling strength K_ϵ which ensures the attractivity of $\mathcal{D}_\epsilon$:

$$K_\epsilon = \frac{\pi^2}{\left(\frac{\pi}{2} - \epsilon\right)\sqrt{N}}\|\tilde{\omega}\|.$$

Noticing that $\sqrt{N}\max_{i,j=1,\dots,N}\|\varpi_i-\varpi_j\|\geq\|\tilde{\omega}\|$, we get that

$$K_\epsilon\leq\frac{\pi^2}{\left(\frac{\pi}{2}-\epsilon\right)}\max_{i,j=1,\dots,N}\|\varpi_i-\varpi_j\|.$$

Since $\left(\frac{\pi}{2}-\epsilon\right)\geq\frac{2}{\pi}\cos(\epsilon)$, for all $0\leq\epsilon\leq\frac{\pi}{2}$, it results that

$$K_\epsilon\leq\frac{\pi^3}{2\cos(\epsilon)}\max_{i,j=1,\dots,N}\|\varpi_i-\varpi_j\|<\pi^3K_{inv},$$

where K_{inv} is the sufficient coupling strength provided in (Chopra and Spong, 2009, Proof of Theorem 4.1). This observation shows that, while the estimate K_ϵ may be more restrictive than the one proposed in (Chopra and Spong, 2009), both are of of the same order, in the sense that $\frac{K_\epsilon}{K_{inv}}<\pi^3$.

For the same region of attraction, a tighter bound K_{suff} for the sufficient coupling strength has recently been given in (Dörfler and Bullo, 2011), where this bound is inversely proportional to the number of oscillators, that is $\frac{K_\epsilon}{K_{suff}}\sim N$. Nonetheless, similarly to (Chopra and Spong, 2009), their rate of convergence is proportional to $\sin(\epsilon)$, leading to a worse bound than ours for large regions of attraction.

In conclusion, Proposition 3.5 partially extends the main results of (Chopra and Spong, 2009; Dörfler and Bullo, 2011) to time-varying inputs. On the one hand, it allows to consider sets of initial conditions larger than those of (Chopra and Spong, 2009), and bounds the convergence rate by a strictly positive value, independently of the region of attraction. On the other hand the required coupling strength is comparable to the one given in (Chopra and Spong, 2009), but more conservative than the lower bound in (Dörfler and Bullo, 2011). Finally for small regions of attraction, the bound on the convergence rate obtained in Proposition 3.5 is not as good as the one of (Chopra and Spong, 2009; Dörfler and Bullo, 2011).

3.4 Robustness of neural synchrony to mean-field feedback

As a corollary of Theorem 3.4 we derive necessary conditions on the intensity of a desynchronizing mean-field feedback. To that end consider the Kuramoto system under mean-field feedback (2.6), and let $\overline{\gamma}$ and $\omega^\perp$ represent the intensity of the mean-field feedback DBS and the heterogeneity of the ensemble of neurons:

$$\overline{\gamma}:=\max_{i,j=1,\dots,N}|\gamma_{ij}|, \tag{3.10}$$

$$\omega^\perp:=\left[\omega_i-\frac{1}{N}\sum_{j=1}^N\omega_j\right]_{i=1,\dots,N}. \tag{3.11}$$

We also define the *grounded mean-field input* $\tilde{I}_{MF}$ of the incremental dynamics associated to (2.6) as

$$\tilde{I}_{MF}(t):=I_{MF}(t)-\overline{I}_{MF}(t)\mathbf{1}_N,\quad\forall t\geq0, \tag{3.12}$$

where, for all $t\geq0$, $I_{MF}(t):=[I_{MF_i}(t)]_{i=1,\dots,N}$,

$$I_{MF_i}(t):=\sum_{j=1}^N\gamma_{ij}\Big(\sin(\theta_i(t)-\theta_j(t))-\sin(\theta_i(t)+\theta_j(t))\Big),$$

is the input of the mean-field feedback (cf. (3.2)) and

$$\overline{I}_{MF}(t) := \frac{1}{N}\sum_{i,j=1}^{N} \gamma_{ij}\Big(\sin(\theta_i(t)-\theta_j(t)) - \sin(\theta_i(t)+\theta_j(t)\Big),$$

for all $t \geq 0$, represents the common drift among the ensemble of neurons due to the mean-field feedback. The grounded mean-field input $\tilde{I}_{MF}$ is the quantity of interest for the aim of desynchronization. Indeed, as already pointed out in (3.5), it is this input, along with the intrinsic heterogeneity of the ensemble (*i.e.* $\omega^{\perp}$), which is responsible for the destabilization of the incremental dynamics of the Kuramoto system under mean-field feedback. An upper bound on the norm of $\tilde{I}_{MF}$ can be easily found as in the proof of Corollary 3.6 (Section 3.6.5), and reads

$$|\tilde{I}_{MF}| \leq 2\overline{\gamma} N\sqrt{N}.$$

The following result, whose proof is given in Section 3.6.5, stresses the robustness of phase-locking with respect to mean-field feedback. It provides a negative answer to the question whether mean-field feedback DBS with arbitrarily small amplitude can effectively desynchronize a network of Kuramoto oscillators.

Corollary 3.6. *Let $k \in \mathbb{R}^{N\times N}_{\geq 0}$ be a given symmetric interconnection matrix and $\omega \in \mathbb{R}^N$ be any (constant) vector of natural frequencies. Let $\gamma \in \mathbb{R}^{N\times N}$ be any feedback gain. Let $\overline{\gamma}$, $\omega^{\perp}$, and $\tilde{I}_{MF}$ be defined as in (3.10)-(3.12). Let the set $\mathcal{O}_k$ be defined as in Definition 3.1 and suppose that it is non-empty. Then there exist a class $\mathcal{KL}$ function β, a class $\mathcal{K}_\infty$ function σ, a positive constant δ_ω, and a neighborhood $\mathcal{P}$ of $\mathcal{O}_k$, such that, for all natural frequencies and all mean-field feedback satisfying*

$$|\omega^{\perp}| + 2\,\overline{\gamma}\, N\sqrt{N} \leq \delta_\omega,$$

the solution of (2.6) satisfies, for all $\tilde{\theta}_0 \in \mathcal{P}$,

$$|\tilde{\theta}(t)|_{\mathcal{O}_k} \leq \beta(|\tilde{\theta}_0|_{\mathcal{O}_k}, t) + \sigma(|\omega^{\perp}| + \|\tilde{I}_{MF}\|),\ \forall t \geq 0,$$

where $\tilde{\theta}$ is defined in (3.6).

Corollary 3.6 states that the phase-locked states associated to the Kuramoto system with any symmetric interconnection topology are robust to sufficiently small mean-field feedbacks. The intensity of the tolerable feedback gain $\overline{\gamma}$ depends on the distribution of natural frequencies, reflecting the fact that a heterogeneous ensemble can be more easily brought to an incoherent state. Similarly to Theorem 3.4, Corollary 3.6 ensures the robustness of the full dynamics (2.3) to small mean-field proportional feedback, only if the coupling strength $|\kappa|$ is sufficiently small to verify condition (2.4), *i.e.* $|\kappa| < \delta_h$.

As stressed in Section 1.1, energy consumption is a critical issue in the DBS framework (Rodriguez-Oroz et al., 2005), mainly due to the short life of the stimulator's batteries and to the side effects that a too strong current injection can bring. Corollary 3.6, along with the explicit input bound δ_ω, which can be computed as in the proof of Theorem 3.4, provides a *lower bound* on the intensity of a proportional mean-field feedback DBS to achieve effective desynchronization for a general symmetric interconnection between the neurons and recording-stimulation setup. Even if hard to know in practice, also an approximate knowledge of the distribution of natural frequencies of the neurons in the STN, of their interconnection topology and of the electrical characteristics of the recording-stimulation setup can be used to compute

this value. In conclusion, Corollary 3.6 answers negatively to the question weather an arbitrarily small feedback gain suffices to induce effective desynchyronization in a neuronal ensemble via mean-field feedback DBS.

A sufficient condition on the feedback gain to bring a neuronal ensemble in a desynchronized state for a generic interconnection topology and feedback setup is provided in Section 5.3.

3.5 A Lyapunov function for the incremental dynamics

In this section, we introduce the Lyapunov function for the incremental dynamics (3.5), that will be referred to as the *incremental Lyapunov function*. It will be used in the proof of Theorem 3.4. We start by showing that the incremental dynamics (3.5) possesses an invariant manifold, that we characterize through some linear relations. This observation allows us to restrict the analysis of the critical points of the Lyapunov function to this manifold. Beyond its technical interest, this analysis shows that phase-locked solutions correspond to these critical points. In particular, it provides an analytic way of computing the set $\mathcal{O}_{\tilde{k}}$ of Definition 3.1, completely characterizing the set of robust asymptotically stable phase-locked solutions.

3.5.1 The incremental Lyapunov function

We start by introducing the *normalized interconnection matrix* associated to $\tilde{k}$

$$E = [E_{ij}]_{i,j=1,\dots,N} := \frac{1}{K} \left[\tilde{k}_{ij}\right]_{i,j=1,\dots,N}, \tag{3.13}$$

where the constant $K > 0$ is defined as

$$K := \begin{cases} 1 & \text{if} \quad \tilde{k} = 0 \\ \max_{i,j=1,\dots,N} \tilde{k}_{ij} & \text{if} \quad \tilde{k} \neq 0. \end{cases} \tag{3.14}$$

Inspired by (Sarlette, 2009), let $V_I : T^{(N-1)^2} \to \mathbb{R}_{\geq 0}$ be the *incremental* Lyapunov function defined by

$$V_I(\tilde{\theta}) := 2 \sum_{i=1}^{N} \sum_{j=1}^{N} E_{ij} \sin^2 \left(\frac{\theta_i - \theta_j}{2} \right), \tag{3.15}$$

where the incremental variable $\tilde{\theta}$ is defined in (3.6). We stress that V_I is independent of the coupling strength K.

3.5.2 The invariant manifold

The presence of an invariant manifold (Lee, 2006; Hirsch et al., 1977) comes from the fact that the components of the incremental variable $\tilde{\theta}$ are not linearly independent. Indeed, we can express $(N-1)(N-2)$ of them in terms of the other $N-1$ independent components. More precisely, by choosing, for instance, $\varphi_i := \theta_i - \theta_N$, $i = 1, \dots, N-1$, as the independent variables, it is possible to write, for all $i = 1, \dots, N-1$,

$$\theta_i - \theta_N = \varphi_i, \tag{3.16a}$$

$$\theta_i - \theta_j = \varphi_i - \varphi_j, \quad \forall j = 1, \dots, N-1. \tag{3.16b}$$

These relations can be expressed in a compact form as

$$\tilde{\theta} = \tilde{B}(\varphi) := B\varphi \mod 2\pi, \quad \varphi \in \mathcal{M}, \tag{3.17}$$

where $\varphi := [\varphi_i]_{i=1,\dots,N-1}$, $B \in \mathbb{R}^{(N-1)^2 \times (N-1)}$, $\mathrm{rank}B = N-1$, $\tilde{B}$ is continuously differentiable, and $\mathcal{M} \subset T^{(N-1)^2}$ is the submanifold defined by the embedding (3.17). The continuous differentiability of $\tilde{B} : \mathcal{M} \to T^{(N-1)^2}$ comes from the fact that $\varphi_i \in T^1$, for all $i = 1, \dots, N-1$, and from the additive group structure of T^1. Formally, this means that the system is evolving on the manifold $\mathcal{M} \subset T^{(N-1)^2}$ of dimension $N-1$. In particular $\mathcal{M}$ is diffeomorphic to T^{N-1}.

3.5.3 Restriction to the invariant manifold

In order to conduct a Lyapunov analysis based on V_I it is important to identify its critical points. Since the system is evolving on the invariant manifold $\mathcal{M}$, only the critical points of the Lyapunov function V_I restricted to this manifold are of interest. Hence we focus on the critical points of the restriction of V_I to $\mathcal{M}$, which is defined by the function $V_I|_{\mathcal{M}} : T^{N-1} \to \mathbb{R}_{\geq 0}$ as

$$V_I|_{\mathcal{M}}(\varphi) := V_I(B\varphi), \quad \forall \varphi \in \mathcal{M}. \tag{3.18}$$

The analysis of the critical points of $V_I|_{\mathcal{M}}$ is not trivial. To simplify this problem, we exploit the fact that the variable φ can be expressed in terms of θ by means of a linear transformation $A \in \mathbb{R}^{(N-1)\times N}$, with $\mathrm{rank}A = N-1$, in such a way that

$$\varphi = \tilde{A}(\theta) := A\theta \mod 2\pi. \tag{3.19}$$

Based on this, we define the function $V : T^N \to \mathbb{R}$ as

$$V(\theta) := V_I|_{\mathcal{M}}(A\theta), \quad \forall \theta \in T^N. \tag{3.20}$$

In contrast with $V_I|_{\mathcal{M}}$, the function V owns the advantage that its critical points are already widely studied in the synchronization literature, see for instance (Sepulchre et al., 2007) and (Sarlette, 2009, Chapter 3). The following lemma allows to reduce the analysis of the critical points of V_I on $\mathcal{M}$ to that of the critical points of V on T^N. Its proof is given in Section 3.6.1.

Lemma 3.7. *Let $\mathcal{M}$, $V_I|_{\mathcal{M}}$, A and V be defined by (3.17)-(3.20). Then $\theta^* \in T^N$ is a critical point of V (i.e. $\nabla_\theta V(\theta^*) = 0$) if and only if $\varphi^* = A\theta^* \in \mathcal{M}$ is a critical point of $V_I|_{\mathcal{M}}$ (i.e. $\nabla_\varphi V_I|_{\mathcal{M}}(\varphi^*) = 0$). Moreover if θ^* is a local maximum (resp. minimum) of V then φ^* is a local maximum (resp. minimum) of $V_I|_{\mathcal{M}}$. Finally the origin of $\mathcal{M}$ is a local minimum of $V_I|_{\mathcal{M}}$.*

3.5.4 Lyapunov characterization of robust phase-locking

The above development allows to characterize phase-locked states through the incremental Lyapunov function V_I. The following lemma, proved in Section 3.6.2, states that the fixed points of the unperturbed incremental dynamics are the critical points of $V_I|_{\mathcal{M}}$, modulo the linear relations (3.16), *i.e.* the critical points of $V_I|_{\mathcal{M}}$ completely characterize phase-locked solutions.

Lemma 3.8. *Let $k \in \mathbb{R}^{N\times N}_{\geq 0}$ be a given symmetric interconnection matrix. Let B and $V_I|_{\mathcal{M}}$ be defined as in (3.17) and (3.18). Then $\varphi^* \in \mathcal{M}$ is a critical point of $V_I|_{\mathcal{M}}$ (i.e. $\nabla_\varphi V_I|_{\mathcal{M}}(\varphi^*) = 0$) if and only if $B\varphi^* \in T^{(N-1)^2}$ is a fixed point of the unperturbed (i.e. $\tilde{\omega} \equiv 0$) incremental dynamics (3.5).*

Remark 3.9. When no inputs apply (*i.e.*, $\tilde{\omega} \equiv 0$), the Lyapunov function V_I is strictly decreasing along the trajectories of (3.5) if and only if the state does not belong to the set of critical points of $V_I|_{\mathcal{M}}$ (cf. Claim 3.11 below). It then follows directly from Lemma 3.8 that isolated local minima of $V_I|_{\mathcal{M}}$ correspond to asymptotically stable fixed points of (3.5). By Definition 3.1 and Theorem 3.4, we conclude that the robust asymptotically stable phase-locked states are completely characterized by the set of isolated local minima of $V_I|_{\mathcal{M}}$. The computation of this set is simplified through Lemma 3.7.

3.5.5 Consequence for the system without inputs

At the light of Lemma 3.8, we can state the following corollary, which recovers, and partially extends, the result of (Sarlette, 2009, Proposition 3.3.2) in terms of the incremental dynamics of the system. It states that, for a symmetric interconnection topology, any disturbance with zero grounded input (3.4) preserves the almost global asymptotic stability of phase-locking for (3.1).

Corollary 3.10. *Let $\varpi : \mathbb{R}_{\geq 0} \to \mathbb{R}^N$ be any signal satisfying $\tilde{\omega}(t) = 0$, for all $t \geq 0$, where $\tilde{\omega}$ is defined in (3.4). If the interconnection matrix $\tilde{k} \in \mathbb{R}_{\geq 0}^{N \times N}$ is symmetric, then almost all trajectories of (3.1) converge to a stable phase-locked solution.*

We stress that Corollary 3.10 is an *almost global* result. It follows from the fact that almost all trajectories converge to the set of local minima of $V_I|_{\mathcal{M}}$. From Lemma 3.8, this set corresponds to asymptotically stable fixed points of the incremental dynamics, that is to asymptotically stable phase-locked solutions. The precise proof is omitted here.

3.6 Main proofs

3.6.1 Proof of Lemma 3.7

By the definition (3.20) of $V(\theta)$, it holds that $\nabla_\theta V(\theta) = \nabla_\theta V_I|_{\mathcal{M}}(A\theta) = A^T \nabla_{A\theta} V_I|_{\mathcal{M}}(A\theta)$. Hence

$$\nabla_{A\theta} V_I|_{\mathcal{M}}(A\theta) = 0 \quad \Rightarrow \quad \nabla_\theta V(\theta) = 0.$$

Since $\text{rank} A = N - 1$, $\ker A^T = \{0\}$, it follows that

$$\nabla_\theta V(\theta) = 0 \quad \Rightarrow \quad \nabla_{A\theta} V_I|_{\mathcal{M}}(A\theta) = 0,$$

which proves the first part of the lemma. To prove the second part, we note that if θ^* is a local minimum of V then there exists a neighborhood U of θ^* such that $V(\theta) \geq V(\theta^*)$ for all $\theta \in U$. That is, $V_I|_{\mathcal{M}}(A\theta) \geq V_I|_{\mathcal{M}}(A\theta^*)$ for all $\theta \in U$. That is $V_I|_{\mathcal{M}}(\varphi) \geq V_I|_{\mathcal{M}}(\varphi^*)$ for all $\varphi \in W = AU$, where $\varphi^* = A\theta^*$. A similar proof holds for maxima. The third part of the lemma follows from the fact the function $V_I|_{\mathcal{M}}$ is positive definite and $V_I|_{\mathcal{M}}(0) = 0$, *i.e.* $\varphi^* = 0$ is a local minimum of $V_I|_{\mathcal{M}}$. □

3.6.2 Proof of Lemma 3.8

From Lemma 3.7, $\varphi^* \in \mathcal{M}$ is a critical point of $V_I|_{\mathcal{M}}$ if and only if $\theta^* \in T^N$ is a critical point of V, where $\varphi^* = A\theta^*$, and A is defined in (3.19). Moreover, when $\tilde{\omega} = 0$, (3.5) can be re-written as

$$\dot{\theta}_i - \dot{\theta}_j = K\left(\chi_j(\theta) - \chi_i(\theta)\right), \quad \forall i, j = 1, \ldots, N,$$

where $\chi(\theta) = [\chi_i(\theta)]_{i=1,\dots,N} := \nabla_\theta V(\theta) = \sum_{j=1}^N E_{ij}\sin(\theta_j - \theta_i)$, and E is defined in (3.13). Hence, $\chi(\theta^*) = \nabla_\theta V(\theta^*) = 0$ if and only if $\varphi^* = A\theta^*$ is a critical point of $V_I|_{\mathcal{M}}$; and $\chi_j(\theta^*) - \chi_i(\theta^*) = 0$, for all $i, j = 1, \dots, N$, if and only if $B\varphi^* = BA\theta^*$ is a fixed point of the unperturbed incremental dynamics, where B is defined in (3.17). To prove the lemma it thus suffices to show that

$$\chi(\theta^*) = 0 \quad \Leftrightarrow \quad \chi_j(\theta^*) - \chi_i(\theta^*) = 0, \quad \forall i, j = 1, \dots, N.$$

One implication is straightforward: if $\chi(\theta^*) = 0$, then in particular all of its components are zero, which implies that $\chi_j(\theta^*) - \chi_i(\theta^*) = 0$, for all $i, j = 1, \dots, N$. On the other hand, if $\chi_j(\theta^*) - \chi_i(\theta^*) = 0$ for all $i, j = 1, \dots, N$, then there exists a constant $\overline{\chi}$, such that $\chi_i(\theta^*) = \overline{\chi}$ for all $i = 1, \dots, N$. Hence, it holds that

$$N\overline{\chi} = \sum_{i=1}^N \chi_i(\theta^*) = \sum_{i=1}^N \frac{\partial V}{\partial \theta_i}(\theta^*) = \sum_{i=1}^N \sum_{j=1}^N E_{ij}\sin(\theta_j^* - \theta_i^*).$$

Since the matrix $\tilde{k}$ is symmetric, so is the matrix E (cf. (3.13)), and thus $\sum_{i=1}^N \sum_{j=1}^N E_{ij}\sin(\theta_j^* - \theta_i^*) = 0$. Consequently, $\chi_i(\theta^*) = \overline{\chi} = 0$ for all $i = 1, \dots, N$, which proves the converse implication. □

3.6.3 Proof of Theorem 3.4

In order to develop the robustness analysis we consider the Lyapunov function (3.15), where the incremental variable $\tilde{\theta}$ is defined in (3.6), and the matrix E is given by (3.13)-(3.14). The derivative of V_I yields $\dot{V}_I(\tilde{\theta}) = (\nabla_{\tilde{\theta}} V_I)^T \dot{\tilde{\theta}}$, where $\dot{\tilde{\theta}}$ is given by (3.5). The following claim, whose proof is given in Section 3.7.1 provides an alternative expression for $\dot{V}_I$.

Claim 3.11. If $\tilde{k} \in \mathbb{R}^{N\times N}$ is symmetric, then $\dot{V}_I = -2(K\chi^T\chi + \chi^T\tilde{\omega})$, where

$$\chi(\tilde{\theta}) := \nabla_\theta V\big(\tilde{\theta}\big) = \left[\sum_{j=1}^N E_{ij}\sin(\theta_j - \theta_i)\right]_{i=1,\dots,N}.$$

From Claim 3.11, it holds that, if $|\chi| \geq \frac{2|\tilde{\omega}|}{K}$, then $\dot{V}_I \leq -K\chi^T\chi$. However, LISS does not follow yet as these regions are given in terms of χ rather than $\tilde{\theta}$. In order to estimate these regions in terms of $\tilde{\theta}$, we define $\mathcal{F}$ as the set of critical points of $V_I|_{\mathcal{M}}$ (*i.e.* $\mathcal{F} := \{\varphi^* \in \mathcal{M} : \nabla_\varphi V_I|_{\mathcal{M}}(\varphi^*) = 0\}$), where $\mathcal{M}$ and $V_I|_{\mathcal{M}}$ are defined in (3.17) and (3.18), respectively. Then, from Lemma 3.7 and recalling that $\chi = \nabla_\theta V_I$, it holds that $|\chi| = 0$ if and only if $\tilde{\theta} \in \mathcal{F}$. Since $|\chi|$ is a positive definite function of the distance from $\tilde{\theta}$ to the set $\mathcal{F}$ and is defined on a compact set, (Khalil, 2001, Lemma 4.3) guarantees the existence of a $\mathcal{K}$ function σ such that

$$|\chi| \geq \sigma(|\tilde{\theta}|_{\mathcal{F}}), \quad \forall \tilde{\theta} \in T^{(N-1)^2}. \tag{3.21}$$

The function σ can then be taken as $\mathcal{K}_\infty$ by choosing a suitable extension outside $T^{(N-1)^2}$. Let $\mathcal{U} := \mathcal{F} \setminus \mathcal{O}_{\tilde{k}}$, where the set $\mathcal{O}_{\tilde{k}}$ is given in Definition 3.1. In view of Lemma 3.8, $\mathcal{U}$ denotes the set of all the critical points of $V_I|_{\mathcal{M}}$ which are not asymptotically stable fixed points of the incremental dynamics. Since $\nabla V_I|_{\mathcal{M}}$ is a Lipschitz function defined on a compact space, it can be different from zero only on a finite collection of open sets. That is, $\mathcal{U}$ and $\mathcal{O}_{\tilde{k}}$ are the finite disjoint unions of closed sets:

$$\mathcal{U} = \bigcup_{i\in I_{\mathcal{U}}} \nu_i, \quad \mathcal{O}_{\tilde{k}} = \bigcup_{i\in I_{\mathcal{O}_{\tilde{k}}}} \{\phi_i\}, \tag{3.22}$$

where $I_{\mathcal{U}}, I_{\mathcal{O}_{\tilde{k}}} \subset \mathbb{N}$ are finite sets, $\{\nu_i,\ i \in I_{\mathcal{U}}\}$ is a family of closed subsets of $\mathcal{M}$, and $\left\{\{\phi_i\},\ i \in I_{\mathcal{O}_{\tilde{k}}}\right\}$ is a family of singletons of $\mathcal{M}$. We stress that $a \neq b$ implies $a \cap b = \emptyset$ for any $a, b \in \{\nu_i,\ i \in I_{\mathcal{U}}\} \bigcup \left\{\{\phi_i\},\ i \in I_{\mathcal{O}_{\tilde{k}}}\right\} =: \mathcal{F}_S$. Define

$$\delta := \min_{a,b \in \mathcal{F}_S, a \neq b} \inf_{\tilde{\theta} \in a} |\tilde{\theta}|_b, \tag{3.23}$$

which represents the minimum distance between two critical sets, and, at the light of Lemma 3.8, between two fixed points of the unpertubed incremental dynamics (3.1). Note that, since $\mathcal{F}_S$ is finite, $\delta > 0$. Define

$$\delta'_\omega = \frac{K}{2}\sigma\left(\frac{\delta}{2}\right), \quad \delta_{\tilde{\theta}} := \frac{\delta}{2}. \tag{3.24}$$

$\delta_{\tilde{\theta}}$ then gives an estimate of the radius of attraction, modulo the shape of the level sets of V_I. The following claim is proved in Section 3.7.2.

Claim 3.12. For all $i \in I_{\mathcal{O}_{\tilde{k}}}$, $\tilde{\theta} \in \mathcal{B}(\phi_i, \delta_{\tilde{\theta}})$, and $|\tilde{\omega}| \leq \delta'_\omega$,

$$|\tilde{\theta} - \phi_i| \geq \sigma^{-1}\left(\frac{2|\tilde{\omega}|}{K}\right) \quad \Rightarrow \quad \dot{V}_I \leq -K\sigma^2(|\tilde{\theta} - \phi_i|).$$

For all $i \in I_{\mathcal{O}_{\tilde{k}}}$, the function $V_I(\tilde{\theta}) - V_I(\phi_i)$ is zero for $\tilde{\theta} = \phi_i$, and strictly positive for all $\theta \in \mathcal{B}(\phi_i, \delta_{\tilde{\theta}}) \setminus \{\phi_i\}$. Noticing that $\mathcal{B}(\phi_i, \delta_{\tilde{\theta}})$ is compact, (Khalil, 2001, Lemma 4.3) guarantees the existence of $\mathcal{K}$ functions $\underline{\alpha}_i, \overline{\alpha}_i$ defined on $[0, \delta_{\tilde{\theta}}]$ such that, for all $\tilde{\theta} \in \mathcal{B}(\phi_i, \delta_{\tilde{\theta}})$,

$$\underline{\alpha}_i(|\tilde{\theta} - \phi_i|) \leq V_I(\tilde{\theta}) - V_I(\phi_i) \leq \overline{\alpha}_i(|\tilde{\theta} - \phi_i|). \tag{3.25}$$

The two functions can then be picked as $\mathcal{K}_\infty$ by choosing a suitable prolongation on $\mathbb{R}_{\geq 0}$. Define the $\mathcal{K}_\infty$ functions

$$\underline{\alpha}(s) := \min_{i \in I_{\mathcal{O}_{\tilde{k}}}} \underline{\alpha}_i(s),\ \overline{\alpha}(s) := \max_{i \in I_{\mathcal{O}_{\tilde{k}}}} \overline{\alpha}_i(s),\ \forall s \geq 0. \tag{3.26}$$

It then holds that, for all $i \in I_{\mathcal{O}_{\tilde{k}}}$ and all $\tilde{\theta} \in \mathcal{B}(\phi_i, \delta_{\tilde{\theta}})$,

$$\underline{\alpha}(|\tilde{\theta} - \phi_i|) \leq V_I(\tilde{\theta}) - V_I(\phi_i) \leq \overline{\alpha}(|\tilde{\theta} - \phi_i|). \tag{3.27}$$

In view of Claim 3.12 and (3.27), it follows from (Isidori, 1999, Remark 10.4.3) that an estimate of the ISS gain and on the tolerated input bound are given by

$$\rho(s) := \underline{\alpha}^{-1} \circ \overline{\alpha} \circ \sigma^{-1}\left(\frac{2}{K}s\right),\ \forall s \geq 0 \tag{3.28}$$

$$\delta_\omega := \rho^{-1}(\delta_{\tilde{\theta}}) \leq \delta'_\omega, \tag{3.29}$$

where σ is defined in (3.21). From (Isidori, 1999, Section 10.4) and Claim 3.12, it follows that, for all $\|\tilde{\omega}\| \leq \delta_\omega$, the set $\mathcal{B}(\mathcal{O}_{\tilde{k}}, \delta_{\tilde{\theta}})$ is forward invariant for the system (3.5). Furthermore, invoking (Sontag and Wang, 1996) and (Isidori, 1999, Section 10.4), Claim 3.12 thus implies LISS with respect to inputs satisfying $\|\tilde{\omega}\| \leq \delta_\omega$, meaning that there exists a class $\mathcal{KL}$ function β such that, for all $\|\tilde{\omega}\| \leq \delta_\omega$, and all $\tilde{\theta}_0 \in \mathcal{B}(\mathcal{O}_{\tilde{k}}, \delta_{\tilde{\theta}})$, the trajectory of (3.5) satisfies $|\tilde{\theta}(t)| \leq \beta(|\tilde{\theta}_0|, t) + \rho(\|\tilde{\omega}\|)$, for all $t \geq 0$. □

3.6.4 Proof of Proposition 3.5

Input-to-State Gain

We start by computing the ISS gain ρ, defined in (3.28), in the particular case of all-to-all coupling and show that it can be taken as a linear function. The first step is to compute the function σ, defined in (3.21), with respect to the origin of the incremental dynamics. That is we have to find a class $\mathcal{K}_\infty$ function σ, such that $|\chi(\tilde{\theta})| \geq \sigma(|\tilde{\theta}|)$ for all $\tilde{\theta}$ in some neighborhood of the origin of the incremental dynamics, where χ is defined in Claim 3.11. The following claim, whose proof is given in Section 3.7.3, gives an explicit expression of this function on the set $\mathcal{D}_0 = \{\tilde{\theta} \in T^{(N-1)^2} : |\tilde{\theta}|_\infty \leq \frac{\pi}{2}\}$, as defined in the statement of Proposition 3.5.

Claim 3.13. In the case of all-to-all coupling , the function χ defined in Claim 3.11 satisfies, for any $\tilde{\theta} \in \mathcal{D}_0$, $|\chi(\tilde{\theta})| \geq \frac{|\tilde{\theta}|}{\pi}$, that is the function σ in (3.21) can be picked as $\sigma(r) = \frac{r}{\pi}$, for all $r \geq 0$.

At the light of Claim 3.13, the ISS gain ρ can be easily computed through (3.28). Indeed, in the all-to-all case, the entries of the matrix E, introduced in (3.13), are all equal to 1, and the Lyapunov function V_I, provided in (3.15), thus becomes

$$V_I(\tilde{\theta}) = 2 \sum_{i,j=1}^{N} \sin^2\left(\frac{\theta_i - \theta_j}{2}\right).$$

Using the fact that $z \geq \sin z \geq \frac{2}{\pi} z$, for all $0 \leq z \leq \frac{\pi}{2}$, it follows that, for all $\tilde{\theta} \in \mathcal{D}_0$,

$$\frac{2}{\pi^2}|\tilde{\theta}|^2 \leq V_I(\tilde{\theta}) \leq \frac{1}{2}|\tilde{\theta}|^2. \tag{3.30}$$

Recalling the definition of the upper $\overline{\alpha}$ and lower $\underline{\alpha}$ estimates of the Lyapunov function with respect to the set of asymptotically stable fixed point (3.26), and that, in the all-to-all case, this set reduces to the origin, we conclude that

$$\underline{\alpha}(r) = \frac{2}{\pi^2} r^2, \quad \overline{\alpha}(r) = \frac{1}{2} r^2, \ \forall r \geq 0.$$

In view of Claim 3.13 and (3.28), it follows that the ISS gain ρ in the statement of Theorem 3.4, can be chosen as

$$\rho(r) = \frac{\pi^2}{K} r. \tag{3.31}$$

Input bound and invariant set

For Claim 3.13, the ISS gain computed in the previous section is valid as soon as $\tilde{\theta}$ belongs to $\mathcal{D}_0$. In the following we compute an input bound which guarantees that trajectories starting in $\mathcal{D}_0$ remain inside $\mathcal{D}_0$. For the sake of generality, we actually show the forward invariance of $\mathcal{D}_\epsilon$ for any $\epsilon \in \left[0, \frac{\pi}{2}\right]$. To that end, we start by the following technical claim, whose proof is given in Section 3.7.4.

Claim 3.14. Given any $0 \leq \delta \leq \pi$, the following holds true:

$$|\tilde{\theta}| \leq \sqrt{N}\delta \ \Rightarrow \ \max_{i,j=1,\dots,N} |\theta_i - \theta_j| \leq \delta.$$

At the light of Claim 3.14, and in view of (3.7) and (3.31), we can compute the input bound δ_ω^ϵ which lets $\mathcal{D}_\epsilon$ be invariant for the systems (3.5) by imposing $\rho(\delta_\omega^\epsilon) = \sqrt{N}\left(\frac{\pi}{2} - \epsilon\right)$, where $\rho(s) = \frac{\pi^2}{K}s$ is the ISS gain in the statement of Theorem 3.4. This gives

$$\delta_\omega^\epsilon = \frac{K\sqrt{N}}{\pi^2}\left(\frac{\pi}{2} - \epsilon\right). \tag{3.32}$$

Exponential convergence and attractivity of $\mathcal{D}_\epsilon$

From Claims 3.12 and 3.13, and (3.30), it holds that, for all $|\tilde{\omega}| \leq \delta_\omega^\epsilon$, and all $\tilde{\theta} \in \mathcal{D}_0$,

$$|\tilde{\theta}| \geq \frac{2\pi}{K}|\tilde{\omega}| \;\Rightarrow\; \dot{V}_I \leq -\frac{K}{\pi^2}|\tilde{\theta}|^2 \leq -\frac{2K}{\pi^2}V_I.$$

Invoking the comparison Lemma (Khalil, 2001, Lemma 3.4), it follows that, for all $t \geq 0$,

$$\min_{0\leq s\leq t}|\tilde{\theta}(s)| \geq \frac{2\pi}{K}\|\tilde{\omega}\| \;\Rightarrow\; V_I(\tilde{\theta}(t)) \leq V_I(\tilde{\theta}(0))e^{-\frac{2K}{\pi^2}t}.$$

From (3.30), this also implies that, for all $t \geq 0$

$$\min_{0\leq s\leq t}|\tilde{\theta}(s)| \geq \frac{2\pi}{K}\|\tilde{\omega}\| \;\Rightarrow\; |\tilde{\theta}(t)| \leq \frac{\pi}{2}|\tilde{\theta}(0)|e^{-\frac{K}{\pi^2}t}.$$

Recalling the explicit expression of ISS gain (3.31), this implies that the system is exponentially input-to-state stable (see for instance (Isidori, 1999, Section 10.4) and (Khalil, 2001, Lemma 4.4 and Theorem 4.10)), and in particular that for all $\|\tilde{\omega}\| \leq \delta_\omega^\epsilon$ and all $\tilde{\theta}_0$ in $\mathcal{D}_0$,

$$|\tilde{\theta}(t)| \leq \frac{\pi}{2}|\tilde{\theta}_0|e^{-\frac{K}{\pi^2}t} + \frac{\pi^2}{K}\|\tilde{\omega}\|,\ \forall t \geq 0.$$

Noticing finally that, if $\|\tilde{\omega}\| \leq \delta_\omega^\epsilon$, (3.32) guarantees that

$$|\tilde{\theta}(t)| \leq \frac{\pi}{2}|\tilde{\theta}_0|e^{-\frac{K}{\pi^2}t} + \sqrt{N}\left(\frac{\pi}{2} - \epsilon\right),\ \forall t \geq 0,$$

Claim 3.14 implies the attractivity of $\mathcal{D}_\epsilon$ for all $\|\tilde{\omega}\| \leq \delta_\omega^\epsilon$. □

3.6.5 Proof of Corollary 3.6

The Corollary is a trivial consequence of Theorem 3.4 by noting that, since $|(\tilde{I}_{MF})_i| = |(I_{MF})_i - \frac{1}{N}\sum_j (I_{MF})_j| \leq \max_j |(I_{MF})_j|$ and $|(I_{MF})_i| < 2N\overline{\gamma}$, for all $i = 1, \ldots, N$, it results that $|\tilde{I}_{MF}| < 2\overline{\gamma}\sqrt{N}N$. By letting δ_ω be defined as in (3.29), from Theorem 3.4, the system is LISS, provided that $|\omega^\perp| + |\tilde{I}_{MF}| < |\omega^\perp| + 2\overline{\gamma}\sqrt{N}N \leq \delta_\omega$. □

3.7 Technical proofs

3.7.1 Proof of Claim 3.11

Consider the derivative of the incremental Lyapunov function V_I, defined in (3.15), along the trajectories of the incremental dynamics (3.5):

$$\begin{aligned}\dot{V}_I(\tilde{\theta}) &:= (\nabla_{\tilde{\theta}} V_I)^T \dot{\tilde{\theta}} \\ &= \sum_{i,j=1}^{N} E_{ij} \sin(\theta_j - \theta_i)(\dot{\theta}_j - \dot{\theta}_i) \\ &= -2 \sum_{i,j=1}^{N} E_{ij} \sin(\theta_j - \theta_i)\dot{\theta}_i,\end{aligned}$$

where the last equality comes from the fact that, since E is a symmetric matrix, $\sum_{i,j=1}^{N} E_{ij} \sin(\theta_j - \theta_i)\dot{\theta}_j = -\sum_{i,j=1}^{N} E_{ij} \sin(\theta_j - \theta_i)\dot{\theta}_i$. For the same reason it holds that $\overline{\omega} \sum_{i,j=1}^{N} E_{ij} \sin(\theta_j - \theta_i) = 0$. Since, from (3.1), $\dot{\theta}_i = \overline{\omega} + \tilde{\omega}_i + K \sum_{h=1}^{N} E_{ih} \sin(\theta_h - \theta_i)$, we get that

$$\begin{aligned}\dot{V}_I &= -2 \sum_{i=1}^{N} \left(\sum_{j=1}^{N} E_{ij} \sin(\theta_j - \theta_i) \right) \left(K \sum_{h=1}^{N} E_{ih} \sin(\theta_h - \theta_i) + \tilde{\omega}_i \right) \\ &= -2(K \nabla V^T \nabla V + \nabla V^T \tilde{\omega}),\end{aligned}$$

which proves the claim. □

3.7.2 Proof of Claim 3.12

From Claim 3.11 it holds that $\dot{V}_I = -2K|\chi|^2 - 2\chi^T \tilde{\omega} \leq -2K|\chi|^2 + 2|\chi||\tilde{\omega}|$. That is

$$|\chi| \geq \frac{2|\tilde{\omega}|}{K}, \quad \Rightarrow \quad \dot{V}_I \leq -K|\chi|^2. \tag{3.33}$$

In view of (3.24), $|\tilde{\omega}| \leq \delta'_\omega$ implies that $\sigma^{-1}\left(\frac{2|\tilde{\omega}|}{K}\right) \leq \delta_{\tilde{\theta}}$. Recalling that, for all $\tilde{\theta} \in \mathcal{B}(\phi_i, \delta_{\tilde{\theta}})$, $|\tilde{\theta}|_{\mathcal{F}} = |\tilde{\theta} - \phi_i|$, it results that

$$|\tilde{\theta} - \phi_i| \geq \sigma^{-1}\left(\frac{2|\tilde{\omega}|}{K}\right) \quad \Rightarrow \quad |\chi| \geq \frac{2|\tilde{\omega}|}{K}. \tag{3.34}$$

Since (3.21) ensures that $-|\chi|^2 \leq -\sigma^2(|\tilde{\theta} - \phi_i|)$, at the light of (3.33) and (3.34), it results that

$$|\tilde{\theta} - \phi_i| \geq \sigma^{-1}\left(\frac{2|\tilde{\omega}|}{K}\right) \quad \Rightarrow \quad \dot{V}_I \leq -K\sigma^2(|\tilde{\theta} - \phi_i|).$$

3.7.3 Proof of Claim 3.13

In the case of all-to-all coupling, the vector χ defined in Claim 3.11 reads

$$\chi(\tilde{\theta}) = \left[\sum_{j=1}^{N} \sin(\theta_j - \theta_i) \right]_{i=1,\ldots,N}.$$

Therefore, the norm inequality $|\tilde{\theta}|_2 \geq |\tilde{\theta}|_\infty$ implies

$$|\chi(\tilde{\theta})|_2 \geq \max_{i=1,\dots,N} \left| \sum_{j=1}^{N} \sin(\theta_j - \theta_i) \right|.$$

Now, since $\tilde{\theta} \in \mathcal{D}_0$, we have $|\theta_i - \theta_j| \leq \frac{\pi}{2}$, which implies that the phases of all oscillators belong to the same quarter of circle. We can thus renumber the indexes of the oscillator phases in such a way that $\theta_i \leq \theta_j$ whenever $i < j$.

First step — For a given $\tilde{\theta}$, in order to find a tight lower bound on $|\chi(\tilde{\theta})|_2$, we are going to show that

$$\max_{i=1,\dots,N} \left| \sum_{j=1}^{N} \sin(\theta_j - \theta_i) \right| = \max \left\{ \sum_{j=1}^{N} \sin|\theta_j - \theta_1|, \sum_{j=1}^{N} \sin|\theta_j - \theta_N| \right\}. \tag{3.35}$$

On the one hand, for all $j = 1, \dots, N$, we have $0 \leq \theta_j - \theta_1 \leq \frac{\pi}{2}$ and $0 \leq \theta_N - \theta_j \leq \frac{\pi}{2}$. It follows that

$$\left| \sum_{j=1}^{N} \sin(\theta_j - \theta_1) \right| = \sum_{j=1}^{N} \sin|\theta_j - \theta_1|, \tag{3.36}$$

and

$$\left| \sum_{j=1}^{N} \sin(\theta_j - \theta_N) \right| = \sum_{j=1}^{N} \sin|\theta_j - \theta_N|. \tag{3.37}$$

On the other hand, for any $i \in \{1, N\}$, we have that, for any $j < i$, $0 \leq \theta_i - \theta_j \leq \frac{\pi}{2}$; while, for any $j > i$, $0 \leq \theta_j - \theta_i \leq \frac{\pi}{2}$. That is

$$\left| \sum_{j=1}^{N} \sin(\theta_j - \theta_i) \right| = \left| \sum_{j=i+1}^{N} \sin|\theta_j - \theta_i| - \sum_{j=1}^{i-1} \sin|\theta_j - \theta_i| \right|.$$

Now, for all $\tilde{\theta} \in \mathcal{D}_0$, if $i > j$, then $|\theta_j - \theta_i| \leq |\theta_j - \theta_N|$, while, if $i < j$, then $|\theta_j - \theta_i| \leq |\theta_j - \theta_1|$. Hence, for all $\tilde{\theta} \in \mathcal{D}_0$,

$$\sum_{j=1}^{i-1} \sin|\theta_j - \theta_i| \leq \sum_{j=1}^{N} \sin|\theta_j - \theta_N|, \quad \forall i \in \{1, N\},$$

and

$$\sum_{j=i+1}^{N} \sin|\theta_j - \theta_i| \leq \sum_{j=1}^{N} \sin|\theta_j - \theta_1|, \quad \forall i \in \{1, N\}.$$

Recalling that, for all $a, b \geq 0$, $|a - b| \leq \max\{a, b\}$, it then follows that, for any $i \in \{1, N\}$,

$$\begin{aligned} \left| \sum_{j=1}^{N} \sin(\theta_j - \theta_i) \right| &\leq \max \left\{ \sum_{j=1}^{i-1} \sin|\theta_j - \theta_i|, \sum_{j=i+1}^{N} \sin|\theta_j - \theta_i| \right\} \\ &\leq \max \left\{ \sum_{j=1}^{N} \sin|\theta_j - \theta_1|, \sum_{j=1}^{N} \sin|\theta_j - \theta_N| \right\}. \end{aligned} \tag{3.38}$$

Therefore, combining (3.36), (3.37), and (3.38), we obtain (3.35), which ends the first step of the proof.

Second step — Using the fact that $\sin z \geq \frac{2}{\pi} z$, for all $z \in \left[0, \frac{\pi}{2}\right]$, Equation (3.35) yields

$$\begin{aligned} |\chi(\tilde{\theta})|_2 &\geq \max\left\{\sum_{j=1}^{N} \sin|\theta_j - \theta_1|, \sum_{j=1}^{N} \sin|\theta_j - \theta_N|\right\} \\ &\geq \frac{2}{\pi} \max\left\{\sum_{j=1}^{N} |\theta_j - \theta_1|, \sum_{j=1}^{N} |\theta_j - \theta_N|\right\} \\ &\geq \frac{2}{\pi} \max\left\{\sum_{j=1}^{N} (\theta_j - \theta_1), \sum_{j=1}^{N} (\theta_N - \theta_j)\right\}. \end{aligned}$$

Or, equivalently, by defining $\delta := \theta_N - \theta_1$, with $0 \leq \delta \leq \frac{\pi}{2}$,

$$|\chi(\tilde{\theta})|_2 \geq \frac{2}{\pi} \max\left\{\sum_{j=1}^{N} (\theta_j - \theta_1), \sum_{j=1}^{N} [\delta - (\theta_j - \theta_1)]\right\}. \tag{3.39}$$

For notation purposes, define $I_{\tilde{\theta}} := [0, \delta]^{N-2}$, $x_i := \theta_{i+1} - \theta_1$, for all $i = 1, \ldots, N-2$, and $x := [x_i]_{i=1,\ldots,N-2} \in I_{\tilde{\theta}}$. Then

$$\begin{aligned} \max\left\{\sum_{j=1}^{N} (\theta_j - \theta_1), \sum_{j=1}^{N} [\delta - (\theta_j - \theta_1)]\right\} &= \max\left\{\delta + \sum_{i=1}^{N-2} x_i,\ \delta + \sum_{i=1}^{N-2} (\delta - x_i)\right\} \\ &= \delta + \max\left\{\sum_{i=1}^{N-2} x_i,\ \sum_{i=1}^{N-2} (\delta - x_i)\right\}. \end{aligned} \tag{3.40}$$

In order to obtain the desired bound, we minimize the function $f : I_{\tilde{\theta}} \to \mathbb{R}_{\geq 0}$, defined by $f(x) := \max\left\{\sum_{i=1}^{N-2} x_i,\ \sum_{i=1}^{N-2} (\delta - x_i)\right\}$. Define the functions

$$a(x) := \sum_{i=1}^{N-2} x_i \quad \text{and} \quad b(x) := \sum_{i=1}^{N-2} (\delta - x_i),$$

and the sets

$$\begin{aligned} A &:= \{x \in I_{\tilde{\theta}} :\ a(x) > b(x)\} \\ B &:= \{x \in I_{\tilde{\theta}} :\ b(x) > a(x)\} \\ C &:= \{x \in I_{\tilde{\theta}} :\ a(x) = b(x)\}. \end{aligned}$$

It then results that $I_{\tilde{\theta}} = A \cup B \cup C$, with $A \cap B = B \cap C = C \cap A = \emptyset$. Observe, moreover, that we obviously have $f|_A = a|_A$ and $f|_B = b|_B$. By the fact that, for all $x \in C$, $\sum_{i=1}^{N-2} x_i = \sum_{i=1}^{N-2} (\delta - x_i)$, we have

$$f(x) = a(x) = b(x) = \frac{N-2}{2}\delta, \quad \forall x \in C. \tag{3.41}$$

Moreover, since $b(x) = (N-2)\delta - a(x)$, it results that

$$a(x) > \frac{N-2}{2}\delta, \quad \forall x \in A,$$

and

$$b(x) > \frac{N-2}{2}\delta, \quad \forall x \in B.$$

That is, since $f|_A = a|_A$, $f|_B = b|_B$, and $A \cup B = I_{\tilde{\theta}} \setminus C$,

$$f(x) > \frac{N-2}{2}\delta, \quad \forall x \in I_{\tilde{\theta}} \setminus C.$$

From (3.41), this also implies that, for all $x \in I_{\tilde{\theta}}$,

$$f(x) \geq \frac{N-2}{2}\delta. \tag{3.42}$$

From (3.39), (3.40), and (3.42), we obtain

$$|\chi(\tilde{\theta})|_2 \geq \frac{2}{\pi}\left(\delta + \frac{N-2}{2}\delta\right) = \frac{N}{\pi}\delta.$$

Finally, recalling that $\delta = |\tilde{\theta}|_\infty$, by the norm inequality $|\tilde{\theta}|_\infty \geq \frac{|\tilde{\theta}|_2}{N-1}$, we conclude that, for all $\tilde{\theta} \in \mathcal{D}_0$,

$$|\chi(\tilde{\theta})|_2 \geq \frac{N}{\pi(N-1)}|\tilde{\theta}|_2 \geq \frac{|\tilde{\theta}|_2}{\pi},$$

which proves the claim.

3.7.4 Proof of Claim 3.14

Since we want to prove that $|\tilde{\theta}|_2 \leq \sqrt{N}\delta \;\Rightarrow\; |\tilde{\theta}|_\infty \leq \delta$, we are going to prove that $|\tilde{\theta}|_\infty \geq \delta \;\Rightarrow\; |\tilde{\theta}|_2 \geq \sqrt{N}\delta$. It is enough to show that, for all $\delta \in [0, \pi]$,

$$|\tilde{\theta}|_\infty = \delta \quad \Rightarrow \quad |\tilde{\theta}|_2 \geq \sqrt{N}\delta. \tag{3.43}$$

Indeed, given $\delta' \geq \delta$, (3.43) implies that, if $|\tilde{\theta}|_\infty = \delta' \geq \delta$, then $|\tilde{\theta}|_2 \geq \sqrt{N}\delta' \geq \sqrt{N}\delta$. In order to prove (3.43) we minimize the Euclidean norm $|\tilde{\theta}|_2$ (or, equivalently, $|\tilde{\theta}|_2^2$), with the constraint that $|\tilde{\theta}|_\infty = \delta$. For the sake of simplicity, renumber the oscillator phases indexes in such a way that $\theta_i \leq \theta_j$ whenever $i < j$, as in the proof of Claim 3. The problem can then be translated into minimizing $|\tilde{\theta}|_2^2$, with the constraint that $\theta_N - \theta_1 = \delta$. Since the square of the Euclidean norm and the constrained function are smooth, we can apply the method of Lagrange multipliers[2]. That is, we can find critical points of $|\tilde{\theta}|_2^2$, under the constraint $\theta_N - \theta_1 = \delta$, by solving the set of equations

$$\frac{\partial}{\partial \theta_i}F(\theta, \lambda) = 0, \; i = 1, \ldots, N, \tag{3.44}$$

$$\frac{\partial}{\partial \lambda}F(\theta, \lambda) = 0, \tag{3.45}$$

where $F(\theta, \lambda) := \sum_{i,j=1}^{N}(\theta_i - \theta_j)^2 - \lambda(\theta_N - \theta_1 - \delta)$, and $\lambda \in \mathbb{R}$ is the *Lagrange multiplier*. (3.44) gives, for $i \in \{1, N\}$, gives

$$\sum_{j=1}^{N}(\theta_i - \theta_j) = 0. \tag{3.46}$$

[2]We present a brief recall of this method in Appendix A on page 67

While (3.45) gives the constraint $\theta_N - \theta_1 = \delta$. In addition, (3.44) gives, for $i = 1$, $4\sum_{j=1}^{N}(\theta_1 - \theta_j) + \lambda = 0$, and, for $i = N$, $4\sum_{j=1}^{N}(\theta_N - \theta_j) - \lambda = 0$,. By solving with respect to λ, we get

$$\sum_{j=1}^{N}(\theta_1 - \theta_j) + \sum_{j=1}^{N}(\theta_N - \theta_j) = 0. \tag{3.47}$$

Equations (3.46)-(3.47), with the constraint $\theta_N - \theta_1 = \delta$, admit a unique solution, modulo a common phase shift among the ensemble (*i.e* $\theta_i \to \theta_i + \alpha$ for all i):

$$\theta_i^* - \theta_j^* = 0, \quad \forall (i,j) \notin \{(1,N),(N,1)\}, \tag{3.48a}$$

$$\theta_i^* - \theta_1^* = \frac{\delta}{2},\ \theta_i^* - \theta_N^* = -\frac{\delta}{2},\ \forall i \notin \{1,N\}. \tag{3.48b}$$

By computing the Hessian of F with respect to the vector $(\tilde{\theta}^T, \lambda)^T$, it is easy to show that its symmetric part is positive semidefinite for all $(\tilde{\theta}^T, \lambda)^T$. Hence the solution (3.48) corresponds to a minimum. To show the uniqueness of this critical point, modulo a common phase shift, note that the set of equations (3.44) can be rewritten as the linear system

$$G\theta := \begin{pmatrix} N-1 & -1 & \dots & -1 & -1 \\ -1 & N-1 & \dots & -1 & -1 \\ \vdots & \vdots & \ddots & \vdots & \vdots \\ -1 & -1 & \dots & N-1 & -1 \\ -1 & -1 & \dots & -1 & N-1 \\ -1 & 0 & \dots & 0 & 1 \end{pmatrix} \begin{pmatrix} \theta_1 \\ \theta_2 \\ \vdots \\ \theta_{N-2} \\ \theta_{N-1} \\ \theta_N \end{pmatrix} \tag{3.49}$$

$$= \begin{pmatrix} \frac{\lambda}{4} \\ 0 \\ \vdots \\ 0 \\ -\frac{\lambda}{4} \\ \delta \end{pmatrix}. \tag{3.50}$$

The matrix $G \in \mathbb{R}^{(N+1)\times N}$ has rank $N-1$, since the minor given by the first N rows is the Laplacian matrix associated to a complete graph, which has rank $N-1$. In particular, it holds that $G\mathbf{1}_N = 0$. Hence the solution to (3.49) is of the form $\theta^* = \theta_\perp^* + \alpha\mathbf{1}_N,\ \alpha \in \mathbb{R}$, where $\theta_\perp^*$ belongs to the ortogonal space to $\mathbf{1}_N$, and is uniquely determined by (3.49). This confirms that the solution (3.48) is unique, modulo a common phase shift. We can then conclude that, if $|\tilde{\theta}|_\infty = \delta$, then

$$\begin{aligned} |\tilde{\theta}|_2^2 &\geq \sum_{i,j=1}^{N}(\theta_i^* - \theta_j^*)^2 \\ &\geq 2\delta^2 + 2\sum_{j=2}^{N-2}\frac{\delta^2}{4} + 2\sum_{j=2}^{N-2}\frac{\delta^2}{4} \\ &\geq N\delta^2, \end{aligned}$$

which proves the claim. □

Appendix A - Lagrange Multipliers

An extremum of a continuously differentiable function $f : \mathbb{R}^n \to \mathbb{R}$, under the constraints $g_i(x) = b_i$, $i = 1, \ldots, m$, where $g_i : \mathbb{R}^n \to \mathbb{R}$ is continuously differentiable, and $b_i \in \mathbb{R}$ belongs to the image of g_i, for all $i = 1, \ldots, m$, can be found by constructing the Lagrangian function F through the Lagrangian multipliers λ_i, $i = 1, \ldots, m$,

$$F(x, \lambda_1, \ldots, \lambda_m) = f(x) - \sum_{i=1}^{m} \lambda_i (g_i(x) - b_i)$$

and by solving the set of equations

$$\frac{\partial}{\partial x_i} F(x, \lambda_1, \ldots, \lambda_m) = 0,$$

$$\frac{\partial}{\partial \lambda_j} F(x, \lambda_1, \ldots, \lambda_m) = 0,$$

for all $i = 1, \ldots, n$ and all $j = 1, \ldots, m$. The optimal value x^*, is found together with the vector of Lagrangian multipliers $\lambda^* = (\lambda_1^*, \ldots, \lambda_m^*)$. See for example (Bliss, 1947).

Chapter 4

Oscillation inhibition via mean-field feedback

Chapters 2 and 3 are mainly concerned with the analysis of network of oscillators under the effect of a closed-loop control signal. They show that no oscillating phase-locked solution can co-exist with the presence of a mean-field feedback (Theorem 2.2). Yet, we have seen that if the feedback gain is too small, the system may converge to an almost phase-locked oscillating solution, still corresponding to a pathological state (Theorem 3.4). In this chapter we investigate a first control goal that can be effectively achieved via closed-loop stimulation of oscillators population.

More precisely, we work under the assumption that the pathological synchronization characterizing neuronal populations in Parkinson's disease can be eliminated by inhibiting the global oscillation. In other words, our aim here is to use the DBS signal to *inactivate* STN neurons, meaning that the stimulation acts by impeding pathological bursting and spiking (Filali et al., 2004). Such an approach basically results as a functional lesion of the STN. This hypothesis is also supported by the fact that, before the invention of DBS, the surgical PD treatment consisted in an ablation of the cerebral zone under concern (Jankovic et al., 1995; Benabid et al., 1996), which corresponds to a radical neuronal inhibition.

The aim of this chapter is thus to provide some insights on how the collective oscillation of a network of nonlinear oscillators, modeling a neuronal population, can be inhibited by proportional feedback when only its average behavior is measured. We rely on the simplified neuron model derived in Chapter 2 to provide preliminary theoretical justifications on how mean-field feedback DBS may yield neuronal inhibition in the STN. We show that for sufficiently small natural frequencies the closed-loop system exhibits a set of almost globally asymptotically stable fixed points, which corresponds to an effective oscillation inhibition. In the case of zero natural frequencies, the feedback signal is vanishing on the stable set, and remains small for small natural frequencies, thus assuring an efficient energy policy of the proposed stimulation signal.

The analysis relies on a gradient dynamics approach. We develop an extensive analysis of the critical sets of the potential function, and completely characterize their stability. The presence of non-isolated equilibria makes the stability analysis rather tricky and tools from invariant normally hyperbolic manifolds theory are used in order to obtain global results. The situation is more involved in the case when the number of oscillators is even, in which case the set of non-isolated critical points is not globally a manifold.

The chapter is structured as follows. In Section 4.1 we recall the mathematical form of the system under studies. In Section 4.2 we consider the ideal case of zero natural frequencies and

homogeneous coupling and feedback gains, and develop an extensive fixed-point and convergence analysis. In Section 4.4, we use the result obtained in Section 4.2 to derive conclusions in the general case of non-zero natural frequencies and heterogeneous gains. The proofs of the main results are provided in Section 4.5, technical proofs are given in Section 4.6.

4.1 Problem formulation

In the following, we consider the Kuramoto system under mean-field feedback (2.6), and let

$$k_0 := \frac{1}{N^2} \sum_{i,j=1}^{N} k_{ij}$$

be the mean of the coupling strengths and

$$\gamma_0 := \frac{1}{N^2} \sum_{i,j=1}^{N} \gamma_{ij}$$

denote the mean of feedback gains. Define moreover the deviations

$$\tilde{k} := [k_{ij} - k_0]_{ij=1,\dots,N} \in \mathbb{R}^{N\times N}$$

and

$$\tilde{\gamma} := [\gamma_{ij} - \gamma_0]_{ij=1,\dots,N} \in \mathbb{R}^{N\times N}$$

of, respectively, the coupling strengths and feedback gains around their means. If the feedback gain γ_0 can be picked in such a way that $\gamma_0 = -k_0$, then (2.6) can be rewritten as

$$\dot{\theta}_i \;=\; k_0 \sum_{j=1}^{N} \sin(\theta_i + \theta_j) + f_i^{\eta}(\theta), \quad \forall i = 1, \dots, N\,. \tag{4.1}$$

where the vector function

$$f^{\eta}(\theta) := \left[\omega_i + \sum_{j=1}^{N} (\tilde{k}_{ij} + \tilde{\gamma}_{ij}) \sin(\theta_j - \theta_i) - \sum_{j=1}^{N} \tilde{\gamma}_{ij} \sin(\theta_j + \theta_i) \right]_{i=1,\dots,N}, \tag{4.2}$$

is parametrized by the matrix

$$\eta := (\omega, \tilde{k}, \tilde{\gamma}) \in \mathbb{R}^{N\times(1+2N)}. \tag{4.3}$$

In this particular situation, one intuitively expects that, if f^{η} is small, then the synchronization of the network of oscillators is compromised, yielding either an oscillating desynchronized state or the end of oscillations. Numerical simulations support these expectations. They reveal that, when f^{η} is small compared to the coupling strength k_0, mean-field feedback inhibits oscillations when γ_0 is picked as $-k_0$: the phase of each oscillator goes to a fixed point (cf. Fig. 4.1 left, in which the feedback is activated at $t = 4$), thus eventually stopping oscillations. On the contrary, when f^{η} is large with respect to the coupling strength k_0, the use of a mean-field feedback with gain $\gamma_0 = -k_0$ desynchronizes the network (cf. Fig. 4.2 left). This problem is addressed in Chapter 5. We stress that the choice $\gamma_0 = -k_0$ implies that the feedback gain is small provided that the original diffusive coupling is small, thus ensuring, in accordance with Assumption 1, the persistence of the oscillators limit cycle attractors in (2.3). The numerical simulations in Figures 4.1(left) and 4.2(left) illustrate this behavior. They show that, even if

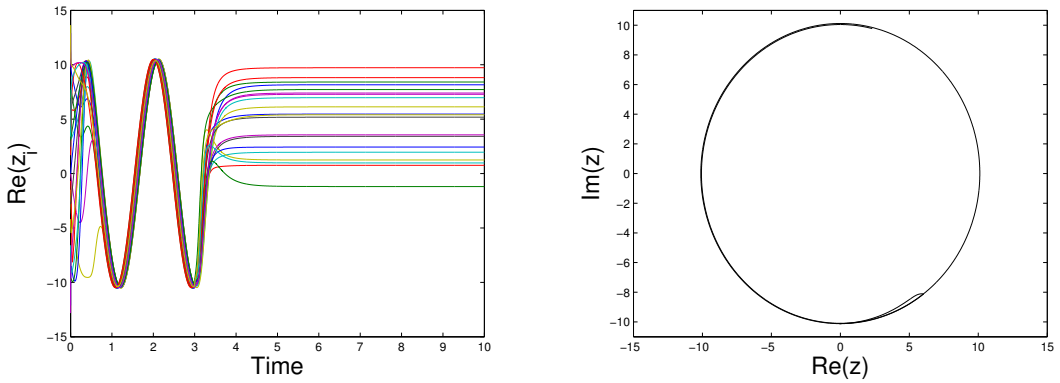

FIGURE 4.1: Small natural frequencies: oscillations inhibition.

the oscillations are blocked or desynchronized, the single oscillators remain near the original limit cycles, where the phase approximation is valid. More precisely, if the coupling strength $|\kappa|$, where the matrix $\kappa \in \mathbb{R}^{N\times N}$ is defined as in (2.4), is sufficiently small that the small coupling condition (2.4) is satisfied, *i.e.* $|\kappa| < \delta_h$, then the choice $\gamma_0 = -k_0$ automatically ensures that the same condition is satisfied for the closed-loop system. To summarize, the analysis contained in this chapter extends to the full dynamics (2.3), provided that the open-loop diffusive coupling strength is sufficiently small. The reader is referred to Appendix A for more details.

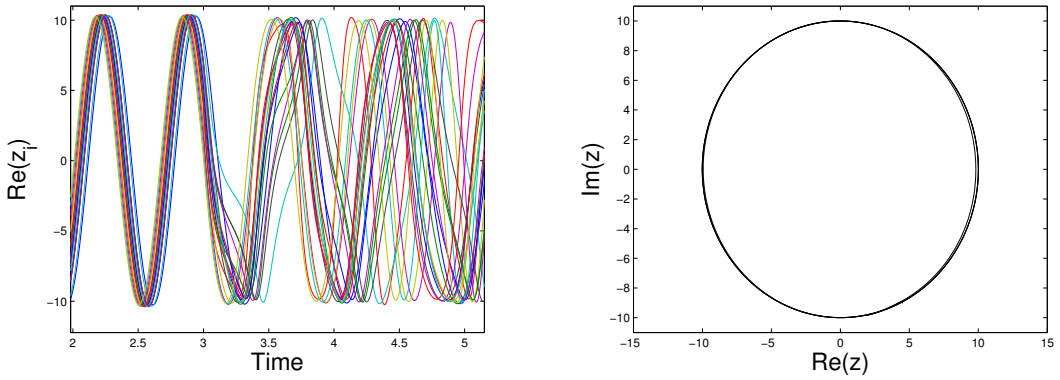

FIGURE 4.2: Large natural frequencies: desynchronization.

Robust oscillation inhibition can be formalized as the existence of an (almost globally) attractive set of fixed points for (4.1). In order to develop an existence and stability analysis of such a set, we start by identifying the fixed points of (4.1) and study their nature in the fictitious case $f^\eta \equiv 0$. Stability properties in the general case (*i.e.* in presence of f^η with sufficiently small amplitude) are derived as a second step, by relying on robustness arguments.

In the remainder of this chapter we lift the oscillators phases from T^N to $\mathbb{R}^N$. This is necessary in view of the gradient analysis developed for $f^\eta \neq 0$. As detailed in Section 4.4, in this case, (4.1) defines a gradient dynamics on $\mathbb{R}^N$, but not necessarily on T^N. We stress that the derived results are independent of this choice, since the 2π-periodicity of the vector field in (4.1) allows to project the lifted vector field, and the associated trajectories, back to the N-torus.

4.2 The case of zero natural frequencies

When $f^\eta \equiv 0$, *i.e.* when the natural frequencies are zero and the coupling is all-to-all, (4.1) reduces to

$$\dot{\theta}_i \;=\; k_0 \sum_{j=1}^{N} \sin(\theta_i + \theta_j), \quad \forall i = 1, \dots, N\,. \tag{4.4}$$

We note that (4.4) can equivalently be written as the gradient system

$$\dot{\theta}_i = -\frac{\partial W}{\partial \theta_i}(\theta), \quad \forall i = 1, \dots, N\,,$$

where the potential function W is given, for all $\theta \in \mathbb{R}^N$, by

$$W(\theta) := -k_0 \sum_{i,j=1}^{N} \sin^2\left(\frac{\theta_i + \theta_j}{2}\right). \tag{4.5}$$

4.2.1 Fixed points identification

We start by computing the fixed points of (4.4) or, equivalently, the critical points of its potential function (4.5). To that aim, we define the following set:

$$\begin{aligned} A_0 \;:=\; \Big\{ & \theta \in \mathbb{R}^N : \theta_i = \frac{\pi}{2} \bmod 2\pi \;\; \forall i \in \mathcal{I}_{\frac{\pi}{2}}\,, \theta_i = \frac{3\pi}{2} \bmod 2\pi \;\; \forall i \in \mathcal{I}_{\frac{3\pi}{2}}, \\ & \mathcal{I}_{\frac{\pi}{2}} \cup \mathcal{I}_{\frac{3\pi}{2}} = \{1, \dots, N\},\; \#\mathcal{I}_{\frac{\pi}{2}} \neq \#\mathcal{I}_{\frac{3\pi}{2}} \Big\}\,. \end{aligned} \tag{4.6}$$

That is, A_0 is made of all the vectors $\theta \in \mathbb{R}^N$ whose components are either $\pi/2$ or $3\pi/2$ (modulo 2π), and for which the number of $\pi/2$ entries is different from the number of $3\pi/2$ entries. In the same way, we define

$$\begin{aligned} B_0 \;:=\; \big\{ & \theta \in \mathbb{R}^N : \theta_i = 0 \bmod 2\pi \;\; \forall i \in \mathcal{I}_0\,, \theta_i = \pi \bmod 2\pi \;\; \forall i \in \mathcal{I}_\pi, \\ & \mathcal{I}_0 \cup \mathcal{I}_\pi = \{1, \dots, N\},\; \#\mathcal{I}_0 \neq \#\mathcal{I}_\pi \big\}\,. \end{aligned} \tag{4.7}$$

In other words, all the vectors of B_0 are made only with 0 and π elements, and the number of their π's differ from the number of their 0's. Finally, we introduce

$$\mathcal{N} := \left\{ \theta \in \mathbb{R}^N : \sum_{i=1}^{N} \sin(\theta_i) = \sum_{i=1}^{N} \cos(\theta_i) = 0 \right\}. \tag{4.8}$$

The following lemma, whose proof is given in Section 4.5.1, shows that A_0, B_0 and $\mathcal{N}$ completely characterize the fixed points of (4.4).

Lemma 4.1. *Given any $k_0 > 0$, the set F_0 of fixed points of (4.4) is given by the disjoint union $F_0 = A_0 \cup B_0 \cup \mathcal{N}$, where $A_0, B_0, \mathcal{N}$ are given in (4.6)-(4.8). That is the sets $A_0, B_0, \mathcal{N}$ form a partition of F_0.*

Lemma 4.1 states in particular that the critical points of W can be divided into two families. The critical points contained in the sets A_0 and B_0 are *isolated* by their definitions (4.6)-(4.7). Their stability can then be easily studied by analyzing the sign definiteness of the Hessian of W at these points. This will be achieved by Lemma 4.2. On the contrary, as we show in the sequel, the fixed points belonging to $\mathcal{N}$ are not isolated. Noticing that $\mathcal{N}$ is defined as a level

set of the function $\theta \mapsto (\sum_{i=1}^{N} \sin(\theta_i), \sum_{i=1}^{N} \cos(\theta_i))^T$, we argue that, at least locally, it is an embedded submanifold. Its stability can then be analyzed through the linearization of (4.4) on the orthogonal subspace of this submanifold. This will be achieved by Lemma 4.3.

4.2.2 Analysis of isolated equilibria

In the following lemma, proved in Section 4.5.2, we address the stability of the fixed points of (4.4) belonging to $A_0 \cup B_0$.

Lemma 4.2. *Let k_0 be any given positive constant. Let W be defined in (4.5), and let*

$$\mathcal{W}_m := \left\{\theta \in \mathbb{R}^N : \theta = \left(\frac{\pi}{2} \ mod \ \pi\right) \mathbf{1}_N\right\} \tag{4.9a}$$

$$\mathcal{W}_M := \left\{\theta \in \mathbb{R}^N : \theta = (0 \ mod \ \pi) \, \mathbf{1}_N\right\} . \tag{4.9b}$$

Then the following holds true:

a) $\mathcal{W}_m$ contains all global minima of W and its points are hyperbolically asymptotically stable for (4.4).

b) $\mathcal{W}_M$ contains all global maxima of W and all its points are hyperbolically unstable for (4.4).

c) All the critical points of W, which are not global extrema, that is all the points in $(A_0 \cup B_0) \setminus (\mathcal{W}_m \cup \mathcal{W}_M)$ where A_0 and B_0 are defined in (4.6)-(4.7), are hyperbolic saddles for (4.4).

We stress that the points belonging to the two sets $\mathcal{W}_m$ and $\mathcal{W}_M$ are multiples of the vector $\mathbf{1}_N$. Thus, for those points, the oscillator phases are all equal. More precisely, points belonging to $\mathcal{W}_m$ are characterized either by all the phases being equal to $\frac{\pi}{2}$ or by all the phases being equal to $-\frac{\pi}{2}$, modulo rotations of 2π. For instance, the vector $(\frac{\pi}{2}, \frac{\pi}{2}, \frac{\pi}{2})$ belongs to $\mathcal{W}_m$, whereas the vector $(\frac{\pi}{2}, \frac{\pi}{2}, -\frac{\pi}{2})$ does not. Similarly for $\mathcal{W}_M$.

4.2.3 Analysis of non-isolated equilibria

The following lemma, whose proof is given in Section 4.5.3, characterizes the non-isolated critical points of the function W, *i.e.* those contained in $\mathcal{N}$.

Lemma 4.3. *Let k_0 be any positive constant and let $\mathcal{N}$ be defined in (4.8). Then, the following holds true:*

a) If N is odd, $\mathcal{N}$ is an embedded submanifold of codimension 2 that is normally hyperbolic[1] for (4.4). In particular, for all $\theta \in \mathcal{N}$, the eigenvalues $\lambda_-(\theta), \lambda_+(\theta)$ of the linearization of (4.4) restricted to the orthogonal directions to $\mathcal{N}$ are such that $\lambda_-(\theta) < 0 < \lambda_+(\theta)$.

b) If N is even, there exists a normally hyperbolic submanifold $\tilde{\mathcal{N}}$ of codimension 2, and 2^N one-dimensional submanifolds $\mathcal{N}_{0i}$, $i = 1, \ldots, 2^N$, such that $\mathcal{N} = \tilde{\mathcal{N}} \cup \bigcup_{i=1}^{2^N} \mathcal{N}_{0i}$. Moreover, for all $\theta \in \tilde{\mathcal{N}}$, the eigenvalues $\lambda_-(\theta), \lambda_+(\theta)$ of the linearization of (4.4) restricted to the orthogonal directions to $\tilde{\mathcal{N}}$ are such that $\lambda_-(\theta) < 0 < \lambda_+(\theta)$, and, for all $i = 1, \ldots, 2^N$, the stable set of $\mathcal{N}_{0i}$ is contained in a submanifold $\mathcal{N}_{0i}^s$ of dimension $\frac{N}{2}$.

[1] An invariant embedded submanifold is normally hyperbolic for a given vector field, if the linearization on its orthogonal subspace is hyperbolic and dominates the tangent behavior. We refer the reader to (Hirsch et al., 1977) for a rigorous introduction to this and related concepts.

Lemma 4.3 states in particular that locally around almost all points θ in $\mathcal{N}$, the dynamics (4.4) can be decomposed in three behaviors: the null behavior tangent to $\mathcal{N}$; the convergent behavior toward $\mathcal{N}$ along the eigenvector associated to $\lambda_-(\theta)$; and the divergent behavior away from $\mathcal{N}$ along the eigenvector associated to $\lambda_+(\theta)$. In the even case, the set $\mathcal{N}$ cannot be globally described as a normally hyperbolic submanifold, due to the presence of the singularities $\mathcal{N}_{0i}$, where the equation

$$\sum_{i=1}^{N} \sin(\theta_i) = \sum_{i=1}^{N} \cos(\theta_i) = 0$$

loses rank. Interestingly, the set $\mathcal{N}$ coincides with the set of non-isolated unstable points of the all-to-all Kuramoto system with all identical natural frequencies (Sepulchre et al., 2007).

4.3 Convergence to the global minima

We have all the ingredients to prove the almost global asymptotic stability of the set of the global minima of W.

Proposition 4.4. *Given any $k_0 > 0$, the set $\mathcal{W}_m$ defined in (4.9a) is almost globally asymptotically stable for the dynamics (4.4).*

Proposition 4.4, whose proof is provided in Section 4.5.4, states that, when neglecting the natural frequencies of the oscillators, the choice $\gamma_0 = -k_0$ of the mean-field feedback gain yields oscillation inhibition for almost all initial conditions, that is the oscillators phases converge almost globally toward an asymptotically stable configuration.

We point out that the output of the system (2.2), defined as

$$y = \sum_{j=1}^{N} \mathrm{Re}(z_j), \qquad z_j = r_j e^{\mathrm{i}\theta_j},\ j = 1, \dots, N, \tag{4.10}$$

where $r_j > 0$ is the radius of the oscillator j (cf. Assumption 1), and thus the applied proportional mean-field feedback, is vanishing on $\mathcal{W}_m$. This fact is of crucial importance in the DBS practice, where inputs magnitude and energy consumption are critical medical issues. See Section 1.1.2.

We point out that the effect of a robust oscillations inhibition is peculiar to the presence of mean-field feedback. In the absence of mean-field feedback, the diffusive coupling of the standard Kuramoto dynamics is invariant with respect to global phase-shifts, commonly denoted as T^1-symmetry[2]. The presence of this symmetry lets the diffusive coupling be ineffective for oscillations inhibition. The T^1 symmetry is indeed associated to a zero eigenvalue of the dynamics with eigenvector $\mathbf{1}_N$ and any nonzero additive constant perturbation of the form $\varpi \mathbf{1}_N$, makes an originally non-oscillating phase-locked solution oscillate with frequency $\varpi \neq 0$.

4.4 The perturbed case $f^\eta \not\equiv 0$

In Section 4.2 we have identified and characterized all the fixed points of (4.4) in the case of zero natural frequencies and all-to-all coupling and feedback, *i.e.* $f^\eta \equiv 0$. We can now plug natural frequencies and coupling and feedback uncertainties back in as perturbations and derive global stability results in the general case $f^\eta \not\equiv 0$.

[2]This symmetry is indeed generated by the torus, when considered as a Lie group, rather than a geometrical space.

Also in the case when $f^\eta \not\equiv 0$, simple computations reveal that, if the dispersion matrices $\tilde{k}, \tilde{\gamma}$ are both symmetric, then (4.1) can be written as the gradient dynamics

$$\dot{\theta}_i = -\frac{\partial W_\eta}{\partial \theta_i}(\theta), \quad \forall i = 1, \dots, N\,,$$

where the perturbed potential function W_η is defined, for all $\theta \in \mathbb{R}^N$, by

$$W_\eta(\theta) := W(\theta) + F^\eta(\theta), \tag{4.11}$$

in which the function W is defined in (4.5) and, for all $\theta \in \mathbb{R}^N$,

$$F^\eta(\theta) := \sum_{i,j=1}^{N} \tilde{\gamma}_{ij} \sin^2\Big(\frac{\theta_i + \theta_j}{2}\Big) - \sum_{i,j=1}^{N} (\tilde{k}_{ij} + \tilde{\gamma}_{ij}) \sin^2\Big(\frac{\theta_j - \theta_i}{2}\Big) - \sum_{i=1}^{N} \omega_i \theta_i.$$

This observation results from the fact that, if $\tilde{k}_{ij} = \tilde{k}_{ji}$ and $\tilde{\gamma}_{ij} = \tilde{\gamma}_{ji}$, for all $i, j = 1, \dots, N$, then $-\frac{\partial F^\eta}{\partial \theta_i} = f_i^\eta$, for all $i = 1, \dots, N$.

Note that the potential function W_ω being not 2π periodic, (4.1) can be written as a gradient dynamics with W_ω as the potential function only when the oscillators phases are lifted to the real line.

4.4.1 Odd number of oscillators

Even though the perturbed potential function W_η is lower unbounded, we expect its local minima to be near the global minima of W and still almost globally asymptotically stable, provided that the perturbation f^η is sufficiently small. The following theorem confirms this expectation in the case when the number of oscillators is odd.

Theorem 4.5. *Let $N \in \mathbb{N}_{\geq 3}$ be odd and $\tilde{k}, \tilde{\gamma} \in \mathbb{R}^{N \times N}$ be symmetric. Then there exists $\delta > 0$ and a class $\mathcal{K}_\infty$ function ρ such that, if the matrix $\eta \in \mathbb{R}^{N \times (1+2N)}$, defined in (4.3), satisfies $|\eta| \leq \delta$, then there exists a set of isolated points $\mathcal{W}_m^\eta \subset \mathbb{R}^N$, satisfying*[3]

$$|\mathcal{W}_m^\eta|_{\mathcal{W}_m} \leq \rho(|\eta|), \tag{4.12}$$

where $\mathcal{W}_m$ is defined in (4.9a), which contains all the local minima of the perturbed potential function W_η. Moreover, $\mathcal{W}_m^\eta$ is almost globally attractive for (4.1), that is, for almost all $\theta_0 \in \mathbb{R}^N$, it holds that

$$\lim_{t \to \infty} |\theta(t; \theta_0)|_{\mathcal{W}_m^\eta} = 0.$$

Theorem 4.5, whose proof is provided below, thus formally establishes the possibility to inhibit oscillations in presence of non-zero natural frequencies and symmetric coupling and feedback uncertainties, at least when the number of oscillators is odd. Note that it guarantees, for almost all $\theta_0 \in \mathbb{R}^N$, that the solution of (4.1) satisfies

$$\limsup_{t \to \infty} |\theta(t; \theta_0)|_{\mathcal{W}_m} \leq \rho(|\eta|),$$

provided that $|\eta| \leq \delta$. Since the mean-field (4.10) is a continuous function which is zero on $\mathcal{W}_m$, this in turns ensures that the mean-field (and thus the applied feedback) is small provided that $|\eta|$ is small. In other words, neuronal inhibition can be achieved via proportional mean-field feedback with an efficient energy policy.

[3] $|\mathcal{W}_m^\eta|_{\mathcal{W}_m}$ denotes the distance between $\mathcal{W}_m$ and $\mathcal{W}_m^\eta$. See notation section for details.

A similar oscillation inhibition result is contained in (Ermentrout and Kopell, 1990). In that reference the authors consider a chain of phase oscillators, and a class of coupling functions that contains the sinusoidal additive coupling considered here as a special case. The result is the existence of a unique stable inhibited solution in the chain of oscillators, provided that the natural frequencies are sufficiently small. Theorem 4.5 complements this analysis, by focusing on a particular coupling function and considering a different interconnection topology. The nature of the derived results is also different. In (Ermentrout and Kopell, 1990), the authors do not exclude the presence of stable oscillating phase-locked solutions. Theorem 4.5, relying on a global gradient dynamics analysis, excludes the presence of any other limit set, except the critical points of the potential function.

4.4.2 Even number of oscillators

The result of Theorem 4.5 is limited to the case when N is odd. In this case the set of non-isolated fixed points $\mathcal{N}$ of the unperturbed system, *i.e.* with $f^\eta \equiv 0$, defines a normally hyperbolic invariant manifold (cf. Lemma 4.3). As seen in the previous subsection, the local analysis around this set can still be developed in the perturbed case by means of the normally hyperbolic invariant manifolds theory. On the contrary, in the even case, the set $\mathcal{N}$ is not a manifold, and no standard mathematical instruments are readily available to analyze its existence and stability under perturbations. The same situation is present, for example, in the standard Kuramoto system (cf. (Sepulchre et al., 2007, Section III)), and also for this system, despite numerical evidences, no results have yet been rigorously proved on the almost global convergence to a phase-locked state in the case of non-identical natural frequencies. Nonetheless, in the case $f^\eta \equiv 0$, Proposition 4.4 states the almost global asymptotic stability of the set of local minima of the potential function also in the even case. In the light of the results of Proposition 4.4 and Theorem 4.5 we conjecture the following result.

Conjecture 4.1. *The result of Theorem 4.5 holds also in the case when N is even.*

4.5 Main proofs

4.5.1 Proof of Lemma 4.1

The fixed points $\theta^* \in \mathbb{R}^N$ of (4.4) satisfy

$$\sum_{j=1}^{N} \sin(\theta_i^* + \theta_j^*) = 0\,, \quad \forall i = 1, \dots, N. \tag{4.13}$$

Using the trigonometric identity $\sin(\alpha+\beta) = \sin\alpha\cos\beta + \sin\beta\cos\alpha$, this condition can be rewritten as

$$\sin(\theta_i^*)a(\theta^*) + \cos(\theta_i^*)b(\theta^*) = 0\,, \quad \forall i = 1, \dots, N, \tag{4.14}$$

where, for all $\theta \in \mathbb{R}^N$,

$$a(\theta) := \sum_{j=1}^{N} \cos(\theta_j), \tag{4.15}$$

and

$$b(\theta) := \sum_{j=1}^{N} \sin(\theta_j). \tag{4.16}$$

We start by showing that the equation

$$\cos(\theta_i^*) = -\frac{a(\theta^*)}{b(\theta^*)}\sin(\theta_i^*),\ \forall i = 1,\dots,N, \tag{4.17}$$

with $a(\theta^*) \neq 0$ and $b(\theta^*) \neq 0$, admits no solution. Suppose indeed that (4.17) holds true. Then, by taking the sum over i of both sides of (4.17), we have

$$\sum_{i=1}^{N}\cos(\theta_i^*) \;=\; -\frac{a(\theta^*)}{b(\theta^*)}\sum_{i=1}^{N}\sin(\theta_i^*),$$

that is, by the definitions (4.15)-(4.16) of a and b,

$$\begin{aligned} a(\theta^*) &= -\frac{a(\theta^*)}{b(\theta^*)}b(\theta^*), \\ &= -a(\theta^*), \end{aligned}$$

which implies $a(\theta^*) = 0$ and thus contradicts the hypothesis.

Recalling (4.14)-(4.16), all the other solutions of (4.13) then necessarily belong to one of the following three sets:

$$\begin{aligned} \tilde{A}_0 &:= \{\theta \in \mathbb{R}^N :\ a(\theta) = 0,\ b(\theta) \neq 0, \cos(\theta_i) = 0,\ \forall i = 1,\dots,N\}, \\ \tilde{B}_0 &:= \{\theta \in \mathbb{R}^N :\ b(\theta) = 0,\ a(\theta) \neq 0, \sin(\theta_i) = 0,\ \forall i = 1,\dots,N\}, \\ \mathcal{N} &= \{\theta \in \mathbb{R} :\ a(\theta) = b(\theta) = 0\}, \end{aligned}$$

where $\mathcal{N}$ is defined in (4.8). To prove the lemma it remains to show that $\tilde{A}_0 = A_0$ and $\tilde{B}_0 = B_0$, where A_0 and B_0 are defined in (4.6) and (4.7) respectively.

Step 1: $\tilde{B}_0 = B_0$.
For all $i = 1,\dots,N$, $\sin(\theta_i) = 0$ implies that $\theta_i = 0 \mod \pi$. Hence, each point $\theta^* \in \tilde{B}_0$ has m_0 elements equal to 0 mod 2π and m_π elements equal to π mod 2π. The sets $\mathcal{I}_0$ and $\mathcal{I}_\pi$ in (4.7) can then be picked as the corresponding index sets, and it holds that $\#\mathcal{I}_0 = m_0$ and $\#\mathcal{I}_\pi = m_\pi$. The condition $a(\theta^*) \neq 0$ then imposes $m_0 \neq m_\pi$, that is $\#\mathcal{I}_0 \neq \#\mathcal{I}_\pi$. This shows that $\tilde{B}_0 \subset B_0$. The converse sense of the inclusion follows by similar reasonings, which establishes that $\tilde{B}_0 = B_0$.

Step 2: $\tilde{A}_0 = A_0$.
We omit the proof of this step, at is follows along the same line as Step 1.

4.5.2 Proof of Lemma 4.2

We start by computing the Hessian of W:

$$H(\theta) := \frac{\partial^2 W}{\partial \theta^2}(\theta).$$

Basic computations reveal that $H = [H_{ij}]_{i,j=1,\dots,N}$ with, for all $i, j = 1,\dots,N$,

$$H_{ii}(\theta) = -k_0(\cos(2\theta_i) + s_i(\theta)) \tag{4.18a}$$
$$H_{ij}(\theta) = -k_0\cos(\theta_i + \theta_j), \quad \forall\ i \neq j, \tag{4.18b}$$

where

$$s_i(\theta) := \sum_{j=1}^{N} \cos(\theta_i + \theta_j) \quad \forall i = 1, \ldots, N. \tag{4.19}$$

Item a): Global minima.
Noticing that $W(\theta) \geq -k_0 N^2$ for all $\theta \in \mathbb{R}^N$, the global minimum of W is attained when $\sin^2\left(\frac{\theta_i^* + \theta_j^*}{2}\right) = 1$, for all $i, j = 1, \ldots, N$, that is, $\theta^* = \left(\frac{\pi}{2} \bmod \pi\right) \mathbf{1}_N$. Recalling (4.9a), it follows that the set $\mathcal{W}_m$ contains all the global minima of W. On this set, it holds that $\cos(\theta_j^* + \theta_i^*) = -1$ for all $i, j = 1, \ldots, N$. Recalling the expression of the Hessian of W, given in (4.18), at the global minima we thus have

$$H|_{\mathcal{W}_m} = k_0\big(N I_N + \mathbf{1}_{N \times N}\big).$$

Since $H|_{\mathcal{W}_m}$ is symmetric diagonally dominant with strictly positive diagonal entries, all its eigenvalues are strictly positive (Horn and Johnson, 1985, Theorem 6.1.10), that is all the points of $\mathcal{W}_m$ are non-degenerate minima of W and thus hyperbolic asymptotically stable for (4.4).

Item b): Global maxima.
The proof of this item is omitted here as it follows along the same lines as for *Item a).*

Item c): Saddles.
In view of Lemma 4.1, after a reordering of the phase indexes, the points $\theta^* \in B_0 \setminus \mathcal{W}_M$ are such that

$$\theta_i = 0 \bmod 2\pi, \ \forall i = 1, \ldots, m_0,$$

and

$$\theta_i = \pi \bmod 2\pi, \ \forall i = m_0 + 1, \ldots, N,$$

where $m_0 \in \{1, \ldots, N\}$. Let $m_\pi := N - m_0$ and consider $i_0, i_0' \in \{1, \ldots, m_0\}$ and $i_\pi, i_\pi' \in \{m_0 + 1, \ldots, N\}$. Since

$$\cos(2\theta_{i_0}) = \cos(\theta_{i_0} + \theta_{i_0'}) = \cos(2\theta_{i_\pi}) = \cos(\theta_{i_\pi} + \theta_{i_\pi'}) = 1,$$

and

$$\cos(\theta_{i_0} + \theta_{i_0 \pi}) = -1,$$

basic computations from (4.18) reveal that, for all $\theta^* \in B_0 \setminus \mathcal{W}_M$, the Hessian of W has the form

$$H(\theta^*) = -k_0 \begin{bmatrix} A & \mathbf{1}_{m_0 \times m_\pi} \\ \mathbf{1}_{m_0 \times m_\pi}^\top & B \end{bmatrix}. \tag{4.20}$$

where $A \in \mathbb{R}^{m_0 \times m_0}$ and $B \in \mathbb{R}^{m_\pi \times m_\pi}$ are defined as

$$A := (m_0 - m_\pi) I_{m_0} + \mathbf{1}_{m_0 \times m_0} \tag{4.21}$$

$$B := (m_\pi - m_0) I_{m_\pi} + \mathbf{1}_{m_\pi \times m_\pi}. \tag{4.22}$$

Consider the two vectors

$$e_1 := (1, 1, 0, \ldots, 0)^T$$

and

$$e_2 := (0, \ldots, 0, 1, 1)^T.$$

Since

$$e_1^T H(\theta^*) e_1 = -2k_0(m_0 - m_\pi)$$

and

$$e_2^T H(\theta^*) e_2 = 2k_0(m_0 - m_\pi),$$

and recalling that $m_0 \neq m_\pi$ in view of Lemma 4.1, $H(\theta^*)$ is sign indefinite. In particular, small variations in the direction given by e_1 or e_2 at this critical points change the values of W by respectively δW_1 and δW_2 with $\delta W_1 \delta W_2 < 0$. Hence, all the points $\theta^* \in B_0 \setminus \mathcal{W}_m$ are saddles. It remains to show that they are also hyperbolic, that is $H(\theta^*)$ is non-singular. Suppose on the contrary that $H(\theta^*)$ is singular. Then its columns are not linearly independent. That is there exists $a_1, \ldots, a_N \in \mathbb{R}$, not all zero, such that

$$\sum_{j=1}^{N} a_j H_{ij}(\theta^*) = 0, \ \forall i = 1, \ldots, N.$$

In particular, using (4.20), (4.21), and (4.22), we get

$$\sum_{j=1}^{N} a_j H_{1j}(\theta^*) = k_0 \left[(m_0 - m_\pi + 1)a_1 + \sum_{j=2}^{m_0} a_j - \sum_{j=m_0+1}^{N} a_j \right] = 0 \tag{4.23}$$

$$\sum_{j=1}^{N} a_j H_{2j}(\theta^*) = k_0 \left[(m_0 - m_\pi + 1)a_2 + \sum_{\substack{j=1 \\ j \neq 2}}^{m_0} a_j - \sum_{j=m_0+1}^{N} a_j \right] = 0. \tag{4.24}$$

Subtracting (4.23) to (4.24), we get $(m_0 - m_\pi + 1)(a_2 - a_1) = (a_2 - a_1)$. Recalling that $m_0 \neq m_\pi$ in view of Lemma 4.1, $(m_0 - m_\pi + 1) \neq 1$. Hence, necessarily $a_2 = a_1$. With similar computations, it follows that that $a_i = a_j$, for all $i, j = 1, \ldots, N$. Plugging this relation in (4.23), and solving for $m_0 - m_\pi$, one gets $m_0 - m_\pi = -\frac{1}{2}$, which is absurd, since $m_0, m_\pi \in \mathbb{N}$. Hence $H(\theta^*)$ is non singular. Through similar computations, the same result holds for the points $\theta^* \in A_0 \setminus \mathcal{W}_M$.

4.5.3 Proof of Lemma 4.3

The set $\mathcal{N}$, defined in (4.8), is the zero level set of the function

$$F(\cdot) := \begin{pmatrix} a(\cdot) \\ b(\cdot) \end{pmatrix} : \mathbb{R}^N \to \mathbb{R}^2, \tag{4.25}$$

where $a, b : \mathbb{R}^N \to \mathbb{R}^2$ are respectively defined in (4.15) and (4.16). The level set of a function defines a submanifold of codimension m if the function has constant rank m (Lee, 2006). In order to check this condition on F, we have to compute its Jacobian's rank in each point $\theta \in \mathcal{N}$. In view of (4.15), (4.16), and (4.25), basic computations reveal that

$$J_F(\theta) := \frac{\partial F}{\partial \theta}(\theta) = \begin{pmatrix} -\sin\theta_1 & \ldots & -\sin\theta_N \\ \cos\theta_1 & \ldots & \cos\theta_N \end{pmatrix}. \tag{4.26}$$

This matrix has rank 2 if and only if it contains two independent columns. A necessary and sufficient condition is then that there exists $(i, j) \in \mathbb{N}_N^{\neq}$, such that

$$\det \begin{pmatrix} -\sin\theta_i & -\sin\theta_j \\ \cos\theta_i & \cos\theta_j \end{pmatrix} = \sin(\theta_j - \theta_i) \neq 0.$$

In other words, the rank of F is strictly smaller than 2 at some point $\overline{\theta} \in \mathcal{N}$ if and only if

$$\sin\left(\overline{\theta}_j - \overline{\theta}_i\right) = 0, \quad \forall i, j = 1, \ldots, N. \tag{4.27}$$

This implies[4] $\overline{\theta}_i - \overline{\theta}_j = 0$ or $\overline{\theta}_i - \overline{\theta}_j = \pi$, for all $i, j = 1, \ldots, N$. That is, reordering the phase index, $\overline{\theta}_i = \theta_0$, $i = 1, \ldots, q_0$, for some $\theta_0 \in [0, 2\pi)$, and $\overline{\theta}_i = \theta_0 + \pi$, $i = q_0 + 1, \ldots, N$, where $0 \leq q_0 \leq N$.

Case 1: *N is odd.*
In the case N is an odd number (4.27) is not compatible with the condition $a(\overline{\theta}) = b(\overline{\theta}) = 0$ imposed in $\mathcal{N}$. Indeed, for any $0 \leq q_0 \leq N$, it holds that

$$a(\overline{\theta}) = q_0 \cos(\theta_0) - (N - q_0)\cos(\theta_0) \neq 0, \ \forall \theta_0 \notin \left\{\frac{\pi}{2}, \frac{3\pi}{2}\right\}.$$

If $\theta_0 \in \left\{\frac{\pi}{2}, \frac{3\pi}{2}\right\}$, then

$$b(\overline{\theta}) = q_0 \sin(\theta_0) - (N - q_0)\sin(\theta_0) \neq 0,$$

for all $0 \leq q_0 \leq N$. Hence (4.27) is not satisfied for all $\bar{\theta} \in \mathcal{N}$. We conclude that, in the case when N is odd, the Jacobian (4.26) of F has rank 2 on $\mathcal{N}$. Hence, $\mathcal{N}$ is a submanifold of codimension 2.
Since $\mathcal{N}$ is a submanifold of codimension 2, we can develop a stability analysis on its orthogonal subspace $\mathcal{N}^{\perp}$. In view of (4.8), a base for this subspace at $\theta \in \mathcal{N}$ is given by $(\nabla a(\theta)^T, \nabla b(\theta)^T)$. We start by computing the expression of the Hessian of W restricted to $\mathcal{N}$ that we denote as

$$\mathcal{H}(\theta) := H|_{\mathcal{N}}(\theta),$$

for all $\theta \in \mathcal{N}$. Notice that the elements s_i, defined in (4.19), satisfy

$$\begin{aligned} s_i|_{\mathcal{N}}(\theta) &= \sum_{j=1}^{N} \cos(\theta_i + \theta_j)|_{a(\theta)=b(\theta)=0} \\ &= \sum_{j=1}^{N} \left[\cos(\theta_i)\cos(\theta_j) - \sin(\theta_i)\sin(\theta_j)\right]|_{a(\theta)=b(\theta)=0} \\ &= \left[\cos(\theta_i)a(\theta) - \sin(\theta_i)b(\theta)\right]|_{a(\theta)=b(\theta)=0} \\ &= 0, \end{aligned}$$

for all $i = 1, \ldots, N$. Consequently, recalling (4.18), we have that

$$\mathcal{H}_{ij}(\theta) = -k_0 \cos(\theta_i + \theta_j), \ \forall \theta \in \mathcal{N}, \ \forall i, j = 1, \ldots, N. \tag{4.28}$$

Moreover, each element of the vector $\mathcal{H}(\theta)\nabla a(\theta)^T$ satisfies

$$\begin{aligned} \left[\mathcal{H}(\theta)\nabla a(\theta)^T\right]_i &= -\frac{k_0}{2}\left(\sum_{j=1}^{N}(-\sin\theta_j)(\cos\theta_i\cos\theta_j - \sin\theta_i\sin\theta_j)\right) \\ &= \frac{k_0}{2}\left(-\sin\theta_i\sum_{j=1}^{N}\sin^2\theta_j + \cos\theta_i\sum_{j=1}^{N}\sin\theta_j\cos\theta_j\right) \\ &= \frac{k_0}{2}\left(\nabla a(\theta)_i\sum_{j=1}^{N}\sin^2\theta_j + \nabla b(\theta)_i\sum_{j=1}^{N}\sin\theta_j\cos\theta_j\right). \end{aligned}$$

[4] All this reasoning holds modulo 2π. We omit to write the modulo operator for clarity.

It follows that, for all $\theta \in \mathcal{N}$,

$$\mathcal{H}(\theta)\nabla a(\theta)^T = \frac{k_0}{2}\left(\nabla a(\theta)^T \sum_{j=1}^{N} \sin^2\theta_j + \nabla b(\theta)^T \sum_{j=1}^{N} \sin\theta_j \cos\theta_j\right). \tag{4.29}$$

With similar computations, we have that, for all $\theta \in \mathcal{N}$,

$$\mathcal{H}(\theta)\nabla b(\theta)^T = \frac{k_0}{2}\left(\nabla a(\theta)^T \sum_{j=1}^{N} \sin\theta_j \cos\theta_j + \nabla b(\theta)^T \sum_{j=1}^{N} \cos^2\theta_j\right). \tag{4.30}$$

Defining

$$\mathcal{H}^{\perp}(\theta) := \mathcal{H}|_{\mathcal{N}^{\perp}}(\theta),$$

for all $\theta \in \mathcal{N}$, it follows from (4.29) and (4.30), that, in the basis $(\nabla a(\theta)^T, \nabla b(\theta)^T)$, $\mathcal{H}^{\perp}(\theta)$ is given by

$$\mathcal{H}^{\perp}(\theta) = \frac{k_0}{2}\begin{pmatrix} \alpha(\theta) & -\gamma(\theta) \\ \gamma(\theta) & -\beta(\theta) \end{pmatrix}, \tag{4.31}$$

where

$$\alpha(\theta) := \sum_{j=1}^{N} \sin^2\theta_j,$$

$$\beta(\theta) := \sum_{j=1}^{N} \cos^2\theta_j,$$

and

$$\gamma(\theta) := \sum_{j=1}^{N} \sin\theta_j \cos\theta_j.$$

The eigenvalues of $\mathcal{H}^{\perp}$ are then given by

$$\lambda_{\pm}(\theta) = \frac{k_0}{2}\left[\left(\sum_{j=1}^{N} \sin^2\theta_j\right) - \frac{N}{2} \pm \sqrt{\frac{N^2}{4} - \left(\sum_{j=1}^{N} \sin\theta_j \cos\theta_j\right)^2}\right]. \tag{4.32}$$

The following claim (proved in Section 4.6.1) ends the proof of the lemma in the case N is odd.

Claim 4.6. The functions λ_- and λ_+ defined in (4.32) satisfy $\lambda_-(\theta) < 0 < \lambda_+(\theta)$ for all $\theta \in \mathcal{N}$.

Case 2: *N is even.*
In the case when N is an even number, consider the groupings of indexes

$$\mathcal{I}_0 = \{i_1, \ldots, i_{\frac{N}{2}}\}, \quad \mathcal{I}_\pi = \{i_{\frac{N}{2}+1}, \ldots, i_N\},$$

where $i_j \in \{1, \ldots, N\}$ for all $j = 1, \ldots, N$, such that

$$\mathcal{I}_0 \cap \mathcal{I}_\pi = \emptyset.$$

Let

$$\mathcal{N}_0 \;:=\; \left\{\theta \in \mathbb{R}^N : \theta_i = \theta_0, \forall i \in \mathcal{I}_0,\ \theta_i = \theta_0 + \pi, \forall i \in \mathcal{I}_\pi, \theta_0 \in \mathbb{R}\right\}. \tag{4.33}$$

$\mathcal{N}_0$ is a 1-dimensional manifold parametrized by θ_0. Condition (4.27) is satisfied for all points in $\mathcal{N}_0$. Moreover, since $a(\theta) = b(\theta) = 0$, for all $\theta \in \mathcal{N}_0$, it holds that $\mathcal{N}_0 \subset \mathcal{N}$. Note that there exists exactly 2^N different groupings $\{\mathcal{I}_0, \mathcal{I}_\pi\}$. Let $\mathcal{N}_{0i}$ be the set of the form (4.33) relative to the i-th grouping. With the same reasoning as in CASE 1, no other sets than $\bigcup_{i=1}^{2^N} \mathcal{N}_{0i}$ in which (4.27) is satisfied are contained in $\mathcal{N}$. Define

$$\tilde{\mathcal{N}} := \mathcal{N} \setminus \mathcal{N}_0.$$

With the same computation as in CASE 1, $\tilde{\mathcal{N}}$ is a normally hyperbolic submanifold of codimension 2 with normal eigenvalues $\lambda_\pm$ as defined in (4.32).

It remains to show that, for each $i = 1, \ldots, 2^N$, the stable set of $\mathcal{N}_{0i}$ is contained in a submanifold of dimension $N/2$. In the following, if no confusion can arise, we omit the index i. Let $e_i \in \mathbb{R}^{N/2}$ be the vector with all zero entries apart 1 in the i-th position, that is $\{e_i\}_{i=1,\ldots,\frac{N}{2}}$ forms the canonical base of $\mathbb{R}^{N/2}$. Recalling (4.18) and (4.33), the Jacobian of the dynamics (4.4) on $\mathcal{N}_0$ can be written, after a reordering of the indexes, as

$$H_0(\theta_0) = -k_0 \sin(2\theta_0) \begin{bmatrix} \mathbf{1}_{N/2\times N/2} & -\mathbf{1}_{N/2\times N/2} \\ -\mathbf{1}_{N/2\times N/2} & \mathbf{1}_{N/2\times N/2} \end{bmatrix}.$$

For all $i, j = 1, \ldots, N/2$ and all $\theta_0 \in \mathbb{R}$,

$$H_0(\theta_0) \begin{pmatrix} e_i \\ e_j \end{pmatrix} = 0.$$

Hence, for all $\theta^\star \in \mathcal{N}_0$ the tangent space to $\mathcal{N}_0$ at $\theta^\star$ contains an $N/2$-dimensional center space E_c, satisfying

$$E_c = \text{span}\left\{ \begin{pmatrix} e_1 \\ e_1 \end{pmatrix}, \begin{pmatrix} e_2 \\ e_2 \end{pmatrix}, \ldots, \begin{pmatrix} e_{N/2} \\ e_{N/2} \end{pmatrix} \right\}.$$

This center space is tangent to the $N/2$-dimensional linear submanifold $\mathcal{M}_c$, defined as

$$\mathcal{M}_c := \left\{ \theta \in \mathbb{R}^N : \ \theta = \theta^\star + \sum_{i=1}^{N/2} a_i \begin{pmatrix} e_i \\ e_i \end{pmatrix}, \ a_i \in \mathbb{R}, \ i = 1, \ldots, N/2 \right\}$$

Noticing that, by construction, $\mathcal{M}_c \subset \mathcal{N}$, all the points in the center submanifold $\mathcal{M}_c$ are fixed points of (4.4), and, thus, they do not belong to the stable set of $\mathcal{N}_0$. From (Sijbrand, 1985, Theorem 3.2' - Case (ii)) this central manifold is unique. By the central manifold theorem (Guckenheimer and Holmes, 2002, Theorem 3.2.1), for all $\theta^\star \in \mathcal{N}_0$, the only other invariant set that contains $\theta^\star$ is given by a $N/2$-dimensional submanifold $\mathcal{M}^\perp$ that is tangent to $E_c^\perp$. Since $\mathcal{N}_0 \subset \mathcal{M}_c$, and since the stable set of $\mathcal{N}_0$ is an invariant set, it is contained in the $N/2$-dimensional submanifold $\mathcal{M}^\perp$.

4.5.4 Proof of Proposition 4.4

CASE 1: *N is even.*
Let $\mathcal{N}$ be as in (4.8), let $\tilde{\mathcal{N}}$ be defined as in Lemma 4.3, and let $\tilde{\mathcal{N}}^s$ denote the stable manifold of $\tilde{\mathcal{N}}$. Since, by Lemma 4.3, $\tilde{\mathcal{N}}$ is normally hyperbolic with one unstable direction, it follows from (Hirsch et al., 1977, Theorem 4.1) that $\tilde{\mathcal{N}}^s$ has zero Lebesgue measure. Moreover, by Lemma 4.3, all the points of $\mathcal{N}$ which are not in $\tilde{\mathcal{N}}$ form a finite set of 1-dimensional manifolds $\mathcal{N}_{0i}$, $i = 1, \ldots, 2^N$. The stable set of each of the $\mathcal{N}_{0i}$ is contained in a $N/2$-dimensional submanifold

$\mathcal{N}_{0i}^s$. Define the set

$$\mathcal{C}_0 := \mathcal{N} \cup \mathcal{N}^s \cup \bigcup_{i=1}^{2^N} \mathcal{N}_{0i}^s.$$

It follows that $\mu(\mathcal{C}_0) = 0$. Consider the domain

$$\mathcal{D} := \mathbb{R}^N \setminus \mathcal{C}_0.$$

By definition $\mathcal{D}$ is open, forward invariant for (4.4), and contains only isolated critical points. Hence by (Hirsch and Smale, 1974, Theorems 1 and 4), the restriction of (4.4) to $\mathcal{D}$ is a well defined gradient dynamics that contains only isolated critical points, and, for almost all $\theta_0 \in \mathcal{D}$, the trajectory starting in θ_0 converges to the global minima $\mathcal{W}_m$ of the potential function. Recalling that $\mu(\mathcal{C}_0) = 0$, we conclude that, for almost all $\theta_0 \in \mathbb{R}^N$, the trajectory starting at θ_0 converges to $\mathcal{W}_m$.

Case 2: *N is odd.*
Let $\mathcal{N}$ be as in (4.8), and let $\mathcal{N}^s$ be its stable manifold. Since, by Lemma 4.3, $\mathcal{N}$ is normally hyperbolic with one unstable direction, it follows from (Hirsch et al., 1977, Theorem 4.1) that $\mathcal{N}^s$ has zero Lebesgue measure. The rest of the proof follows along the same line of the even case with $\mathcal{C}_0 = \mathcal{N}^s$.

4.5.5 Proof of Theorem 4.5

The potential function W_η defined in (4.11) is nothing else than the potential function W defined in (4.5), perturbed by the function F^η. From Lemmas 4.1, 4.2, and 4.3, all the invariant sets of (4.4), given by the critical points of (4.5), are either hyperbolic fixed points or normally hyperbolic invariant manifolds. Hence, they persist under sufficiently small perturbations along with their stable and unstable manifolds (Hirsch et al., 1977, Theorem 4.1). Nonetheless, we can not conclude almost global convergence to the local minima of (4.11) directly since, (4.11) being lower unbounded, there may exists trajectories that run off to infinity. After having introduced some notation and a technical result, we organize the proof in two steps. In the first, we study the boundedness of the trajectories, whereas in the second we exploit the perturbed gradient structure and the classical persistence result of Hirsch et al. (Hirsch et al., 1977, Theorem 4.1) to conclude.

We start by introducing some notation that we use in the remainder of the proof. Given a bounded function $F : \mathbb{R}^N \to \mathbb{R}^N$, we denote by $\overline{\|F\|}$ its sup-Euclidean norm, that is $\overline{\|F\|} := \sup_{\theta \in \mathbb{R}^N} |F(\theta)|$. We next introduce the C^∞-topology in the space of smooth bounded functions with bounded derivative (Golubitsky and Guillemin, 1973, Chapter 2, Section 3). In order to formally define this topology, we need some further notation. Given $n \in \mathbb{N}$, $m_1, \dots, m_n \in \mathbb{N}$, and $M \in \mathbb{R}^{m_1 \times \dots \times m_n}$, we denote as $|M|$ the (entry-wise) Euclidean norm of M, that is $|M| := \sqrt{\sum_{i_1=1}^{m_1} \cdots \sum_{i_n=1}^{m_n} M_{i_1,\dots,i_n}^2}$. Note that $|\cdot|$ is a norm on $\mathbb{R}^{m_1 \times \dots \times m_n}$ as can be formally shown by isomorphically mapping $\mathbb{R}^{m_1 \times \dots \times m_n}$ to $\mathbb{R}^{m_1 m_2 \dots m_n}$. For instance, in the case $n = 1$, $|\cdot|$ is the Euclidean norm, while for $n = 2$ it is the Frobenius norm. Given a smooth bounded function $F : \mathbb{R}^N \to \mathbb{R}^{m_1 \times \dots \times m_n}$, we denote its sup-Euclidean norm as $\overline{\|F\|} := \sup_{\theta \in \mathbb{R}^N} |F(\theta)|$. Finally, given $r \in \mathbb{N}$, we define the C^r-norm of a smooth bounded function $F : \mathbb{R}^N \to \mathbb{R}^N$ with bounded derivatives as $\overline{\|F\|}_r := \sup_{n=0,\dots,r} \overline{\|F^{(n)}\|}$, where $F^{(n)} : \mathbb{R}^N \to \mathbb{R}^{\overbrace{N \times \dots \times N}^{n+1 \text{ times}}}$ denotes the n-th partial derivative of F, that is, for all $i, i_1, \dots i_n \in 1, \dots, N$, $\left(F_i^{(n)}\right)_{i_1 \dots i_n}(\theta) = \frac{\partial^n F_i}{\partial \theta_{i_1} \dots \partial \theta_{i_n}}(\theta)$, if $n \geq 1$, and $F_i^{(0)}(\theta) = F_i(\theta)$. The C^∞ topology is the topology generated by the collection of all the open balls defined by the C^r norms, $r \in \mathbb{N}$. Convergence in this topology is denoted

by $\xrightarrow{C^\infty}$. Given a family of functions $\{F^\nu\}_{\nu\in\mathbb{R}^{n\times m}}$ parametrized by $\nu \in \mathbb{R}^{n\times m}$, it holds that $F^\nu \xrightarrow[|\nu|\to 0]{C^\infty} 0$ if and only if F^ν and all its partial derivatives $(F^\nu)^{(r)}$, $r \in \mathbb{N}$, converge uniformly to zero as $|\nu| \to 0$ (Golubitsky and Guillemin, 1973, Page 43).

We next state the following claim, whose proof is provided in Section 4.6.2, which shows that the perturbation f^η converges to zero in the C^∞ topology as $|\eta|$ tends to zero. In particular, f^η is small in the C^r-norms, provided that $|\eta|$ is small. We use this technical result at different steps of the proof.

Claim 4.7. Consider the function f^η defined in (4.2) and the parameter matrix $\eta \in \mathbb{R}^{N\times(1+2N)}$ introduced in (4.3). Then it holds that

$$f^\eta \xrightarrow[|\eta|\to 0]{C^\infty} 0.$$

In particular, for all $r \in \mathbb{N}$, there exists a $\mathcal{K}_\infty$ function ϱ, such that $\overline{\|f^\eta\|}_r \leq \varrho(|\eta|)$.

The proof then follows from the two following steps.

STEP 1: *Boundedness of the trajectories.*
We use the potential function W as a (lower bounded) Lyapunov function for (4.1). Since (4.1) is a gradient dynamics with potential function W_η, the derivative of W along the trajectories of (4.1) reads

$$\begin{aligned}\dot{W}(\theta) := -\nabla W_\eta^\top(\theta)\nabla W(\theta) &= -\nabla\left(W(\theta)+F^\eta(\theta)\right)^\top \nabla W(\theta)\\ &= -|\nabla W(\theta)|^2 + (f^\eta(\theta))^\top \nabla W(\theta). \end{aligned} \tag{4.34}$$

Equation (4.34) implies that

$$|\nabla W(\theta)| > 2\overline{\|f^\eta\|} \quad \Rightarrow \quad \dot{W}(\theta) < -\frac{|\nabla W(\theta)|^2}{2}. \tag{4.35}$$

Note that, since f^η is 2π-periodic and smooth, it is bounded, and thus $\overline{\|f^\eta\|}$ is well defined. Let F_0 be the set of critical points of W as defined in Lemma 4.1. By definition

$$\nabla W(\theta) = 0 \quad \Leftrightarrow \quad \theta \in F_0. \tag{4.36}$$

Consequently, the continuous function $|\nabla W| : \mathbb{R}^N \to \mathbb{R}_{\geq 0}$ is positive outside F_0. In view of the periodicity of $|\nabla W|$, it follows from (Khalil, 2001, Lemma 4.3) that there exists a $\mathcal{K}$ function σ such that

$$|\nabla W(\theta)| \geq \sigma(|\theta|_{F_0}),\ \forall \theta \in \mathbb{R}^N. \tag{4.37}$$

Let

$$\delta_\sigma := \frac{1}{2}\lim_{s\to\infty}\sigma(s). \tag{4.38}$$

Note that, by (4.37), $\sigma \in \mathcal{K}\setminus\mathcal{K}_\infty$ (*i.e.* σ is bounded) and thus δ_σ is well defined. If $\overline{\|f^\eta\|} < \delta_\sigma$, then $\sigma^{-1}\left(2\overline{\|f^\eta\|}\right)$ is well defined and Equations (4.35) and (4.37) yield

$$|\theta|_{F_0} \geq \sigma^{-1}\left(2\overline{\|f^\eta\|}\right) \quad \Rightarrow \quad \dot{W}(\theta) < -\frac{|\nabla W(\theta)|^2}{2}. \tag{4.39}$$

In other words, the derivative of W is negative outside the set $\mathcal{B}\left(F_0, \sigma^{-1}\left(2\overline{\|f^\eta\|}\right)\right)$. Let δ_1 be the minimum Euclidean distance between any two critical sets of W, *i.e.*

$$\delta_1 := \min\left\{\min_{\theta_a,\theta_b\in A_0\cup B_0\cup\mathcal{W}_m\cup\mathcal{W}_M,\theta_a\neq\theta_b}|\theta_a-\theta_b|, \inf_{\theta\in A_0\cup B_0\cup\mathcal{W}_m\cup\mathcal{W}_M}|\theta|_{\mathcal{N}}\right\}. \tag{4.40}$$

We claim that $\delta_1 > 0$. Indeed, by periodicity of W, we can compute δ_1 on any hypercube $C_{2\pi} \subset \mathbb{R}^N$ of side 2π, which defines a compact subset of $\mathbb{R}^N$. Since $\mathcal{N}$ is an embedded submanifold, its intersection with any compact subset is compact. Moreover, the intersection of the set $A_0\cup B_0\cup\mathcal{W}_m\cup\mathcal{W}_M$ with any compact subset contains only a finite number of points. δ_1 is thus defined as the Euclidean distance between a finite number of points and a disjoint compact set, which shows its positivity.

Relation (4.39) permits to study the decrease of W far from its critical sets, which are separated, in the light of $\delta_1 > 0$. This study, together with an analysis of the behavior of (4.1) near the unstable critical sets of W, permits to compute an upper bound on the size of η, and thus of f^η (cf. Claim 4.7 above), such that the trajectories of (4.1) converge in finite time to a forward invariant neighborhood of the minima of W, thus ensuring boundedness. The following claim, whose proof is provided in Section 4.6.3 and is inspired from (Angeli and Praly, 2011, Proof of Claim 1), proves this conjecture.

Claim 4.8. There exists $\overline{\delta} > 0$, such that, if $|\eta| < \overline{\delta}$, then there exists a sublevel set Q_c of W, with $Q_c \subset \mathcal{B}\left(\mathcal{W}_m, \frac{\delta_1}{4}\right)$, such that, for almost all initial conditions $\theta_0 \in \mathbb{R}^N$, there exists $T > 0$, such that the trajectory of (4.1) starting in θ_0 satisfies

$$\theta(t;\theta_0) \in Q_c, \quad \forall t \geq T.$$

In particular, for almost all initial conditions, the trajectory of (4.1) is bounded.

STEP 2: *Almost global convergence.*
Since almost all the trajectories of (4.1) are bounded, all the trajectories that do not start on the stable manifolds of unstable critical points must converge to the minima of the potential function W_η. It thus remains to show that, also in the perturbed case $f^\eta \not\equiv 0$, the stable set of all the critical points of W_η which are not local minima is of zero Lebesgue measure. We do this invoking the normal hyperbolicity of these sets and (Hirsch et al., 1977, Theorem 4.1), where it is shown that a normally hyperbolic invariant manifold persists under sufficiently small smooth perturbations, along with its stable and unstable manifolds. The qualifier "small" here, is intended in the C^∞, or Whitney, topology sense (Golubitsky and Guillemin, 1973, Chapter 2, Section 3), as introduced above.

More precisely, Claim 4.7 ensures that perturbation f^η are small in the C^∞-norm, provided that $|\eta|$ is small. Then, for each hyperbolic critical point θ^* of (4.5) contained in $A_0\cup B_0\cup\mathcal{W}_m\cup\mathcal{W}_M$, where A_0 and B_0 are defined in (4.6) and (4.7) and $\mathcal{W}_m$ and $\mathcal{W}_M$ are defined in (4.9a) and (4.9b), (Hirsch et al., 1977, Theorem 4.1) implies the existence of some $\delta_{\theta^*} > 0$ such that, if $|\eta| \leq \delta_{\theta^*}$, then the perturbed potential function (4.11) still has a unique hyperbolic critical point θ^*_η that is $|\eta|$-near to θ^*, that is

$$\lim_{\eta\to 0}|\theta^*_\eta - \theta^*| = 0.$$

In addition, the stable and unstable manifolds of θ^*_η have the same dimensions as and are $|\eta|$-near in the C^∞ topology[5] to those of θ^*. Let

$$\delta_{isolated} := \min\{\delta_{\theta^*} : \theta^* \in A_0 \cup B_0 \cup \mathcal{W}_m \cup \mathcal{W}_M\},$$

which is positive, since the set $A_0 \cup B_0 \cup \mathcal{W}_m \cup \mathcal{W}_M$ is 2π-periodic and contains only a finite number of points in each hypercube $C_{2\pi} \subset \mathbb{R}^N$ of side 2π. Invoking again Claim 4.7 and (Hirsch et al., 1977, Theorem 4.1), there exists $\delta_2 > 0$, such that, if $|\eta| \leq \delta_2$, then f^η has a unique smooth normally hyperbolic invariant manifold $\mathcal{N}_\eta$, $|\eta|$-near to $\mathcal{N}$ in the C^∞ topology, that is

$$\mathcal{N}_\eta \xrightarrow[|\eta|\to 0]{C^\infty} \mathcal{N},$$

and whose stable and unstable manifolds have the same dimensions as and are $|\eta|$-near in the C^∞ topology to those of $\mathcal{N}$. For $|\eta| \leq \min\{\delta_2, \delta_{isolated}\}$, all the isolated local minima of W_η are contained in the set $\mathcal{W}^\eta_m$, which is non empty, and which satisfies

$$\lim_{\eta\to 0} |\mathcal{W}^\eta_m|_{\mathcal{W}_m} = 0.$$

This also implies the existence of a $\mathcal{K}_\infty$ function ρ satisfying (4.12) (Khalil, 2001). The first part of the statement of the theorem is thus proved for all

$$\delta \leq \min\{\delta_2, \delta_{isolated}\}.$$

For the rest of the statement, we proceed as in Proposition 4.4 and we construct an open, forward invariant set that contains only isolated critical points, and whose complement is of zero Lebesgue measure. For $|\eta| \leq \delta_2$, let $\mathcal{N}^s_\eta$ denote the stable manifold of $\mathcal{N}_\eta$ and consider the domain

$$\mathcal{D}_\eta = \mathbb{R}^N \setminus \mathcal{N}^s_\eta.$$

Since $\mathcal{N}$ has one unstable orthogonal direction, so does $\mathcal{N}^s_\eta$. Thus $\mu(\mathcal{N}^s_\eta) = 0$, that is the complement of the domain $\mathcal{D}_\eta$ has zero Lebesgue measure. Moreover, if $|\eta| \leq \min\{\delta_{isolated}, \delta_2\}$, by definition $\mathcal{D}_\eta$ is open, forward invariant for (4.4), and contains only isolated critical points. Hence, the restriction of (4.1) to $\mathcal{D}_\eta$ is a well defined gradient dynamics that contains only isolated critical points. From (Hirsch and Smale, 1974, Theorems 1 and 4) almost all the bounded trajectories belonging to $\mathcal{D}_\eta$ converge to the set $\mathcal{W}^\eta_m$ of local minima of W_η, which is non-empty since of $|\eta| \leq \delta_{isolated}$. Invoking Claim 4.8, it follows that, for all η such that $|\eta| < \overline{\delta}$, almost all trajectories are bounded. Therefore, for

$$|\eta| < \delta := \min\{\delta_{isolated}, \delta_2, \overline{\delta}\},$$

almost all trajectories belonging to $\mathcal{D}_\eta$ converge to the set of isolated local minima $\mathcal{W}^\eta_m$ of W_η. Recalling that the complement of $\mathcal{D}_\eta$ in $\mathbb{R}^N$ has zero Lebesgue measure, the second part of the statement of the theorem is proved. □

[5]The C^∞ topology for embedded submanifolds is induced by the C^∞ topology on the space of smooth embeddings with image in the embedding space. Embedded submanifolds are indeed in one-to-one correspondence with smooth embeddings (Lee, 2006, Corollary 8.4)

4.6 Technical proofs

4.6.1 Proof of Claim 4.6

We start by showing that $\tilde{\lambda}_{\pm}(\theta) \neq 0$ for all $\theta \in \tilde{\mathcal{N}}$. Suppose, on the contrary, that $\tilde{\lambda}_{\pm}(\theta) = 0$. This implies from (4.32) that

$$2\sum_{j=1}^{N} \sin^2\theta_j - N = \mp\sqrt{N^2 - 4\left(\sum_{j=1}^{N} \sin\theta_j \cos\theta_j\right)^2},$$

that is

$$\left(\sum_{j=1}^{N} \sin^2\theta_j\right)^2 - N\sum_{j=1}^{N} \sin^2\theta_j + \left(\sum_{j=1}^{N} \sin\theta_j \cos\theta_j\right)^2 = 0. \tag{4.41}$$

Noticing that $\left(\sum_{j=1}^{N} \sin^2\theta_j\right)^2 = \sum_{ij=1}^{N} (\sin\theta_i \sin\theta_j)^2$, using the trigonometric identity $\sin a \sin b = \frac{1}{2}(\sin(a-b) - \sin(a+b))$, it follows that

$$\left(\sum_{j=1}^{N} \sin^2\theta_j\right)^2 = \frac{1}{4}\sum_{ij=1}^{N} \big[\cos(\theta_i - \theta_j) - \cos(\theta_i + \theta_j)\big]^2. \tag{4.42}$$

Noticing that

$$\left(\sum_{j=1}^{N} \sin\theta_j \cos\theta_j\right)^2 = \sum_{ij=1}^{N} \sin\theta_i \cos\theta_i \sin\theta_j \cos\theta_j,$$

and using the trigonometric identity $\sin a \cos b = \frac{1}{2}(\sin(a+b) + \sin(a-b))$, it follows that

$$\begin{aligned}
\left(\sum_{j=1}^{N} \sin\theta_j \cos\theta_j\right)^2 &= \frac{1}{4}\sum_{ij=1}^{N} \big[\sin^2(\theta_i + \theta_j) - \sin^2(\theta_i - \theta_j)\big] \\
&= \frac{1}{4}\sum_{ij=1}^{N} \big[\sin(\theta_i + \theta_j) + \sin(\theta_i - \theta_j)\big]^2 - \frac{1}{4}\sum_{ij=1}^{N} 2\sin(\theta_i + \theta_j)\sin(\theta_i - \theta_j) - \\
&\quad \frac{1}{4}\sum_{ij=1}^{N} 2\sin^2(\theta_i - \theta_j) \\
&= \frac{1}{4}\sum_{ij=1}^{N} \big[\sin(\theta_i + \theta_j) + \sin(\theta_i - \theta_j)\big]^2 - \frac{1}{4}\sum_{ij=1}^{N} 2\sin^2(\theta_i - \theta_j),
\end{aligned}$$

where the third equality comes from the fact that $\sum_{i,j=1}^{N} \sin(\theta_i + \theta_j)\sin(\theta_i - \theta_j) = 0$ for all θ. Moreover we have that

$$\begin{aligned}
&\frac{1}{4}\Big[\sum_{ij=1}^{N} \big(\cos(\theta_i - \theta_j) - \cos(\theta_i + \theta_j)\big)^2 + \big(\sin(\theta_i + \theta_j) + \sin(\theta_i - \theta_j)\big)^2\Big] \\
= \;& \frac{1}{2}N^2 - \frac{1}{2}\sum_{ij=1}^{N} \Big[\big(\cos(\theta_i - \theta_j)\cos(\theta_i + \theta_j) - \sin(\theta_i + \theta_j)\sin(\theta_i - \theta_j)\big)\Big] \\
= \;& \frac{1}{2}N^2 - \frac{1}{2}N^2 + N\sum_{j=1}^{N} \sin^2\theta_j = N\sum_{j=1}^{N} \sin^2\theta_j,
\end{aligned} \tag{4.43}$$

where in the third equality we have used the fact that

$$\sum_{ij=1}^{N} \cos(\theta_i - \theta_j)\cos(\theta_i + \theta_j) = \sum_{ij=1}^{N} \frac{1}{2}(\cos 2\theta_i + \cos 2\theta_j) = N\sum_{j=1}^{N} \cos 2\theta_j = N^2 - 2N\sum_{j=1}^{N} \sin^2 \theta_j.$$

Finally, plugging (4.42)-(4.43) into (4.41), we have that

$$\tilde{\lambda}_{\pm}(\theta) = 0 \quad \Longrightarrow \quad \sum_{ij=1}^{N} 2\sin^2(\theta_i - \theta_j) = 0,$$

that is $\sin(\theta_i - \theta_j) = 0$, for all $i, j = 1, \ldots, N$. Recalling (4.27), we conclude that $\tilde{\lambda}_{\pm}(\theta) \neq 0$, for all $\theta \in \tilde{\mathcal{N}}$.

Since $\tilde{\lambda}_{\pm}$ are continuous functions that do not cross zero, they cannot change sign. To prove the claim it then remains to find θ^*, such that $\tilde{\lambda}_{+}(\theta^*) > 0$ and $\tilde{\lambda}_{-}(\theta^*) < 0$.
Consider θ^* such that $\theta_i^* = 2\pi\frac{(i-1)}{N}$, that is the oscillator phases are uniformly distributed on the circle[6]. Recalling (4.32), it holds that

$$\tilde{\lambda}_{\pm}(\theta^*) = 2\sum_{j=1}^{N} \sin^2 \theta_j^* - N \pm N.$$

That is

$$\tilde{\lambda}_{+}(\theta^*) = 2\sum_{j=1}^{N} \sin^2 \theta_j^* > 0,$$

and, since $\sum_{j=1}^{N} \sin^2 \theta_j^* < N$,

$$\tilde{\lambda}_{-}(\theta^*) = -2N - 2\sum_{j=1}^{N} \sin^2 \theta_j^* < 0.$$

□

4.6.2 Proof of Claim 4.7

The statement of the claim is equivalent to requiring that f^{η} and all its partial derivatives converge uniformly to zero as $|\eta| \to 0$ (Golubitsky and Guillemin, 1973, Chapter 2, Section 3). That is we have to show that, for all $n \in \mathbb{N}$ and for all $\epsilon > 0$, there exists $\delta > 0$, such that, if $|\eta| \leq \delta$, then $\bar{\|}(f^{\eta})^{(n)}\bar{\|} \leq \epsilon$. In the rest of the proof we let $\mathcal{S}$ be the set of functions defined as $\mathcal{S} := \{\sin(\cdot), -\sin(\cdot), \cos(\cdot), -\cos(\cdot)\}$.

[6] This phase configuration is called the *split configuration* in (Sepulchre et al., 2007).

In order to give an estimate of $\overline{\|}(f^\eta)^{(n)}\overline{\|}$ we claim that, for all $n \in \mathbb{N}$ and for all $i, i_1, \ldots, i_n \in 1, \ldots, N$, it holds that, for all $\theta \in \mathbb{R}^N$,

$$\frac{\partial^n f_i^\eta}{\partial\theta_{i_n}\ldots\partial\theta_{i_1}}(\theta) = \begin{cases} (a): \ \omega_i + \sum_{j=1}^N (\tilde{k}_{ij} + \tilde{\gamma}_{ij})\varsigma_1(\theta_j - \theta_i) - \sum_{j=1}^N \tilde{\gamma}_{ij}\varsigma_2(\theta_j + \theta_i), & \text{or} \\ (b): \ \sum_{j=1}^N (\tilde{k}_{ij} + \tilde{\gamma}_{ij})\varsigma_3(\theta_j - \theta_i) - \sum_{j=1}^N \tilde{\gamma}_{ij}\varsigma_4(\theta_j + \theta_i), & \text{or} \\ (c): \ (\tilde{k}_{ii_j} + \tilde{\gamma}_{ii_j})\varsigma_5(\theta_{i_j} - \theta_i) - \gamma_{ii_j}\varsigma_6(\theta_{i_j} + \theta_i), \ j \in \{1, \ldots, n\} & \text{or} \\ (d): \ 0, \end{cases} \tag{4.44}$$

where $\varsigma_1, \ldots, \varsigma_6 \in \mathcal{S}$. Since (4.44) holds for $n = 0$, we proceed by induction. Suppose that (4.44) holds for some $n \in \mathbb{N}$. Then, in cases $(a), (b)$, simple computations lead to

$$\frac{\partial^{n+1} f_i^\eta}{\partial\theta_{i_{n+1}}\ldots\partial\theta_{i_1}}(\theta) = \begin{cases} \sum_{j=1}^N (\tilde{k}_{ij} + \tilde{\gamma}_{ij})\varsigma_7(\theta_j - \theta_i) - \sum_{j=1}^N \tilde{\gamma}_{ij}\varsigma_8(\theta_j + \theta_i), & \text{if } i_{n+1} = i, \\ (k_{ii_{n+1}} + \tilde{\gamma}_{ii_{n+1}})\varsigma_9(\theta_{i_{n+1}} - \theta_i) - \gamma_{ii_{n+1}}\varsigma_{10}(\theta_{i_{n+1}} + \theta_i), & \text{if } i_{n+1} \neq i, \end{cases}$$

where $\varsigma_7, \ldots, \varsigma_{10} \in \mathcal{S}$. Furthermore, in case (c),

$$\frac{\partial^{n+1} f_i^\eta}{\partial\theta_{i_{n+1}}\ldots\partial\theta_{i_1}}(\theta) = \begin{cases} (\tilde{k}_{ii_j} + \tilde{\gamma}_{ii_j})\varsigma_{11}(\theta_{i_j} - \theta_i) - \gamma_{ii_j}\varsigma_{12}(\theta_{i_n} + \theta_i), & \text{if } i_{n+1} \in \{i, i_j\}, \\ 0, & \text{if } i_{n+1} \notin \{i, i_j\}, \end{cases}$$

where $\varsigma_{11}, \varsigma_{12} \in \mathcal{S}$. Finally, in case (d),

$$\frac{\partial^{n+1} f_i^\eta}{\partial\theta_{i_{n+1}}\ldots\partial\theta_{i_1}}(\theta) = 0,$$

which proves that (4.44) holds for $n + 1$. By induction, (4.44) therefore holds for all $n \in \mathbb{N}$. Given a matrix $M \in \mathbb{R}^{n\times m}$, let $|M|_{max}$ denote its max (entry-wise) norm, that is $|M|_{max} := \max_{\substack{i=1,\ldots,n,\\ j=1,\ldots,m}} |M_{ij}|$. Then, noticing that $|\varsigma(\vartheta)| \leq 1$, for all $\varsigma \in \mathcal{S}$ and all $\vartheta \in \mathbb{R}$, it follows from (4.44) that, for all $\theta \in \mathbb{R}^N$

$$\left|\frac{\partial^n f_i^\eta}{\partial\theta_{i_n}\ldots\partial\theta_{i_1}}(\theta)\right| \leq (1 + 3N)\max\left\{|\omega|_{max}, |\tilde{k}|_{max}, |\tilde{\gamma}|_{max}\right\},$$

and, thus,

$$\begin{aligned} \overline{\|}(f^\eta)^{(n)}\overline{\|} &\leq N^{n+1}(1 + 3N)\max\left\{|\omega|_{max}, |\tilde{k}|_{max}, |\tilde{\gamma}|_{max}\right\} \\ &\leq N^{n+1}(1 + 3N)|\eta|. \end{aligned} \tag{4.45}$$

Hence, given $n \in \mathbb{N}$ and $\epsilon > 0$, it holds that $\overline{\|}(f^\eta)^{(n)}\overline{\|} < \epsilon$ for all η such that $|\eta| < \frac{\epsilon}{N^{n+1}(1+3N)}$, which proves the first part of the statement of the claim. Given $r \in \mathbb{N}$, the second part follows from (4.45) by picking, for all $x \in \mathbb{R}_{\geq 0}$, $\varrho(x) = N^{r+1}(1 + 3N)x$

4.6.3 Proof of Claim 4.8

We start by noticing a useful relationship, which follows directly from Claim 4.7: there exists a class $\mathcal{K}_\infty$ function ρ_1, such that, for all $\eta \in \mathbb{R}^{N\times(1+2N)}$, it holds that

$$\overline{\|f^\eta\|} \leq \rho_1(|\eta|). \tag{4.46}$$

Relation (4.39) implies that, if $\overline{\|f^\eta\|} < \delta_\sigma$, then the trajectories of (4.1) can spend at most a finite time outside the set $\mathcal{B}\left(F_0, \sigma^{-1}\left(2\overline{\|f^\eta\|}\right)\right)$. To show this, note that, from (4.37),

$$\inf_{\theta\in\mathbb{R}^N\setminus\mathcal{B}\left(F_0,\sigma^{-1}\left(2\overline{\|f^\eta\|}\right)\right)} \frac{|\nabla W(\theta)|^2}{2} \geq \frac{1}{2}\sigma\left(\sigma^{-1}\left(2\overline{\|f^\eta\|}\right)\right)^2 = 2\overline{\|f^\eta\|}^2. \tag{4.47}$$

Relations (4.39) and (4.47) imply that, for all initial conditions $\theta_0 \in \mathbb{R}^N$, the solution of (4.1) satisfies

$$W(\theta(t,\theta_0)) < W(\theta_0) - 2\overline{\|f^\eta\|}^2 t, \tag{4.48}$$

for all t such that $\theta(s;\theta_0) \in \mathbb{R}^N \setminus \mathcal{B}\left(F_0, \sigma^{-1}\left(2\overline{\|f^\eta\|}\right)\right)$ for all $s \in [0,t)$. Suppose that

$$\theta(t,\theta_0) \in \mathbb{R}^N \setminus \mathcal{B}\left(F_0, \sigma^{-1}\left(2\overline{\|f^\eta\|}\right)\right),\ \forall t \geq 0.$$

Then, from (4.48), $W(\theta(t,\theta_0)) \to -\infty$ as $t \to +\infty$, which contradicts the fact that W is lower bounded. Hence, for all initial condition θ_0, there exists $0 \leq T < \infty$, such that the solution of (4.1) starting at θ_0 enters the set $\mathcal{B}\left(F_0, \sigma^{-1}\left(2\overline{\|f^\eta\|}\right)\right)$ at time T. Without loss of generality, we can then assume that the initial condition θ_0 lies in $\mathcal{B}\left(F_0, \sigma^{-1}\left(2\overline{\|f^\eta\|}\right)\right)$.

Case 1: $\theta_0 \in \mathcal{B}\left(\mathcal{W}_m, \sigma^{-1}\left(2\overline{\|f^\eta\|}\right)\right)$.
We construct explicitly a forward invariant sublevel set Q_c of W that contains $\mathcal{B}\left(\mathcal{W}_m, \sigma^{-1}\left(2\overline{\|f^\eta\|}\right)\right)$. In order to do this, consider the largest sublevel set Q_c of W contained in $\mathcal{B}\left(\mathcal{W}_m, \frac{\delta_1}{4}\right)$. Note that, by the definition (4.9a) of $\mathcal{W}_m$, Q_c can be written as

$$Q_c = \bigcup_{k\in\mathbb{Z}} Q_{c,k}, \tag{4.49}$$

where

$$Q_{c,k} := \mathcal{B}\left(\left(\frac{\pi}{2} + k\pi\right)\mathbf{1}_N, \frac{\delta_1}{4}\right) \cap Q_c,\ \forall k \in \mathbb{Z}, \tag{4.50}$$

is compact. Moreover, recalling the definition of δ_1 in (4.40), it holds that $\mathcal{B}\left(\left(\frac{\pi}{2} + k\pi\right)\mathbf{1}_N, \frac{\delta_1}{4}\right) \cap \mathcal{B}\left(\left(\frac{\pi}{2} + k'\pi\right)\mathbf{1}_N, \frac{\delta_1}{4}\right) = \emptyset$, for all $k, k' \in \mathbb{Z}$, $k \neq k'$, and thus

$$Q_{c,k} \cap Q_{c,k'} = \emptyset,$$

whenever $k \neq k'$. Pick $\delta_m > 0$ small enough that

$$\mathcal{B}\left(\mathcal{W}_m, \sigma^{-1}\left(2\delta_m\right)\right) \subset Q_c. \tag{4.51}$$

If $\overline{\|f^\eta\|} < \min\{\delta_m, \delta_\sigma\}$, then for all $\theta \in \partial Q_c$, it holds that $|\theta|_{\mathcal{W}_m} > \sigma^{-1}(2\overline{\|f^\eta\|})$ and $|\theta|_{F_0\setminus\mathcal{W}_m} > \frac{\delta_1}{4} > \sigma^{-1}(2\overline{\|f^\eta\|})$. It thus follows from (4.39) that, if $\overline{\|f^\eta\|} < \min\{\delta_m, \delta_\sigma\}$, then

$$\max_{\theta\in\partial Q_c} \dot{W}(\theta) < 0,$$

which implies (cf. e.g. (Isidori, 1999, Remark 10.1.2)) that Q_c is forward invariant. By (4.51), if $\bar{\|}f^\eta\bar{\|} < \min\{\delta_m, \delta_\sigma\}$, then $\mathcal{B}\left(\mathcal{W}_m, \sigma^{-1}\left(2\bar{\|}f^\eta\bar{\|}\right)\right) \subset Q_c$, and thus the trajectories of (4.1) satisfy

$$\theta_0 \in \mathcal{B}\left(\mathcal{W}_m, \sigma^{-1}\left(2\bar{\|}f^\eta\bar{\|}\right)\right) \quad \Rightarrow \quad \theta(t;\theta_0) \in Q_c, \ \forall t \geq 0.$$

In particular, since Q_c is given by the disjoint union of compact sets (cf. (4.49)), for all initial conditions $\theta_0 \in \mathcal{B}\left(\mathcal{W}_m, \sigma^{-1}\left(2\bar{\|}f^\eta\bar{\|}\right)\right)$, the trajectory of (4.1) is bounded, provided that $|\eta| \leq \rho_1^{-1}(\min\{\delta_m, \delta_\sigma\})$, where the $\mathcal{K}_\infty$ function ρ_1 is defined in (4.46).

Case 2: $\theta_0 \in \mathcal{B}\left(\xi, \sigma^{-1}\left(2\bar{\|}f^\eta\bar{\|}\right)\right)$, with $\xi \in \mathcal{F}_0$, where $\mathcal{F}_0 := \left\{\mathcal{N}, \left\{\{x\} : x \in \{A_0 \cup B_0 \cup \mathcal{W}_M\}\right\}\right\}$. We stress that by $\xi \in \mathcal{F}_0$ we mean that ξ is either a singleton made of an unstable isolated critical point, *i.e.* $\xi = \{x\}$, with $x \in A_0 \cup B_0 \cup \mathcal{W}_M$, or that ξ is the unstable normally hyperbolic invariant manifold $\mathcal{N}$, *i.e.* $\xi = \mathcal{N}$. We start by showing that, for sufficiently small $|\eta|$, all the trajectories starting in the set $\mathcal{B}\left(\xi, \sigma^{-1}\left(2\bar{\|}f^\eta\bar{\|}\right)\right)$, $\xi \in \mathcal{F}_0$, leaves the set $\mathcal{B}\left(\xi, \frac{\delta_1}{2}\right)$ in finite time, where δ_1 is defined in (4.40). From Lemmas 4.2 and 4.3, ξ is either made of an isolated hyperbolic fixed point, or an invariant normally hyperbolic manifold. As proved in Claim 4.7 above, in the C^∞ topology, the perturbation f^η is small provided that $|\eta|$ is small. More precisely,

$$f^\eta \xrightarrow[|\eta|\to 0]{C^\infty} 0.$$

Theorem 4.1 in (Hirsch et al., 1977) then implies that there exists $\delta_\xi > 0$ such that, if $|\eta| < \delta_\xi$, then the perturbed dynamics (4.1) still has a hyperbolic fixed point, or an invariant normally hyperbolic manifold, ξ_η, that is also $|\eta|$-near from ξ in the C^∞ topology, that is

$$\xi_\eta \xrightarrow[|\eta|\to 0]{C^\infty} \xi,$$

and whose stable and unstable manifolds have the same dimension as and are $|\eta|$-near in the C^∞ topology to those of ξ. For

$$|\eta| < \min\left\{\rho_1^{-1}\left(\frac{1}{2}\sigma\left(\frac{\delta_1}{4}\right)\right), \delta_\xi\right\},$$

it follows from (4.39) that no other critical sets apart from ξ_η are contained in $\mathcal{B}\left(\xi, \frac{\delta_1}{2}\right)$. It also follows from (Hirsch et al., 1977, Theorem 4.1) that the only forward invariant set in $\mathcal{B}\left(\xi, \frac{\delta_1}{2}\right)$ is the stable manifold of ξ_η. Since, for all $\xi \in \mathcal{F}_0$, ξ has at least one unstable direction, the stable manifold of ξ, and thus that of ξ_η, has zero Lebesgue measure. By construction, if $|\eta| < \min\left\{\rho_1^{-1}\left(\frac{1}{2}\sigma\left(\frac{\delta_1}{4}\right)\right), \delta_\xi\right\}$, then

$$\mathcal{B}\left(\xi, \sigma^{-1}\left(2\bar{\|}f^\eta\bar{\|}\right)\right) \subset \mathcal{B}\left(\xi, \frac{\delta_1}{4}\right) \subset \mathcal{B}\left(\xi, \frac{\delta_1}{2}\right).$$

It follows that, for almost all initial conditions $\theta_0 \in \mathcal{B}\left(\xi, \sigma^{-1}\left(2\bar{\|}f^\eta\bar{\|}\right)\right)$, there exists $0 < T_1 < T_2$, such that the trajectory of (4.1) satisfies

$$\theta(T_1;\theta_0) \notin \mathcal{B}\left(\xi, \frac{\delta_1}{4}\right), \quad \theta(T_2;\theta_0) \notin \mathcal{B}\left(\xi, \frac{\delta_1}{2}\right).$$

Let

$$\underline{\delta} = \min_{\xi \in \mathcal{F}_0} \delta_\xi,$$

which is positive, by the 2π-periodicity of W and since the set $\mathcal{F}_0$ contains only a finite number of elements in each hypercube $C_{2\pi} \subset \mathbb{R}^N$ of side 2π.

As already shown, using (4.48), the trajectories of (4.1) can spend at most a finite time outside the ball $\mathcal{B}\left(F_0, \sigma^{-1}\left(2\overline{\|f^\eta\|}\right)\right)$, where F_0 is defined in (4.36). At the light of the above analysis, if

$$|\eta| < \min\left\{\rho_1^{-1}\left(\frac{1}{2}\sigma\left(\frac{\delta_1}{4}\right)\right), \underline{\delta}\right\},$$

we can find, for almost all $\theta_0 \in \mathcal{B}\left(\xi, \sigma^{-1}\left(2\overline{\|f^\eta\|}\right)\right)$, $\xi \in \mathcal{F}_0$, a succession of time instants $0 \leq \tau_1 < \tau_2 < \tau_3 < \tau_4 < \tau_5$, such that the trajectory of (4.1) starting in θ_0 satisfies

$$|\theta(\tau_1, \theta_0)|_\xi = \sigma^{-1}\left(2\overline{\|f^\eta\|}\right), \tag{4.52a}$$

$$|\theta(\tau_2, \theta_0)|_\xi = \frac{\delta_1}{4}, \tag{4.52b}$$

$$|\theta(\tau_3, \theta_0)|_\xi = \frac{\delta_1}{2}, \tag{4.52c}$$

$$|\theta(\tau_4, \theta_0)|_{\xi'} = \frac{\delta_1}{4}, \tag{4.52d}$$

$$|\theta(\tau_5, \theta_0)|_{\xi'} = \sigma^{-1}\left(2\overline{\|f^\eta\|}\right), \tag{4.52e}$$

where

$$\xi' \in \mathcal{F}_0 \cup \left\{\{x\} : \ x \in \mathcal{W}_m\right\}.$$

We now show that, if $|\eta|$ is sufficiently small then it necessary holds that

$$x \in \xi, x' \in \xi' \quad \Rightarrow \quad W(x') < W(x),$$

that is the trajectory has moved toward a critical set corresponding to a lower W-level set. We know from (4.39) that W is strictly decreasing on $[\tau_1, \tau_2) \cup (\tau_4, \tau_5]$. Moreover, we can give an explicit estimate of the decreasing of W on $[\tau_2, \tau_4]$. Let

$$\epsilon_0 = \frac{1}{2} \min_{\theta \in \mathbb{R}^N \setminus \mathcal{B}\left(F_0, \frac{\delta_1}{4}\right)} |\nabla W(\theta)|^2 \tag{4.53}$$

be half of the minimum rate of decreasing of W away from the critical points in the unperturbed case ($\omega = 0$). It follows from (4.34) that there exists $\delta' > 0$ such that, if $\overline{\|f^\eta\|} < \delta'$, then in the perturbed case we have

$$\max_{\theta \in \mathbb{R}^N \setminus \mathcal{B}\left(F_0, \frac{\delta_1}{4}\right)} \dot{W}_\eta(\theta) = \max_{\theta \in \mathbb{R}^N \setminus \mathcal{B}\left(F_0, \frac{\delta_1}{4}\right)} \left(-|\nabla W(\theta)|^2 + f^\eta(\theta)^\top \nabla W(\theta)\right) < -\epsilon_0. \tag{4.54}$$

Moreover, let

$$M_f := 2 \max_{\theta \in \mathbb{R}^N \setminus \mathcal{B}\left(F_0, \frac{\delta_1}{4}\right)} |\nabla W(\theta)|, \tag{4.55}$$

be an upper bound on the magnitude of the vector field away from the critical points in the unperturbed case, and, again by continuity, pick $\delta'' > 0$ such that

$$\overline{\|f^\eta\|} < \delta'' \quad \Rightarrow \quad \max_{\theta \in \mathbb{R}^N \setminus \mathcal{B}\left(F_0, \frac{\delta_1}{4}\right)} |\nabla W(\theta) + f^\eta(\theta)| \ \leq \ M_f. \tag{4.56}$$

It follows from (4.52b), (4.52c), and (4.52d) that in the time interval $[\tau_2, \tau_4]$ the trajectory has traveled a distance at least equal to $\frac{\delta_1}{2}$. From (4.56) it then follows that, if $|\eta| <$

$\min\left\{\rho_1^{-1}\left(\frac{1}{2}\sigma\left(\frac{\delta_1}{4}\right)\right), \underline{\delta}, \rho_1^{-1}(\delta'')\right\}$, then the time interval $[\tau_2, \tau_4]$ to travel this distance satisfies

$$\tau_4 - \tau_2 \geq \frac{\delta_1}{2M_f}.$$

Using (4.54), if

$$|\eta| < \min\left\{\rho_1^{-1}\left(\frac{1}{2}\sigma\left(\frac{\delta_1}{4}\right)\right), \underline{\delta}, \rho_1^{-1}(\delta'), \rho_1^{-1}(\delta'')\right\},$$

then

$$W(\theta(\tau_4, \theta_0)) - W(\theta(\tau_2, \theta_0)) < \Delta W_{min} := -\epsilon_0 \frac{\delta_1}{2M_f}. \tag{4.57}$$

Define the maximum variation $\delta W_{in}(\overline{\|f^\eta\|})$ of W inside the sets $\mathcal{B}\left(\xi, \sigma^{-1}\left(2\overline{\|f^\eta\|}\right)\right)$, for $\xi \in \mathcal{F}_0$ as

$$\delta W_{in}(\overline{\|f^\eta\|}) := \max_{\xi \in \mathcal{F}_0} \left(\max_{\theta \in \mathcal{B}\left(\xi, \sigma^{-1}\left(2\overline{\|f^\eta\|}\right)\right)} W(\theta) - \min_{\theta \in \mathcal{B}\left(\xi, \sigma^{-1}\left(2\overline{\|f^\eta\|}\right)\right)} W(\theta) \right). \tag{4.58}$$

If $\Delta W_{min} > \delta W_{in}(\overline{\|f^\eta\|})$, then the trajectory of (4.1) must enter at time τ_5 a set $\mathcal{B}\left(\xi', \sigma^{-1}\left(2\overline{\|f^\eta\|}\right)\right)$ with $W(x') < W(x)$, for all $x' \in \xi'$ and all $x \in \xi$. Indeed, by definition, for all $\theta \in \mathcal{B}\left(\xi, \sigma^{-1}\left(2\overline{\|f^\eta\|}\right)\right)$, it holds that

$$W(\theta) \geq \max_{\theta \in \mathcal{B}\left(\xi, \sigma^{-1}\left(2\overline{\|f^\eta\|}\right)\right)} W(\theta) - \delta W_{in}(\overline{\|f^\eta\|}).$$

Since

$$W(\theta(\tau_1, \theta_0)) \leq \max_{\theta \in \mathcal{B}\left(\xi, \sigma^{-1}\left(2\overline{\|f^\eta\|}\right)\right)} W(\theta),$$

if $\Delta W_{min} > \delta W_{in}(\overline{\|f^\eta\|})$, then

$$W(\theta(\tau_5, \theta_0)) < \max_{\theta \in \mathcal{B}\left(\xi, \sigma^{-1}\left(2\overline{\|f^\eta\|}\right)\right)} W(\theta) - \delta W_{in}(\overline{\|f^\eta\|}).$$

Hence necessarily $W(x') < W(x)$, for all $x' \in \xi'$ and all $x \in \xi$. Noticing that, by continuity, $\delta W_{in}(\overline{\|f^\eta\|})$ tends continuously to zero as $\overline{\|f^\eta\|} \to 0$, we can find $\delta''' > 0$, such that, if $\overline{\|f^\eta\|} < \delta'''$, then

$$\delta W_{in}(\overline{\|f^\eta\|}) < \Delta W_{min}.$$

By construction, if

$$|\eta| < \min\left\{\rho_1^{-1}\left(\frac{1}{2}\sigma\left(\frac{\delta_1}{4}\right)\right), \underline{\delta}, \rho_1^{-1}(\delta'), \rho_1^{-1}(\delta''), \rho_1^{-1}(\delta''')\right\},$$

almost all the trajectories starting in $\mathcal{B}\left(\xi, \sigma^{-1}\left(2\overline{\|f^\eta\|}\right)\right)$, for $\xi \in \mathcal{F}_0$, converge in finite time to some set $\mathcal{B}\left(\xi', \sigma^{-1}\left(2\overline{\|f^\eta\|}\right)\right)$, $\xi' \in \mathcal{F}_0 \cup \left\{\{x\} : \ x \in \mathcal{W}_m\right\}$, with ξ' such that

$$x \in \xi, x' \in \xi' \quad \Rightarrow \quad W(x') < W(x).$$

Repeating this construction iteratively, and noticing that W assumes only a finite set of values at its critical points, we conclude that almost all trajectories converge to $\mathcal{B}\left(\mathcal{W}_m, \sigma^{-1}\left(2\overline{\|f^\eta\|}\right)\right)$, in finite time.

From the analysis developed in CASE 1 and CASE 2, it follows that, if

$$|\eta| < \min\left\{\rho_1^{-1}\left(\frac{1}{2}\sigma\left(\frac{\delta_1}{4}\right)\right), \underline{\delta}, \rho_1^{-1}\left(\min\{\delta', \delta'', \delta''', \delta_\sigma, \delta_m\}\right)\right\},$$

then, for almost all initial condition θ_0, there exists $T > 0$ such that the trajectories of (4.1) satisfies $\theta(t;\theta_0) \in Q_{c,k}$, for some $k \in \mathbb{Z}$, for all $t \geq T$, where $Q_{c,k}$ is defined in (4.50) and is compact for all $k \in \mathbb{Z}$, which proves the claim by picking

$$\overline{\delta} := \min\left\{\rho_1^{-1}\left(\frac{1}{2}\sigma\left(\frac{\delta_1}{4}\right)\right), \underline{\delta}, \rho_1^{-1}\left(\min\{\delta', \delta'', \delta''', \delta_\sigma, \delta_m\}\right)\right\}.$$

Chapter 5

Desynchronization via mean-field feedback

In this chapter we explore the possibility of eliminating the pathological neuronal synchronization by effectively desynchronizing the population activity.

While desynchronization owns quite an intuitive meaning, its formal definition is not straightforward. One way of guaranteeing sufficient disorder in a network of oscillators is to induce chaos in the incremental dynamics of their outputs (*i.e.* the dynamics ruling the phase differences of each pair of oscillators). This is the approach followed by chaotification techniques, cf. *e.g.* (Zhang et al., 2009; Gao and Chau, 2002; Chen, 2003; Chen and Yang, 2003). However, chaos may be too strong a requirement in some particular applications and most anti-control techniques may require too much knowledge on the oscillators state to be practically implemented in a DBS device.

On the other hand, simply guaranteeing that phases are not synchronized is not enough in most practical applications. To see this, consider a pair of oscillators whose phases difference, although not constant, remains at all times in a small neighboorhood of a given value. In this case, all classical definitions of synchronization are violated as the oscillators are neither phase synchronized (Strogatz, 2000), nor phase-locked or frequency-synchronized (Blekhman et al., 1997), as their phases difference is not constant. Nevertheless, for practical concerns, such a system cannot be considered as desynchronized since the phases difference remains "almost constant" at all times. In fact, such a situation would rather correspond to "approximative synchronization" as defined in (Blekhman et al., 1997). In a nutschell, desynchronization is not simply the negation of synchronization.

In the textbook (Pikovsky et al., 2001), and references therein, desynchronization is implicitly intended as the absence of approximate synchronization. This requirement translates in asking that the phase difference between each pair of oscillators grows unbounded when lifted to the real line. The existence of unbounded trajectories is treated in a general framework in (Orsi et al., 2001). As we show in Example 5.1, asking that the phase-difference is unbounded may not suffice to exclude asymptotic synchronization either.

The objective of this chapter is to define desynchronization in a rigorous manner for general networks of interconnected phase oscillators, and to provide a geometric and topological interpretation of this property by linking it to existing concepts of instability (Nemytskii and Stepanov, 1960). Roughly speaking, a pair of oscillators will be considered as desynchronized if their phases are permanently drifting away. This concept (referred to as strong desynchronization in Section 5.1) is quite demanding due to the requirement of all-time phase drift. We therefore propose a relaxed notion, called practical desynchronization, that imposes phase

drift only in average over a given time window (Section 5.2). For each of these properties, we propose a characterization involving the grounded variables of the system, *i.e.* the differences between the oscillators' phases and their mean.

Based on this theoretical background, we show, by relying on the model derived in Chapter 2, that practical desynchronization can be induced in an interconnected neuronal population via mean-field feedback (Theorem 5.10). More precisely, we provide a sufficient condition involving the differences in the natural frequencies, the interconnection topology, and the stimulation/registration setup to ensure that a given pair of oscillators is practically desynchronized. This condition can readily be used for mean-field feedback control design, and to compute a lower bound on the number of desynchronized pairs. We specialize this analysis to the all-to-all case in Corollary 5.11.

The chapter is structured as follows. In Section 5.1 we derive the proposed definition of strong desynchronization and mathematically characterize it. We derive the notion of practical desynchronization and characterize it mathematically in Section 5.2. A rigorous analysis on how these properties can be induced in the Kuramoto system via proportional mean-field feedback is provided in Section 5.3. We give the proofs of the main results in Section 5.4, while technical proofs are given in Section 5.5.

5.1 Strong desynchronization

The dynamics of a network of coupled nonlinear phase oscillators can be expressed as

$$\dot{\theta} = F(\theta, t), \tag{5.1}$$

where $F : T^N \times \mathbb{R} \to \mathbb{R}^N$ satisfies the Caratheodory conditions (Hale, 1969) and $F(\cdot, t)$ is locally Lipschitz for each $t \in \mathbb{R}$. Since $F(\cdot, t)$ is defined on T^N, it is 2π-periodic, and since it is also locally Lipschitz, it is bounded and globally Lipschitz. This ensures, together with the Caratheodory conditions, existence and unicity of the solution of (5.1), cf. *e.g.* (Hale, 1969, Theorems 3.1 and 5.1). Each component θ_i, $i = 1, \ldots, N$, of θ is the phase of the oscillator i. The function F describes both the internal dynamics of each oscillator and the coupling between different oscillators. This class of systems encompasses the phase oscillators studied in (Brown et al., 2003), of which the Kuramoto system (Kuramoto, 1984) is probably the most famous representative (cf. Section 5.3 for a deeper analysis). In what follows we derive a suitable definition of desynchronization and provide a mathematical characterization.

5.1.1 Definitions

A pair $(i, j) \in \mathbb{N}_N^{\neq}$ of coupled oscillators (5.1) undergoes *frequency synchronization* (Blekhman et al., 1997) if, given $t_0 \in \mathbb{R}$ and $\theta_0 \in T^N$,

$$|\dot{\theta}_i(t) - \dot{\theta}_j(t)| = 0, \quad \forall t \in \mathbb{R}, \tag{5.2}$$

where $\dot{\theta}_i(\cdot) := \dot{\theta}_i(\cdot; t_0, \theta_0)$ and similarly for $\theta_j(\cdot)$. This relation, which is also referred to as *phase-locking*, guarantees a constant phase difference between the oscillators i and j. A particular case of phase-locking is when this phase difference is zero, thus making $\theta_i(t)$ and $\theta_j(t)$ equal at all times. This stronger property is referred to as *phase synchronization*. When these properties hold asymptotically (*i.e.* as time goes to infinity), we refer to these properties as asymptotic phase-locking and asymptotic synchronization respectively (Strogatz, 2000; Pikovsky et al., 2001).

Asymptotic phase-locking is guaranteed (at least locally) if an asymptotically stable fixed point exists for the incremental dynamics ruling $\theta_i - \theta_j$. In the presence of exogenous disturbances or unmodelled dynamics, this asymptotically stable fixed point may present some robustness properties. We speak in this case of *practical phase-locking* (see Chapter 3), which can be formally characterized as[1]

$$|\theta_i(t) - \theta_j(t) - \delta\theta_{ij}| \leq \varepsilon_{ij}, \quad \forall t \in \mathbb{R}, \tag{5.3}$$

where $\delta\theta_{ij} \in [0; 2\pi)$ and $\varepsilon \geq 0$. When (5.3) holds only for a subset of pairs of oscillators, it is also referred to as *partial entrainment* (Aeyels and Rogge, 2004). Since $\theta \in T^N$, the above constraint is trivially satisfied if ε_{ij} is greater than π. On the other hand, for small values of ε_{ij}, the condition (5.3) imposes that the phase difference between oscillators i and j, while not remaining constant, exhibit small oscillations around some constant values $\delta\theta_{ij}$.

For desynchronization to have a practical relevance in most applications, it must exclude the two situations described by (5.2) and (5.3) and their asymptotic counterparts. Simply asking that the phase difference between two oscillators becomes unbounded when lifted on the real line may not be enough, as illustrated in the following example.

Example 5.1. *Given $t_0 > 0$, consider the non-autonomous dynamics*

$$\dot{\theta}_{\pm}(t; t_0, \theta^0_{\pm}) = \omega \pm \frac{\delta\omega}{t}, \ \forall t \geq t_0.$$

Then

$$\theta_+(t; t_0, \theta^0_+) - \theta_-(t; t_0, \theta^0_-) = 2\delta\omega\big(\ln(t) - \ln(t_0)\big) + \theta^0_+ - \theta^0_-,$$

which grows unbounded, yet

$$\lim_{t\to\infty} \big(\dot{\theta}_+(t; t_0, \theta^0_+) - \dot{\theta}_-(t; t_0, \theta^0_-)\big) = 0,$$

meaning that asymptotic phase-locking is achieved.

Another natural requirement to make sure that the system is desynchronized is then to ask that the phases of oscillators i and j permanently drift away from one another, *i.e.*

$$|\dot{\theta}_i(t) - \dot{\theta}_j(t)| > 0, \ \forall t \in \mathbb{R}.$$

However, this requirement alone may not be enough either, since, for example, asymptotic phase-locking, that is

$$\lim_{t\to\infty} \dot{\theta}_i(t) - \dot{\theta}_j(t) = 0,$$

may satisfy it (if the convergence is achieved in infinite time only). For a pair of oscillators to be desynchronized, we therefore ask that the relative drift be *uniformly* bounded away from zero. This requirement ensures that the considered oscillators have their phases mutually drifting at all times and keeping on evolving in the torus with uniformly non-zero frequency difference. These conditions can be cast in a compact form in the following definition.

Definition 5.1. A pair $(i, j) \in \mathbb{N}_N^{\neq}$ of oscillators is said to be *strongly desynchronized* for (5.1) if there exists $\Omega_{ij} > 0$ such that, for all $\theta_0 \in T^N$ and all $t_0 \in \mathbb{R}$,

$$|\dot{\theta}_i(t; t_0, \theta_0) - \dot{\theta}_j(t; t_0, \theta_0)| \geq \Omega_{ij}, \quad \forall t \in \mathbb{R}. \tag{5.4}$$

[1] We stress that the constant $\delta\theta_{ij}$ and ε_{ij} may depend on the inital conditions (t_0, θ_0).

Given $m \in \left\{1, \ldots, \frac{N(N-1)}{2}\right\}$, the network of coupled phase oscillators (5.1) is said to be *m-strongly desynchronized* if it contains m distinct pairs of desynchronized oscillators. If $m = \frac{N(N-1)}{2}$ then (5.1) is said to be *completely strongly desynchronized*.

Definition 5.1 satisfies two basic requirements: 1) it excludes synchronization and practical synchronization, also asymptotically; 2) it is naturally satisfied by an ensemble of uncoupled oscillators, provided the natural frequencies are not identical. We stress, however, that Definition 5.1 does not exclude $p : q$ resonances[2] with $p \neq q$.

5.1.2 Mathematical characterization of desynchronization

In order to give a geometrical interpretation of this property, we introduce the *grounded variable* $\psi \in \mathbb{R}^N$ associated to (5.1). Given some $\theta_0 \in T^N$ and some $t_0 \in \mathbb{R}$, the evolution of ψ is defined as

$$\begin{aligned} \dot{\psi}(t; t_0, \theta_0) &:= \left(I_N - \frac{1}{N}\mathbf{1}_N\mathbf{1}_N^\top\right)\dot{\theta}(t; t_0, \theta_0), \ \forall t \in \mathbb{R} \\ \psi(t_0; t_0, \theta_0) &= \theta_0 \end{aligned} \tag{5.5}$$

which constitutes a non-autonomous dynamics on $\mathbb{R}^N$. We refer to (5.5) as the *grounded dynamics* of (5.1). We stress that (5.5) could have been equivalently defined on either $\mathbb{R}^N$ or T^N. Note indeed that, since the right hand side of (5.1) satisfies the Charatheodory conditions and is globally Lipschitz in θ, (5.1) is forward complete (Khalil, 2001, Theorem 3.2). Hence, $\dot{\theta}(t; t_0, \theta_0) \in \mathbb{R}^N$, for all $t, t_0 \in \mathbb{R}$ and all $\theta_0 \in T^N$, and thus (5.5) induces a well defined non-autonomous vector field on both $\mathbb{R}^N$ and T^N. For future convenience we define here (5.5) as non-autonomous dynamics on $\mathbb{R}^N$. Noticing that

$$\frac{1}{N}\mathbf{1}_N^\top\dot{\theta} = \frac{1}{N}\sum_{i=1}^{N}\dot{\theta}_i,$$

this dynamics describes the evolution of the system (5.1) in a moving reference frame with speed equal to the instantaneous mean frequency $\frac{1}{N}\sum_{j=1}^{N}\dot{\theta}_j(t)$. This implies that $\dot{\psi}(t) \in \mathbf{1}_N^\perp \subset \mathbb{R}^N$, for all $t \in \mathbb{R}$, where $\psi(\cdot) := \psi(\cdot; t_0, \theta_0)$, that is the grounded dynamics has zero mean-drift, and $\mathbf{1}_N^\top\psi(t) \equiv \mathbf{1}_N^\top\theta_0$. In addition, it is possible to show that asymptotic phase-locking of (5.1) corresponds to the existence of an asymptotically stable set for (5.5) (cf. *e.g.* (Jadbabaie et al., 2004)), and, similarly, that practical phase-locking corresponds to bounded trajectories.

We introduce here some concepts that serves as the basis of the mathematical characterization of strong desynchronization. This concept pertains to non-autonomous dynamical systems of the form

$$\dot{x} = G(x, t), \tag{5.6}$$

where $G : \mathbb{R}^n \times \mathbb{R} \to \mathbb{R}^n$ satisfies the Caratheodory conditions, and $G(\cdot, t)$ is continuous and locally Lipschitz, which ensures existence and unicity of the solution (Hale, 1969, Theorems 3.1 and 5.1).

Definition 5.2. (Nemytskii and Stepanov, 1960). The dynamical system (5.6) is said to be *completely unstable* if all its points are wandering, that is for all $x_0 \in \mathbb{R}^n$ and all $t_0 \in \mathbb{R}$, there exists a neighborhood U of x_0 and a time $T > 0$, such that

$$x(t; t_0, U) \cap U = \emptyset, \ \forall t \geq T + t_0.$$

[2] A pair of oscillator is said to be in a $p : q$ resonance, if the difference $|p\theta_i - q\theta_j|$ lifted to the real line remains bounded for all time, for some $p, q \in \mathbb{N}_{>0}$.

Complete instability can be considered as the complementary of asymptotic stability. Indeed, complete instability implies that, given *any* point, one can find a sufficiently small neighborhood around it, such that, after a sufficiently long time, the trajectories of the system leave the neighborhood and never go back in. The above definition is of no relevance to systems evolving in a compact space, as in this case the α- and ω-limit sets[3] are always non-empty (Bhatia and Szegö, 1970).

In the following lemma we give a sufficient condition for (5.6) to be completely unstable. Its proof is provided in Section 5.4.1.

Lemma 5.3. *Suppose that (5.6) is forward complete. Suppose moreover that there exists a vector $\alpha \in \mathbb{R}^n$ and a constant $\overline{\alpha} > 0$ such that, for all $x_0 \in \mathbb{R}^n$ and all $t_0 \in \mathbb{R}$, the solution of (5.6) satisfies*

$$\alpha^\top G(x(t; t_0, x_0), t) \geq \overline{\alpha}, \quad \forall t \in \mathbb{R}.$$

Then (5.6) is completely unstable.

Based on the above considerations, we now state the following theorem, which gives a geometrical and topological characterization of strong desynchronization in the sense of Definition 5.1. The proof is provided in Section 5.4.2.

Theorem 5.4. *The pair $(i, j) \in \mathbb{N}_N^{\neq}$ of oscillators is strongly desynchronized for the system (5.1), if and only if there exists a constant $\bar{\alpha} > 0$, such that, for all $\theta_0 \in T^N$ and $t_0 \in \mathbb{R}$, the grounded dynamics (5.5) satisfies*

$$\dot{\psi}(t; t_0, \theta_0)^\top (e_i - e_j) \geq \bar{\alpha}, \quad \forall t \in \mathbb{R}, \tag{5.7}$$

along the solutions of (5.1). In particular, if the pair (i, j) is strongly desynchronized, then the grounded dynamics (5.5) associated to (5.1) is completely unstable.

Theorem 5.4 highlights two properties of desynchronized dynamical systems: one geometrical, and the other topological. The first one, geometrical property, is contained in (5.7). It states that the grounded dynamics (5.5) is uniformly drifting away along the direction given by $e_i - e_j \in \mathbf{1}_N^\perp$. If we plug the mean-drift back in, and project the resulting dynamics on the torus (to recover the original phase dynamics (5.1)), this means that in the (θ_i, θ_j) sub-torus the trajectories of (5.1) are (locally) uniformly drifting away from the synchronization sub-manifold

$$\mathcal{D}_{ij} := \{\theta \in T^N : \ \theta_i = \theta_j\}.$$

This is described by Figure 5.1.

The topological characterization comes directly from the second part of the statement. In particular the grounded dynamics associated to a desynchronized system satisfies the complete instability property of Definition 5.2. We point out that this characterization complements the one associated to phase-locking, that is the asymptotic stability of the grounded dynamics.

Given $m \in \left\{1, \ldots, \frac{N(N-1)}{2}\right\}$, the following corollary, which is a direct consequence of Theorem 5.4, gives a characterization of m-strong desynchronization and therefore of complete strong desynchronization. We stress that the above geometrical interpretation (Figure 5.1) extends to all the m pairs of strongly desynchronized oscillators.

Corollary 5.5. *Given $m \in \left\{1, \ldots, \frac{N(N-1)}{2}\right\}$, if the system (5.1) is m-strongly desynchronized then its associated grounded dynamics (5.5) is completely unstable.*

[3] The ω- (resp. α-) limit set of a point x_0 is the union of all the points $\bar{x}$ for which there exists an increasing (resp. decreasing) and unbounded sequence of time instants $\{t_n\}_{n\in\mathbb{N}} \subset \mathbb{R}$ such that $\lim_{n\to\infty} x(t_n; t_0, x_0) = \bar{x}$.

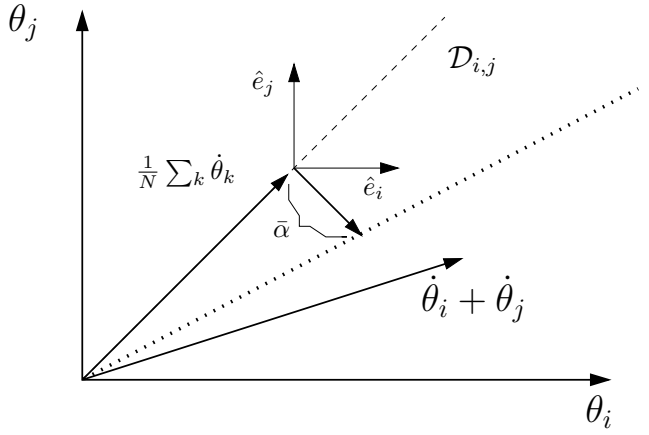

FIGURE 5.1: Geometric interpretation of desynchronization

5.2 Practical desynchronization

5.2.1 Definition

For particular applications, strong desynchronization may appear to be too demanding a requirement. For example, in electrical treatment of neurological diseases, only the average rate of discharge of the neurons is of interest (Volkmann et al., 1996; Sarma et al., 2010; Lopez-Azcarate et al., 2010; Plenz and Kital, 1999; Rosa et al., 2010). More generally, the presence of exogenous disturbances, small coupling, or unmodelled dynamics may let the requirement of Definition 5.1 be too restrictive. The permanent phase drift imposed in Definition 5.1 impedes the instantaneous frequencies to be equal even on short time intervals. Intuitively, such a frequency similarity would not affect the overall desynchronization if it happens sufficiently rarely. Hence, we relax that definition by replacing the pointwise inequality (5.4) by the less restrictive assumption that the difference of frequencies be bounded from below in average, uniformly over some moving window of length T.

Definition 5.6. A pair $(i,j) \in \mathbb{N}_N^{\neq}$ of oscillators is said to be *practically desynchronized* for (5.1) if there exists $\Omega_{ij}, T_{ij} > 0$ such that, for all $\theta_0 \in T^N$ and $t_0 \in \mathbb{R}$,

$$\frac{1}{T_{ij}} \left| \int_t^{t+T_{ij}} \left(\dot{\theta}_i(\tau; t_0, \theta_0) - \dot{\theta}_j(\tau; t_0, \theta_0) \right) d\tau \right| \geq \Omega_{ij}, \tag{5.8}$$

for all $t \in \mathbb{R}$. Given $m \in \left\{1, \ldots, \frac{N(N-1)}{2}\right\}$, the network of coupled phase oscillators (5.1) is said to be *m-practically desynchronized* if it contains m distinct pairs of practically desynchronized oscillators. If $m = \frac{N(N-1)}{2}$ then (5.1) is said to be *completely practically desynchronized*.

Even though the computation of the time window length T_{ij} can seem a hard task in general, the intrinsic periodicity of phase oscillators can help to find it. As shown in Theorem 5.10 and Corollary 5.11 below, in the case of Kuramoto oscillators under mean-field feedback (2.6), T_{ij} can simply be picked as twice the mean period of the uncoupled and unforced oscillations, *i.e.* $T_{ij} = \frac{\pi}{\bar{\omega}}$, where $\bar{\omega} := \frac{1}{N}\sum_{i=1}^N \omega_i$ is the mean natural frequency of the ensemble. Note that (5.8) implies that the scalar function $\theta_i(\cdot) - \theta_j(\cdot)$ is persistently exciting on each time interval $[t, t+T_{ij}]$ (Panteley et al., 2001). The converse implication is not necessarily true.

The following example, inspired by the textbook (Pikovsky et al., 2001) (see also (Pazó et al., 2003; Popovych et al., 2007)), illustrates another important case in which Definition 5.6 applies [4].

Example 5.2. *An interesting phenomenon exhibited by some coupled oscillators is that of "phase-slips" (Pikovsky et al., 2001, Sections 3.1.3 and 3.4.2). See also (Pazó et al., 2003; Popovych et al., 2007). Roughly speaking, two oscillators undergo phase-slips when their phase difference remains constant, or with small variations, most of the time, apart from periods in which it abruptly increases (a slip). The typical time-course of the phase difference between two coupled oscillators undergoing phase-slips is depicted in Figure 5.2.*

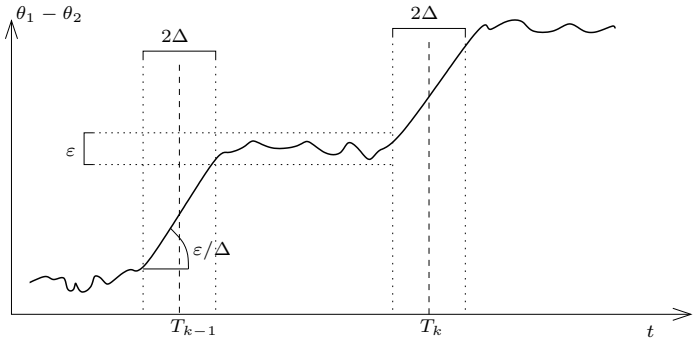

FIGURE 5.2: Time-course of the phase difference between two couple oscillators undergoing successive phase-slips on the intervals $[T_k - \Delta, T_k + \Delta]$. The constants ε, Δ are defined in (5.11) below.

If the length of the time intervals between two successive phase-slips varies in an unpredictable way, it might be hard to figure out a suitable time window over which the property (5.8) can be checked. In order to find conditions under which this is possible, let us formalize the phase-slip behavior in a slightly more general context. Given initial conditions $t_0 \in \mathbb{R}$, $\theta_1^0, \theta_2^0 \in T^N$, *consider a pair of forced coupled oscillators*

$$\dot{\theta}_1 = F_1(\theta_1, \theta_2, u_1(t)), \tag{5.9}$$
$$\dot{\theta}_2 = F_2(\theta_1, \theta_2, u_2(t)), \tag{5.10}$$

for all $t \in \mathbb{R}$, *where* $u_1, u_2 : \mathbb{R} \to \mathbb{R}$ *are exogenous inputs. Suppose that the time instants* $\{T_k\}_{k\in\mathbb{Z}} \subset \mathbb{R}$ *at which phase-slips occur form a lower and upper unbounded increasing sequence and that, moreover, the increments* $T_k - T_{k-1}$ *are uniformly bounded, that is there exists* $\bar{T} > 0$ *such that* $T_k - T_{k-1} < \bar{T}$ *for all* $k \in \mathbb{Z}$. *Defining, for all* $t \in \mathbb{R}$, *the set* A_t *as*

$$A_t := [t, t + \bar{T}] \setminus \bigcup_{k\in\mathbb{Z}} [T_k - \Delta, T_k + \Delta],$$

we can then formalize the phase-slip behavior depicted in Figure 5.2 as follows. For all $t_0 \in \mathbb{R}$, *all* $\theta_1^0, \theta_2^0 \in T^1$, *and all* $k \in \mathbb{Z}$, *there exists* $\varepsilon > 0$ *and* $\Delta \in (0, \bar{T}/2)$, *such that*

$$\left| \int_{A_t} \left(\dot{\theta}_1(\tau) - \dot{\theta}_2(\tau) \right) d\tau \right| \leq \varepsilon, \ \forall t \in \mathbb{R}, \tag{5.11a}$$
$$\dot{\theta}_1(t) - \dot{\theta}_2(t) \geq \frac{\varepsilon}{\Delta}, \ \forall t \in [T_k - \Delta, T_k + \Delta]. \tag{5.11b}$$

[4] The authors are thankful to an anonymous reviewer of the first version of this paper for bringing their attention to this example.

where $\dot\theta_1(\cdot) = \dot\theta_1(\cdot; t_0, \theta_1^0)$, and similarly for θ_2. Condition (5.11a) implies that outside the intervals $[T_k - \Delta, T_k + \Delta]$, $k \in \mathbb{Z}$, the two oscillators remain practically phase-locked. In particular their phase difference does not vary more than ε. Conversely, (5.11b) implies that on each time interval $[T_k - \Delta, T_k + \Delta]$ the phase θ_1 slips away from θ_2 faster than ε/Δ.

A similar behavior is observed in forced coupled oscillators subject to strong noise, as the ones considered in (Pikovsky et al., 2001, Section 3.4.2), in which case u_1, u_2 are the realization of a given stochastic process. Another example is provided by coupled chaotic oscillators before the "phase-synchronization" transition, like the ones considered in (Pikovsky et al., 2001, Section 3.1.3) and (Pazó et al., 2003; Popovych et al., 2007). In these cases, if condition (5.11) holds, then

$$\begin{aligned}\frac{1}{\bar T}\left|\int_t^{t+\bar T}\big(\dot\theta_1(\tau)-\dot\theta_2(\tau)\big)\,d\tau\right| &\geq \frac{1}{\bar T}\left|\int_{[t,t+\bar T]\setminus A_t}\big(\dot\theta_1(\tau)-\dot\theta_2(\tau)\big)\,d\tau\right| \\ &\quad -\frac{1}{\bar T}\left|\int_{A_t}\big(\dot\theta_1(\tau)-\dot\theta_2(\tau)\big)\,d\tau\right| \\ &\geq \frac{2\varepsilon}{\bar T}-\frac{\varepsilon}{\bar T}\geq\frac{\varepsilon}{\bar T},\end{aligned}$$

that is the two oscillators are practically desynchronized in the sense of Definition 5.6. This example thus illustrates the fact that phase-slips do not prevent practical synchronization, provided that the slips are sufficiently important. ♢

In the following proposition, whose proof is provided in Section 5.4.3, we show that if (5.1) is time-invariant, then uniformity of (5.8) in θ_0 suffices to ensure its uniformity in time. This lets (5.8) be easier to check in practice (see also Theorem 5.10 below).

Proposition 5.7. *Suppose that (5.1) is time-invariant. Given $T_{ij}, \Omega_{ij} > 0$, assume that there exists a pair of oscillators $(i,j) \in \mathbb{N}_N^{\neq}$ satisfying (5.8) for all $\theta_0 \in T^N$, and for some $t = T^* \in \mathbb{R}$. Then (5.8) holds for all $t \in \mathbb{R}$.*

5.2.2 Characterization of practical desynchronization

In order to extend the interpretation developped in Section 5.1.2 to the case of practical synchronization, we introduce an averaged system associated to (5.1). Given any $T > 0$, any $\theta_0 \in T^N$, and any $t_0 \in \mathbb{R}$, the *T-averaged* system associated to (5.1) is defined as

$$\begin{aligned}\dot{\widehat{\langle\theta(t;t_0,\theta_0)\rangle_T}} &:= \frac{1}{T}\int_T^{t+T}\dot\theta(\tau;t_0,\theta_0)d\tau, \\ \langle\theta(t_0;t_0,\theta_0)\rangle_T &:= \theta_0,\end{aligned} \tag{5.12}$$

for all $t \in \mathbb{R}$. The averaged system evolves with the average instantaneous frequency of the system (5.1) over a sliding time window of length T. We point out that, since, by forward completeness of (5.1),

$$\frac{1}{T}\int_T^{t+T}\dot\theta(\tau;t_0,\theta_0)d\tau \in \mathbb{R}^N,\ \forall t\in\mathbb{R},$$

the system (5.12) is a well defined non-autonomous dynamics on T^N.

The following lemma, whose proof is trivial and is omitted, shows that the practical desynchronization of (5.1) corresponds to the strong desynchronization of its averaged system.

Lemma 5.8. *There pair $(i,j) \in \mathbb{N}_N^{\neq}$ of oscillators is practically desynchronized for the system (5.1), that is θ_i, θ_j satisfy (5.8) for some $\Omega_{ij}, T_{ij} > 0$, if and only if the T_{ij}-averaged system*

(5.12) associated to (5.1), satisfies, for all $t_0 \in \mathbb{R}$ and all $\theta \in T^N$,

$$|\widehat{\dot{\langle\theta_i(t;t_0,\theta_0)\rangle}}_{T_{ij}} - \widehat{\dot{\langle\theta_j(t;t_0,\theta_0)\rangle}}_{T_{ij}}| \geq \Omega_{ij}, \ \forall t \in \mathbb{R}, \tag{5.13}$$

that is $\langle\theta_i\rangle_{T_{ij}}$ and $\langle\theta_j\rangle_{T_{ij}}$ are strongly desynchronized.

At the light of the above lemma we are able to give a characterization of practical desynchronization. For all $T \geq 0$, the *T-averaged grounded dynamics* $\psi_T \in \mathbb{R}^N$ associated to (5.12) is given by

$$\begin{aligned} \dot{\psi}_T(t;t_0,\theta_0) &:= \left(I_N - \frac{1}{N}\mathbf{1}_N\mathbf{1}_N^\top\right)\widehat{\dot{\langle\theta(t;t_0,\theta_0)\rangle}}_T \\ \psi_T(t_0;t_0,\theta_0) &= \theta_0. \end{aligned} \tag{5.14}$$

The following corollary, which is a direct consequence of Theorem 5.4 and Lemma 5.8, provides a complete characterization of practical desynchronization.

Corollary 5.9. *There exists a pair $(i,j) \in \mathbb{N}_N^{\neq}$ of practically desynchronized oscillators for system (5.1) if and only if there exist some constants $\bar{\alpha}, T > 0$, such that, for all $\theta_0 \in T^N$ and all $t_0 \in \mathbb{R}$, the T-averaged grounded dynamics (5.14) satisfies*

$$\dot{\psi}_T(t;t_0,\theta_0)^\top(e_i - e_j) \geq \bar{\alpha}, \quad \forall t \in \mathbb{R}. \tag{5.15}$$

In particular, if the pair (i,j) is practically desynchronized, the T-averaged grounded dynamics (5.14) associated to (5.1) is completely unstable.

5.3 Desynchronization of the Kuramoto system through mean-field feedback

Let us recall the phase model derived in Chapter 2 for an interconnected neuronal population under mean-field feedback:

$$\dot{\theta}_i = \omega_i + \sum_{j=1}^{N}(k_{ij}+\gamma_{ij})\sin(\theta_j - \theta_i) - \sum_{j=1}^{N}\gamma_{ij}\sin(\theta_j + \theta_i), \ \forall i = 1,\ldots,N, \tag{5.16}$$

where θ_i represents the phase of the oscillator i, the parameters k_{ij} represent the interconnection gains between two oscillators, and γ_{ij} are gains resulting from the application of the proportional mean-field feedback.

It was shown in Chapter 2 that, for almost all interconnection topology and almost all value of the feedback gain, phase-locking is impossible under MFF. In the next theorem, whose proof is provided in Section 5.4.4, we show that practical desynchronization can actually be achieved by MFF. In other words, we give a sufficient condition to assure that a given couple of oscillators is practically desynchronized while the ensemble keeps on oscillating (Figure 5.3).

Theorem 5.10. *Suppose that there exists $i,j \in \mathbb{N}_N^{\neq}$, such that*

$$\Omega_{ij} := |\omega_i - \omega_j| - \sum_{h=1}^{N}|\gamma_{ih}+\gamma_{jh}|\left(\frac{\pi\nu}{2\overline{\omega}} + \frac{\nu^2}{6\overline{\omega}^2}\right) - \sum_{h=1}^{N}|\varepsilon_{ih}+\varepsilon_{jh}| > 0, \tag{5.17}$$

where $\nu := 2\max_{h=1,\ldots,N}\left(|\tilde{\omega}_h| + \sum_{h'=1}^{N}|\gamma_{hh'}+\varepsilon_{hh'}|\right)$, $\overline{\omega} := \frac{1}{N}\mathbf{1}_N^\top\omega$, $\tilde{\omega}_h := \omega_h - \bar{\omega}$, and $\varepsilon_{hh'} := k_{hh'} + \gamma_{hh'}$, for all $h,h' = 1,\ldots,N$.
Then the pair of oscillators (i,j) is practically desynchronized.

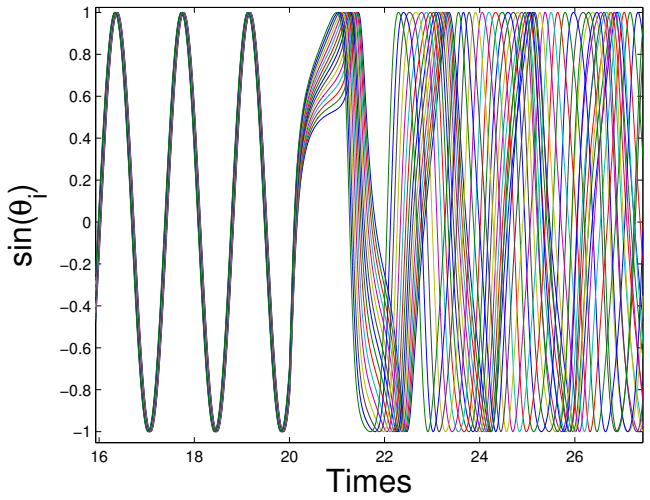

FIGURE 5.3: Evolution of the phases of (5.18) for large natural frequencies when a proportional mean-field feedback with gain $\gamma_0 = -2k_0$ is switched on at time $t = 20$. The mean-field feedback induces desynchronization.

The sufficient condition (5.17) can readily be used in practical applications to explicitly compute the minimum number of desynchronized pairs of oscillators. The term

$$\sum_{h=1}^{N} |\gamma_{ih} + \gamma_{jh}| \left(\frac{\pi \nu}{2\bar{\omega}} + \frac{\nu^2}{6\bar{\omega}^2} \right)$$

is small provided the mean natural frequency $\bar{\omega}$ is large. In the opposite case, one rather expects the mean-field feedback to block the oscillations, as described in Chapter 4. The term

$$\sum_{h=1}^{N} |\varepsilon_{ih} + \varepsilon_{jh}|$$

guides the feedback gain design to obtain oscillators desynchronization by imposing to minimize the closed-loop diffusive coupling strength $k_{ij} + \gamma_{ij}$. In terms of the grounded dynamics associated to (5.19), Corollary 5.9 implies that its average system is completely unstable (Figure 5.4).

Note that, in order to minimize the closed-loop diffusive coupling strength, the feedback gains must be of the same magnitude as the diffusive coupling gains. This ensures that, if the open-loop diffusive coupling strength satisfies the small coupling condition (2.4), *i.e.* $|\kappa| < \delta_h$, then the same holds for the closed-loop coupling. In particular, the practical desynchronization sufficient condition of Theorem 5.10 extends to the full dynamics (2.3), provided that the open-loop coupling strength is sufficiently small. The sufficient coupling strength ensuring phase-locking solely depends on the natural frequency dispersion, whereas the small coupling condition (2.4) solely depends on the natural radius. Thus, imposing a sufficiently large diffusive coupling to ensure phase-locking of the open-loop system (*i.e.* without mean-field feedback) is compatible with the small coupling condition (2.4), provided the natural frequency dispersion is sufficiently small.

In the case when the coupling is given by the all-to-all topology, and each oscillator contributes in the same way at the measured mean-field and receives the input with same intensity, the interconnection and feedback gains become $k_{ij} = k_0$ and $\gamma_{ij} = \gamma_0$, for all $i, j = 1, \ldots, N$. In

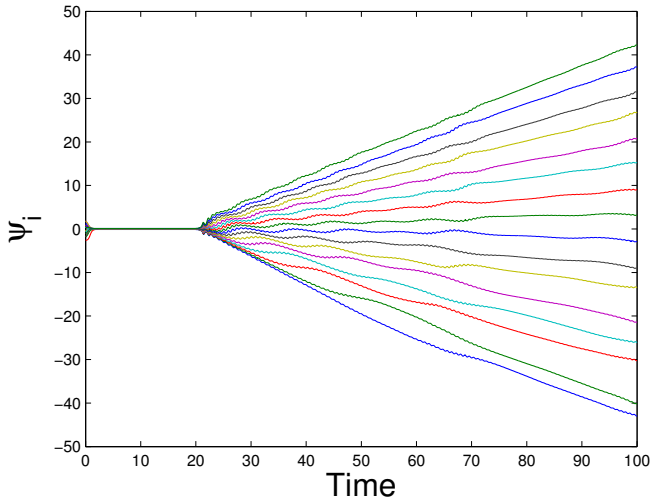

FIGURE 5.4: Evolution of the grounded dynamics of (5.18) for large natural frequencies when a proportional mean-field feedback with gain $\gamma_0 = -k_0$ is switched on at time $t = 20$

this case (5.16) reduces to

$$\dot{\theta}_i \quad = \quad \omega_i + (k_0 + \gamma_0) \sum_{j=1}^{N} \sin(\theta_j - \theta_i) - \gamma_0 \sum_{j=1}^{N} \sin(\theta_j + \theta_i), \ \forall i = 1, \dots, N. \tag{5.18}$$

The diffusive coupling term $(k_0 + \gamma_0) \sum_{j=1}^{N} \sin(\theta_j - \theta_i)$ can be eliminated by choosing $\gamma_0 = -k_0$, and (5.18) reduces to

$$\dot{\theta}_i = \omega_i + k_0 \sum_{j=1}^{N} \sin(\theta_j + \theta_i), \ \forall i = 1, \dots, N. \tag{5.19}$$

Theorem 5.10 then relaxes in this case to the following corollary, whose proof is a direct consequence of Theorem 5.10 and is omitted.

Corollary 5.11. *Suppose that there exists $i, j \in \mathbb{N}_N^{\neq}$, such that*

$$\Omega_{i,j} := |\omega_i - \omega_j| - 2Nk_0 \left(\frac{\pi\nu}{2\overline{\omega}} + \frac{\nu^2}{6\overline{\omega}^2} \right) > 0, \tag{5.20}$$

where $\nu := 2 \max_{h=1,\dots,N} (|\tilde{\omega}_h| + Nk_0)$, $\overline{\omega} := \frac{1}{N} \mathbf{1}_N^\top \omega$, and $\tilde{\omega}_h := \omega_h - \bar{\omega}$, for all $h = 1, \dots, N$. Then the pair of oscillators (i, j) is practically desynchronized.

Inequality (5.20) is always satisfied, provided that $\omega_i \neq \omega_j$ and $\bar{\omega}$ is sufficiently large (Figures 5.3 and 5.4). Indeed, the minimum coupling strength that ensures asymptotic phase-locking of (5.18) in the absence of mean-field feedback does not depend on the absolute magnitude of the natural frequencies, but only on their dispersion (Dörfler and Bullo, 2011; Jadbabaie et al., 2004; Aeyels and Rogge, 2004; Chopra and Spong, 2009). One thus expects the value of k_0 guaranteeing phase-locking in the absence of MFF to be independent of $\bar{\omega}$.

Interestingly, conditions (5.20) and (5.17) provide somehow complementary results to those in (Aeyels and Rogge, 2004). There the authors derive, in the case of a three oscillators network, several sufficient conditions for a pair of oscillators to be practically phase-locked (partial entrainment). Conversely, Theorem 5.10 and Corollary 5.11 provide sufficient conditions for a pair of oscillators to be practically desynchronized. A combination of the two investigations

might shade more light on both partial entrainment and desynchronization under mean-field feedback.

5.4 Main proofs

5.4.1 Proof of Lemma 5.3.

From the assumption of the lemma it simply holds by integration that

$$\alpha^\top(x(t;t_0,x_0),t) - x_0) \geq \bar{\alpha}(t-t_0). \tag{5.21}$$

Recalling that, by the Cauchy-Schwartz inequality, for all $y \in \mathbb{R}^n$, $|\alpha||y| \geq \alpha^\top y$, (5.21) implies that

$$|x(t;t_0,x_0),t) - x_0| \geq \frac{\bar{\alpha}}{|\alpha|}(t-t_0). \tag{5.22}$$

Given $T > 0$, consider the neighborhood U of x_0 defined as $U := \mathcal{B}(x_0, r_0)$, where $r_0 := \frac{\bar{\alpha}T}{4|\alpha|}$. From (5.22) it follows that $x(t;t_0,x_0),t) \notin U$ for all $t \geq \frac{T}{2} + t_0$, which ends the proof. □

5.4.2 Proof of Theorem 5.4

Necessity: Assume that the pair (i,j) is strongly desynchronized. Then there exists a constant $\Omega_{ij} > 0$ such that, given any $\theta_0 \in T^N$ and $t_0 \in \mathbb{R}$, it holds that $|\dot{\theta}_i(t) - \dot{\theta}_j(t)| \geq \Omega_{ij}$ for all $t \in \mathbb{R}$, where $\theta(\cdot) := \theta(\cdot;t_0,\theta_0)$. Without loss of generality, we can pick i,j in such a way that $\dot{\theta}_i(t) - \dot{\theta}_j(t) \geq \Omega_{ij}$ for all $t \in \mathbb{R}$ (otherwise, just flip the indexes i and j). Then, it holds from (5.5) that, for all $t \in \mathbb{R}$,

$$\dot{\psi}(t)^\top(e_i - e_j) = \dot{\psi}_i(t) - \dot{\psi}_j(t) = \dot{\theta}_i(t) - \dot{\theta}_j(t) \geq \Omega_{ij},$$

where $\psi(\cdot) := \psi(\cdot;t_0,\theta_0)$. In particular, the solutions of (5.5) integrated along (5.1) satisfy $\dot{\psi}(t)^\top(\hat{e}_i - \hat{e}_j) \geq \Omega_{ij}$. The necessity part is then proved by picking $\bar{\alpha} = \Omega_{ij}$.
Sufficiency: Given $\theta_0 \in T^N$ and $t_0 \in \mathbb{R}$, let (5.7) hold for some $\bar{\alpha} > 0$. Then, for all $t \in \mathbb{R}$, it holds that

$$\bar{\alpha} \leq \dot{\psi}(t)^\top(e_i - e_j) = \dot{\psi}_i(t) - \dot{\psi}_j(t) = \dot{\theta}_i(t) - \dot{\theta}_j(t).$$

The sufficiency part is then proved by picking $\Omega_{ij} = \overline{\alpha}$.
The rest of the statement follow by Lemma 5.3. □

5.4.3 Proof of Proposition 5.7

Since the dynamics (5.1) is time invariant we can pick, without loss of generality, $T^* = 0$ in the statement of the proposition. Let $\theta_0 \in T^N$. Since (5.1) defines a smooth bounded dynamics, $\theta(t;t_0,\theta_0)$ exists for all time, (Khalil, 2001, Theorem 3.2). Fix any $t \in \mathbb{R}$, and let $\theta(t) := \theta(t;t_0,\theta_0)$. The system (5.1) being time invariant, and since (5.8) holds uniformly in

the initial conditions, it also holds that

$$\begin{aligned} & \frac{1}{T_{ij}} \left| \int_t^{t+T_{ij}} \left(\dot{\theta}_i(\tau; t_0, \theta_0) - \dot{\theta}_j(\tau; t_0\theta_0) \right) d\tau \right| \\ = \; & \frac{1}{T_{ij}} \left| \int_0^{T_{ij}} \left(\dot{\theta}_i(\tau; t_0, \theta(t)) - \dot{\theta}_j(\tau; t_0, \theta(t)) \right) d\tau \right| \\ \geq \; & \Omega_{ij}. \end{aligned}$$

Since $t \in \mathbb{R}$ is arbitrary, the proposition is proved. □

5.4.4 Proof of Theorem 5.10

The whole proof is based on the following claim, whose proof is provided in Section 5.5.1.

Claim 5.12. For all $\theta_0 \in T^N$, the trajectory of (5.19) satisfies, for all $i, j = 1, \ldots, N$,

$$\frac{\overline{\omega}}{\pi} \left| \int_0^{\pi/\overline{\omega}} \sin\left(\theta_i(\tau) + \theta_j(\tau)\right) d\tau \right| \leq \left(\frac{\pi\nu}{2\overline{\omega}} + \frac{\nu^2}{6\overline{\omega}^2} \right).$$

Invoking Proposition 5.7 and Claim 5.12, it follows that, for all $\theta_0 \in T^N$, all $i, j \in \mathbb{N}_N^{\neq}$, and all $t \in \mathbb{R}$, the trajectory of (5.19) satisfies

$$\begin{aligned} & \frac{\overline{\omega}}{\pi} \left| \int_T^{t+\pi/\overline{\omega}} \left(\dot{\theta}_i(\tau) - \dot{\theta}_j(\tau) \right) d\tau \right| \\ \geq \; & |\omega_i - \omega_j| \\ & - \sum_{l=i,j} \sum_{h=1}^{N} \frac{\gamma_{lh}}{N} \frac{\overline{\omega}}{\pi} \left| \int_T^{t+\pi/\overline{\omega}} \sin(\theta_l(\tau) + \theta_h(\tau)) d\tau \right| \\ & - \sum_{l=i,j} \sum_{h=1}^{N} \frac{\varepsilon_{lh}}{N} \frac{\overline{\omega}}{\pi} \left| \int_T^{t+\pi/\overline{\omega}} \sin(\theta_l(\tau) - \theta_h(\tau)) d\tau \right|, \; \forall t \geq 0 \\ \geq & |\omega_i - \omega_j| - \frac{1}{N} \sum_{h=1}^{N} |\gamma_{ih} + \gamma_{jh}| \left(\frac{\pi\nu}{2\overline{\omega}} + \frac{\nu^2}{6\overline{\omega}^2} \right) - \frac{1}{N} \sum_{h=1}^{N} |\varepsilon_{ih} + \varepsilon_{jh}| \\ > & 0, \end{aligned}$$

where the last inequality comes from assumption (5.17). Recalling Definition 5.6, this proves the theorem. □

5.5 Technical proofs

5.5.1 Proof of Claim 5.12

For all $i, j = 1, \ldots, N$, let

$$\varphi_{ij}(t) := \tilde{\omega}_i t + \tilde{\omega}_j t + \int_0^t \sum_{l=i,j} \sum_{h=1}^{N} \left(\varepsilon_{lh} \sin(\theta_h(\tau) - \theta_l(\tau)) - \gamma_{hl} \sin(\theta_h(\tau) + \theta_l(\tau)) \right) d\tau, \; \forall t \geq 0. \quad (5.23)$$

where, for all $h, l = 1, \dots, N$, ε_{hl} is defined as in the statement of Theorem 5.10. Note that, for all $i, j = 1, \dots, N$ and all $t \geq 0$,

$$|\varphi_{ij}(t)| \quad \leq \quad |\tilde{\omega}_i + \tilde{\omega}_j|t + \sum_{l=i,j} \sum_{h=1} |\varepsilon_{lh} + \gamma_{hl}|t \leq \nu t. \tag{5.24}$$

Moreover, integrating (5.16) we obtain that, for all $i, j = 1, \dots, N$ and all $t \geq 0$,

$$\theta_i(t) = \overline{\omega} t + \tilde{\omega}_i t + \int_0^t \sum_{j=1}^{N} \Big(\varepsilon_{ij} \sin(\theta_j(\tau) - \theta_i(\tau)) - \gamma_{ij} \sin(\theta_j(\tau) + \theta_i(\tau)) \Big) d\tau + \theta_{0i},$$

and, recalling (5.23),

$$\theta_i(t) + \theta_j(t) = 2\overline{\omega} t + \theta_{0i} + \theta_{0j} + \varphi_{ij}(t). \tag{5.25}$$

It then follows that

$$\begin{aligned}
& \frac{\overline{\omega}}{\pi} \left| \int_0^{\pi/\overline{\omega}} \sin\big(\theta_i(\tau) + \theta_j(\tau)\big) d\tau \right| \\
= \; & \frac{\overline{\omega}}{\pi} \left| \int_0^{\pi/\overline{\omega}} \sin(2\overline{\omega} t + \theta_{0i} + \theta_{0j} + \varphi_{ij}(t)) dt \right| \\
\leq \; & \frac{\overline{\omega}}{\pi} \left| \int_0^{\pi/\overline{\omega}} \cos(2\overline{\omega} t + \theta_{0i} + \theta_{0j}) \sin \varphi_{ij}(t) dt \right| + \frac{\overline{\omega}}{\pi} \left| \int_0^{\pi/\overline{\omega}} \sin(2\overline{\omega} t + \theta_{0i} + \theta_{0j}) \cos \varphi_{ij}(t) dt \right|,
\end{aligned}$$

where the first equality comes from (5.25), and the second inequality from the trigonometric identity $\sin(a + b) = \cos a \sin b + \sin a \cos b$ and the triangular inequality.

From (5.24) it follows that $\sin \varphi_{ij}(t) \leq \nu t$ for all $t \geq 0$. Hence, we can give the following upper bound:

$$\frac{\overline{\omega}}{\pi} \left| \int_0^{\pi/\overline{\omega}} \cos(2\overline{\omega} t + \theta_{0i} + \theta_{0j}) \sin \varphi_{ij}(t) dt \right| \leq \frac{\overline{\omega}}{\pi} \int_0^{\pi/\overline{\omega}} \nu t dt \leq \frac{\pi \nu}{2\overline{\omega}}. \tag{5.26}$$

Furthermore, note that

$$\begin{aligned}
& \frac{\overline{\omega}}{\pi} \left| \int_0^{\pi/\overline{\omega}} \sin(2\overline{\omega} t + \theta_{0i} + \theta_{0j}) \cos \varphi_{ij}(t) dt \right| \\
= \; & \frac{\overline{\omega}}{\pi} \left| \int_0^{\pi/\overline{\omega}} \sin(2\overline{\omega} t + \theta_{0i} + \theta_{0j}) dt \right| + \frac{\overline{\omega}}{\pi} \left| \int_0^{\pi/\overline{\omega}} \sin(2\overline{\omega} t + \theta_{0i} + \theta_{0j}) (\cos \varphi_{ij}(t) - 1) dt \right| \\
= \; & 0 + \frac{\overline{\omega}}{\pi} \left| \int_0^{\pi/\overline{\omega}} \sin(2\overline{\omega} t + \theta_{0i} + \theta_{0j}) (\cos \varphi_{ij}(t) - 1) dt \right|.
\end{aligned}$$

Recalling that $\cos \varphi_{ij}(t) \geq 1 - \frac{1}{2} \varphi_{ij}(t)^2$, it follows from (5.24) that $\cos \varphi_{ij}(t) \geq 1 - \frac{1}{2} (\nu t)^2$, that is $\cos \varphi_{ij}(t) - 1 \geq -\frac{1}{2} (\nu t)^2$, and, finally, $|\cos \varphi_{ij}(t) - 1| \leq \frac{1}{2} (\nu t)^2$, for all $t \geq 0$. It then follows

that

$$\begin{aligned} & \frac{\overline{\omega}}{\pi}\left|\int_0^{\pi/\overline{\omega}} \sin(2\overline{\omega}t+\theta_{0i}+\theta_{0j})\cos\varphi_{ij}(t)dt\right| \\ = \; & \frac{\overline{\omega}}{\pi}\left|\int_0^{\pi/\overline{\omega}} \sin(2\overline{\omega}t+\theta_{0i}+\theta_{0j})(\cos\varphi_{ij}(t)-1)dt\right| \\ \leq \; & \frac{\overline{\omega}}{\pi}\int_0^{\pi/\overline{\omega}} \frac{1}{2}(\nu t)^2 dt \\ \leq \; & \frac{\nu^2}{6\overline{\omega^2}}. \end{aligned} \tag{5.27}$$

The claim follows directly from (5.26), (5.26) and (5.27). □

Appendix A

Extensions to Part I[1]

In this chapter we will study a generalization of the closed-loop dynamics proposed in Chapter 2. More precisely, in Section A.1, we consider more general form of diffusive coupling and mean-field proportional feedback. The importance of such generalizations is discussed below. Based on the generalized dynamics, we provide in Section A.2 a formal derivation of the small coupling condition permitting to introduce Assumption 1 in a less artificial way. All the results of Chapter 2 are then rigorously re-derived in Section A.3 for the new extended dynamics. Finally, in Sections A.4, A.5, and A.6, we provide sufficient conditions for and a sketch of some possible extensions of the results in Chapters 2, 3, 4, and 5 to the new generalized dynamics.

A.1 A more general model

This section extends the model derivation of Chapter 2 to a wider class of interconnected oscillators. Given $\rho_i > 0$, $i = 1, \dots, N$, consider the following dynamics on $\mathbb{C}^N$

$$\dot{z}_i = (\mathrm{i}\omega_i + \rho_i^2 - |z_i|^2) z_i + \sum_{j=1}^{N} \kappa_{ij} e^{\mathrm{i}\delta_{ij}} (e^{\mathrm{i}\eta_j} z_j - e^{\mathrm{i}\eta_i} z_i) + u_i \tag{A.1}$$

where $\kappa := [\kappa_{ij}]_{i,j=1,\dots,N} \in \mathbb{R}^{N \times N}$,

$$u_i := \sum_{j=1}^{N} \tilde{\gamma}_{ij} e^{\mathrm{i}\phi_{ij}} \left[\cos\varphi_j \mathrm{Re}(e^{\mathrm{i}\psi_j} z_j) + \mathrm{i} \sin\varphi_j \mathrm{Im}(e^{\mathrm{i}\psi_j} z_j) \right], \tag{A.2}$$

$\tilde{\gamma} := [\tilde{\gamma}_{ij}]_{i,j=1,\dots,N} \in \mathbb{R}^{N \times N}$, and where

$$\Phi := ([\delta_{ij}]_{i,j=1,\dots,N}, [\eta_i]_{i=1,\dots,N}, [\varphi_i]_{i=1,\dots,N}, [\phi_{ij}]_{i,j=1,\dots,N}, [\psi_i]_{i=1,\dots,N}) \in \mathbb{R}^{N \times (2N+3)} \tag{A.3}$$

The phase matrix Φ accounts for possible imprecision in the association between physical (voltages, conductances, ion concentrations, etc.) and mathematical (real and imaginary parts) variables. For instance:

- The phases $[\eta_i]_{i=1,\dots,N}$ rotate the oscillator contributions to the diffusive coupling. This permits to consider the case when, in the simplification from the full coupled limit cycles to the reduced ones, we can not exactly associate the voltages and recovery variables of each oscillator to the real and imaginary parts, respectively.

[1] This chapter results for the reviewer's (Prof. Ermentrout and Prof. Aeyels) comments on a preliminary version of this thesis.

- The phases $[\delta_{ij}]_{i,j=1,\dots,N}$ rotate the diffusive coupling terms in such a way that the imaginary part of the coupling influences the real one and vice-versa.
- Similarly, the phases $([\varphi_i]_{i=1,\dots,N}, [\phi_{ij}]_{i,j=1,\dots,N}, [\psi_i]_{i=1,\dots,N})$ accounts for the same type of inaccuracies in the feedback coupling. In particular, the phases $[\varphi_i]_{i=1,\dots,N}$ permit to consider the case when the real and the imaginary parts of the oscillations contribute to the mean-field measurement with different gains.

We point out that this generalized model includes two important situations as special cases:

Reduction to the original mean-field proportional feedback scheme in Equation (2.3) By picking $\delta_{ij} = \eta_i = \phi_{ij} = \psi_j = \varphi_j = 0$ and by setting $\tilde{\gamma}_{ij} = \beta_i \alpha_j$, for all $i, j = 1, \dots, N$, trivial computations reveal that (A.1) reduces to

$$\dot{z}_i = (\mathrm{i}\omega_i + \rho_i^2 - |z_i|^2) z_i + \sum_{j=1}^{N} \kappa_{ij}(z_j - z_i) + \beta_i \sum_{j=1}^{N} \alpha_j \mathrm{Re}(z_j),$$

thus recovering the dynamics in Equation (2.3).

Reduction to the normal form (A.4) in (Aronson et al., 1990) . With the choice $\varphi_i = \frac{\pi}{4}$, $\eta_i = \psi_i = 0$, and $\phi_{ij} = \delta_{ij}$, for all $i, j = 1, \dots, N$, the sum of the coupling and feedback terms in Equations (A.1)-(A.2) can be re-written as

$$\sum_{j=1}^{N} e^{\mathrm{i}\delta_{ij}} \left[(\kappa_{ij} + \tilde{\gamma}_{ij}) z_j - \kappa_{ij} z_i \right] = \sum_{j=1}^{N} (\kappa_{ij} + \tilde{\gamma}_{ij}) e^{\mathrm{i}\delta_{ij}} \left[z_j - \frac{\kappa_{ij}}{\kappa_{ij} + \tilde{\gamma}_{ij}} z_i \right]. \tag{A.4}$$

Clearly, for $\kappa_{ij} = 0$, we obtain a purely direct coupling, which recovers the coupling term in Equation (A.4) of (Aronson et al., 1990) with $\tilde{\kappa}_i = 0$. Otherwise, given $\tilde{\kappa}_i \in (0, 1]$, we let

$$\frac{\kappa_{ij}}{\kappa_{ij} + \tilde{\gamma}_{ij}} = \tilde{\kappa}_i,$$

which is equivalent to asking

$$\tilde{\gamma}_{ij} = \frac{(1 - \tilde{\kappa}_i)\kappa_{ij}}{\tilde{\kappa}_i}. \tag{A.5}$$

By plugging (A.5) into (A.4), we can further transform the coupling and feedback terms as

$$\sum_{j=1}^{N} \left(\kappa_{ij} + \frac{1 - \tilde{\kappa}_i}{\tilde{\kappa}_i} \kappa_{ij} \right) e^{\mathrm{i}\delta_{ij}} (z_j - \tilde{\kappa}_i z_i) = \sum_{j=1}^{N} \kappa'_{ij} e^{\mathrm{i}\delta_{ij}} (z_j - \tilde{\kappa}_i z_i),$$

where $\kappa'_{ij} := \frac{\kappa_{ij}}{\tilde{\kappa}_i}$, which recovers the coupling term of Equation (A.4) of (Aronson et al., 1990) with $\tilde{\kappa}_i \in (0, 1]$.

The normal form (A.4) in (Aronson et al., 1990) constitutes the basis of many theoretical works on synchronization phenomena between coupled oscillators, including, in particular, works on desynchronization via mean-field feedback, e.g. (Hauptmann et al., 2005a; Popovych et al., 2006a) and references therein.

A.2 Formal reduction to the phase dynamics

The goal of this section is to derive the phase dynamics of the closed-loop system (A.1)-(A.2). More precisely, we rigorously derive conditions justifying Assumption 1, that is conditions for which the oscillator radius variations can be neglected in the associated phase dynamics.

We start by writing the oscillator states in polar coordinates, that is $z_i =: r_i e^{\mathrm{i}\theta_i}$, for all $i = 1, \dots, N$, where $r_i = |z_i| \in \mathbb{R}_{\geq 0}$ and $\theta_i = \arg(z_i) \in T^1$. We stress that the oscillator phases θ_i are defined only for $|z_i| = r_i > 0$. In these coordinates the dynamics (A.1)-(A.2) reads

$$\dot{r}_i e^{\mathrm{i}\theta_i} + \mathrm{i} r_i \dot{\theta}_i e^{\mathrm{i}\theta_i} = (\mathrm{i}\omega_i + \rho_i^2 - r_i^2) r_i e^{\mathrm{i}\theta_i} + \sum_{j=1}^{N} \kappa_{ij} e^{\mathrm{i}\delta_{ij}} (e^{\mathrm{i}\eta_j} r_j e^{\mathrm{i}\theta_j} - e^{\mathrm{i}\eta_i} r_i e^{\mathrm{i}\theta_i}) + u_i$$

with

$$u_i := \sum_{j=1}^{N} \tilde{\gamma}_{ij} e^{\mathrm{i}\phi_{ij}} \left[\cos\varphi_j \mathrm{Re}(e^{\mathrm{i}\psi_j} r_j e^{\mathrm{i}\theta_j}) + \mathrm{i} \sin\varphi_j \mathrm{Im}(e^{\mathrm{i}\psi_j} r_j e^{\mathrm{i}\theta_j}) \right].$$

By multiplying both sides of this dynamics by $\frac{e^{-\mathrm{i}\theta_i}}{r_i}$, extracting the real and imaginary part, and using some basic trigonometry, we get, for $r_i > 0$, $i = 1, \dots, N$,

$$\dot{\theta}_i = \omega_i + f_i(\theta, r, \kappa, \tilde{\gamma}, \Phi) \tag{A.6a}$$
$$\dot{r}_i = r_i(\rho_i^2 - r_i^2) + g_i(\theta, r, \kappa, \tilde{\gamma}, \Phi), \tag{A.6b}$$

where, for all $i = 1, \dots, N$,

$$\begin{aligned} f_i(\theta, r, \kappa, \tilde{\gamma}, \Phi) := & -\sum_{j=1}^{N} \kappa_{ij} \sin(\delta_{ij} + \eta_i) + \sum_{j=1}^{N} \frac{\kappa_{ij} r_j}{r_i} \sin(\theta_j - \theta_i + \delta_{ij} + \eta_j) \\ & + \sum_{j=1}^{N} \frac{\tilde{\gamma}_{ij} r_j}{r_i} \left[\frac{\sin\varphi_j + \cos\varphi_j}{2} \sin(\theta_j - \theta_i + \phi_{ij} + \psi_j) \right. \\ & \left. + \frac{\sin\varphi_j - \cos\varphi_j}{2} \sin(\theta_j + \theta_i - \phi_{ij} + \psi_j) \right] \end{aligned} \tag{A.7}$$

$$\begin{aligned} g_i(\theta, r, \kappa, \tilde{\gamma}, \Phi) := & -r_i \sum_{j=1}^{N} \kappa_{ij} \cos(\delta_{ij} + \eta_i) + \sum_{j=1}^{N} \kappa_{ij} r_j \cos(\theta_j - \theta_i + \delta_{ij} + \eta_j) \\ & + \sum_{j=1}^{N} \tilde{\gamma}_{ij} r_j \left[\frac{\sin\varphi_j + \cos\varphi_j}{2} \cos(\theta_j - \theta_i + \phi_{ij} + \psi_j) \right. \\ & \left. + \frac{\cos\varphi_j - \sin\varphi_j}{2} \cos(\theta_j + \theta_i - \phi_{ij} + \psi_j) \right] \end{aligned} \tag{A.8}$$

which defines the phase/radius dynamics of (A.1)-(A.2) on $T^N \times \mathbb{R}^N_{>0}$.

Let $f := [f_i]_{i=1,\dots,N}$ and $g := [g_i]_{i=1,\dots,N}$. When the diffusive coupling and the mean-field proportional feedback are both zero, that is $\kappa = \tilde{\gamma} = 0$, it holds that $f \equiv g \equiv 0$. Hence, in this case, (A.6) reduces to

$$\dot{\theta}_i = \omega_i \tag{A.9a}$$
$$\dot{r}_i = r_i(\rho_i^2 - r_i^2), \tag{A.9b}$$

for all $i = 1, \dots, N$. Let $\rho := [\rho_i]_{i=1,\dots,N} \in \mathbb{R}^{N \times N}$. It is evident that the N-torus $T^N \times \rho \subset T^N \times \mathbb{R}^N_{>0}$ is invariant for (A.9), since all its points are fixed points of the radius dynamics (A.9b). Moreover, it is normally hyperbolic, since the linearization of (A.9) on its tangent space[2] is $\frac{\partial \dot{\theta}}{\partial \theta} \equiv 0$, whereas the linearization on the orthogonal space, *i.e.* $\frac{\partial \dot{r}}{\partial r}$, has eigenvalues

[2]Since r is constant on $T^N \times [\rho_i]_{i=1,\dots,N}$, the tangent space at a point $(\theta, [\rho_i]_{i=1,\dots,N}) \in T^N \times [\rho_i]_{i=1,\dots,N}$ is spanned by $\left\{ \frac{\partial}{\partial \theta_i}\Big|_{(\theta,[\rho_i]_{i=1,\dots,N})} \right\}$, $i = 1, \dots, N$, whereas the orthogonal space is spanned by $\left\{ \frac{\partial}{\partial r_i}\Big|_{(\theta,[\rho_i]_{i=1,\dots,N})} \right\}$, $i = 1, \dots, N$.

$-2\rho_i^2$, $i = 1, \dots, N$. Thus, it is also (exponentially) attractive.

We are now going to apply a classical result of Hirsch et. al (Hirsch et al., 1977, Theorem 4.1) to show that, if $\kappa, \tilde{\gamma}$ are sufficiently small, then (A.6) still has an attractive normally hyperbolic invariant torus in a neighborhood of $\mathcal{T}_0 := T^N \times \rho$.

Proposition A.1. *Given $\rho_i > 0$, $i = 1, \dots, N$, there exists constants δ_h, $C_h > 0$ depending only ρ_i, $i = 1, \dots, N$, such that, if $|(\kappa, \tilde{\gamma})| \leq \delta_h$, then there exists an attractive invariant manifold $\mathcal{T}_p \subset T^N \times \mathbb{R}^N_{>0}$ normally hyperbolic for (A.6) and satisfying*

$$|r - \rho| \leq C_h |(\kappa, \tilde{\gamma})|, \quad \forall (\theta, r) \in \mathcal{T}_p. \tag{A.10}$$

Proof Even though for $\kappa = \tilde{\gamma} = 0$ it holds that $f \equiv g \equiv 0$, as soon as $(\kappa, \tilde{\gamma}) \neq 0$, f and g are unbounded, due to singularities at $r_i = 0$ and $r_i = \infty$, for some $i \in \{1, \dots, N\}$. However, the persistence of the normally hyperbolic invariant torus solely relying on local arguments, we can construct a locally defined auxiliary smooth dynamical system, which is identical to (A.6) near $\mathcal{T}_0$. The auxiliary system possesses a normally hyperbolic invariant manifold $\mathcal{T}_p$ near $\mathcal{T}_0$ if and only if the same holds for the original dynamics (A.6).

Step 1: *Compactification.*
The result of (Hirsch et al., 1977, Theorem 4.1) applies for dynamical systems defined on compact manifolds. Thus, we construct our auxiliary dynamics on a compact manifold containing $\mathcal{T}_0$. To this end, we consider some smooth functions $G_i : \mathbb{R}_{\geq 0} \to [0, 1]$ such that (see (Lee, 2006, Page 54))

$$G_i(r_i) = \begin{cases} 0 & \text{if } r_i \in \left[0, \ \frac{\rho_i}{2}\right] \\ 1 & \text{if } r_i \in \left[\frac{3\rho_i}{4}, \ \frac{5\rho_i}{4}\right] \\ 0 & \text{if } r_i > \frac{3\rho_i}{2}. \end{cases} \tag{A.11}$$

By denoting

$$\overline{P} := \left\{ r \in \mathbb{R}^N_{>0} : \ r_i \in \left[\frac{\rho_i}{2}, \ \frac{3\rho_i}{2}\right], \ i = 1, \dots, N \right\},$$

we let $\overline{\mathcal{M}}$ be the compact submanifold

$$\overline{\mathcal{M}} := T^N \times \overline{P}.$$

We define our auxiliary dynamical as a dynamical system on the compact submanifold $\overline{\mathcal{M}}$ as follows:

$$\dot{\theta}_i = \omega_i + f_i(\theta, r, \kappa, \tilde{\gamma}, \Phi), \qquad \theta \in T^N \tag{A.12a}$$
$$\dot{r}_i = r_i(\rho_i^2 - r_i^2) + G_i(r_i) g_i(\theta, r, \kappa, \tilde{\gamma}, \Phi), \quad r \in \overline{P}. \tag{A.12b}$$

Note that, by definition, the two dynamics (A.6) and (A.12) coincide on

$$\underline{\mathcal{M}} := T^N \times \underline{P}, \tag{A.13}$$

where

$$\underline{P} := \left\{ r \in \mathbb{R}^N_{>0} : \ r_i \in \left[\frac{3\rho_i}{4}, \ \frac{5\rho_i}{4}\right], \ i = 1, \dots, N \right\}.$$

In particular (A.6) has an attractive normally hyperbolic invariant manifold $\mathcal{T}_p \subset \underline{\mathcal{M}}$ if and only if (A.12) does.

Step 2: *Invariance.*
In order to apply (Hirsch et al., 1977, Theorem 4.1) to (A.12) with κ and $\tilde{\gamma}$ as the perturbation parameters, we also have to show that the compact manifold $\overline{\mathcal{M}}$ is invariant with respect to

the flow of (A.12) independently of $(\kappa, \tilde{\gamma}) \in \mathbb{R}^{N\times 2N}$. In this case, the flow of (A.12) maps $\overline{\mathcal{M}}$ into itself independently of the perturbation parameters, as required by (Hirsch et al., 1977, Theorem 4.1). By construction of the functions G_i in (A.11), the border of $\overline{\mathcal{M}}$, *i.e.*

$$\partial\overline{\mathcal{M}} := T^N \times \frac{\rho}{2} \cup T^N \times \frac{3\rho}{2}$$

are fixed points of the radius dynamics (A.12b), independently of the value of the parameters $\kappa, \tilde{\gamma}, \Phi$. In other words, for all $(\kappa, \tilde{\gamma}, \Phi) \in \mathbb{R}^{N\times(4N+3)}$, the border of $\overline{\mathcal{M}}$ is given by the union of the two invariant torus $T^N \times \frac{\rho}{2}$ and $T^N \times \frac{3\rho}{2}$. This in turn ensures that $\overline{\mathcal{M}}$ is invariant for (A.12). Indeed, if a trajectory exists crossing the border of $\overline{\mathcal{M}}$, then the image of the crossing point through the flow of (A.12) falls out of $\partial\overline{\mathcal{M}}$, which violates its invariance.

STEP 3: *The nominal invariant manifold and construction of the perturbed one.*
For $\kappa = \tilde{\gamma} = 0$, the N-torus $\mathcal{T}_0 = T^N \times \rho$ is attractive normally hyperbolic invariant for (A.12), since $\mathcal{T}_0 \subset \underline{\mathcal{M}}$ and the same holds for (A.6).

It remains to show that, if $|(\kappa, \tilde{\gamma})|$ is small, then the C^1-norm[3] of the functions

$$\begin{aligned} \overline{\mathcal{M}} &:\longrightarrow \mathbb{R}^N \\ (\theta, r) &\longmapsto f\big|_{\overline{\mathcal{M}}}(\theta, r, \kappa, \tilde{\gamma}, \Phi) \end{aligned}$$

and

$$\begin{aligned} \overline{\mathcal{M}} &:\longrightarrow \mathbb{R}^N \\ (\theta, r) &\longmapsto G\big|_{\overline{\mathcal{M}}}(r) g\big|_{\overline{\mathcal{M}}}(\theta, r, \kappa, \tilde{\gamma}, \Phi) \end{aligned}$$

where $G := [G_i]_{i=1,\dots,N}$, is small as well. To this aim, note that f and its derivative $\frac{\partial f}{\partial(\theta,r)}$ are linear in $(\kappa, \tilde{\gamma})$. Furthermore, the coefficients, which depend only on (θ, r, Φ), are uniformly bounded on $\overline{\mathcal{M}} \times \mathbb{R}^{N\times(2N+3)}$. Similarly, for the function Gg and its derivative $\frac{\partial(Gg)}{\partial(\theta,r)}$. It follows that there exists C_f, $C_g > 0$, C_f, C_g independent of κ, $\tilde{\gamma}$, ω, and Φ, such that

$$\bar{\|} f|_{\overline{\mathcal{M}}}(\cdot, \cdot, \kappa, \tilde{\gamma}, \Phi)\bar{\|}_1 \leq C_f |(\kappa, \tilde{\gamma})| \tag{A.14a}$$

$$\bar{\|} G|_{\overline{\mathcal{M}}}(\cdot) g|_{\overline{\mathcal{M}}}(\cdot, \cdot, \kappa, \tilde{\gamma}, \Phi)|_{\overline{\mathcal{M}}}\bar{\|}_1 \leq C_g |(\kappa, \tilde{\gamma})|, \tag{A.14b}$$

that is both f and g are $|(\kappa, \tilde{\gamma})|$-small in the C^1-norm. Note that the constants C_f, C_g solely depend on the natural radius ρ_i.

We can finally apply (Hirsch et al., 1977, Theorem 4.1) to conclude the existence of $\delta'_h > 0$, independent of κ, $\tilde{\gamma}$, ω, and Φ, such that, if

$$|(\kappa, \tilde{\gamma})| \leq \delta'_h, \tag{A.15}$$

then (A.6) still has an attractive normally hyperbolic invariant N-torus $\mathcal{T}_p \subset \overline{\mathcal{M}}$, which is $|(\kappa, \tilde{\gamma})|$-near in the C^1-norm to $\mathcal{T}_0$. The fact that δ'_h depends only on the natural radius ρ_i, comes from the fact that the linear part of the unperturbed dynamics (A.9) solely depends on ρ_i, $i = 1, \dots, N$. In particular, there exists $C_h > 0$ such that, if $|(\kappa, \tilde{\gamma})| < \delta'_h$, then

$$|r - \rho| \leq C_h |(\kappa, \tilde{\gamma})|, \quad \forall (\theta, r) \in \mathcal{T}_p, \tag{A.16}$$

where again C_h is independent of κ, $\tilde{\gamma}$, ω, and Φ.

[3] The C^1-norm of a C^1 bounded function with bounded derivatives $F : \overline{\mathcal{M}} \to \mathbb{R}^N$ is defined as $\bar{\|} F\bar{\|}_1 := \max\{\max_{x\in\overline{\mathcal{M}}} |F(x)|, \max_{x\in\overline{\mathcal{M}}} |\partial F/\partial x(x)|\}$, where $|F(x)|$ (resp. $|\partial F/\partial x(x)|$) is the Euclidean (resp. Frobenius) norm of $F(x)$ (resp. $\partial F/\partial x(x)$).

To prove the proposition, it remains to pick $|(\kappa, \tilde{\gamma})|$ sufficiently small that $\mathcal{T}_p \subset \underline{\mathcal{M}}$, where $\underline{\mathcal{M}}$, defined in (A.13), is the region where (A.12) coincides with (A.6). To this aim, from (A.15), (A.16), and the definition (A.13) of $\underline{\mathcal{M}}$, it suffices to pick

$$\delta_h := \frac{\min_{i=1,\dots,N} \rho_i}{4C_h}, \tag{A.17}$$

and

$$|(\kappa, \tilde{\gamma})| \leq \delta_h, \tag{A.18}$$

□

Remark A.2. We refer to condition (A.18) as the *small coupling condition*. Note that the constant δ_h, and thus the small coupling condition, depends only on the oscillator natural radius ρ_i. In particular, it is independent of the natural frequencies ω.

If the small coupling condition is verified, then Proposition A.1 has two important consequences:

1. On the attractive normally hyperbolic invariant torus $\mathcal{T}_p$, the oscillator radius variations around their natural radius are bounded by $|r(t) - \rho| \leq C_h|(\kappa, \tilde{\gamma})|$, for all $t \geq 0$. In particular, they are small, provided that $|(\kappa, \tilde{\gamma})|$ is small.

2. To the first order in $|(\kappa, \tilde{\gamma})|$ the phase dynamics does not depend on the radius dynamics. Indeed from (A.10) and (A.14) it follows that

$$\begin{aligned}\left|\frac{\partial f}{\partial r}(\theta, r, \kappa, \tilde{\gamma}, \Phi)(r - \rho)\right| &\leq \left|\frac{\partial f}{\partial r}(\theta, r, \kappa, \tilde{\gamma}, \Phi)\right| |r - \rho| \\ &\leq C_f|(\kappa, \tilde{\gamma})|C_h|(\kappa, \tilde{\gamma})| \\ &= C_f C_h|(\kappa, \tilde{\gamma})|^2.\end{aligned}$$

Items 1 and 2 justify Assumption 1. In particular, to the first order in $|(\kappa, \tilde{\gamma})|$, *i.e.* to the first order in the coupling and feedback strength, if the small coupling condition (A.18) holds true, then

$$\dot{\theta}_i = \omega_i - \sum_{j=1}^{N} \kappa_{ij} \sin(\delta_{ij} + \eta_i) + \bar{f}_i(\theta, k, \gamma, \Phi), \tag{A.19a}$$

where

$$\bar{f}_i(\theta, k, \gamma, \Phi) := \omega_i - \sum_{j=1}^{N} \kappa_{ij} \sin(\delta_{ij} + \eta_i) + \sum_{j=1}^{N} k_{ij} \sin(\theta_j - \theta_i + \delta_{ij} + \eta_j) \tag{A.20a}$$

$$+ \sum_{j=1}^{N} \gamma_{ij} \left[\frac{\sin\varphi_j + \cos\varphi_j}{2} \sin(\theta_j - \theta_i + \phi_{ij} + \psi_j)\right. \tag{A.20b}$$

$$\left. + \frac{\sin\varphi_j - \cos\varphi_j}{2} \sin(\theta_j + \theta_i - \phi_{ij} + \psi_j)\right], \tag{A.20c}$$

with $k := [k_{ij}]_{ij=1,\dots,N} := \left[\frac{\kappa_{ij}\rho_j}{\rho_i}\right]$ and $\gamma := [\gamma_{ij}]_{ij=1,\dots,N} := \left[\frac{\tilde{\gamma}_{ij}\rho_j}{\rho_i}\right]$. We stress that the error between the nominal phase dynamics (A.6) and (A.19) is of the same order as $|(\kappa, \tilde{\gamma})|^2$. It is thus small provided that $|(\kappa, \tilde{\gamma})|$ is small.

The generalized phase dynamics (A.19) constitutes the object of our analyses in this chapter.

A.3 Generalization of the results of Chapter 2

In this section we extend the results contained in Lemmas 2.3 and 2.4 and Theorem 2.2, to the generalized phase dynamics (A.19). We stress that all the forthcoming analysis is valid, provided that the small coupling condition (A.18) is satisfied, independently of the natural frequencies.

A.3.1 Generalized fixed point equation

Similarly to Chapter 2, we start by identifying the phase-locked solutions or, equivalently, the fixed points of the incremental dynamics of (A.19), *i.e.* $\dot{\theta}_i - \dot{\theta}_j = 0$, for all $i, j = 1, \dots, N$. Given some initial conditions $\theta^*(0)$, this fixed points equation reads

$$0 = \omega_i - \sum_{h=1}^{N} \kappa_{ih} \sin(\delta_{ih} + \eta_i) + \sum_{h=1}^{N} k_{ih} \sin(\Delta_{ih} + \delta_{ih} + \eta_h) \tag{A.21a}$$

$$+ \sum_{h=1}^{N} \gamma_{ih} \frac{\sin\varphi_h + \cos\varphi_h}{2} \sin(\Delta_{ih} + \phi_{ih} + \psi_h) \tag{A.21b}$$

$$-\omega_j + \sum_{h=1}^{N} \kappa_{jh} \sin(\delta_{jh} + \eta_j) - \sum_{h=1}^{N} k_{jh} \sin(\Delta_{jh} + \delta_{jh} + \eta_h) \tag{A.21c}$$

$$- \sum_{h=1}^{N} \gamma_{jh} \frac{\sin\varphi_h + \cos\varphi_h}{2} \sin(\Delta_{jh} + \phi_{jh} + \psi_h) \tag{A.21d}$$

$$+ \sum_{h=1}^{N} \frac{\sin\varphi_h - \cos\varphi_h}{2} \sin(2\Lambda_\Omega(t) + \Delta_{ih} + 2\theta_i^*(0) - \phi_{ih} + \psi_h) \tag{A.21e}$$

$$- \sum_{h=1}^{N} \frac{\sin\varphi_h - \cos\varphi_h}{2} \sin(2\Lambda_\Omega(t) + \Delta_{jh} + 2\theta_j^*(0) - \phi_{jh} + \psi_h). \tag{A.21f}$$

where the phase differences $\Delta \in \mathbb{R}^{N\times N}$ and the common frequency of oscillation $\Omega : \mathbb{R} \to \mathbb{R}$ are defined in (2.12) and (2.13), respectively.

Let us introduce some notation. The fixed point equation (A.21) must be solved in Δ and Ω. It is parametrized, apart from the natural frequencies ω, by the elements of the matrix $\Upsilon \in \mathbb{R}^{N\times(4N+3)}$, which is defined as

$$\Upsilon := (k, \kappa, \Phi). \tag{A.22}$$

Let us denote the first four (time-independent) lines of (A.21) as the function $\Phi_{ij}^{TI} : \mathbb{R}^N \times \mathbb{R}^{N\times(4N+3)} \times \mathbb{R}^{N\times N} \to \mathbb{R}$, that is

$$\begin{aligned}\Phi_{ij}^{TI}(\omega, \Upsilon, \Delta) = \omega_i &- \sum_{h=1}^{N} \kappa_{ih} \sin(\delta_{ih} + \eta_i) + \sum_{h=1}^{N} k_{ih} \sin(\Delta_{ih} + \delta_{ih} + \eta_h) \\ &+ \sum_{h=1}^{N} \gamma_{ih} \frac{\sin\varphi_h + \cos\varphi_h}{2} \sin(\Delta_{ih} + \phi_{ih} + \psi_h) \\ &-\omega_j + \sum_{h=1}^{N} \kappa_{jh} \sin(\delta_{jh} + \eta_j) - \sum_{h=1}^{N} k_{jh} \sin(\Delta_{jh} + \delta_{jh} + \eta_h) \\ &- \sum_{h=1}^{N} \gamma_{jh} \frac{\sin\varphi_h + \cos\varphi_h}{2} \sin(\Delta_{jh} + \phi_{jh} + \psi_h).\end{aligned} \tag{A.23}$$

Similarly we denote the last two (time-dependent) lines of (A.21) as the function $\Phi_{ij}^{TD} : \mathbb{R} \times \mathbb{R}^{N\times(4N+3)} \times \mathbb{R}^{N\times N} \times \mathbb{R}^N \to \mathbb{R}$, that is

$$\begin{aligned}\Phi_{ij}^{TD}(t,\Upsilon,\Delta,\theta^*(0)) := &\sum_{h=1}^{N} \frac{\sin\varphi_h - \cos\varphi_h}{2} \sin(2\Lambda_\Omega(t) + \Delta_{ih} + 2\theta_i^*(0) - \phi_{ih} + \psi_h) \\ &- \sum_{h=1}^{N} \frac{\sin\varphi_h - \cos\varphi_h}{2} \sin(2\Lambda_\Omega(t) + \Delta_{jh} + 2\theta_j^*(0) - \phi_{jh} + \psi_h).\end{aligned} \tag{A.24}$$

Then we can generalize Lemma 2.3 as follows.

Lemma A.3. *For all initial conditions $\theta^*(0) \in T^N$, all natural frequencies $\omega \in \mathbb{R}^N$, all parameters $\Upsilon \in \mathbb{R}^{N\times(4N+3)}$, if system (A.19) admits an oscillating phase-locked solution starting in $\theta^*(0)$ with phase differences Δ and collective frequency of oscillation Ω, then, for all $1 \le i < j \le N$, the functions defined in (A.23) and (A.24) satisfy*

$$\Phi_{ij}^{TI}(\omega,\Upsilon,\Delta) = 0, \tag{A.25a}$$

$$\Phi_{ij}^{TD}(t,\Upsilon,\Delta,\theta^*(0)) = 0. \tag{A.25b}$$

Proof The proof follows along the same lines as those of the original lemma. Firstly, note that, by definition, the fixed point equation (A.21) can be rewritten as

$$\Phi_{ij}^{TI}(\omega,\Upsilon,\Delta) + \Phi_{ij}^{TD}(t,\Upsilon,\Delta,\theta^*(0)) = 0.$$

Since $\Phi_{ij}^{TI}(\omega,\Upsilon,\Delta)$ is constant, this is equivalent to writing

$$\begin{aligned}\Phi_{ij}^{TI}(\omega,\Upsilon,\Delta) &= c_{ij}, \\ \Phi_{ij}^{TD}(t,\Upsilon,\Delta,\theta^*(0)) &= -c_{ij},\end{aligned} \tag{A.26}$$

for some constant $c_{ij} \in \mathbb{R}$. We claim that, if the phase-locked solution is oscillating, then necessarily $c_{ij} = 0$. To see this, differentiate (A.26) with respect to time. We obtain, for all $t \ge 0$,

$$\begin{aligned}0 = 2\Omega(t)\times& \\ \Bigg\{ &\sum_{h=1}^{N} \gamma_{ih}\Big[\cos\psi_h \cos(2\Lambda_\Omega(t) + \Delta_{ih} - \phi_i + 2\theta_i^*(0)) - \sin\psi_h \sin(2\Lambda_\Omega(t) + \Delta_{ih} - \phi_i + 2\theta_i^*(0))\Big] \\ - &\sum_{h=1}^{N} \gamma_{jh}\Big[\cos\psi_h \cos(2\Lambda_\Omega(t) + \Delta_{jh} - \phi_j + 2\theta_j^*(0)) - \sin\psi_h \sin(2\Lambda_\Omega(t) + \Delta_{jh} - \phi_j + 2\theta_j^*(0))\Big]\Bigg\}.\end{aligned} \tag{A.27}$$

Since the solution is oscillating, Ω is a non-identically zero continuous function, and, thus, there exists an open interval $(\underline{t},\bar{t})$, such that $\Omega(t) \neq 0$, for all $t \in (\underline{t},\bar{t})$. Hence, (A.27) implies that

$$\begin{aligned}&\sum_{h=1}^{N} \gamma_{ih}\Big[\cos\psi_h \cos(2\Lambda_\Omega(t) + \Delta_{ih} - \phi_i + 2\theta_i^*(0)) - \sin\psi_h \sin(2\Lambda_\Omega(t) + \Delta_{ih} - \phi_i + 2\theta_i^*(0))\Big] \\ &- \sum_{h=1}^{N} \gamma_{jh}\Big[\cos\psi_h \cos(2\Lambda_\Omega(t) + \Delta_{jh} - \phi_j + 2\theta_j^*(0)) - \sin\psi_h \sin(2\Lambda_\Omega(t) + \Delta_{jh} - \phi_j + 2\theta_j^*(0))\Big] = 0,\end{aligned} \tag{A.28}$$

for all $t \in (\underline{t}, \bar{t})$. By differentiating (A.28) with respect to time and considering once again that $\Omega(t) \neq 0$ for all $t \in (\underline{t}, \bar{t})$, one gets

$$\Phi_{ij}^{TD}(t, \Upsilon, \Delta, \theta^*(0)) = 0$$

for all $t \in (\underline{t}, \bar{t})$, that is, at the light of (A.26), $c_{ij} = 0$, which concludes the proof. □

A.3.2 Invertibility of the time-independent part of the generalized fixed point equation

In the following lemma, which generalizes Lemma 2.4, we show that the time-independent part (A.25a) of the fixed point equation (A.21) can be inverted for a generic choice of the parameters.

Lemma A.4. *There exists a set $\mathcal{N} \subset \mathbb{R}^N \times \mathbb{R}^{N\times(4N+3)}$, and a set $\mathcal{N}_0 \subset \mathcal{N}$ satifying $\mu(\mathcal{N}_0) = 0$, such that (A.25a) with natural frequencies $\omega^* \in \mathbb{R}^N$ and parameters $\Upsilon^* \in \mathbb{R}^{N\times(4N+3)}$ admits a solution $\Delta^* \in \mathbb{R}^{N\times N}$ if and only if $(\omega^*, \Upsilon^*) \in \mathcal{N}$. Moreover, for all $(\omega^*, \Upsilon^*) \in \mathcal{N} \setminus \mathcal{N}_0$, there exists a neighborhood U of (ω^*, Υ^*), a neighborhood W of Δ^*, and an analytic function $f : U \to W$, such that, for all $(\omega, \Upsilon) \in U$, $\big(\omega,\ \Upsilon,\ \Delta := f(\omega, \Upsilon)\big)$ is the unique solution of (A.25a) in $U \times W$.*

Remark A.5. In this generalized version, we prove the analyticity of f, instead of simply smoothness as for Lemma 2.4, since this permits to largely simplify the proof of the existence Theorem A.6.

Proof (SKETCH) The first part of the proof follows exactly the same steps as that of Lemma 2.4, with the matrix Υ at the place of the matrix Γ, and with the two function F and $\hat{F}$ (currently defined in (2.21) and (2.33), respectively) redefined as follows. By letting $y_i := \Delta_{iN}$, $i = 1, \ldots, N-1$, we let

$$F_i(\omega, \Upsilon, y) := \Phi_{iN}^{TI}(\omega, \Upsilon, \Delta(y)),$$

and

$$\hat{F}_i(\hat{\omega}_i, \Upsilon, y) := \Phi_{iN}^{TI}(0, \Upsilon, \Delta(y)) + \hat{\omega}_i,$$

where $\Delta_{iN}(y) := y_i$, $i = 1, \ldots, N-1$, and $\Delta_{nm}(y) = y_m - y_n$, $n = 1, \ldots, N$, $m = 1, \ldots, N-1$. The end of the proof is slightly different since, to prove the analyticity of f, instead of just smoothness, one has to invoke the fact that F is analytic and then apply the analytic implicit function theorem (Krantz and Parks, 2002, Theorem 2.3.5). For more details, we invite the reader to retrace the proof of Lemma 2.4, with the above modifications in mind. □

A.3.3 Non-existence of oscillating phase-locked solutions in the generalized dynamics

In the following theorem, which generalizes Theorem 2.2, we show that, for a generic choice of the parameters, no oscillating phase-locked solution exists in the phase dynamics (A.19).

Theorem A.6. *For all initial conditions $\theta^*(0)$, and for almost all $\omega \in \mathbb{R}^N$ and $\Upsilon \in \mathbb{R}^{N\times(4N+3)}$, (A.19) admits no oscillating phase-locked solution starting in $\theta^*(0)$.*

Proof

Observe that, if $(\omega, \Upsilon) \notin \mathcal{N}$, then, by Lemma A.4, the time-independent part of the fixed point equation (A.25a) admits no solutions and, thus, by Lemma A.3, the phase dynamics (A.19) admits no oscillating phase-locked solution.

Therefore, let us assume that $(\omega, \Upsilon) \in \mathcal{N}$. We claim that there exists $\mathcal{M}_0 \subset \mathcal{N}$, with $\mu(\mathcal{M}_0) = 0$, such that, given initial conditions $\theta^*(0)$, if there exists an oscillating phase-locked solution of (A.19) starting in $\theta^*(0)$, then $(\omega, \Upsilon) \in \mathcal{N}_0 \cup \mathcal{M}_0$, where $\mathcal{N}_0$ is defined in Lemma A.4 in Section A.3.2. If our claim holds true, noticing that $\mu(\mathcal{M}_0 \cup \mathcal{N}_0) = 0$, then the theorem is proved.

We want to construct $\mathcal{M}_0$ as the zeros of a suitable analytic function, thus ensuring that it has zero Lebesgue measure (Krantz and Parks, 2002, Page 83).
Given $(\omega, \Upsilon) \in \mathcal{N} \setminus \mathcal{N}_0$, it follows from Lemma A.4 that there exists a unique $\Delta(\omega, \Upsilon)$ such that $(\omega,\ \Upsilon,\ \Delta(\omega, \Upsilon))$ is solution to (A.25a). That is the function

$$\begin{aligned} \mathcal{N} \setminus \mathcal{N}_0 &:\longrightarrow \mathbb{R}^{N \times N} \\ (\omega, \Upsilon) &\longmapsto \Delta(\omega, \Upsilon) \end{aligned}$$

is well defined. It is also analytic, since, again by Lemma A.4, for all $(\omega, \Upsilon) \in \mathcal{N} \setminus \mathcal{N}_0$ it is analytic in a neighborhood $U \ni (\omega, \Upsilon)$. Given a pair of indexes $i \neq j$, consider the function

$$\mathcal{N} \setminus \mathcal{N}_0 :\longrightarrow \mathbb{R} \tag{A.29a}$$

$$(\omega, \Upsilon) \longmapsto G(\omega, \Upsilon) := \Phi_{ij}^{TD}(0, \Upsilon, \Delta(\omega, \Upsilon), \theta^*(0)) \tag{A.29b}$$

where Φ_{ij}^{TD} is defined in (A.24). The function G defined by (A.29) is analytic on $\mathcal{N} \setminus \mathcal{N}_0$, since it is the composition of two analytic functions (Krantz and Parks, 2002, Proposition 1.4.2). We define $\mathcal{M}_0$ as the zero set of G, that is

$$\mathcal{M}_0 := \{(\omega, \Upsilon) \in \mathcal{N} \setminus \mathcal{N}_0 : G(\omega, \Upsilon) = 0\}. \tag{A.30}$$

As anticipated above, since G is analytic, $\mu(\mathcal{M}_0) = 0$. By construction, if $(\omega, \Upsilon) \in (\mathcal{N} \setminus \mathcal{N}_0) \setminus \mathcal{M}_0$, then $G(\omega, \Upsilon) \neq 0$, that is, by the definition of G in (A.29), the time-dependent part of the fixed point equation (A.25b) admits no solutions. By Lemma A.3, this implies that, if there exists an oscillating phase-locked solution starting from $\theta^*(0)$, then necessarily

$$\begin{aligned} (\omega, \Upsilon) &\in \mathcal{N} \setminus \left[(\mathcal{N} \setminus \mathcal{N}_0) \setminus \mathcal{M}_0\right] \\ &= \mathcal{N} \setminus \left[\mathcal{N} \setminus (\mathcal{N}_0 \cup \mathcal{M}_0)\right] \\ &= \mathcal{N}_0 \cup \mathcal{M}_0, \end{aligned}$$

which proves the claim. □

A.3.4 A particular parameter configuration

Theorem A.6 holds only generically in the space of natural frequencies and parameters. This means that there exist sets of zero Lebesgue measure in this space where oscillating phase-locked solutions may indeed exist. In Section 2.4.2 we provide one examples (Example 2.3). Here we relate this zero measure set to the normal form (A.4) in (Aronson et al., 1990).

It is proved in that reference that the normal (A.4) admits asymptotically stable (oscillating) phase-locked solutions. At the same time, as discussed in Section A.1, this normal form can be obtained from our generalized dynamics via a suitable choice of the parameter matrix Φ, defined in (A.3). However, this does not contradict Theorem A.6. The normal form (A.4) falls indeed in the parameter zero measure set for which Theorem A.6 does not apply.

We stress that this intrinsic difference between our analysis and the analysis in (Aronson et al., 1990) reflects the different assumptions in the derivation of the phase-dynamics:

- ⋆ Under the assumption that the attractivity of the limit cycles in (A.1) is large, compared to the diffusive coupling and feedback strengths, to the first order, the radius dynamics can be ignored and the phase dynamics has the form (A.19), as derived in Section A.2.
- ⋆⋆ Under the assumption that the oscillators are near the Hopf bifurcation, as in that reference, the attractivity of the limit cycle is small and, to the first order, the phase dynamics depends only on the phase differences. At the same time, the effects of the radius variations are not negligible.

Beyond the purely existence result of Theorem A.6 (which is not so informative about the possible phenomena that can be observed), we stress in Section 4.3 and Section A.5 below that the presence of non-diffusive terms in the phase dynamics is crucial to obtain robust oscillation inhibition without death of the oscillation amplitude. The same fact is thoroughly stressed in (Ermentrout and Kopell, 1990). In other words, oscillation inhibition can not be robustly observed in the normal form (A.4) derived in (Aronson et al., 1990) without death of the oscillation amplitude. At the same time, ignoring the radius dynamics necessarily leads to ignoring the existence of other types of phenomena, in particular, the existence of stable phase-trapped and phase-drift solutions, as defined and observed in that reference.

It would be interesting to explore an ensemble, or a couple, of Landau-Stuart oscillators in the intermediate case between the strong attractivity assumption considered here and the weak attractivity assumption considered in (Aronson et al., 1990). This is left to future work.

A.4 Extension of the results of Chapters 3

The result of Theorem 3.4, which characterizes the robustness of phase-locking between Kuramoto oscillators, relies on the existence of an ISS Lyapunov function for the incremental phase dynamics, whose local minima characterize asymptotically stable phase-locked solutions. In this section we provide sufficient conditions for which the generalized incremental dynamics associated to (A.19) still admits a Lyapunov function. The phase-locking robustness analysis can then be generalized by retracing the steps in Chapter 3.

A.4.1 The generalized incremental dynamics with inputs

In the more general case (A.19), the incremental dynamics with inputs reads, for all $i, j = 1, \dots, N$,

$$\dot{\theta}_i(t) - \dot{\theta}_j(t) = \tilde{\omega}_i(t) - \tilde{\omega}_j(t) + \sum_{h=1}^{N} k_{ih} \sin(\theta_h - \theta_i + \delta_{ih} + \eta_h) - \sum_{h=1}^{N} k_{jh} \sin(\theta_h - \theta_j + \delta_{jh} + \eta_h) \quad \text{(A.31)}$$

where, for all $i = 1, \dots, N$ and all $t \in \mathbb{R}$, the grounded inputs $\tilde{\omega}_i(t)$ are given by

$$\tilde{\omega}_i(t) = \varpi_i(t) - \frac{1}{N} \sum_{j=1}^{N} \varpi_j(t). \quad \text{(A.32)}$$

and, as in (3.2), the time-varying natural frequencies ϖ_i account for generic time-varying perturbations to the oscillators, including, in particular, heterogeneities and the effects of

mean-field proportional feedback. They are given by

$$\begin{aligned}\varpi_i(t) = p_i(t) + \omega_i - \sum_{j=1}^{N} \kappa_{ij} \sin(\delta_{ij} + \eta_i) \\ + \sum_{j=1}^{N} \gamma_{ij} \Big[\frac{\sin\varphi_j + \cos\varphi_j}{2} \sin(\theta_j(t) - \theta_i(t) + \phi_{ij} + \psi_j) \\ + \frac{\sin\varphi_j - \cos\varphi_j}{2} \sin(\theta_j(t) + \theta_i(t) - \phi_{ij} + \psi_j) \Big],\end{aligned} \tag{A.33}$$

and $p_i : \mathbb{R} \to \mathbb{R}$, $i = 1, \ldots, N$, are measurable functions.

A.4.2 The generalized Lyapunov function

We want to find and ISS Lyapunov function for the generalized incremental dynamics with inputs (A.31). To this aim, consider the following function

$$V_I(\tilde{\theta}) := 2 \sum_{i=1}^{N} \sum_{j=1}^{N} E_{ij} \sin^2 \Big(\frac{\theta_j - \theta_i + \delta_{ij} + \eta_j}{2} \Big), \tag{A.34}$$

where $E_{ij} = \frac{k_{ij}}{K}$, and $K = \max_{ij} |k_{ij}|$, if $k \neq 0$, or $K = 1$, otherwise.

We now provide sufficient conditions on the parameter matrix Υ, defined in (A.22), for which (A.34) is an ISS Lyapunov function for the incremental dynamics (A.31) with inputs $\tilde{\omega}$. More precisely, we require that the coupling matrix k is symmetric and that, moreover, the phases $\delta_{ij} + \eta_j$ are antisymmetric under the exchange of i and j, that is

$$k_{ij} = k_{ji} \quad \forall i, j = 1, \ldots, N, \tag{A.35a}$$

$$\delta_{ij} + \eta_j = -\delta_{ji} - \eta_i, \quad \forall i, j = 1, \ldots, N. \tag{A.35b}$$

Condition (A.35a) is the same symmetric coupling assumption made in Chapter 3, whereas (A.35b) ensures that the diffusive coupling terms $\sin(\theta_j - \theta_i + \delta_{ij} + \eta_j)$ are antisymmetric. We stress that, if (A.35) is not exactly verified, the resulting dynamical uncertainties can be embedded in the perturbation term p_i in (A.33). This ensures, in particular, that our robustness analysis extends to a full neighborhood of the subset of parameters defined by (A.35).

If (A.35) holds, then the derivative of the Lyapunov function V_I along the trajectories of the incremental dynamics (A.31) reads

$$\begin{aligned}\dot{V}_I(\tilde{\theta}) &:= (\nabla_{\tilde{\theta}} V_I)^T \dot{\tilde{\theta}} \\ &= -\sum_{i,j=1}^{N} E_{ij} \sin(\theta_j - \theta_i + \delta_{ij} + \eta_j)(\dot{\theta}_i - \dot{\theta}_j) \\ &= -2 \sum_{i,j=1}^{N} E_{ij} \sin(\theta_j - \theta_i + \delta_{ij} + \eta_j) \dot{\theta}_i,\end{aligned}$$

where the last equality comes from the fact that, since by definition and (A.35a) E is a symmetric matrix, whereas, by (A.35b), $\sin(\theta_j - \theta_i + \delta_{ij} + \eta_j)$ is antisymmetric, $\sum_{i,j=1}^{N} E_{ij} \sin(\theta_j - \theta_i + \delta_{ij} + \eta_j) \dot{\theta}_j = -\sum_{i,j=1}^{N} E_{ij} \sin(\theta_j - \theta_i + \delta_{ij} + \eta_j) \dot{\theta}_i$. Since, for the same reason, it also holds

that $\sum_{i,j=1}^{N} E_{ij} \sin(\theta_j - \theta_i + \delta_{ij} + \eta_j) \sum_{h=1}^{N} \varpi_h(t) = 0$, we finally get that

$$\begin{aligned} \dot{V}_I &= -2 \sum_{i=1}^{N} \left(\sum_{j=1}^{N} E_{ij} \sin(\theta_j - \theta_i + \delta_{ij} + \eta_j) \right) \left(K \sum_{h=1}^{N} E_{ih} \sin(\theta_h - \theta_i + \delta_{ij} + \eta_j)) + \tilde{\omega}_i \right) \\ &= -2(K \nabla V^T \nabla V + \nabla V^T \tilde{\omega}), \end{aligned}$$

which proves that V_I is, at least locally near its local minima, an ISS Lyapunov function for (A.31).

A.4.3 Statement of the generalized result

Based on the function (A.34), we can retrace the same steps of Chapter 3 for the generalized phase dynamics (A.19) and derive the following result.

Theorem A.7. *Let k be a given symmetric interconnection matrix and suppose that $\delta_{ij} + \eta_j = -\delta_{ji} - \eta_i$ for all $i, j = 1, \dots, N$. Suppose, moreover, that the set $\mathcal{O}_k$ of asymptotically stable fixed points of the unperturbed, i.e. $\tilde{\omega} = 0$, incremental dynamics (A.31) in non-empty. Then $\mathcal{O}_k$ is locally input-to-state stable with respect to small $\tilde{\omega}$.*

Similarly to the original Theorem 3.4, the proof of Theorem A.7 relies on the existence of the explicit (incremental) Lyapunov function (A.34), which permits to compute explicitly the different ISS gain and bounds. At the light of this, a similar result to Corollary 3.6 also holds. More precisely, if no other exogenous disturbances but the mean-field proportional feedback are present, then the necessary condition for desynchronization becomes:

$$\left| \omega_i - \frac{1}{N} \sum_{j=1}^{N} \omega_j - \sum_{j=1}^{N} \kappa_{ij} \sin(\delta_{ij} + \eta_i) - \frac{1}{N} \sum_{h=1}^{N} \kappa_{hj} \sin(\delta_{hj} + \eta_h) \right| + 2\bar{\gamma} N \sqrt{N} \leq \delta_\omega,$$

where again $\bar{\gamma}$ is the feedback intensity and is defined as in 3.10, and where the constant $\delta_\omega > 0$ depends only on the interconnection matrix k.

A.5 Extension of the results of Chapters 4

The analysis of Chapter 4 entirely relies on the gradient nature of the closed-loop dynamics. In the all-to-all case analyzed in Chapter 4, we show, in particular, that the critical set of the potential function consists of only normally hyperbolic invariant manifolds (including isolated critical points, which are zero-dimensional invariant manifolds) and that all its minima are isolated. This ensures robust almost-global convergence to the set of isolated local minima, corresponding to robust oscillation inhibition.

A.5.1 Generalized gradient dynamics

Here we want to derive conditions on the parameter matrix Υ, defined in (A.22), for which (A.19) still admits a gradient dynamics structure. We claim in particular that, if

$$k_{ij} = k_{ji}, \quad \forall i, j = 1, \dots, N, \tag{A.36a}$$
$$\gamma_{ij} = \gamma_{ji}, \quad \forall i, j = 1, \dots, N, \tag{A.36b}$$
$$\varphi_i = \varphi_j, \quad \forall i, j = 1, \dots, N, \tag{A.36c}$$
$$\delta_{ij} + \eta_j = -\delta_{ji} - \eta_i, \quad \forall i, j = 1, \dots, N, \tag{A.36d}$$
$$\psi_i = -\phi_{ij} \quad \forall i, j = 1, \dots, N. \tag{A.36e}$$

then (A.19) can be written as a gradient dynamics. Condition (A.36a) is the known symmetric coupling assumption. Simple computations, reveal that conditions (A.36b,c) are equivalent to asking that both $\gamma_{ij}(\sin\varphi_j + \cos\varphi_j)$ and $\gamma_{ij}(\sin\varphi_j - \cos\varphi_j)$ are symmetric under the exchange of i and j. This ensures that the effective gains

$$\gamma_{ij}^{\mp} := \gamma_{ij} \frac{\sin\varphi_j \pm \cos\varphi}{2} \tag{A.37}$$

in front of both the diffusive and the additive feedback terms (A.19c) and (A.19d) are symmetric, that is $\gamma_{ij}^{\mp} = \gamma_{ji}^{\mp}$, for all $i, j = 1, \dots, N$. As in Section A.4, condition (A.36d) ensures that the diffusive coupling terms $\sin(\theta_j - \theta_i + \delta_{ij} + \eta_j)$ are antisymmetric. Finally, simple computations reveal that (A.36e) is equivalent to asking that the diffusive feedback terms $\sin(\theta_j - \theta_i + \phi_{ij} + \psi_j)$ are antisymmetric, whereas the additive terms $\sin(\theta_j + \theta_i - \phi_{ij} + \psi_j)$ are symmetric.

Consider the function

$$W(\theta, \omega, \kappa, k, \gamma, \Phi) = \sum_{i,j=1}^{N} k_{ij} \sin^2\left(\frac{\theta_j - \theta_i + \delta_{ij} + \eta_j}{2}\right) \tag{A.38a}$$
$$+ \sum_{i,j=1}^{N} \gamma_{ij}^{-} \sin^2\left(\frac{\theta_j - \theta_i + \phi_{ij} + \psi_j}{2}\right) \tag{A.38b}$$
$$- \sum_{i,j=1}^{N} \gamma_{ij}^{+} \sin^2\left(\frac{\theta_j + \theta_i - \phi_{ij} + \psi_j}{2}\right) \tag{A.38c}$$
$$- \sum_{i=1}^{N} \left(\omega_i - \sum_{j=1}^{N} \kappa_{ij} \sin(\delta_{ij} + \eta_i)\right) \theta_i. \tag{A.38d}$$

We claim that, if (A.36) holds true, then (A.19) can be written as the gradient dynamics $\dot{\theta} = -\nabla_\theta W$. Let us denote by $\frac{\partial(\text{A.38q})}{\partial\theta_h}$, where $q \in \{a, b, c\}$ and $h \in \{1, \dots, N\}$, the partial derivatives of the different right terms in (A.38) with respect to θ_h. Then we have

$$\begin{aligned} -\frac{\partial(\text{A.38a})}{\partial\theta_h} &= \frac{1}{2}\left[\sum_{j=1}^{N} k_{hj} \sin(\theta_j - \theta_h + \delta_{hj} + \eta_j) - \sum_{i=1}^{N} k_{ih} \sin(\theta_h - \theta_i + \delta_{ih} + \eta_h)\right] \\ &= \frac{1}{2}\left[\sum_{j=1}^{N} k_{hj} \sin(\theta_j - \theta_h + \delta_{hj} + \eta_j) + \sum_{i=1}^{N} k_{hi} \sin(\theta_i - \theta_h + \delta_{hi} + \eta_i)\right] \\ &= \sum_{j=1}^{N} k_{hj} \sin(\theta_j - \theta_h + \delta_{hj} + \eta_j) \end{aligned} \tag{A.39}$$

where the second equality comes from the fact that, by assumption (A.36a,d), for all $i, j = 1, \dots, N$, $-k_{ji} \sin(\theta_i - \theta_j + \delta_{ji} + \eta_i) = k_{ij} \sin(\theta_j - \theta_i + \delta_{ij} + \eta_j)$. Similar computations for the diffusive feedback term (A.38b) reveal that

$$-\frac{\partial(\text{A.38b})}{\partial \theta_h} = \sum_{j=1}^{N} \gamma_{hj}^{-} \sin(\theta_j - \theta_h + \phi_{hj} + \psi_j). \tag{A.40}$$

For the diffusive additive term (A.38c), we have

$$\begin{aligned} -\frac{\partial(\text{A.38c})}{\partial \theta_h} &= \frac{1}{2}\left[\sum_{j=1}^{N} \gamma_{hj}^{+} \sin(\theta_j + \theta_h - \phi_{hj} + \psi_j) + \sum_{i=1}^{N} \gamma_{ih}^{+} \sin(\theta_h + \theta_i + \phi_{ih} + \psi_h)\right] \\ &= \frac{1}{2}\left[\sum_{j=1}^{N} \gamma_{hj}^{+} \sin(\theta_j + \theta_h - \phi_{hj} + \psi_j) + \sum_{i=1}^{N} \gamma_{hi}^{+} \sin(\theta_i + \theta_h + \phi_{hi} + \psi_i)\right] \\ &= \sum_{j=1}^{N} \gamma_{hj}^{+} \sin(\theta_j + \theta_h - \phi_{hj} + \psi_j), \end{aligned} \tag{A.41}$$

where the second equality come from the fact that, by assumption (A.36b,c,e), for all $i, j = 1, \dots, N$, $\gamma_{ij}^{+} \sin(\theta_j + \theta_i - \phi_{ij} + \psi_j) = \gamma_{ji}^{+} \sin(\theta_i + \theta_j - \phi_{ji} + \psi_i)$. Finally, by noticing that

$$-\frac{\partial}{\partial \theta_h}\left(-\sum_{i=1}^{N}\left(\omega_i - \sum_{j=1}^{N} \kappa_{ij} \sin(\delta_{ij} + \eta_i)\right)\theta_i\right) = \omega_h - \sum_{j=1}^{N} \kappa_{hj} \sin(\delta_{hj} + \eta_h),$$

Equations (A.39)-(A.40)-(A.41) show that, if (A.36) holds true, then $-\frac{\partial W}{\partial \theta_h} = \dot{\theta}_h$, which shows that W is a potential function for (A.19).

A.5.2 Statement of the generalized result

In Sections 4.2.1, 4.2.2, and 4.2.3 we thoroughly analyze the critical set of the potential function W in the ideal case of all-to-all coupling and feedback, and zero natural frequencies. A similar analysis can be developed for the generalized potential function (A.38). More precisely, one should analyze the critical set of (A.38) under condition (A.36) and in the ideal case $\omega_i - \sum_{j=1}^{N} \kappa_{ij} \sin(\delta_{ij} + \eta_i) = 0$, for all $i = 1, \dots, N$. This translates into studying the critical set of the unperturbed potential function

$$W_0(\theta, k, \gamma, \Phi) = \sum_{i,j=1}^{N} k_{ij} \sin^2\left(\frac{\theta_j - \theta_i + \delta_{ij} + \eta_j}{2}\right) \tag{A.42a}$$

$$+ \sum_{i,j=1}^{N} \gamma_{ij}^{-} \sin^2\left(\frac{\theta_j - \theta_i + \phi_{ij} + \psi_j}{2}\right) \tag{A.42b}$$

$$- \sum_{i,j=1}^{N} \gamma_{ij}^{+} \sin^2\left(\frac{\theta_j + \theta_i - \phi_{ij} + \psi_j}{2}\right), \tag{A.42c}$$

under the assumption that (A.36) holds true. Note that $-\nabla_\theta W_0 = \bar{f}(\theta, k, \gamma, \Phi)$, where $\bar{f}$ is defined in (A.19b). Similarly to Chapter 4, if the parameters are such that the critical set of W_0 consists of only normally hyperbolic invariant manifolds and all its minima are isolated, then one can plug the effective natural frequencies $\omega_i - \sum_{j=1}^{N} \kappa_{ij} \sin(\delta_{ij} + \eta_i)$ back in as perturbations and conclude robust oscillation inhibition. We can formalize this discussion as follows.

Theorem A.8. *Consider the dynamics (A.19) and suppose that (k, γ, Φ) satisfy (A.36). Suppose, moreover, that the critical set of the unperturbed potential function W_0 is made of only normally hyperbolic invariant manifolds, and that the set $\mathcal{W}_m$ of its local minima is non-empty and made of isolated critical points. Then, there exists $\delta > 0$ and a class $\mathcal{K}_\infty$ function ρ such that, if*

$$\left| \omega - \left[\sum_{j=1}^{N} \kappa_{ij} \sin(\delta_{ij} + \eta_i) \right]_{i=1,\dots,N} \right| \leq \delta \tag{A.43}$$

then there exists a set of isolated points $\tilde{\mathcal{W}}_m$, satisfying

$$|\tilde{\mathcal{W}}_m|_{\mathcal{W}_m} \leq \rho \left(\left| \omega - \left[\sum_{j=1}^{N} \kappa_{ij} \sin(\delta_{ij} + \eta_i) \right]_{i=1,\dots,N} \right| \right),$$

which contains all the local minima of the potential function W and which is almost globally attractive for (A.19).

Theorem A.8 provides a condition on the coupling and feedback gains, and on the phases Φ, for which oscillation inhibition can be robustly achieved via mean-field proportional feedback. We stress that the analysis of the critical set of W can be a hard task in general. However, once the system dimension N is fixed, numerical analysis can come into play to check whether this set is hyperbolic or not.

Remark A.9. The phase dynamics associated to the normal form (A.4) derived in (Aronson et al., 1990) does not satisfy the assumptions of Theorem A.8. Recalling the discussion in Item 2 in Section A.1, it is easy to verify that for the set of parameters associated to this normal form, the phase dynamics (A.19) and, thus, the potential function W contain only diffusive terms. As a consequence, all the critical points of W are non-isolated. Indeed, given a critical point θ^*, all the points of the form $\theta^* + a\mathbf{1}_N$, with $a \in \mathbb{R}$, are again critical points of W. When the closed-loop dynamics contains only diffusive coupling terms, robust oscillation inhibition is thus impossible. Indeed, all the fixed points are at most stable, but never asymptotically, thus excluding robustness by converse Lyapunov theorems (Khalil, 2001, Theorem 4.17),(Sontag and Wang, 1999). The same fact is stressed, with different arguments, in the introduction of (Ermentrout and Kopell, 1990), where the authors study oscillation inhibition (without death of the amplitude) in pairs or chains of coupled neuronal oscillators.

A.6 Extension of the results of Chapters 5

The practical desynchronization condition in Chapter 5 relies on two main points:

- **A)** The mean natural frequency must be sufficiently large, in such a way that the average contribution of the additive coupling terms is small (cf. Claim 5.12 in the proof of Theorem 5.10).
- **B)** The closed-loop diffusive coupling must be small.

A): In the general case (A.19), the average contribution of the additive feedback terms can still be analyzed via Claim 5.12 in the proof of Theorem 5.10. Indeed, Claim 5.12 naturally extends to the case when an arbitrary phase is added in the sine argument. Thus, the average contribution of each additive term admits the same upper bound as for the original phase dynamics (2.6).

B): The closed-loop diffusive coupling requires more attention.
With the notation $\zeta_{ij} := \phi_{ij} + \psi_j - \delta_{ij} - \psi_j$, for all $i, j = 1, \dots, N$, we start by rewriting the diffusive feedback terms as follows:

$$\begin{aligned}\sin(\theta_j - \theta_i + \phi_{ij} + \psi_j) &= \sin(\theta_j - \theta_i + \delta_{ij} + \eta_j) + \sin(\theta_j - \theta_i + \delta_{ij} + \eta_j + \zeta_{ij}) \\ &\quad - \sin(\theta_j - \theta_i + \delta_{ij} + \eta_j) \\ &= \sin(\theta_j - \theta_i + \delta_{ij} + \eta_j) \\ &\quad + 2\sin\left(\frac{\zeta_{ij}}{2}\right)\cos\left(\theta_j - \theta_i + \delta_{ij} + \eta_j + \frac{\zeta_{ij}}{2}\right),\end{aligned} \tag{A.44}$$

where the second equality comes from the trigonometric identity $\sin a - \sin b = 2\sin\left(\frac{a-b}{2}\right)\cos\left(\frac{a+b}{2}\right)$. By plugging (A.44) in (A.19), the closed-loop diffusive coupling becomes, for all $i = 1, \dots, N$,

$$\sum_{j=1}^{N} k_{ij}\sin(\theta_j - \theta_i + \delta_{ij} + \eta_j) + \sum_{j=1}^{N}\gamma_{ij}\frac{\sin\varphi_j + \cos\varphi_j}{2}\sin(\theta_j - \theta_i + \phi_{ij} + \psi_j) =$$

$$\sum_{j=1}^{N}(k_{ij} + \gamma_{ij}^{-})\sin(\theta_j - \theta_i + \delta_{ij} + \eta_j) + 2\sum_{j=1}^{N}\gamma_{ij}^{-}\sin\left(\frac{\zeta_{ij}}{2}\right)\cos\left(\theta_j - \theta_i + \delta_{ij} + \eta_j + \frac{\zeta_{ij}}{2}\right). \tag{A.45}$$

where γ_{ij}^{-} are defined in (A.37). In the ideal case

$$\delta_{ij} + \eta_j = \phi_{ij} + \psi_j, \quad \forall i, j = 1, \dots, N, \tag{A.46}$$

it holds that $\zeta_{ij} = 0$ and thus the closed-loop diffusive coupling can be directly modified via γ_{ij}^{-}. In this case, we fall back to the same analysis as the the original case. In particular, if (A.46) holds true, by retracing the proof of Theorem 5.10, it follows that the practical desynchronization condition (5.17) becomes

$$\Omega_{ij} := |\omega_i - \omega_j| - \sum_{h=1}^{N}\left(|\gamma_{ih}^{+}| + |\gamma_{jh}^{+}|\right)\left(\frac{\pi\nu}{2\overline{\omega}} + \frac{\nu^2}{6\overline{\omega}^2}\right) - \sum_{h=1}^{N}\left(|\varepsilon_{ih}| + |\varepsilon_{jh}|\right) > 0,$$

where

$$\nu := 2\max_{h=1,\dots,N}\left(|\tilde{\omega}_h| + \sum_{h'=1}^{N}\left(|\gamma_{hh'}^{+}| + |\varepsilon_{hh'}|\right)\right), \tag{A.47a}$$

$$\overline{\omega} := \frac{1}{N}\sum_{i=1}^{N}\omega_i, \tag{A.47b}$$

$$\tilde{\omega}_h := \omega_h - \bar{\omega}, \ \forall h = 1, \dots, N, \tag{A.47c}$$

$$\varepsilon_{hh'} := k_{hh'} + \gamma_{hh'}^{-}, \ \forall h, h' = 1, \dots, N. \tag{A.47d}$$

Conversely, if $[\zeta_{ij}]_{ij=1,\dots,N} \neq 0$, the term $-\sum_{h=1}^{N}\left(\left|\gamma_{ih}^{-}\sin\left(\frac{\zeta_{ih}}{2}\right)\right| + \left|\gamma_{jh}^{-}\sin\left(\frac{\zeta_{jh}}{2}\right)\right|\right)$ must be added to the desynchronization condition. To summarize, we have the following result, which generalizes Theorem 5.10 to the extended phase dynamics (A.19).

Theorem A.10. *Suppose that there exists $(i, j) \in \mathbb{N}_N^{\neq}$, such that*

$$\begin{aligned}\Omega_{ij} := |\omega_i - \omega_j| &- \sum_{h=1}^{N}\left(|\gamma_{ih}^{+}| + |\gamma_{jh}^{+}|\right)\left(\frac{\pi\nu}{2\overline{\omega}} + \frac{\nu^2}{6\overline{\omega}^2}\right) - \sum_{h=1}^{N}\left(|\varepsilon_{ih}| + |\varepsilon_{jh}|\right) \\ &- \sum_{h=1}^{N}\left(\left|\gamma_{ih}^{-}\sin\left(\frac{\zeta_{ih}}{2}\right)\right| + \left|\gamma_{jh}^{-}\sin\left(\frac{\zeta_{jh}}{2}\right)\right|\right) > 0.\end{aligned} \tag{A.48a}$$

where $\nu, \overline{\omega}, \tilde{\omega}_h, \varepsilon_{h,h'}$, $h, h' = 1, \ldots, N$, are defined in (A.47). Then the pair of oscillators (i, j) is practically desynchronized for (A.19) in the sense of Definition 5.6.

Remark A.11. We stress that the generalized practical desynchronization condition (A.48) can be robustly obtained on an open set of parameters. Indeed, if (A.46) is not exactly verified, the contribution associated to the parametric uncertainties, *i.e.* $-\sum_{h=1}^{N}\left(\left|\gamma_{ih}^{-}\sin\left(\frac{\zeta_{ih}}{2}\right)\right|+\left|\gamma_{jh}^{-}\sin\left(\frac{\zeta_{jh}}{2}\right)\right|\right)$, is small, provided that those uncertainties are small. This ensures that, if (A.48) holds true in the ideal case $\zeta_{ij} = 0$, for all $i, j = 1, \ldots, N$, then we can find an upper bound $\delta_{desynch} > 0$, such that (A.48) is still verified in the perturbed case $\zeta_{ij} \neq 0$, provided that $|\zeta_{ij}| < \delta_{desynch}$, for all $i, j = 1, \ldots, N$.

A.7 Numerical simulations on Van der Pol and Hodgkin-Huxley models

In this section we numerically explore the effect of proportional mean-field feedback on ensembles of coupled Van der Pol and Hodgkin-Huxley oscillators. We pick the parameters in such a way that, in the absence of stimulation, the ensembles are frequency synchronized.

The main result is the (numerical) evidence that the phenomenology observed and analytically explained for strongly attractive Landau-Stuart oscillators in Chapter 3 (robustness of phase-locking to small feedback intensity), Chapter 4 (oscillation inhibition for small natural frequencies), and Chapter 5 (desynchronization for large natural frequencies) also hold for these more complex models. This opens the way to future analytical investigation.

A.7.1 Van der Pol oscillators under proportional mean-field feedback

We consider an ensemble of all-to-all interconnected Van der Pol oscillators under the effect of a homogeneous proportional mean-field feedback. Their dynamics read

$$\dot{V}_i = 5V_i - V_i^3 - a_i w_i + \frac{K}{N}\left(\sum_{j=1}^{N} V_j - NV_i\right) + \frac{\gamma}{N}\sum_{j=1}^{N} V_j \tag{A.49}$$

$$\dot{w}_i = a_i V_i + 0.1\frac{K}{N}\left(\sum_{j=1}^{N} w_j - Nw_i\right) \tag{A.50}$$

for all $i = 1, \ldots, N$. In order to obtain a heterogeneous ensemble, in the large frequency configuration, the coefficients a_i are centered at $\bar{a} = 1$ as follows

$$a_i = 0.95 + 0.1\frac{i-1}{N-1},$$

$i = 1, \ldots, N$, whereas in the small natural frequency configuration they are centered at $\underline{a} = 0.1$ as follows

$$a_i = 0.095 + 0.01\frac{i-1}{N-1},$$

$i = 1, \ldots, N$. The coupling strength is given by $K = 0.5$. The small feedback configuration is obtained for $\gamma = -1.7K$, whereas the large feedback configuration for $\gamma = -2K$. The result of simulations, is provided in Figures A.1, A.2, and A.3.

As illustrated in Figure A.1, when the oscillator frequency is large, the effect of the mean-field feedback is to desynchronize the oscillators, provided that the feedback gain is sufficiently large

(cf. Chapter 5 and Section A.6). For smaller feedback gain, phase-locking robustly persists (Figure A.2), even though the irregularity increases (cf. Chapter 3 and Section A.4). Conversely, as illustrated in Figure A.3, for small natural frequencies, the mean-field proportional feedback inhibits the oscillations (cf. Chapter 4 and Section A.5). We stress that, as depicted in Figure A.3(right), even though oscillation inhibition is robustly achieved, the trajectories of the single oscillators remain close to the original limit cycle attractor (cf. Section A.2).

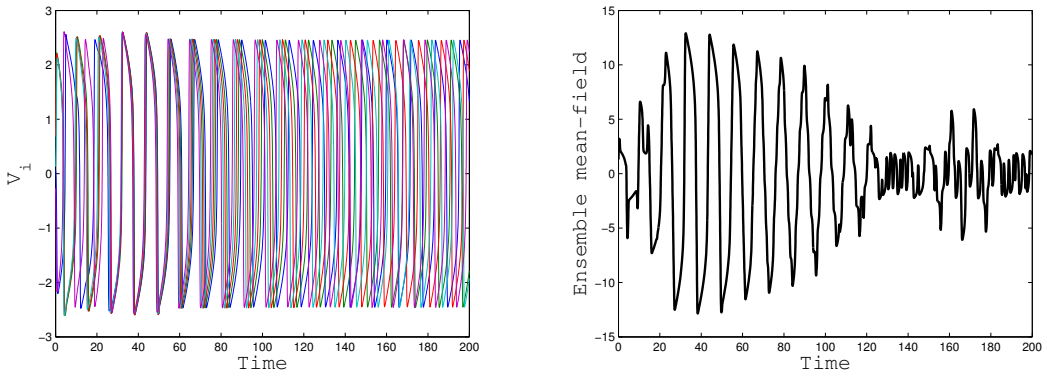

FIGURE A.1: Response of all-to-all coupled ($N = 5$) Van der Pol oscillators to proportional mean-field feedback. The feedback is switched on at $t = 50$. Large natural frequencies: desynchronization. Left: voltages. Right: ensemble mean-field.

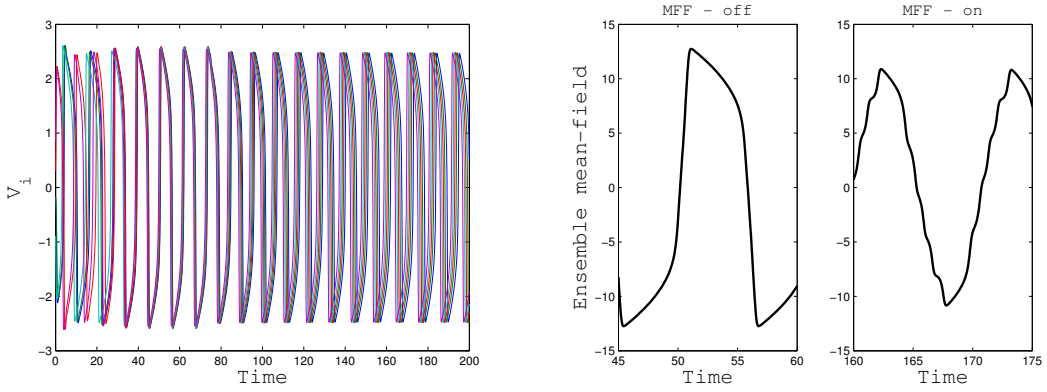

FIGURE A.2: Response of all-to-all coupled ($N = 5$) Van der Pol oscillators to proportional mean-field feedback. The feedback is switched on at $t = 50$. Small feedback gain: robust phase-locking. Left: voltages. Right: ensemble mean-field before and after the feedback is switched on.

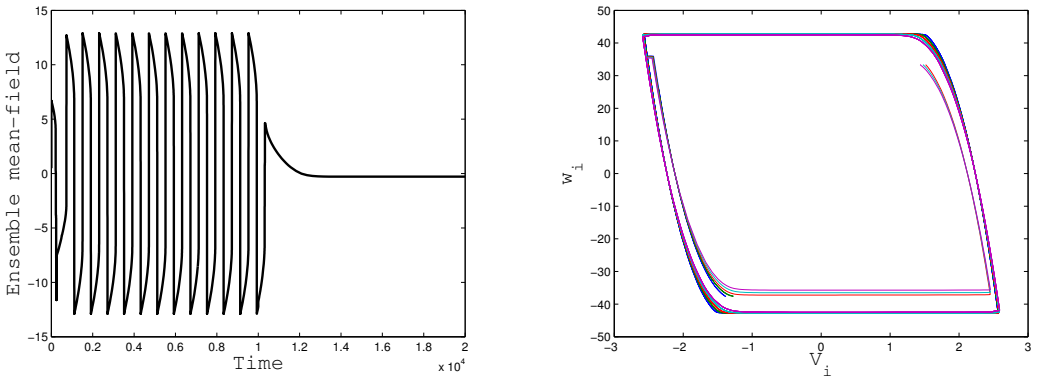

FIGURE A.3: Response of all-to-all coupled ($N = 5$) Van der Pol oscillators to proportional mean-field feedback. The feedback is switched on at $t = 50$. Small natural frequencies: oscillation inhibition. Left: ensemble mean-field. Right: trajectory behavior in the V_i, w_i planes.

A.7.2 Hodgkin-Huxley neurons under mean-field proportional feedback

We consider an ensemble of $N = 7$ diffusively coupled Hodgkin-Huxley dynamics under proportional mean-field feedback

$$\begin{aligned}
C\dot{V}_i &= I_{app} - g_{K,i}n_i^4(V_i - V_K) - g_{Na,i}m_i^3h_i(V_i - V_{Na}) - g_l(V_i - V_l) \\
&\quad + \frac{K}{N}\left(\sum_{j=1}^{N} V_j - NV_i\right) + \frac{\gamma}{N}\sum_{j=1}^{N} V_j \\
\dot{n}_i &= \alpha_n(V_i)(1 - n_i) - \beta_n(V_i)n_i \\
\dot{m}_i &= \alpha_m(V_i)(1 - m_i) - \beta_m(V_i)m_i \\
\dot{h}_i &= \alpha_h(V_i)(1 - h_i) - \beta_h(V_i)h_i,
\end{aligned}$$

for all $i = 1, \ldots, 7$, where the functions α_x, β_x, $x = n, m, h$, can be found in the paper Hodgkin and Huxley (1952). The value for the potassium Nernst potential $V_K = -12$ is the same as in Hodgkin and Huxley (1952), while the sodium Nersnt and the leak Nernst potentials are rounded to $V_{Na} = 120$ and $V_l = 10.6$, respectively. The leak current conductance is $g_l = 0.3$. In order to obtain an heterogeneous ensemble, the maximum sodium and potassium conductances are defined as

$$\begin{aligned}
g_{K,i} &= \bar{g}_K(1 + i) \\
g_{Na,i} &= \bar{g}_{Na}(1 + 2i),
\end{aligned}$$

where $\bar{g}_K = 36$ and $g_{Na} = 120$. The large natural frequencies configuration is obtained for $I_{app} = 60$, whereas the small natural frequency configuration for $I_{app} = 0$. The coupling strength is given by $K = 2$. The large feedback configuration is obtained for $\gamma = -2K$, whereas the small feedback configuration for $\gamma = -1.41K$. The result of simulations is provided in Figures A.4, A.5, and A.6.

As illustrated in Figure A.1, when the oscillator frequency is large, the effect of the mean-field feedback is to desynchronize the oscillators, provided that the feedback gain is sufficiently large (cf. Chapter 5 and Section A.6). For smaller feedback gain, phase-locking robustly persists (Figure A.2), even though the irregularity increases (cf. Chapter 3 and Section A.4). Conversely, as illustrated in Figure A.3, for small natural frequencies, the mean-field proportional

feedback inhibits the oscillations (cf. Chapter 4 and Section A.5).

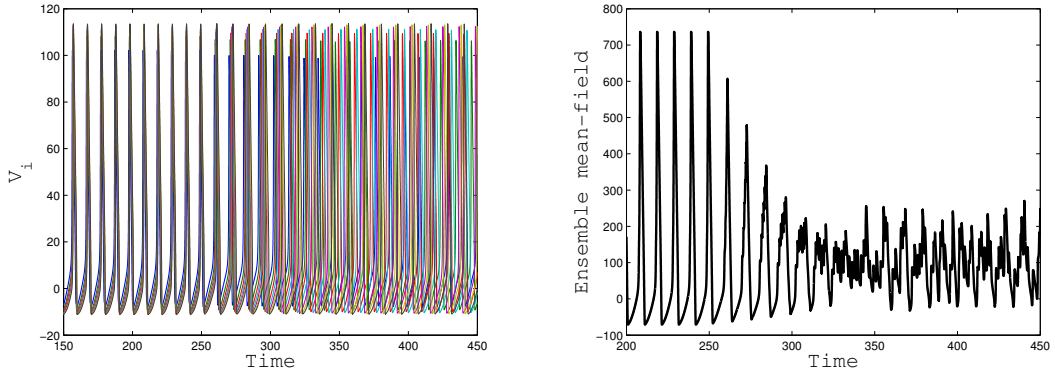

FIGURE A.4: Response of all-to-all coupled ($N = 7$) Hodgkin-Huxley neuron model to proportional mean-field feedback. The feedback is switched on at $t = 250$. Large natural frequencies: desynchronization. Left: voltages. Right: ensemble mean-field.

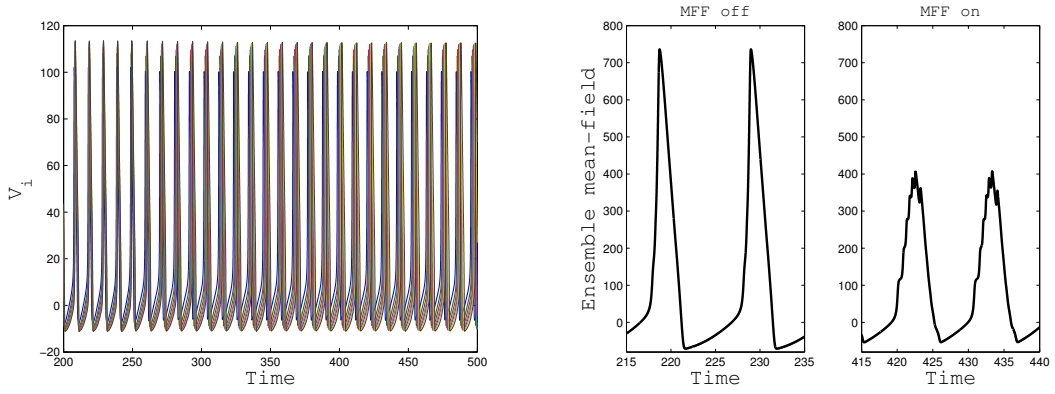

FIGURE A.5: Response of all-to-all coupled ($N = 7$) Hodgkin-Huxley neuron model to proportional mean-field feedback. The feedback is switched on at $t = 250$. Small feedback gain: robust phase-locking. Left: voltages. Right: ensemble mean-field before and after the feedback is switched on.

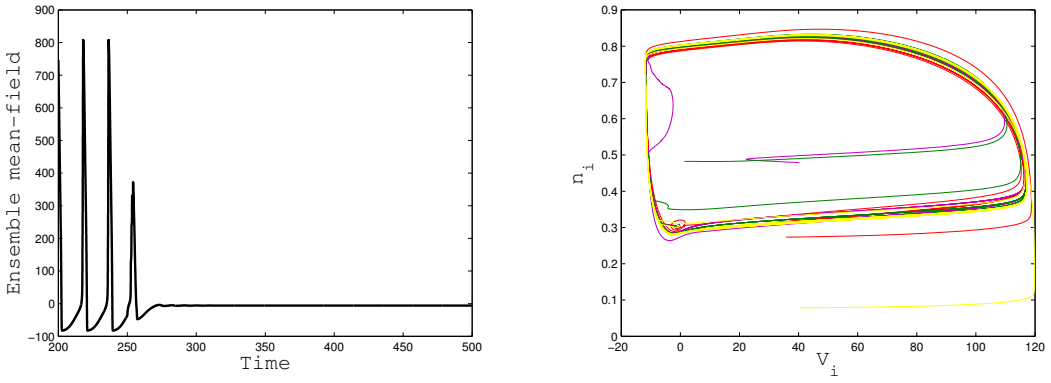

FIGURE A.6: Response of all-to-all coupled ($N = 7$) Hodgkin-Huxley neuron model to proportional mean-field feedback. The feedback is switched on at $t = 250$. Small natural frequencies: oscillation inhibition. Left: ensemble mean-field. Right: trajectory projection on the V_i, n_i planes.

Part II

More realistic neuron models

Chapter 6

Reduced modeling of calcium-gated Hodgkin-Huxley neuronal dynamics[1]

Motivated by the need for a deeper mathematical understanding of the synchronization phenomena exhibited by dopaminergic neurons (Drion et al., 2011a,b) illustrated in Section 1.6, we develop in this chapter a mathematical analysis of calcium-gated Hodgkin-Huxley dynamics based on reduced models. Calcium currents are involved in the regulation of the spiking behavior of a large family of neurons, including dopaminergic, but also STN, and other central nervous system's neurons, suggesting that they might play a central role also in the electrophysiological mechanisms behind PD. We refer the reader to Sections 1.4.2 and, in particular, page 16 for more details and some references.

Hybrid reduced models of the Izhikevich type (Izhikevich, 2010) offer a valuable tool for the mathematical modeling of neuron dynamics. In their simple form they are indeed able to reproduce with fidelity the behavior of a large family of neurons (Izhikevich, 2003).

We show, however, that the Izhikevich model fails at reproducing some physiological behaviors exhibited by dopaminergic neurons, namely robust periodic spiking (pacemaking) and after-depolarization potentials, or ADPs, (Guzman et al., 2009). We show that this deficiency is intrinsically due to a specific type of bifurcation in the fast voltage dynamics of calcium-gated neurons that is absent in the Izhikevich model. We therefore propose a new hybrid neuron model, embedding this calcium-gated bifurcation and reproducing the robust pacemaking of dopaminergic (DA) neurons, as we are going to briefly illustrate in this introduction.

The pacemaking activity of DA neurons, as the one depicted in Figure 6.1, is characterized by ADPs, a hallmark of voltage-regulated calcium currents (Chen and Yaari, 2008). See also Section 1.4.2. ADPs are tightly linked to the excitability properties of neurons, since they are associated to a post-spike phase of high excitability that is due to the persistent activation of depolarizing calcium currents (Chen and Yaari, 2008; Beurrier et al., 1999). At the same time, DA neurons pacemaking and ADPs generation are very robust in biologically meaningful conditions (Guzman et al., 2009), meaning that the spiking rhythm and ADPs shape are barely influenced in the presence of small exogenous perturbations.

[1] The results presented in this chapter were obtained under the supervision of Prof. R. Sepulchre at the University of Liège, Belgium. This work was supported by the Belgian Network DYSCO (Dynamical Systems, Control, and Optimization), funded by the Interuniversity Attraction Poles Programme, initiated by the Belgian State, Science Policy Office, and by the European Union Seventh Framework Programme [FP7/2007-2013] under grant agreement n.257462 HYCON2 Network of excellence. The obtained results were also the motivating subject of a submitted "CALL CREDITS AND PROJECTS F.R.S.-FNRS 2011 (CC)" project.

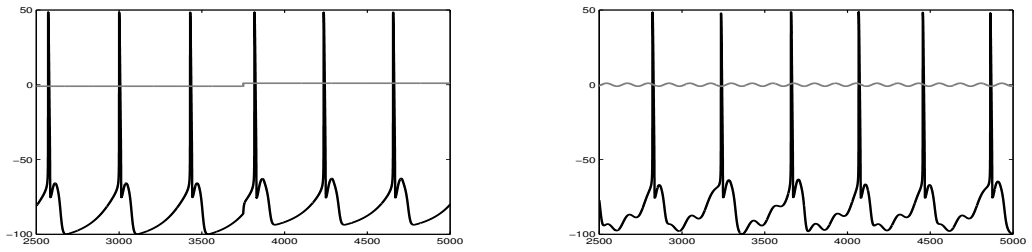

FIGURE 6.1: Robust pacemaking and afterdepolarization potentials in a detailed computational model of dopaminergic neurons. The gray trace depicts the injected stimulus.

In order to study DA neurons mathematically, we proceed with a planar hybrid reduction by fitting the parameters of the Izhikevich model to the DA neurons spiking pattern. In the absence of exogenous inputs, the obtained hybrid dynamics reproduces with fidelity the behavior of DA neurons. Interestingly, however, even tiny amounts of current completely disrupt its pacemaking activity and ADPs shape. These numerical observations are reported in Figure 6.13. This lack of robustness compromises the realism of the obtained modeling, thus making it unsuitable to use in biologically meaningful conditions and, in particular, in the presence of exogenous inputs. The forthcoming analysis thus aims at deriving an alternative simple neuron model that captures the essential dynamical mechanisms behind the robustness of pacemaking and ADPs.

More precisely, since we are interested in qualitative aspects, instead of considering a particular and detailed neuron model, we propose in Section 6.2 a simple modification of the original Hodgkin-Huxley dynamics exhibiting the typical behaviors of calcium-gated neurons, that is ADPs (Chen and Yaari, 2008), plateau oscillations (Brown and Randall, 2009), and spike latency (Molineux et al., 2005). See also Section 1.4.2 for an informal description of this phenomena and other references. Following the standard reduction of the Hodgkin-Huxley equations, we reduce the proposed model to a planar dynamics exhibiting the same qualitative behavior, and explain in Sections 6.2.2 and 6.2.3 the origin of ADPs, plateau oscillations, and spike latency via phase-portrait and numerical bifurcation analysis. In Section 6.3, we deepen further this investigation. We show, in particular, the existence of a *transcritical bifurcation* in the fast voltage dynamics of the reduced model. The same bifurcation is absent in the Izhikevich model, as well as in other existing simple neuron models, such as FitzHugh-Nagumo (FitzHugh, 1961) or Hindmarsh-Rose (Hindmarsh and Rose, 1984). We identify this bifurcation as the mathematical signature of calcium-gated neurons.

Based on normal forms, we derive a simple dynamics that captures the qualitative behavior associated to this transcrtical bifurcation. We prove analytically, with the help of geometrical singular perturbations, the existence of a saddle-homoclinic bifurcation, as highlighted by the numerical bifurcation analysis on the calcium-gated Hodgkin-Huxley model.

Inspired by the above normal form, we propose in Section 6.4 a novel reduced hybrid neuron model. Similarly to the Izhikevich model, its parameters can be chosen to reproduce qualitatively the spiking pattern of DA neurons. As opposed to the Izhikevich model, however, the proposed model exhibits the same robustness properties of DA neurons. At the light of the analysis developed in the rest of the chapter, we illustrate how this difference is closely related to the different bifurcations of the fast voltage dynamics in the two models: fold, for the Izhikievich model, and transcritical, for the proposed model.

As a conclusion to this analysis, we propose the novel reduced model as a suitable choice for the mathematical analysis of calcium-gated neurons and, in particular, for the study of

the response of the latter to exogenous inputs. As discussed in Section 1.6.1, apart from neuronal synchronization analysis and control, the potentiality of the proposed hybrid modeling of neurons involved in PD/DBS could also be relevant for the DBS computational model-based approach (Schiff, 2010).

6.1 A short survey on the ionic basis of spiking

We start with a brief recall of the ionic mechanism underlying neurons electrical activity that will be useful in the sequel.

6.1.1 Electrical properties of the neuron membrane

Neurons, as living cells, have a membrane that separates them from the outside world (Trevors and Saier Jr, 2011, Second Law of Biology). The electrical activity of neurons is due to a potential difference between the interior and the exterior of the cell and to currents across its membrane. In the following, we briefly describe this mechanism. All the information reported here, and many more details, can be found elsewhere. For an electro-physiological perspective, see in (Hille, 1984, Chapters 1-5), and references therein. For an elementary dynamical perspective, see (Izhikevich, 2007, Chapters 5-9), and references therein. For a more advanced mathematical discussion, see (Ermentrout and Terman, 2010, Chapters 1-7), and references therein.

The neuron membrane is endowed with ionic channels that transport different ions, mainly sodium Na^+, potassium K^+, and calcium Ca^{2+} ions. The flow of these ions through the neuron membrane generates a net current I_{ions}, and the difference in ions concentration between the intracellular and extracellular mediums a net membrane voltage V_m.

The neuron membrane plays itself an electrical role. Via its lipid bilayer, it acts as an insulator between two charged mediums (the interior and the exterior), that is it acts as a capacitance C_m. The rate of change of V_m under a current I_{ions} is thus given by

$$C_m \frac{dV_m}{dt} = I_{ions}. \tag{6.1}$$

Since it is also a conductive medium, the neuron membrane must also satisfy Ohm's law. Let I be an externally applied current. If g is the membrane conductance, then it holds that

$$I + I_{ions} + gV_m = 0. \tag{6.2}$$

By plugging (6.2) into (6.1), we get

$$C_m \frac{dV_m}{dt} = -gV_m + I,$$

that is the membrane voltage dynamics can be described by a RC-circuit. As such, a neuron would not even be able to autonomously generate an oscillatory electrical activity. The complex behavior exhibited by real neurons relies on a number of important properties that we have hidden until now, and that we present in what follows.

6.1.2 Ionic dynamics in the neuron membrane

Due to chemical kinetics, each ion crossing the neuron membrane possesses a different equilibrium Nernst[2] potential. Ions with a negative Nernst potential (like K^+) tend to flow outside the cell generating negative (outward) currents. Conversely, ions with a positive Nernst potential (Na^+ and, even more, Ca^{2+}) tend to generate positive (inward) currents.

The membrane conductance is also ion-dependent, meaning that its permeability, through selective ionic channels, depends on the ion type. Moreover, the different conductances are not static, but they change dynamically and nonlinearly following voltage changes.

More precisely, each selective ionic channel is endowed with voltage-sensitive gates. There are two types of gates: activation gates, and inactivation gates. Activation gates open (activate) ionic channels, and, conversely, inactivation gates close (inactivate) ionic channels. Ionic channels can exhibit activation, inactivation, or both types of gates. The probability that a sodium activation gate is in the open state is usually denoted by m, while the probability that a sodium inactivation gate is not closed by h. Similarly, we use n and d for potassium and calcium activation gates[3]. As a representative example, in the Hodgkin-Huxley model (Hodgkin and Huxley, 1952) the membrane conductances g_{Na} and g_K with respect to sodium and potassium ions are given by

$$g_{Na} = \bar{g}_{Na} m^3 h, \qquad g_K = \bar{g}_K n^4, \tag{6.3}$$

where $\bar{g}_{Na}, \bar{g}_K > 0$ are the maximal conductances and are proportional to the number of ionic channels of the given ion type. The exponent on each gating variable is the number of gates of that type for each channel. So, for instance, when all the potassium activation gates are open, then $n = 1$ and the potassium conductance is maximal. Similarly, if the 20% of the sodium activation gates are open, and the 60% of the inactivation gates are not closed, then $g_{Na} = \bar{g}_{Na} 0.2^3 0.6 = 0.048 \bar{g}_{Na}$.

The different gates evolve dynamically following voltage changes and the rapidity with which they react is ion-dependent. In particular, the Na^+ activation gate m is much faster to react than its inactivation h, and both K^+ and Ca^{2+} activation gates n and d. Conversely, h, n, and d, evolve on a similar time-scale.

The co-operation of all these properties transform the first order linear RC-circuit (6.1.1) in a higher order nonlinear RC-circuit with voltage dependent conductances and timescale separations. The first conductance-based model able to capture all these important properties of neuron dynamics is the aforementioned Hodgkin-Huxley model (Hodgkin and Huxley, 1952), whose equivalent circuit is depicted in Figure 6.2. As an emblematic choice, we pick the Hodgkin-Huxley model for all the forthcoming analysis.

6.2 Reduction of a calcium-gated Hodgkin-Huxley models

Consider the Hodgkin-Huxley model (Hodgkin and Huxley, 1952) provided with an extra non-inactivating calcium current $I_{Ca} = -\bar{g}_{Ca} d^a (V - V_{Ca})$, where $\bar{g}_{Ca}$ is the maximum calcium conductance, V_{Ca} is the calcium Nernst potential, and a is the number of activation gates per calcium channel. Since they evolve on a similar time-scale, we assume for simplicity that the behavior of the calcium activation gating variable d can be well approximated as a function

[2]The Nerst potential V_X of an ion X is the voltage of a permeable membrane separating two mediums containing X for which kinetic equilibrium is achieved. It depends on the difference in ion concentration between the two mediums. More precisely, $V_X \propto \log \frac{[X]_{in}}{[X_{out}]}$ (Hille, 1984, Chapters 1).

[3]In the following we only consider potassium and calcium channels that do not inactivate.

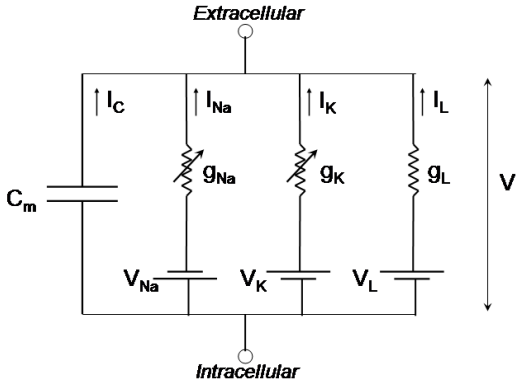

FIGURE 6.2: Electrical circuit equivalent to the Hodgkin-Huxley model. C_m denotes the neuron membrane capacitance. V_{Na} and V_K are, respectively, the sodium and potassium Nernst potential. The nonlinear conductances g_{Na} and g_K are given by (6.3). $I_C = C_m dV/dt$ is the current at membrane capacitance. I_{Na} and I_K are the ionic currents generated by, respectively, sodium and potassium ions. The leak current I_L approximates passive properties of the cell. Adapted from (Skinner, 2006), with permission.

$f(n)$ of the potassium activation gating variable n, for some function $f : [0,1] \to [0,1]$. The obtained model reads

$$\begin{aligned}
\dot{V} &= I - \bar{g}_K n^4 (V - V_K) - \bar{g}_{Na} m^3 h (V - V_{Na}) - g_l (V - V_l) - \bar{g}_{Ca} f(n)^a (V - V_{Ca}) + I_{pump} \\
\dot{n} &= \alpha_n(V)(1-n) - \beta_n(V) n \\
\dot{m} &= \alpha_m(V)(1-m) - \beta_m(V) m \\
\dot{h} &= \alpha_h(V)(1-h) - \beta_h(V) h,
\end{aligned} \tag{6.4}$$

where the extra DC-current I_{pump} accounts for the effects of outward calcium pumps currents (Hille, 1984, Chapters 4). For the Hodgkin-Huxley part, we use the parameters of the original paper (Hodgkin and Huxley, 1952). As a simple choice, we pick in our analysis $f(n) := n$, and $a := 3$, corresponding to calcium activation gates with the same kinetics of potassium activation gates and three activation gates per channel. In the following, we let the state "I_{Ca}-off" correspond to $g_{Ca} = I_{pump} = 0$, and the state "I_{Ca}-on" to $g_{Ca} = 2.7$ and $I_{pump} = -19$. Such parameters do not reflect any precise physiological calcium current. We choose them as a simple prototypical example. Figure 6.3 depicts the spiking behavior in the two configurations.

Compared to the original Hodgkin-Huxley model (see Figure 6.3a), the presence of the calcium current (see Figure 6.3b) is characterized by three hallmarks: A) spike latency (the burst initiates with a delay with respect to the onset of the stimulation); B) plateau oscillations (spike train oscillations are generated at higher voltage than the hyperpolarized state); C) after-depolarization potential, or ADP, (the burst terminates with a small depolarization). Such behavior is typical for neurons with sufficiently strong calcium currents. See for instance: spike latency (Rekling and Feldman, 1997; Molineux et al., 2005), plateau oscillations (Beurrier et al., 1999), ADPs (Azouz et al., 1996; Chen and Yaari, 2008). See Sections 1.4.2. In the following we analyze and explain the origin of this behavior mathematically, relying on reduced models.

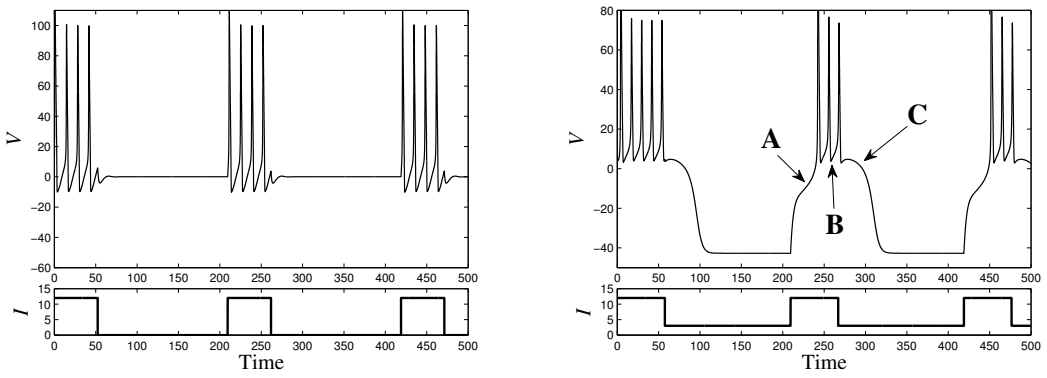

(a) I_{Ca} off (b) I_{Ca} on

FIGURE 6.3: Exogenous bursting in the Hodgkin-Huxley model (6.4) with and without calcium current.

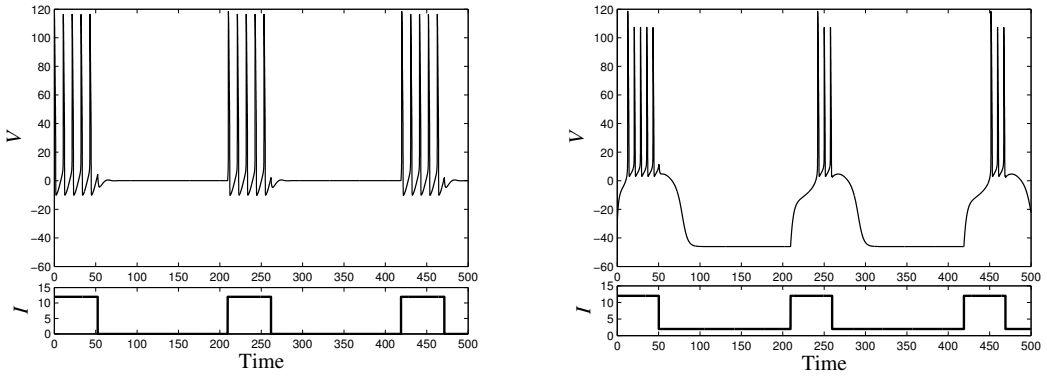

(a) I_{Ca} off (b) I_{Ca} on

FIGURE 6.4: Exogenous bursting in the reduced Hodgkin-Huxley model with and without calcium current.

6.2.1 Planar reduction

The original Hodgkin-Huxley model can be reduced in a standard way to a two dimensional system by: i) assuming an instantaneous sodium activation, $m \equiv m_\infty(V)$, where $m_\infty(V) = \alpha_m(V)/(\alpha_m(V) + \beta_m(V))$; ii) exploiting the approximate linear relation, originally proposed in (FitzHugh, 1961), $h + sn = c$, with $s, c \simeq 1$. Applying the same reduction to (6.4) with parameters as above we obtain the planar system

$$\begin{aligned} \dot{V} &= I - \bar{g}_K n^4 (V - V_K) - \bar{g}_{Na} m_\infty(V)^3 (0.89 - 1.1n)(V - V_{Na}) - g_l(V - V_l) \\ &\quad -\bar{g}_{Ca} n^3 (V - V_{Ca}) + I_{pump} \\ \dot{n} &= \alpha_n(V)(1 - n) - \beta_n(V) n \end{aligned} \tag{6.5}$$

exhibiting the same qualitative behavior as the full model, as depicted in Figure 6.4.

6.2.2 Phase portrait analysis

The beauty of planar reductions is that they permit to understand complex phenomena through phase-portrait analysis. In what follows, we define the "nullcline" associated to a variable x, with $x = V, n$, as the set $\{(V, n) \in \mathbb{R}^2 : \dot{x} = 0\}$.

Figure 6.5 (left) depicts the phase-portrait of the reduced Hodgkin-Huxley model. This phase portrait and the associated reduced dynamics are well studied in the literature. See (FitzHugh, 1961) for FitzHugh paper, and (Ermentrout and Terman, 2010, Section 3.6) and (Izhikevich, 2007, Section 5.2) for a recent discussion and more references. We recall them for comparison purposes only. The resting state is a stable focus, lying near the minimum of the V-nullcline, which exhibits the familiar N-shape. When the stimulation is turned on, this fixed point loses stability in a subcritical Andronov-Hopf bifurcation, as discussed in Section 6.2.3 through bifurcation analysis, and the trajectory rapidly converges to the periodic spiking limit cycle attractor. As the stimulation is turned off, the resting state becomes again globally stable, and the burst terminates with small subthreshold oscillations (cf. Figure 6.4 (a)).

In the presence of the calcium current the phase-portrait changes drastically, as in Figure 6.5 (right). In the "stimulation off" configuration, the resting state is a stable node lying on the far left of the phase-plane. The V-nullcline exhibits an original "hourglass" shape. Its left branch is stable and guides the relaxation toward the resting state after a spike has been generated. In this phase $\dot{V}$ changes sign from positive to negative approximately at the funnel of the hourglass, corresponding to the ADP apex. The right branch is unstable and its two intersections with the n-nullcline are a saddle and an unstable focus. When the stimulation is turned on, the V-nullcline breaks up in two branches. The upper one exhibits the familiar N-shape and contains an unstable focus surrounded by a stable limit cycle. Around this branch the dynamics is basically equivalent to that of the original Hodgkin-Huxley model. Note that a comparison between Figure 6.5 (b) and (d) of the position of, respectively, the resting state and the spiking limit cycle explains the presence of plateau oscillations. The lower branch of the V-nullcline lies now below the n-nullcline, and no more fixed points are present in this region. While converging toward the spiking limit cycle attractor, the trajectory, originally at rest, travels in the small region between the two nullclines where the vector field is small. As a consequence, the first spike is fired with a latency with respect to the onset of the stimulation, as observed in Figures 6.3 and 6.4 in the presence of the calcium current.

6.2.3 Bifurcation analysis

We can shed more light on the transition mechanism between the stimulation-on and off configurations by computing the bifurcation diagram of (6.5) with I as the bifurcation parameter, as depicted in Figure 6.6. We use XPPAUT (Ermentrout, 2002, 2004) for this numerical analysis. In both the I_{Ca}-on and off configurations we draw the bifurcation diagram only for small I, corresponding to the hyperpolarized-spike transition. In both cases the stable limit cycle disappears for higher values of I in a supercritical Andronov-Hopf bifurcation, which leads to a stable depolarized, *i.e.* high-voltage, state.

Figure 6.6 (left) illustrates the bifurcation diagram of the original Hodgkin-Huxley model. As anticipated, for $I < I_{AH}$ the unique fixed point is a stable focus that loses stability at $I = I_{AH}$ in a subcritical Andronov-Hopf bifurcation. At this bifurcation the trajectory converges to the stable spiking limit cycle. When I is lowered again below I_{SNLC}, the spiking limit cycle disappears in a saddle-node of limit cycles, the unstable one (not drawn) being born from the subcritical Andronov-Hopf bifurcation, and the trajectory relaxes back to rest.

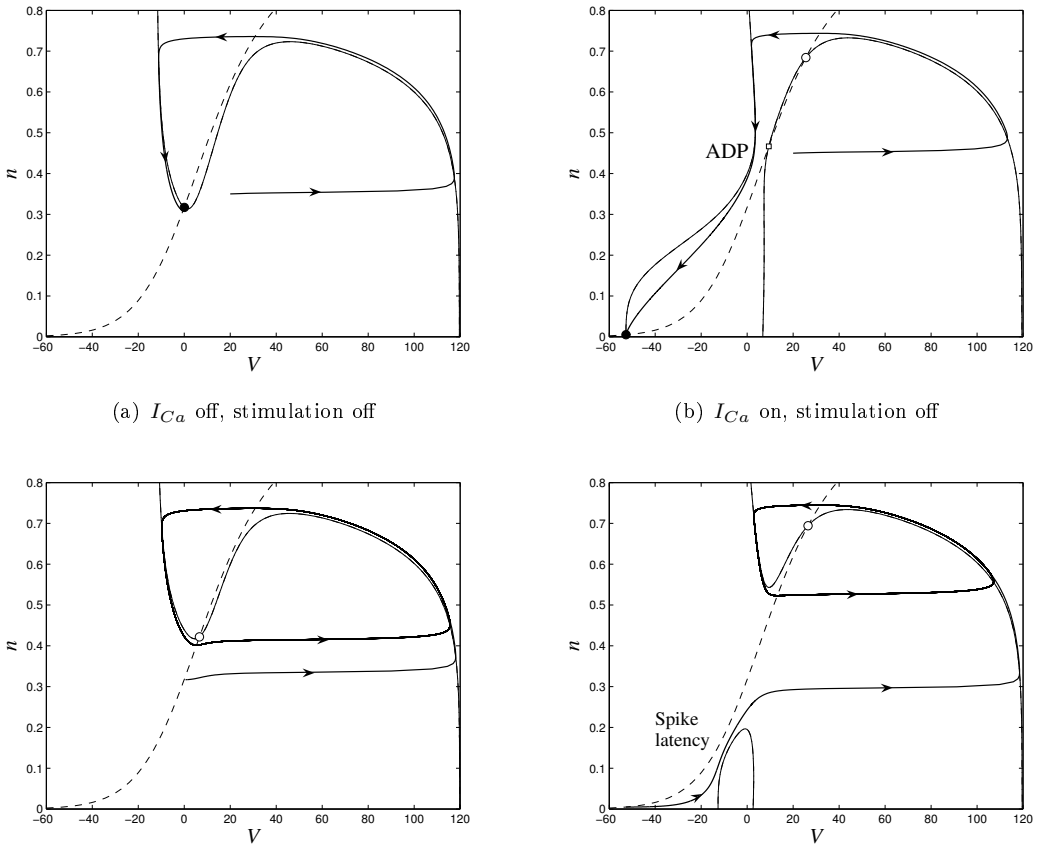

(a) I_{Ca} off, stimulation off

(b) I_{Ca} on, stimulation off

(c) I_{Ca} off, stimulation on

(d) I_{Ca} on, stimulation on

FIGURE 6.5: Phase portraits of the reduce Hodgkin-Huxley model with and without calcium current. The V-nullcline is drawn as a solid thin line, the n-nullcline as a dashed thin line. Trajectories are drawn as solid oriented lines. Black circles denote stable focus, black squares stable nodes, white circles unstable focus, and white square saddle points.

Figure 6.6 (right) illustrates the bifurcation diagram of the calcium-gated Hodgkin-Huxely model. For $I < I_{SN}$ there are a stable node (lower branch), a saddle (central branch), and an unstable focus (upper branch), like in Figure 6.5 (b). The node and the saddle coalesce in a supercritical fold bifurcation at $I = I_{SN}$, and disappear for $I > I_{SN}$ letting the trajectory converge toward the stable limit cycle. The spike latency observed in the I_{Ca}-on configuration unmasks the ghost of this bifurcation, when we expect the lower branch of V-nullcline in Figure 6.5 (d) be tangent to the n-nullcline, as depicted in Figure 6.7. The stable limit cycle disappears in a saddle homoclinic bifurcation as I diminishes below I_{SH}, which lets the trajectory relax back to the hyperpolarized state. Note that this bifurcation diagram is qualitatively identical to that of the detailed computational model of dopaminergic neuron derived in (Drion et al., 2011a).

In the next section we provide further mathematical details about the mechanism underlying the homoclinic bifurcation exhibited by the calcium-gated Hodgkin-Huxley model.

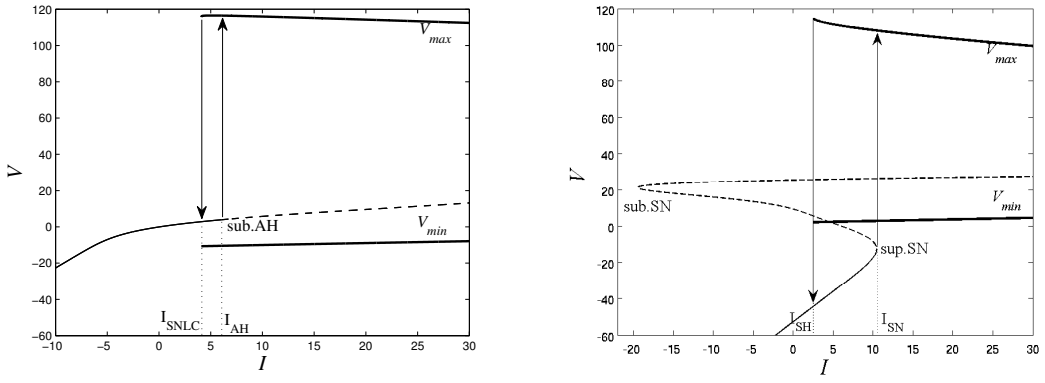

(a) I_{Ca} off (b) I_{Ca} on

FIGURE 6.6: One parameter bifurcation diagram of the reduced Hodgkin-Huxley model with and without calcium current. Thin solid lines represents stable fixed points, while dashed lines unstable fixed points or saddle points. The thick lines labeled V_{min} and V_{max} represent, respectively, the minimum and the maximum voltage of limit cycles. (a): Hodgkin-Huxley model. (b): calcium-gated Hodgkin-Huxley model. I_x, with $x = SNLC, AH, SH, SN$, denotes the value of the input current for which the system undergoes the bifurcation x. See the text for more details.

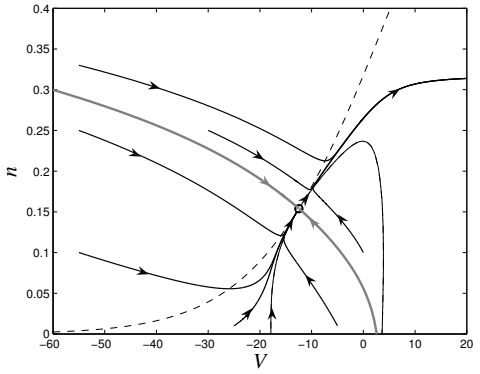

FIGURE 6.7: Saddle-node in the reduced Hodgkin-Huxley model with calcium current for $I \sim I_{SN}$. The gray thick trajectory depict the stable manifold of the saddle-node.

6.3 Calcium gated transcritical and saddle-homoclinic bifurcation

As highlighted in Figure 6.5, the sharp time scale separation

$$\left|\frac{dV}{dt}\right| \gg \left|\frac{dn}{dt}\right|$$

between V and n lets the trajectory spend most of the time near the attractive branches of the V-nullcline. The shape of this set is thus crucial in determining the behavior of the associated dynamics.

In this section, we first provide a qualitative description of the shape of the V-nullcline. We do this based on the existence of an algebraic bifurcation in the defining equation that is associated

to a transcritical bifurcation of the fast V-dynamics. We then exploit this analysis to derive rigorously the mechanisms underlying the homoclinic bifurcation discussed in Section 6.2.3.

6.3.1 Transcritical bifurcation of the fast dynamics

A graphical comparison of Figure 6.8 (a) and (b) suggests that, by the differentiability of $\dot{V}$ with respect to I and the implicit function theorem (Lee, 2006), there must exist a critical value $I_{tc} \in (2.4, 2.46)$ of the input current for which the V-nullcline has a self-intersection. Let $f_V(V, n, I)$ be the voltage dynamics of the reduced model (6.5) in the presence of calcium currents, that is

$$f_V(V, n, I) := \dot{V}\Big|_{I_{Ca}\text{-on}} \quad , \tag{6.6}$$

where $\dot{V}$ is defined in (6.5) and all the other parameters are unchanged. We claim that there exists $(V_{tc}, n_{tc}) \in \mathbb{R}^2$, such that

$$f_V(V_{tc}, n_{tc}, I_{tc}) = 0 \tag{6.7a}$$

$$\frac{\partial f_V}{\partial V}(V_{tc}, n_{tc}, I_{tc}) = 0 \tag{6.7b}$$

$$\frac{\partial f_V}{\partial n}(V_{tc}, n_{tc}, I_{tc}) = 0 \tag{6.7c}$$

$$\begin{vmatrix} \frac{\partial^2 f_V}{\partial V^2}(V_{tc}, n_{tc}, I_{tc}) & \frac{\partial^2 f_V}{\partial V \partial n}(V_{tc}, n_{tc}, I_{tc}) \\ \frac{\partial^2 f_V}{\partial V \partial n}(V_{tc}, n_{tc}, I_{tc}) & \frac{\partial^2 f_V}{\partial n^2}(V_{tc}, n_{tc}, I_{tc}) \end{vmatrix} < 0 \tag{6.7d}$$

$$\frac{\partial^2 f_V}{\partial V^2}(V_{tc}, n_{tc}, I_{tc}) \neq 0, \tag{6.7e}$$

describing a non-degenerate (transversal) self-intersection (Seydel, 2010, Section 5.5.2, Th. 5.7) of the V-nullcline at (V_{tc}, n_{tc}), and satisfying the additional condition that both intersecting branches are not parallel to the V axis, as implied by Condition (6.7e). Condition (6.7a) is the V-nullcline equation. Noticing that $\frac{\partial f_V}{\partial n}$ and $\frac{\partial f_V}{\partial V}$ do not depend on I, conditions (6.7b) and (6.7c) follows by the fact that, as $I < I_{tc}$ varies, as in Figure 6.8(a), the right and left extrema of, respectively, the left and right branches of the V-nullcline lie, by definition, on the line $\frac{\partial f_V}{\partial n} = 0$, and, similarly, as $I > I_{tc}$ varies, as in Figure 6.8(b), the minimum and the maximum of, respectively, the upper and lower branches of the V-nullcline lie, by definition, on the line $\frac{\partial f_V}{\partial V} = 0$. Since at the intersection the four extrema coincide, conditions (6.7b) and (6.7c) follow. We stress that (6.7b) and (6.7c) define the point (V_{tc}, n_{tc}) in a unique way as the intersection of two planar lines (cf. Figure 6.8 (a)). Conditions (6.7d) and (6.7e) are generic and can be easily verified numerically.

In the singular limit $\dot{n} = 0$, the self intersection described by conditions (6.7) corresponds to a transcritical bifurcation (Strogatz, 2001) of the voltage dynamics, with n as the bifurcation parameter. That is, as sketched in Figure 6.9, for $I = I_{tc}$, the two intersecting branches exchange their stability at $n = n_{tc}$. More precisely, the two branches lying in the region on the left of the line $\frac{\partial \dot{V}}{\partial V} = 0$ are stable, since there $\frac{\partial \dot{V}}{\partial V} < 0$. Conversely, the two branches on the right of the line $\frac{\partial \dot{V}}{\partial V} = 0$ are unstable. This bifurcation is absent in the reduced Hodgkin-Huxley equation without calcium current and constitutes the mathematical signature of the new reduced model.

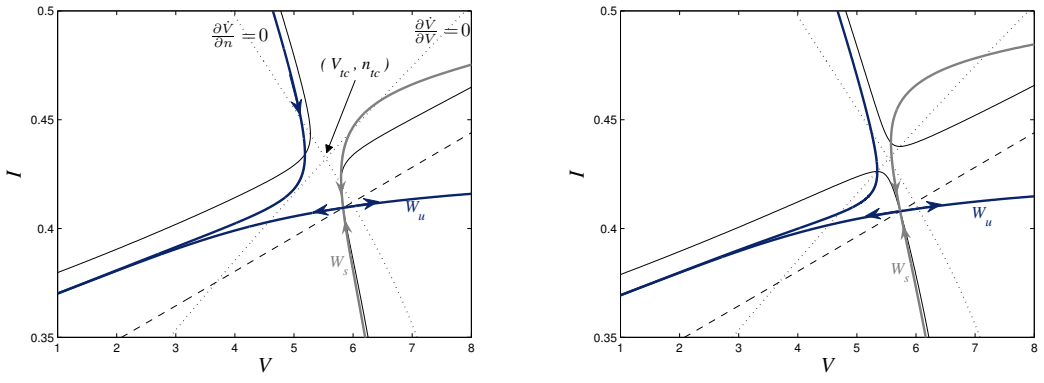

(a) $I = 2.4$

(b) $I = 2.46$

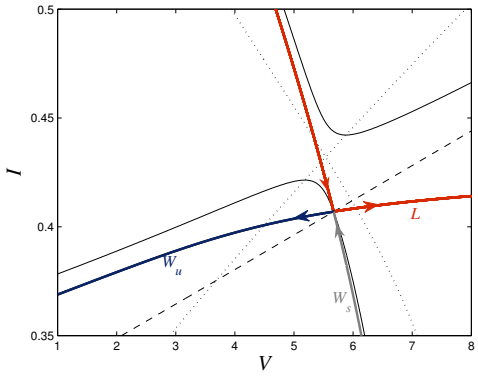

(c) $I = I_{SH} \sim 2.497$

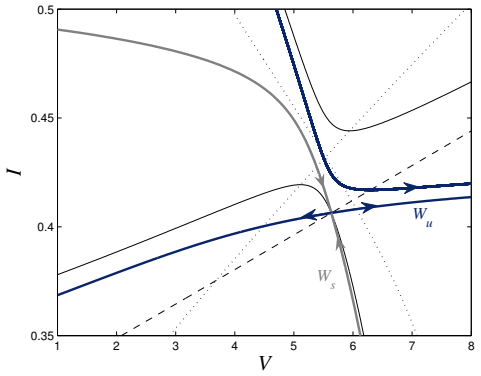

(d) $I = 2.52$

FIGURE 6.8: Phase portrait in the I_{Ca}-on configuration for different values of the input current. The V-nullcline is drawn as a solid thin line, the n-nullcline as a dashed thin line. W_s denotes the stable manifold of the saddle point, and W_u its unstable manifold. L denotes a saddle-homoclinic trajectory.

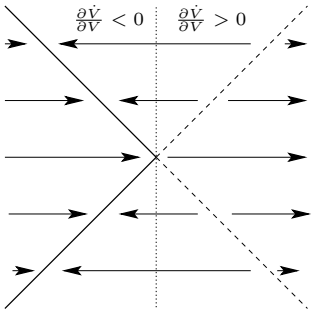

FIGURE 6.9: Sketch of the voltage dynamics of (6.5) for $I = I_{tc}$ near the V-nullcline self-intersection in the singular limit $\dot{n} = 0$. Thick lines are stable fixed points, dashed lines unstable. The dotted line is the locus $\frac{\partial \dot{V}}{\partial V} = 0$. Arrows delineate the sign of $\dot{V}$ in the different regions. The intersection point is a degenerate singular point of the voltage dynamics, corresponding to a transcritical bifurcation.

6.3.2 A normal form lemma

In this technical section we compute a normal form of (6.5) associated to conditions (6.7).

Let

$$\epsilon g(V,n) := \dot{n}, \tag{6.8}$$

where $\dot{n}$ is defined in (6.5), and

$$g_0 := g(V_{tc}, n_{tc}), \tag{6.9}$$

where V_{tc} and n_{tc} satisfy the defining conditions (6.7b)-(6.7b). The form (6.8) is a rescaling of the recovery variable dynamics to highlight the timescale separation between V and n. The following lemma is an application of (Krupa and Szmolyan, 2001b, Lemma 2.1) to the reduced calcium-gated Hodgkin-Huxley model.

Lemma 6.1. *Suppose that $g_0 < 0$. Then there exists an affine change of coordinates and a rescaling of ϵ and I that transform the dynamical system*

$$\dot{V} = f_V(V,n,I) \tag{6.10a}$$
$$\dot{n} = \epsilon g(V,n), \tag{6.10b}$$

where f_V and g are respectively defined in (6.6) and (6.8), into the following normal form

$$\dot{v} = v^2 - w^2 + I + h_1(v,w,\epsilon) \tag{6.11a}$$
$$\dot{w} = \epsilon(-1 + h_2(v,w,\epsilon)), \tag{6.11b}$$

where $h_1(v,w,\epsilon) = O(v^3, v^2w, vw^2, w^3, \epsilon v, \epsilon w, \epsilon^2)$ and $h_2(v,w,\epsilon) = O(v,w,\epsilon)$.

Proof Let $\alpha := \frac{1}{2}\frac{\partial^2 f_V}{\partial V^2}(V_{tc}, n_{tc}, I_{tc})$, $\beta := \frac{1}{2}\frac{\partial^2 f_V}{\partial V \partial n}(V_{tc}, n_{tc}, I_{tc})$, $\gamma := \frac{1}{2}\frac{\partial^2 f_V}{\partial n^2}(V_{tc}, n_{tc}, I_{tc})$, and $\lambda := \frac{-\beta}{\sqrt{\beta^2 - \gamma\alpha}}$. From (6.7) and (Krupa and Szmolyan, 2001b, Lemma 2.1), it follows that, for $I = I_{tc}$, the affine change of variable $v = \alpha(V - V_{tc}) + \beta(n - n_{tc})$, $w = \sqrt{\beta^2 - \gamma\alpha}(n - n_{tc})$, transforms (6.10), after a suitable rescaling of ϵ, into the equation

$$\dot{v} = v^2 - w^2 + \lambda\epsilon + h_1(v,w,\epsilon)$$
$$\dot{w} = \epsilon(-1 + h_2(v,w,\epsilon)).$$

Noticing that f_V is affine in the input current, in the case $I \neq I_{tc}$ the extra term $\alpha(I - I_{tc})$ must be added to $\dot{v}$. The result follows by defining the rescaled input current $\tilde{I} := \lambda\epsilon + \alpha(I - I_{tc})$. □

For the dynamical system (6.11) with $I = 0$ the self intersection of the V-nullcline discussed in Section 6.3.1 becomes evident, with the two intersecting branches given by $w = \pm\sqrt{v^2}$.

6.3.3 Singularly perturbed saddle-homoclinic bifurcation

Figures 6.8 (b),(c),(d) provide a graphical evidence of the calcium-gated homoclinic bifurcation highlighted in Section 6.2.3 through numerical bifurcation analysis. In order to prove the existence of this bifurcation rigorously, we rely on the normal form introduced in Lemma 6.1 and exploit the timescale separation between v and w through geometrical singular perturbations theory (GSPT).

Let us briefly recall some basic of GSPT. The interested reader will find in (Jones, 1995) an excellent introduction to the topic, and in (Krupa and Szmolyan, 2001c,b,a) some recent extensions on which we rely for the forthcoming analysis.

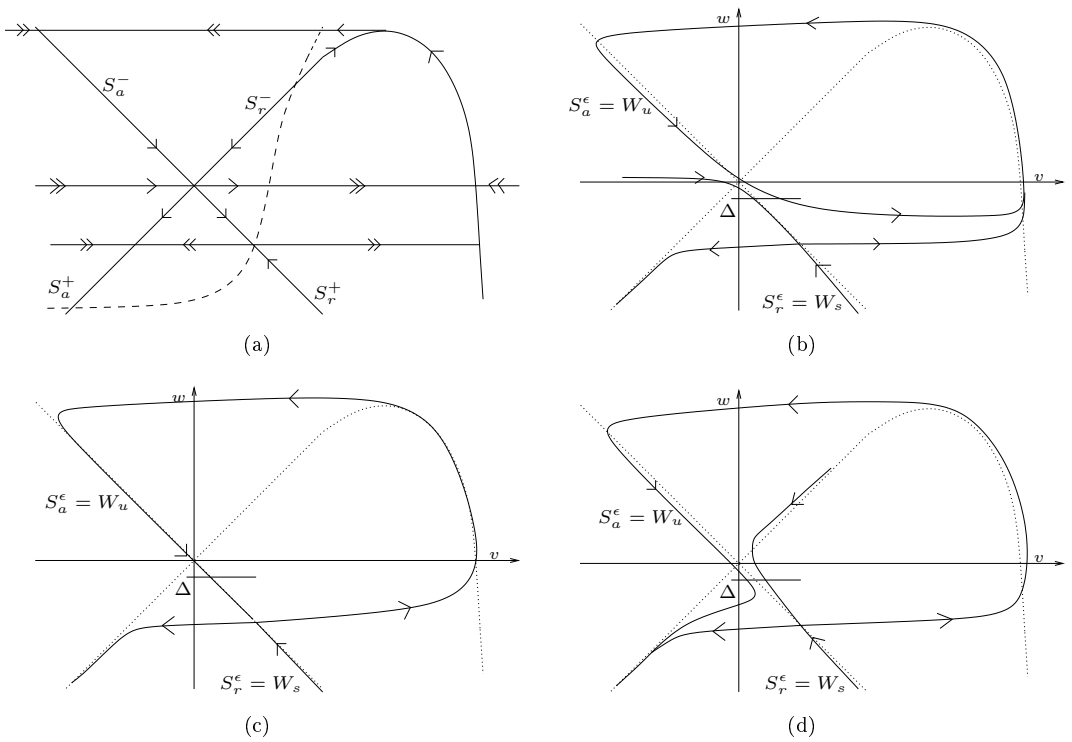

FIGURE 6.10: Phase-portrait of (6.11) for different values of ϵ and I. (a): fast-slow dynamics of (6.11) for $\epsilon = I = 0$. (b): Continuation of the slow attractive S_a^ϵ and repelling S_r^ϵ manifolds for $\epsilon > 0$ and $I > I_c(\sqrt{\epsilon})$, where $I_c(\sqrt{\epsilon})$ is defined as in Theorem 6.2. (c): Continuation of S_a^ϵ and S_r^ϵ for $\epsilon > 0$ and $I = I_c(\sqrt{\epsilon})$. (d): Continuation of S_a^ϵ and S_r^ϵ for $\epsilon > 0$ and $I < I_c(\sqrt{\epsilon})$.

The time rescaling $t := \epsilon\tau$ transforms (6.11) into the equivalent system

$$\epsilon \dot{v} = v^2 - w^2 + I + h_1(v, w, \epsilon) \tag{6.12a}$$
$$\dot{w} = (-1 + h_2(v, w, \epsilon)), \tag{6.12b}$$

which describes the dynamics (6.5) in the slow timescale τ. In the limit $\epsilon = 0$, commonly referred to as the *singular limit*, one obtains from (6.11) and (6.12) the two new dynamical systems

$$0 = v^2 - w^2 + I + h_1(v, w, \epsilon) \tag{6.13a}$$
$$\dot{w} = (-1 + h_2(v, w, \epsilon)), \tag{6.13b}$$

called the *reduced problem* and evolving on the slow timescale τ, and

$$\dot{v} = v^2 - w^2 + I + h_1(v, w, \epsilon) \tag{6.14a}$$
$$\dot{w} = 0, \tag{6.14b}$$

called the *layer problem* and evolving on the fast timescale t. Figure 6.10 (a) depicts the fast-slow dynamics associated to (6.13)-(6.14). The main idea behind GSPT is to combine the analysis of the reduced and layer problems to derive conclusion on the behavior of the associated non-singular system, *i.e.* with $\epsilon > 0$.

The reduced problem (6.13) is a dynamical system on the set $S_0 := \{(v, w) \in \mathbb{R}^2 : v^2 - w^2 + I + h_1(v, w, \epsilon) = 0\}$, usually called the *critical manifold*. The points in S_0 are indeed

critical points of the layer problem (6.14). More precisely, portions of S_0 on which $\frac{\partial \dot{V}}{\partial V}$ is non-vanishing are normally hyperbolic invariant manifolds of equilibria of the layer problem, whose stability is determined by the sign of $\frac{\partial \dot{V}}{\partial V}$. Conversely, points in S_0 where $\frac{\partial \dot{V}}{\partial V} = 0$ constitute degenerate equilibria. In particular, the layer problem (6.14) exhibits, for $I = 0$, two degenerate fixed points. As depicted in Figure 6.10 (a), they are given by the self-intersection of the V-nullcline, corresponding to a transcritical singularity, and and by the fold singularity at the right knee of the upper branch of the V-nullcline.

The basic result of GSPT, firstly derived by Fennichel (Fenichel, 1979), is that, for ϵ sufficiently small, non-degenerate portions of S_0 persist as nearby normally hyperbolic locally invariant manifolds S_ϵ of (6.10). More precisely, the *slow manifold* S_ϵ lies in a neighborhood of S_0 of radius $O(\epsilon)$. The dynamics on S_ϵ is a small perturbation of the reduced problem (6.13). We point out that S_ϵ may not be unique, but is determined only up to $O(e^{c/\epsilon})$, for some $c > 0$. That is, two different choices of S_ϵ are exponentially close (in ϵ) one to the other. Since the presented results are independent of the particular S_ϵ considered, we let this choice be arbitrary. The trajectories of the layer problems perturb to a stable and an unstable invariant foliations with basis S_ϵ.

The analysis near degenerates point is more delicate. Only recently some works have treated this problem for different types of degenerate singularities (Krupa and Szmolyan, 2001c,b,a). Figure 6.10 (b),(c),(d) sketch the extension of the slow manifold S_ϵ after the fold point, and the three possible way in which S_ϵ can continue after the trascritical singularity, depending on the injected current.

The result depicted in Figure 6.10 relies on the following theorem, adapted from (Krupa and Szmolyan, 2001b).

Let $\Delta := \{(v, w) \in \mathbb{R}^2 : \ v_- \leq v \leq v_+, \ w = \rho\}$, be the section depicted in Figure 6.10, where $\rho < 0$ and $|\rho|$ is sufficiently small, and v_-, v_+ are such that $\Delta \cap S_r^+ \neq \emptyset$. For a given $\epsilon > 0$, let $q_{a,\epsilon} := \Delta \cap S_a^\epsilon$ and $q_{r,\epsilon} := \Delta \cap S_r^\epsilon$ be the intersections, whenever they exist, of respectively the locally attractive and locally repelling invariant submanifolds S_a^ϵ and S_r^ϵ with the section Δ. The following theorem reformulates in a compact way the discussion contained in Remark 2.2 and Section 3 of (Krupa and Szmolyan, 2001b)[4] for systems with inputs of the form (6.11).

Theorem 6.2 (Krupa and Szmolyan (2001b))**.** *Consider the system (6.11). Then there exists $\epsilon_0 > 0$ and a smooth function $I_c(\sqrt{\epsilon})$, defined on $[0, \epsilon_0]$ and satisfying $I_c(0) = 0$, such that, for all $\epsilon \in (0, \epsilon_0]$, the following assertions hold*

1. *$q_{a,\epsilon} = q_{r,\epsilon}$ if and only if $I = I_c(\sqrt{\epsilon})$*
2. *there exists an open interval $A \ni I_c(\sqrt{\epsilon})$, such that, for all $I \in A$, it holds that $\Delta \cap S_a^\epsilon \neq \emptyset$, $\Delta \cap S_r^\epsilon \neq \emptyset$, and*

$$\frac{\partial}{\partial I}\left(q_{a,\epsilon} - q_{r,\epsilon}\right) > 0.$$

Figure 6.10 illustrates this result.

Remark 6.3. The function $I_c(\sqrt{\epsilon})$ is related to the function $\lambda_c(\sqrt{\epsilon})$ defined in (Krupa and Szmolyan, 2001b, Remark 2.2) by $I_c(\sqrt{\epsilon}) := \epsilon\lambda_c(\sqrt{\epsilon})$. Similarly, for $\epsilon > 0$, the parameter I appearing in Theorem 6.2 is just the re-scaling $I = \epsilon\lambda$ of the parameter λ appearing in (Krupa and Szmolyan, 2001b, Remark 2.2 and Sections 3).

Theorem 6.2 can readily be applied to prove the existence of a saddle-homoclinic bifurcation for the dynamics (6.11). By Lemma 6.1, the same result then holds for the reduced calcium-gated Hodgkin-Huxley model (6.5).

[4] The author is thankful to Prof. Szmolyan for his useful comments in this regard.

Firstly, note that, as depicted in Figure 6.10, the slow repelling one-dimensional manifold S_r^ϵ coincides with the stable manifold of the saddle point W_s. To see this, assume that the saddle point belongs to S_r^ϵ. Then for all initial condition in S_r^ϵ the trajectory converges to the saddle point, that is $S_r^\epsilon \subset W_s$. Since from the stable manifold theorem (Guckenheimer and Holmes, 2002, Theorem 1.3.2) W_s is also a one dimensional submanifold, $W_s = S_r^\epsilon$. It remains to show that the saddle point belongs to S_r^ϵ. Suppose the converse is true. Then for $\epsilon > 0$, the slow manifold S_r^ϵ passes in a neighborhood U of the saddle of radius $O(\epsilon)$ and is roughly parallel to the repelling branch of the critical manifold S_0. Pick ϵ sufficiently small in such a way that: i) no other critical points but the saddle lie in U; ii) the unstable invariant foliation, and thus the unstable manifold of the saddle W_u, are approximately horizontal in U. Under these conditions S_r^ϵ and W_u must intersect somewhere in U. Since this intersection is an invariant point, it is a fixed point, which contradicts the fact that no other fixed points but the saddle lie in U.

We also claim that S_a^ϵ can be chosen in such a way that $S_a^\epsilon = W_u$, as depicted in Figure 6.10. Consider the branch of W_u leaving on the left of the saddle. For ϵ sufficiently small, this branch follows the unstable invariant foliation toward the right attractive branch of the critical manifold. There, from standard GSPT arguments, it slides up toward the fold point at the right knee. From (Krupa and Szmolyan, 2001a, Theorem 2.1), it follows that W_u continues after the fold point, approximately following the associated critical fiber[5], and arrives in the vicinity of the left attractive branch of the critical manifold. Again, by standard GSPT arguments, W_u continues there as a perturbation S_a^ϵ of S_0, which proves the claim.

At the light of this analysis the existence of the homoclinic bifurcation is a direct corollary of Theorem 6.2. For $I > I_c(\sqrt{\epsilon})$, the unstable manifold of the saddle W_u continues after the transcritical singularity on the right of W_s, and spirals toward an exponentially stable limit cycle, whose existence can be proved with similar GSPT arguments (see for instance (Krupa and Szmolyan, 2001c)). This situation is the one depicted in Figure 6.8 (d) and Figure 6.10 (b). As I tends to $I_c(\sqrt{\epsilon})$, W_u tends to W_s. At $I = I_c(\sqrt{\epsilon})$, W_u extends after the transcritical point to W_s, forming the saddle-homoclinic trajectory, as depicted in Figure 6.8 (c) and Figure 6.10 (c). For $I < I_c(\sqrt{\epsilon})$, the unstable manifold W_u continues after the transcritical singularity on the left of W_s, toward the stable node. See Figure 6.8 (a) and (b) and Figure 6.10 (d).

6.4 A new reduced hybrid model of calcium-gated neuronal dynamics

Inspired by the normal form (6.11) computed in Lemma 6.1, and in the same spirit of the Izhikevich reduction of neuronal dynamics to simple hybrid models (Izhikevich, 2010), we consider the following hybrid dynamical system as a simple representation of the calcium-gated Hodgkin-Huxley model

$$\dot{v} = v^2 - w^2 + I \qquad \text{if } v \geq v_{th}, \text{ then} \tag{6.15a}$$

$$\dot{w} = \epsilon(av - w + w_0) \qquad v \leftarrow c,\ u \leftarrow d, \tag{6.15b}$$

where $a, c, d, w_0, I, v_{th} \in \mathbb{R}$ are parameters. Hybrid neuronal models are intended to capture the neuron subthreshold dynamics, in particular the bifurcation mechanism involved in the resting-spiking transition. The spike generation mechanism is accounted for by the hybrid reset mechanism: when v reaches a high threshold v_{th}, both v and w are reseted to fixed values c and d respectively. This reset mechanism has essentially the same role of the return

[5] The critical fiber is defined as the trajectory of the layer problem passing by the fold point, cf. Figure 6.10

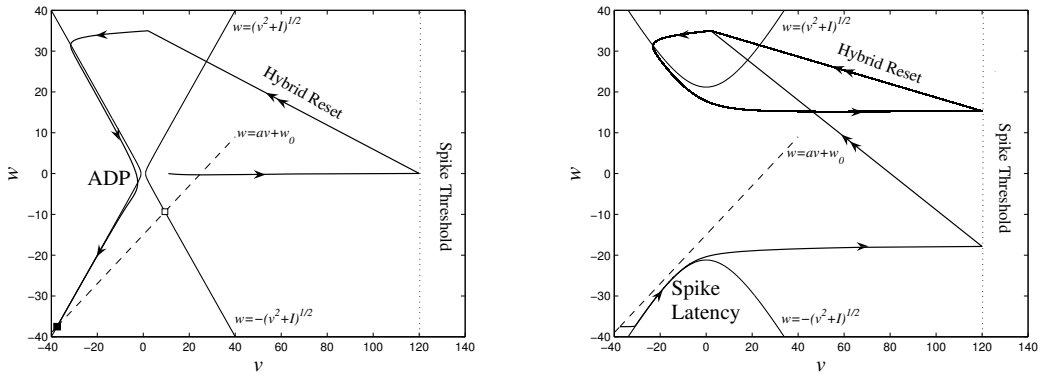

(a) $I = -1$ (b) $I = 450$

FIGURE 6.11: Simple model (6.15) with $a = 0.6, c = 2, d = 35, w_0 = -15, v_{th} = 120$. exhibiting the same qualitative behavior of the calcium-gated Hodgkin-Huxley model. The legend for the phase-portrait is the same as Figure 6.5.

mechanism provided by the left attractive branch of the V-nullcline in the full model, as depicted in Figures 6.5 and 6.10, and discussed in Section 6.3.3 in terms of GSPT.

As illustrated by Figure 6.11, the hybrid dynamics (6.15) captures the qualitative properties of the subthreshold dynamics in the reduced calcium-gated Hodgkin-Huxley model (Cf. Figure 6.5). As discussed in the Sections 6.2.2 and 6.3, due to the time scale separation between v and w, the shape of the v-nullcline plays a major role in generating the observed behavior. That is why we do not expect other hybrid neuron models with a concave v-nullcline, like the aforementioned Izhikevich model, to exhibit the same characteristics.

6.4.1 Hybrid singularly perturbed saddle-homoclinic bifurcation

The saddle-homoclinic bifurcation analysis provided in Section 6.3.3 for the reduced calcium-gated Hodgkin-Huxley model naturally extends to the hybrid dynamics (6.15). By construction indeed, if $w_0 < 0$, this model can be transformed in the normal form (6.11) derived in Lemma 6.1, and Theorem 6.2 applies directly.

Similarly to the derivation in Section 6.3.3, we can associate to (6.15) two new dynamical systems describing its singular dynamics, *i.e.* with $\epsilon = 0$, in the fast timescale t and in the slow timescale $\tau := t/\epsilon$, respectively. More precisely, the dynamics

$$0 = v^2 - w^2 + I \qquad \text{if } v \geq v_{th}, \text{ then} \tag{6.16a}$$
$$\dot{w} = av - w + w_0 \qquad v \leftarrow c,\ u \leftarrow d, \tag{6.16b}$$

and

$$\dot{v} = v^2 - w^2 + I \qquad \text{if } v \geq v_{th}, \text{ then} \tag{6.17a}$$
$$\dot{w} = 0 \qquad v \leftarrow c,\ u \leftarrow d, \tag{6.17b}$$

define, respectively, the *hybrid reduced problem* and *hybrid layer problem* associated to (6.15). Figure 6.12 (a) depicts the associated slow-fast hybrid dynamics for parameters as in Figure 6.11.

The analysis of the non-singular limit follows the same line of the analysis developed in Section 6.3.3 for the continuous time case. The only difference is that the return mechanism provided by

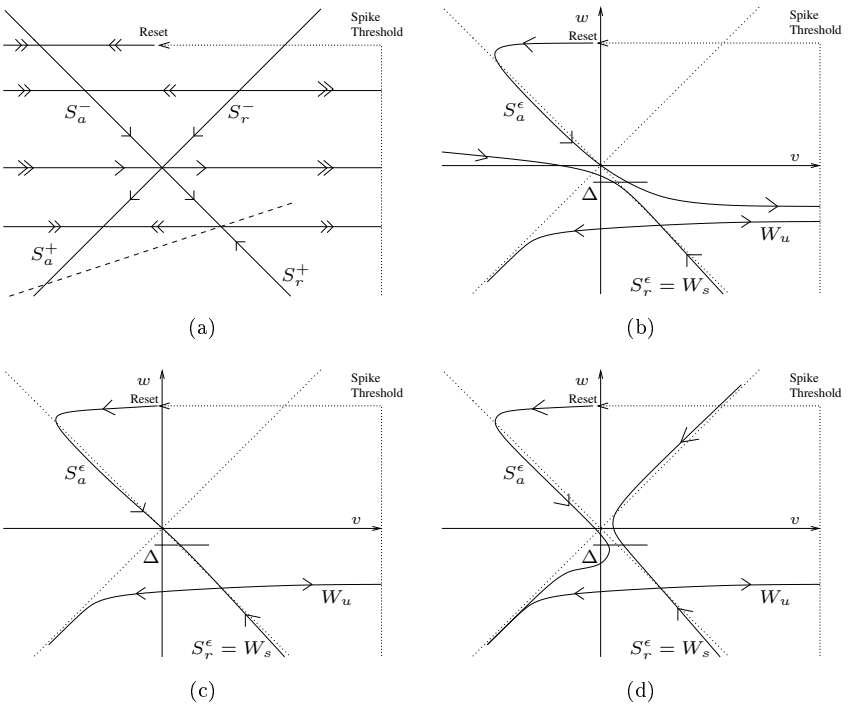

FIGURE 6.12: Phase-portrait of the hybrid dynamics (6.15) for different values of ϵ and I. (a): Fast-slow dynamics for $\epsilon = I = 0$. (b): Continuation of the slow manifolds for $\epsilon > 0$ and $I > I_c(\sqrt{\epsilon})$, where $I_c(\sqrt{\epsilon})$ is defined as in Theorem 6.2. (c): Continuation of the slow manifolds for $\epsilon > 0$ and $I = I_c(\sqrt{\epsilon})$. (d): Continuation of the slow manifolds for $\epsilon > 0$ and $I < I_c(\sqrt{\epsilon})$.

the right attractive branch of the critical manifold S_0 is replaced by the hybrid reset mechanism. The result is summarized in Figure 6.12 (b),(c),(d). The slow attractive manifold S_a^ϵ is chosen as the continuation of the trajectory starting at the reset point. In this way it also coincides with the image of the unstable manifold of the saddle W_u through the hybrid reset mechanism. As in the continuous time case, the stable manifold of the saddle W_s can be shown to coincide with the slow repelling manifold S_r^ϵ. Let $I_c(\sqrt{\epsilon})$ be defined as in Theorem 6.2. For $I > I_c(\sqrt{\epsilon})$, the unstable manifold W_u is brought by the rest mechanism on the right of W_s and directly into the hybrid limit cycle attractor, as in Figure 6.12 (b). At $I = I_c(\sqrt{\epsilon})$ the hybrid reset connects W_u and W_s, corresponding to a hybrid homoclinic bifurcation. The associated phase-portrait is shown in Figure 6.12 (c). Finally for $I < I_c(\sqrt{\epsilon})$, the unstable manifold W_u is brought back on the left of W_s, and the resting state becomes globally stable.

We stress that the existence of the hybrid homoclinic bifurcation in (6.15) is independent of the reset point (c, d), provided that the trajectory starting from it is attracted toward the left upper branch of the critical manifold, as in Figure 6.12. As discussed in Section 6.3.3, under this condition two different choices of the reset point are associated to two slow manifolds that are $O(e^{c/\epsilon})$ near, for some $c > 0$. By the result in Theorem 6.2, the two values of the critical current I_c for which the slow attractive manifold extends to the slow repelling manifold are again $O(e^{c/\epsilon})$ near. This also ensures that the value for which the hybrid homoclinic bifurcation happens is independent of the reset point, modulo variations that are $O(e^{c/\epsilon})$. The same robustness properties do not hold for other hybrid models with a concave v-nullclines. There, the existence and the critical value of a hybrid homoclinic bifurcation heavily relies on the reset point. The main reason for this is the lack in these models of an attractive singular connection between the stable and the unstable manifold of the saddle, as in Figure 6.12 (a), that can persist in the non-singular limit.

6.4.2 Hybrid modeling of calcium gated neurons

For quantitative modeling purposes we can modify (6.15) to obtain the equivalent dynamics

$$\dot{v} = v^2 + bvw - w^2 + I \qquad \text{if } v \geq v_{th}, \text{ then} \tag{6.18a}$$

$$\dot{w} = \epsilon(av - w + w_0) \qquad v \leftarrow c, \; u \leftarrow d. \tag{6.18b}$$

The extra parameter $b \in \mathbb{R}$ changes the inclination of the v-nullcline branches, similarly to the reduced Hodgkin-Huxley model in Figure 6.5, and permits to fit with more fidelity the behavior of (6.18) to that of more detailed models. In this section we illustrate this possibility by reproducing the behavior of the dopaminergic neuron model developed in (Drion et al., 2011a), and which also constitutes, as discussed in Section 1.6, the main experimental motivation for the analysis developed in this chapter. We compare the observed behavior with that of the original Izhikevich model (Izhikevich, 2010), and explain the observed phenomena through the analysis developed in Section 6.4.1.

More precisely, we focus on the generation of *robust* ADPs. By *robust* we mean that the model behavior is only slightly perturbed in biologically meaningful conditions, *i.e.* in the presence of small disturbances and parameters uncertainties and variability. Figure 6.13(top) depicts the robust pacemaking activity and ADPs generation in the detailed computational model of dopaminergic neurons (Drion et al., 2011a). A small amplitude DC current step or an alternating current of the same amplitude only slightly change the pacemaking rhythm and the ADP shape.

In order to generate a similar pacemaking activity in both the reduced model (6.18), and in the Izhikevich model, we provide them with a slower adaptation variable z modeling the variation of the intracellular calcium concentration. The adaptation variable variable z follows the linear dynamics

$$\dot{z} = -\epsilon_z z, \qquad \text{if } v \geq v_{th}, \text{ then } z \leftarrow z + d_z. \tag{6.19}$$

The term $-z$, accounting for outward calcium pumps currents, is added to the v dynamics of both the reduced models (6.18) and Izhikevich model. The dynamics equations and parameters used for the Izhikevich model can be found in Appendix A on page 154.

Figures 6.13 and 6.14 provides a comparison of the nominal and perturbed pacemaking, and of the ADPs generation mechanism in the two reduced hybrid models.

As already described in Section 6.2.2 for the calcium-gated Hodgkin-Huxley model and in Figure 6.11 for the reduced model (6.15), the voltage reaches the ADP apex approximately at the hourglass funnel of the voltage nullcline. As illustrated in Figure 6.14, the mathematical analysis in Section 6.4.1 highlights the presence in that region of an attractive normally hyperbolic manifold S_a^ϵ. This manifold attracts the trajectories and steers them through the ADP apex and toward the resting point. That is why the ADP height and shape barely depend on the chosen reset point. At the same time, the persistence to small perturbations of this invariant manifold (Hirsch et al., 1977) ensures, as required in biologically meaningful conditions, the robustness of the pacemaking and ADP generation mechanism to small inputs.

To generate ADPs in the Izhikevich model we follow (Izhikevich, 2007, Section 8.1.4) and we use the parameters provided in http://www.izhikevich.org/publications/figure1.m (see the end of the chapter for the used equations and parameters).

In the Izhikevich model, ADPs are generated when trajectories cross the v-nullcline from below. The unperturbed pacemaking activity of the Izhikevich model is strikingly similar to that of the complex computational model in Figure 6.13(top). As illustrated in Figure 6.14, the lack of any attractive structure lets, however, the ADP height and shape heavily rely on the reset

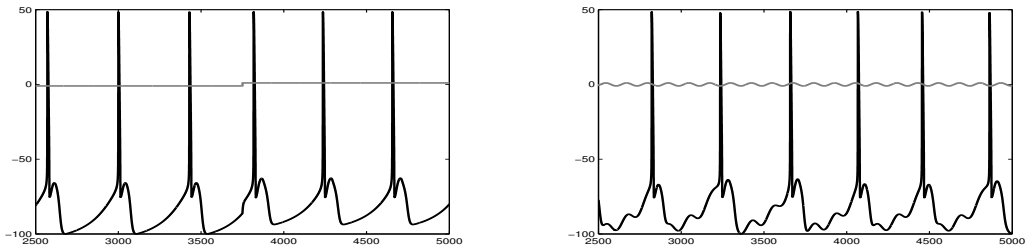

(a) Detailed model of dopaminergic neuron.

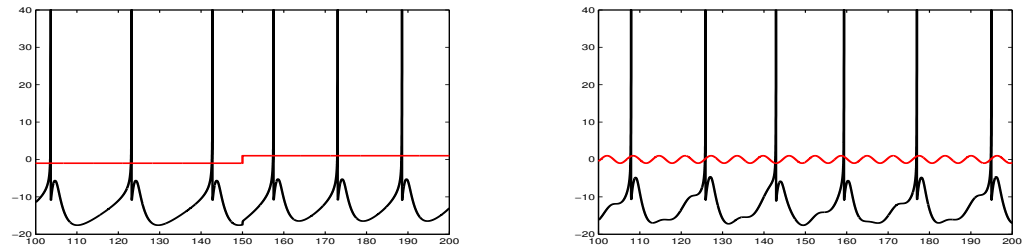

(b) Novel reduced model (6.15).

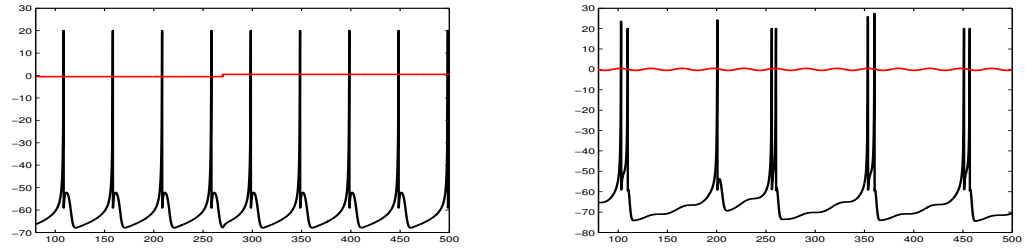

(c) Izhikevich model.

FIGURE 6.13: Nominal and perturbed pacemaking in (a) the computational model of DA nuerons (Drion et al., 2011a), (b) the new reduced hybrid model (6.15), and (c) the Izhikevich model (Izhikevich, 2010). The parameter for the novel reduced model (6.15) are: $b = -1.5, I = 100, \epsilon = 1, a = 0.25, w_0 = -5, v_{th} = 40, c = -10, d = 20, \epsilon_z = 0.1, d_z = 150$. Equations and parameters for the Izhikevich model and the computational model are provided in Appendix A on page 154.

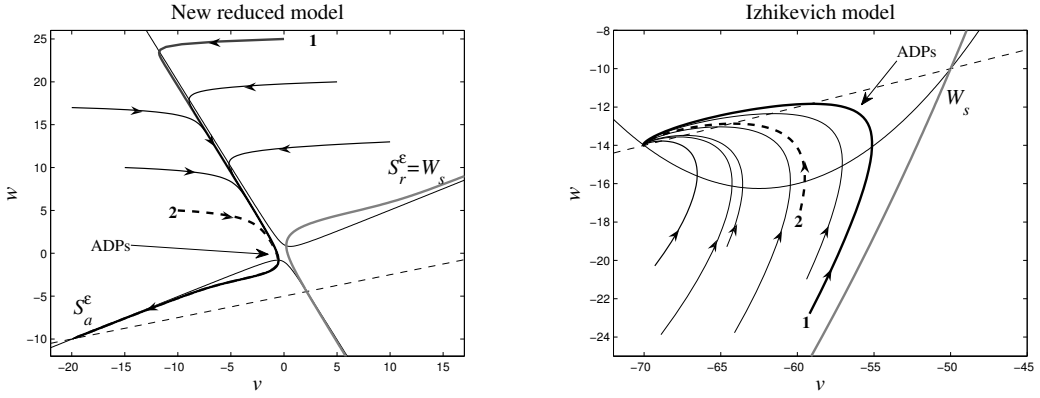

FIGURE 6.14: ADPs generation comparison in the proposed and in the Izhikevich hybrid models. Legend as in Figure 6.5. Parameters for the new reduced model (6.15) as in Figure 6.13, apart that here $I = 1$. Equations and parameters for the Izhikevich model are provided at the end of the chapter

point. When a step of DC current is applied the model barely changes the spiking pattern and ADP shape, indicating that the perturbation intensity is small. Conversely, when a sinusoidal current of the same amplitude is applied, the pace-making and ADP generation mechanisms are completely disrupted. Even if small, due to the time-varying input the reset point changes indeed at each spiking cycle and the lack of a robust attractive structure makes the spiking behavior non robust to these variations. The proximity of the stable manifold of the saddle lets even the reset point falls out of the basin of attraction of the stable fixed point, generating doublets. This behavior does not correspond to the one exhibited by the detailed computational model and is not satisfactory in biologically meaningful conditions.

In conclusion, even though in the absence of perturbations the Izhikevich model reproduces with fidelity the spiking pattern of the computational model, its lack of robustness makes it unsuitable to analyze the neuron response to exogenous inputs. Conversely, the simple model (6.15) captures the dynamical essence of the pacemaking and ADP generation mechanism of dopaminergic neurons in the normally hyperbolic invariant manifold structure associated to the the transcritical bifurcation of its voltage dynamics. That is why we propose (6.15) as a simple choice to analyze mathematically synchronization and control properties of dopaminergic neurons, and, more in general, of calcium-gated neurons.

Appendix A - Equations and parameters of Izhikevich and dopaminergic neuron models

Equations and parameters for the Izhikevich model in Figures 6.13 and 6.14

$$\begin{aligned} &\dot{v} = 0.04v^2 + 5v + 140 - w + I - z && \text{if } v \geq v_{th}, \text{ then} \\ &\dot{w} = a(bv - w) && v \leftarrow c,\ u \leftarrow u + d, \\ &\dot{z} = -a_z z && z \leftarrow z + d_z. \end{aligned}$$

where $I = 0$ for the phase-portrait analysis and ADPs comparison and $I = 5$ for the time plots, and $a = 1, b = 0.2, v_{th} = 30, c = -60, d = -21, d_z = 5, a_z = 0.1$.

Equations and parameters for the DA neuron model in Figure 6.13

$$\begin{aligned} C\dot{V} &= -\bar{g}_{Na} m^3 h (V - V_{Na}) - \bar{g}_K n^4 (V - V_K) - \bar{g}_{Ca(L)} \frac{K_{M,L}}{K_{M,L} + [Ca^{2+}]} d_L (V - V_{Ca}) \\ &\quad - g_l (V - V_l) - I_{Ca,pump,max} \left(1 + \frac{K_{M,P}}{[Ca^{2+}]}\right)^{-1} - \bar{g}_{K,Ca} \left(\frac{[Ca^{2+}]}{K_D [Ca^{2+}]}\right)^2 (V - V_K), \\ \dot{m} &= (m_\infty(V) - m)/\tau_m(V), \\ \dot{h} &= (h_\infty(V) - h)/\tau_h(V), \\ \dot{n} &= (n_\infty(V) - n)/\tau_n(V), \\ \dot{d_L} &= (d_{L\infty}(V) - d_L)/\tau_{d_L}(V), \\ [\dot{Ca^{2+}}] &= -k_1 (I_{Ca(L)} + I_{Ca,pump}) - k_2 I_{Na}, \end{aligned}$$

where $C = 10^{-3}\ \mu F/cm^2$, $V_{Na} = 50\ mV$, $V_K = -95\ mV$, $V_l = -54.3\ mV$, $V_{Ca} = 120\ mV$, $\bar{g}_{Na} = 0.16\ S/cm^2$, $\bar{g}_K = 0.024\ S/cm^2$, $g_l = 0.3\ 10^{-3}\ S/cm^2$, $\bar{g}_{Ca(L)} = 3.1\ 10^{-3}\ S/cm^2$, $\bar{g}_{K,Ca} = 5\ 10^{-3}\ S/cm^2$, $I_{Ca,pump,max} = 0.0156\ mA/cm^2$, $K_{M,P} = 0.0001\ mM$, $K_{M,L} = 0.00018\ mM$, $k_1 = 0.1375\ 10^{-3}$, $K_D = 0.4\ 10^{-3}\ mM$, $k_2 = 0.018\ 10^{-4}$.

Chapter 7

Neuronal synchrony from an input-output viewpoint[1]

Motivated by the generalization of the results in Part I to more realistic neuron models, in the present chapter we extend an input/output approach recently proposed to analyze synchronization in networks of nonlinear operators and apply this result to a network of heterogeneous Hindmarsh-Rose neurons. We also provide in this way an analytical justification of rather counter-intuitive and physiologically meaningful synchronization phenomena observed in simulation.

As already discussed, synchronization in a network of agents can be interpreted as the appearance of a correlated behavior among its constituting dynamical systems. It finds applications in many physical, engineering, medical, and biological fields. The problem of finding sufficient conditions under which synchronization can be guaranteed is particularly challenging when the components of the network are heterogeneous. Nonetheless, such a heterogeneity is common in many biological applications, in particular in the study of neuronal synchronization. A similar problem is cast in Chapter 3 for the particular case of periodically spiking neurons, modeled as a simple complex oscillators.

Recently, a promising method has been developed (Scardovi et al., 2010) to provide explicit conditions on the agents' dynamics and on their interconnection topology for a network of identical systems to synchronize. This approach relies on the input/output properties of the agents involved, and thus requires little knowledge on the individual dynamics. This feature is of particular interest for neuronal synchronization, in which parameter and identification are often hard to achieve in a precise manner. However, that result imposes for the time-being that all agents composing the network have the same dynamics, which constitutes a restrictive constraint in view of the typical heterogeneities between neuronal cells. The aim of this chapter is therefore to extend this method to make it cope some heterogeneity between the agents and to apply it to a population of heterogeneous Hindmarsh-Rose neuronal models (Hindmarsh and Rose, 1984).

As discussed in Section 1.6, in networks of neuronal cells, signaling occurs both internally, through the interaction of the different ionic currents, and externally, through synaptic coupling. Following the framework introduced in (Scardovi et al., 2010), the model we rely on explicitly takes into account internal and external interconnections by viewing each component of the network (referred to as a *compartment*) as an interconnection of subsystems (referred

[1] The results presented in this chapter were obtained under the supervision of Prof. L. Scardovi at TUM, Munich, Germany. This work was supported by the European Union Seventh Framework Programme [FP7/2007-2013] under grant agreement n.257462 HYCON2 Network of excellence.

to as *species*) represented by nonlinear input-output operators. The input to each operator includes both the influence of the other species within the same compartment, and a diffusive coupling term between the same species in different compartments, as well as exogenous disturbances. Similarly to (Scardovi et al., 2010; Arcak and Sontag, 2006; Sontag, 2006b; Arcak and Sontag, 2008), the dynamical properties of the isolated subsystems as well as the algebraic properties of the interconnection are summarized in the so-called *dissipativity* matrix, whose diagonal stability implies the robust synchronization of the network. This approach is similar to classical works on large-scale systems such as (Vidyasagar, 1981; Moylan and Hill, 1978). The robustness property is quantified through L_2 gain conditions that can be explicitly computed for particular interconnection structures.

Recently, other works have approached the study of synchronization in networks of nonlinear systems. In (Stan and Sepulchre, 2007; Hamadeh et al., 2008; Stan et al., 2007; Oud and Tyukin, 2004) the authors exploits the incremental passivity of the underlying dynamics. In (Spong, 1996; Pavlov et al., 2004, 2006; Pham and Slotine, 2007; Lohmiller and Slotine, 1998; Wang and Slotine, 2004; Steur et al., 2009) the authors use a convergent and contracting dynamics approach. All these works heavily use a state-space formalism, which requires a detailed knowledge of the underlying dynamics, as opposed to the purely input-output approach used in this chapter.

This chapter generalizes the results in (Scardovi et al., 2010) in the following ways: i) the elements belonging to the same species are not required to be identical, ii) the obtained synchronization conditions are weaker, and iii) the bound on the synchronization error is explicitly computed, thus paving the way to the study of interconnected systems forced by external inputs (*e.g.* control signals).

The chapter is organized as follows. In Section 7.1, we recall the formalism of (Scardovi et al., 2010) and adapt it to heterogenous compartments. In Section 7.2, the needed input/output properties are defined and illustrated through some academic examples. The main result is provided in Section 7.3, and its application to a network of Hindmarsh-Rose neuronal models is presented in Section 7.4. Proofs are given in Section 7.5.

7.1 Preliminaries and problem statement

The needed notation is recalled in Section Notation at page 25.

The system under analysis is given by the diffusive interconnection of n compartments, each composed of N subsystems that we refer to as species (Scardovi et al., 2010). The compartments are structurally identical, in the sense that they contain the same number of species, and that the internal interconnection is common to all compartments. The heterogeneity comes into play at the level of the species, *i.e.* the members of one species in different compartments are allowed to be different. The class of heterogeneities that we can take into account with the present approach will be detailed in the following sections.

Each species $k \in \{1, \dots, N\}$ in the compartment $j \in \{1, \dots, n\}$ is described through a nonlinear operator $H_{k,j} : L_{2e}^m \to L_{2e}^m$, and its input-output behavior is given by

$$y_{k,j} = H_{k,j} v_{k,j}, \quad v_{k,j} \in L_{2e}^m. \tag{7.1}$$

The inputs are given by

$$v_{k,j} = w_{k,j} + \sum_{i=1}^{N} \sigma_{k,i} y_{i,j} + \sum_{z=1}^{n} a_{j,z}^k (y_{k,z} - y_{k,j}), \tag{7.2}$$

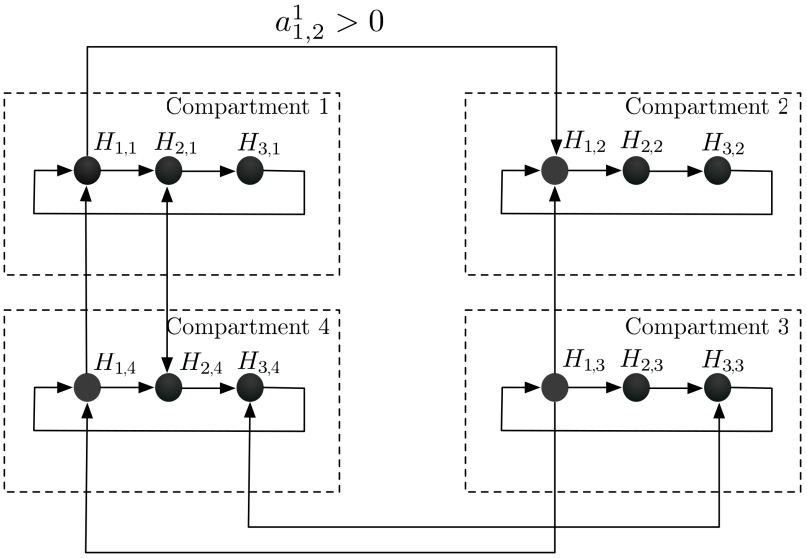

FIGURE 7.1: An illustration of the interconnection structure.

where $w_{k,j}$ models exogenous disturbances, $\sum_{i=1}^{N} \sigma_{k,i} y_{i,j}$ models the input-output coupling among different species in the same compartment j, and $\sum_{z=1}^{n} a^k_{j,z}(y_{k,z} - y_{k,j})$ represents the diffusive coupling between the same species k in different compartments (see Figure 7.1). The coefficients $a^k_{i,j}$, $k = 1, \dots, N$, $i, j = 1, \dots, n$ are non-negative. They represent the interconnection structure among different compartments. We assume no self-loops, that is $a^k_{j,j} = 0$, for all $k = 1, \dots, N$ and all $j = 1, \dots, n$. As highlighted by the species superscript k, the coefficient $a^k_{i,j}$ may vary from species to species, allowing for different interconnection topologies between different species.

The internal interconnection structure is quantified by the $N \times N$ matrix

$$\Sigma := [\sigma_{k,i}]_{k,i=1,\dots,N}. \tag{7.3}$$

Moreover, for all $\eta \in \mathbb{R}^N$, let

$$E_\eta := \Sigma - \operatorname{diag}(\eta_1, \dots, \eta_N). \tag{7.4}$$

We respectively denote by $Y_k := \operatorname{col}(y_{k,1}, \dots, y_{k,n})$, $V_k := \operatorname{col}(v_{k,1}, \dots, v_{k,n})$, $W_k := \operatorname{col}(w_{k,1}, \dots, w_{k,n})$, the vectors of outputs, inputs, and exogenous disturbances of the same species k. Given a set of vectors Z_k, $k = 1, \dots, N$, we indicate the stacked vector by $Z := \operatorname{col}(Z_1, \dots, Z_N)$, for example we indicated the stacked vector of outputs by $Y := \operatorname{col}(Y_1, \dots, Y_N) \in L^{nN}_{2e}$.

The closed-loop input (7.2) can then be condensed as

$$V_k = W_k + \sum_{i=1}^{N} \sigma_{k,i} Y_i - L_k Y_k, \ \forall k = 1, \dots, N, \tag{7.5}$$

where $L_k := \left[l^k_{i,j}\right]_{i,j=1,\dots,n} \in \mathbb{R}^{n \times n}$ is the Laplacian matrix associated to the k-th diffusive interconnection, defined as

$$l^k_{i,j} := \begin{cases} \sum_{z=1}^{n} a^k_{i,z}, & i = j \\ -a^k_{i,j}, & i \neq j. \end{cases} \tag{7.6}$$

The connectivity properties of the diffusive interconnection can be associated to the algebraic

properties of L_k (Godsil and Royle, 2001). In particular, the algebraic connectivity λ_k can be extended to the case of directed graphs (Wu, 2005) as

$$\lambda_k := \min_{z \in \mathbf{1}_n^\perp, |z|=1} z^T L_k z. \tag{7.7}$$

To analyze the synchronization of the interconnected system (7.1)-(7.2), we compare the outputs of the same species in different compartments. The mean output $\overline{Y}_k \in L_{2e}^m$ of a species k is defined as

$$\overline{Y}_k := \frac{1}{n} \sum_{j=1}^{n} y_{k,j}, \ k = 1, \ldots, N. \tag{7.8}$$

By defining the vector of synchronization error

$$Y_k^\Delta := \mathrm{col}(y_{k,1} - \overline{Y}_k, \ldots, y_{k,n} - \overline{Y}_k), \tag{7.9}$$

we have that $Y_k^\Delta = 0$ if and only if the outputs are synchronized, meaning that $y_{k,1} = y_{k,2} = \ldots = y_{k,n}$. A natural quantity to characterize the degree of synchronization of the species k over the time window $[0, T]$, $T \geq 0$, is thus given by $\|Y_k^\Delta\|_T$. In the sequel, the same notation is used to define the vectors V_k^Δ and W_k^Δ.

7.2 Definitions and first examples

In order to study synchronization properties of the system (7.1)-(7.2) we introduce some operator properties that will be extensively used in the paper

The next definition characterizes an *incremental* input-output property that relates output differences to input differences for operators pairs. It thus constitutes a natural instrument to study synchronization of input-output operators. This definition is the natural generalization of (Scardovi et al., 2010, Definition 1) to the case of heterogeneous populations.

Definition 7.1. Given $\gamma \in \mathbb{R}$ and $\mathcal{I} \subset \mathbb{N}$, a family $\mathcal{H}$ of input-output operators $H_i : L_{2e}^m \to L_{2e}^m$, $i \in \mathcal{I}$, is said to be γ-*mutual relaxed co-coercive* if, for all $i, j \in \mathcal{I}$, there exists $\beta_{i,j} \in \mathbb{R}$, such that, for all $u_i, u_j \in L_{2e}^m$, and all $T \geq 0$,

$$\gamma \|H_i u_i - H_j u_j\|_T^2 \leq \langle (H_i u_i - H_j u_j), (u_i - u_j) \rangle_T + \beta_{i,j}. \tag{7.10}$$

The constants $\beta_{i,j}$ are called the *biases*.

Let us illustrate Definition 7.1 through some examples that will be useful for the development of Section 7.4.

Example 7.1. *With the same computation as in (Scardovi et al., 2010, Section V.A), a scalar dynamical system $\dot{x} = -f(x) + u$ with arbitrary initial conditions and output $y = x$ can be shown to define mutually relaxed co-coercive operators, provided its right-hand side satisfies a one-sided Lipschitz condition as the one studied in (Pavlov et al., 2004). In particular, a scalar linear dynamics $\dot{x} = -ax + bu$, with arbitrary initial conditions defines mutually co-coercive operators with co-coercivity constant $\gamma = \frac{a}{b}$.*

For state space models Definition 7.1 is satisfied by incrementally output feedback passive systems (Stan and Sepulchre, 2007; Oud and Tyukin, 2004) with small heterogeneities as shown in the following proposition, whose proof is given in Section 7.5.1.

Proposition 7.2. *Consider a family of input-output dynamics*

$$\left\{\begin{array}{rcl} \dot{x}_j & = & f(x_j,u_j)+\delta f_j(x_j,v_j) \\ x_j(0) & = & x_j^0 \\ y_j & = & h_k(x_j) \end{array}\right. \tag{7.11}$$

where $u_j, y_j \in \mathbb{R}^m$, $x_j \in \mathbb{R}^p$, and $v_j \in \mathbb{R}^q$, for all all $j = 1,\ldots,n$. Note that $f : \mathbb{R}^p \times \mathbb{R}^m \to \mathbb{R}^p$ is common to all x_j, while the heterogeneity comes from the term $\delta f_j : \mathbb{R}^p \times \mathbb{R}^q \to \mathbb{R}^p$. Suppose that there exists a smooth function $V : \mathbb{R}^p \to \mathbb{R}_{\geq 0}$ and a constant $\gamma \in \mathbb{R}$ such that along the trajectories of (7.11), for all $i, j = 1,\ldots,n$,

$$\dot{V}(x_i - x_j) \leq -\gamma(y_i - y_j)^2 + (u_i - u_j)^T(y_i - y_j) + \left[\frac{\partial V}{\partial x}(x_i - x_j)\right]^T (\delta f_i(x_i,v_i) - \delta f_j(x_j,v_j)). \tag{7.12}$$

Given two functions $v_i, v_j : \mathbb{R}_{\geq 0} \to \mathbb{R}^q$, suppose that, for all initial conditions x_i^0, x_j^0, there exists a constant $C \geq 0$ such that, for all input functions $u_i, u_j \in L^m_{2e}$, along the trajectories of (7.11),

$$\left\| \left[\frac{\partial V}{\partial x}(x_i - x_j)\right]^T (\delta f_i(x_i,v_i) - \delta f_j(x_j,v_j)) \right\|_T \leq C, \tag{7.13}$$

for all $T \geq 0$. Then the input-output operators associated to (7.11) are mutually relaxed co-coercive with co-coercivity constant γ and biases $\beta_{i,j} = V(x_i^0 - x_j^0) + C$.

The heterogeneity $\delta f_j(x_j, v_j)$ depends both on the state of the system, and on the (possibly time varying) parametric uncertainties v_j. The right hand side of (7.13) represents the energy added to incremental storage function V by the presence of heterogeneities. Relation (7.13) requires this energy to be finite and independent from the systems inputs. When $\delta f_j = 0$, for all $j = 1,\ldots,n$, the only heterogeneities are due to different initial conditions. In this case Proposition 7.2 says that identical incrementally passive systems define a family of mutually relaxed co-coercive operators. The following example illustrates a particular situation in which condition (7.13) can be checked

Example 7.2. *Consider a family of non-controllable passive system with (possibly nonlinear) heterogeneities in the non-controllable part of the form*

$$\left\{\begin{array}{rcl} \dot{x}_j^c & = & A_c x_j^c + B u_j + A_{uc} x_u, \\ \dot{x}_j^u & = & A_u x_j^u + \delta f_j(x_j^u) \\ x_j(0) & = & x_j^0 \\ y_j & = & C x_j^c \end{array}\right. \tag{7.14}$$

where $y_j, u_j \in \mathbb{R}^m$, $x_j^c \in \mathbb{R}^{p_c}$, $x_j^u \in \mathbb{R}^{p_u}$, and $[A_c, B]$ is controllable, for all all $j = 1,\ldots,n$. Suppose that A_u is Hurwitz, that δf_j is continuous, and that the non-controllable part x_j^u is exponentially stable, that is there exists $\alpha_j, b_j > 0$ such that, for all initial condition $x_j^u(0)$,

$$|x_j^u(t)| \leq b_j |x_j^u(0)| e^{-\alpha_j t}, \ \forall t \geq 0, \tag{7.15}$$

for all $j = 1,\ldots,n$. Suppose moreover that controllable part x_j^c is output feedback passive. From these assumptions, it follows that there exists a symmetric positive definite matrix $Q := \begin{bmatrix} Q_c & 0 \\ 0 & Q_u \end{bmatrix}$, where $Q_c \in \mathbb{R}^{p_c \times p_c}$ and $Q_u \in \mathbb{R}^{p_u \times p_u}$, and a constant $\gamma \in \mathbb{R}$, such that, for all

$i, j = 1, \dots, n$,

$$\begin{aligned}
& \frac{d}{dt}\frac{1}{2}(x_i - x_j)^T Q (x_i - x_j) \\
= \; & \frac{d}{dt}(x_i^c - x_j^c)^T Q_c (x_i^c - x_j^c) + \\
& \frac{d}{dt}(x_i^u - x_j^u)^T Q_u (x_i^u - x_j^u) \\
\leq \; & \gamma (y_i - y_j)^2 + (y_i - y_j)^T (u_i - u_j) + \\
& \frac{1}{2}(x_i^u - x_j^u)^T (Q_u A_u + A_u^T Q_u)(x_i^u - x_j^u) + \\
& (x_i^u - x_j^u)^T Q_u (\delta f_i(x_i^u) - \delta f_j(x_j^u)) \\
\leq \; & \gamma (y_i - y_j)^2 + (y_i - y_j)^T (u_i - u_j) + \\
& (x_i^u - x_j^u)^T Q_u (\delta f_i(x_i^u) - \delta f_j(x_j^u)),
\end{aligned} \tag{7.16}$$

where the first inequality comes from the fact the controllable part is linear and output feedback passive, hence, it is also output feedback incrementally passive, and the second inequality comes from the fact that A_u is Hurwitz. Moreover, recalling (7.15), and that δf_j is continuous, it follows that, for all initial conditions $x_j^u(0), x_i^u(0)$,

$$\int_0^T (x_i^u - x_j^u)^T Q_u (\delta f_i(x_i^u) - \delta f_j(x_j^u)) dt \leq$$

$$2 \max(b_j |x_j^u(0)|, b_i |x_i^u(0)|) \frac{1}{\min_{j=1,\dots,n} \alpha_j} C_\delta, \tag{7.17}$$

where

$$C_\delta = \max_{a \in \mathbb{R}^{p_u},\ |a| \leq \max_{j=1,\dots,n} b_j |x_j^u(0)|} .$$

It follows from (7.16) and (7.17) that (7.12) and (7.13) are satisfied, hence (7.14) defines a family of mutually co-coercive operators.

7.3 Robust synchronization results

7.3.1 Main result

The following theorem is an extension of (Scardovi et al., 2010, Theorem 1) to the case of heterogeneous dynamics. Its proof is given in Section 7.5.2.

Theorem 7.3. *Consider the network (7.1)-(7.2). Suppose that the following assumptions are satisfied:*

1. *For each $k = 1, \dots, N$, the family of operators $\mathcal{H}_k := \{H_{k,j}\}_{j=1,\dots,n}$ is γ_k-mutually relaxed co-coercive, $\gamma_k \in \mathbb{R}$.*
2. *For each $k = 1, \dots, N$, $\tilde{\gamma}_k := \gamma_k + \lambda_k > 0$, where λ_k is the algebraic connectivity (7.7) of the interconnection graph associated to the species k.*
3. *The dissipation matrix $E_{\tilde{\gamma}}$, as defined in (7.4), is diagonally stable[2].*

[2] A matrix M is said to be diagonally stable if there exists a diagonal matrix $D > 0$ such that $DM + M^T D < 0$.

Then, there exist $\rho, \beta > 0$, such that

$$\|Y^{\Delta}\|_T \leq \rho \|W^{\Delta}\|_T + \beta, \quad \forall T \geq 0. \tag{7.18}$$

In particular, letting $d_i > 0$, $i = 1, \ldots, N$, be such that $DE_{\tilde{\gamma}} + E_{\tilde{\gamma}}^T D < 0$, where $D = \mathrm{diag}(d_1, \ldots, d_N)$, the L_2-gain ρ in (7.18) is given by

$$\rho := \frac{\max_{i=1,\ldots,N}\{d_i\}}{\min\left\{\mathrm{spect}(-DE_{\tilde{\gamma}} - E_{\tilde{\gamma}}^T D)\right\}}. \tag{7.19}$$

Theorem 7.3 ensures that the synchronization error Y^{Δ} of the system is small (in the L_2 norm) provided that the input dispersion W^{Δ} is small. In particular the closed-loop system has finite incremental L_2-gain from the incremental input W^{Δ} to the incremental output Y^{Δ}. With respect to (Scardovi et al., 2010), apart from the less conservative assumptions, Theorem 7.3 provides an explicit expression for the L_2-gain. Notice that the gain can be made arbitrarily small, by reducing the eigenvalues of the matrix $DE_{\tilde{\gamma}} + E_{\tilde{\gamma}}^T D$.

7.3.2 L_2-gain for particular interconnection topologies

In the following lemmas, whose proofs are given in Section 7.5.3, we give the explicit computation of the incremental L_2-gain ρ, appearing in Theorem 7.3 for two particular compartmental interconnection topologies.

Lemma 7.4. *Suppose that the dissipativity matrix $E_{\tilde{\gamma}}$ has the form*

$$E_{\tilde{\gamma}} = \begin{bmatrix} -\tilde{\gamma}_1 & 0 & \ldots & 0 & -1 \\ 1 & -\tilde{\gamma}_2 & \ddots & & 0 \\ 0 & 1 & -\tilde{\gamma}_3 & \ddots & \vdots \\ \vdots & \ddots & \ddots & \ddots & 0 \\ 0 & \ldots & 0 & 1 & -\tilde{\gamma}_N \end{bmatrix}, \tag{7.20}$$

that is the compartmental coupling is given by a cyclic feedback (Arcak and Sontag, 2006). If $\tilde{\gamma}_i > 0$, for all $i = 1, \ldots, N$, and

$$1 - r\cos\left(\frac{\pi}{N}\right) > 0, \tag{7.21}$$

where

$$r := \sqrt[N]{\prod_{i=1}^{N} \frac{1}{\tilde{\gamma}_i}}, \tag{7.22}$$

then the dissipativity matrix $E_{\tilde{\gamma}}$ is diagonally stable, and the incremental L_2-gain (7.19) of the closed-loop system is given by

$$\rho = \frac{1}{(1 - r\cos\left(\frac{\pi}{N}\right)) \min_{i=1,\ldots,N} \tilde{\gamma}_i} \tilde{\delta} \tag{7.23}$$

where

$$\tilde{\delta} = \frac{\max\left\{1, (r\tilde{\gamma}_2)^2, (r^2\tilde{\gamma}_2\tilde{\gamma}_3)^2, \ldots, \left(r^{N-1}\tilde{\gamma}_2 \ldots \tilde{\gamma}_N\right)^2\right\}}{\min\left\{1, (r\tilde{\gamma}_2)^2, (r^2\tilde{\gamma}_2\tilde{\gamma}_3)^2, \ldots, (r^{N-1}\tilde{\gamma}_2 \ldots \tilde{\gamma}_N)^2\right\}}.$$

The form of the incremental L_2-gain for a cyclic interconnection (7.23) can be readily used for synthesis purposes. It suggests in particular that the algebraic connectivity of the interconnection topologies associated to different species must be chosen in such a way that the secant condition (7.21) is satisfied with a large margin, that is $r\cos(\pi/N) \ll 1$ and that the minimum closed-loop co-coercivity constant $\min_{i=1,\dots,N}\tilde{\gamma}_i$ should be large. Noticing that r is given by the inverse of the geometrical mean $\overline{\gamma}$ of the algebraic connectivities, that is

$$\overline{\gamma} := \sqrt[N]{\prod_{i=1}^{N}\tilde{\gamma}_i},$$

the term $\tilde{\delta}$ imposes that the set $\{\tilde{\gamma}_i\}_{i=1,\dots,N}$ should be as homogeneous as possible, meaning that $\frac{\tilde{\gamma}_i}{\overline{\gamma}} \sim 1$, for all $i = 1,\dots,N$. The last condition can be interpreted as avoiding "bottlenecks" effects in the feedback cycle given by species that synchronize with a slower rate than the others. This kind of homogeneity conditions is often encountered in the study of the *synchronizability* of a given interconnection topology (Motter et al., 2005; Hao et al., 2009).

In the following lemma we specialize the computation of the incremental L_2 gain to the case of antisymmetric input-output interconnections. Its proof is provided in Section 7.5.4

Lemma 7.5. *Suppose that the dissipativity matrix $E_{\tilde{\gamma}}$ has the form*

$$E_{\tilde{\gamma}} = A_N - diag(\tilde{\gamma}_1,\dots,\tilde{\gamma}_N),$$

where A_N denotes an antisymmetric $N\times N$ matrix and $\tilde{\gamma}_i > 0$ for all $i = 1,\dots,N$. Then $E_{\tilde{\gamma}}$ is diagonally stable and the incremental L_2-gain (7.19) is given by

$$\rho := \frac{1}{\min_{i=1,\dots,N}\{\tilde{\gamma}_i\}}.$$

The L_2 gain obtained for antisymmetric input-output interconnections is independent of the size of the system, and takes into account the minimum co-coercivity constant only. This fact reflects the observation that any antisymmetric input-output interconnection can be decomposed into a family of two-dimensional negative feedbacks. Notice that both Lemma 7.4 and Lemma 7.5 provide the same L_2-gain for a two-dimensional negative feedback.

7.3.3 Apllication to state-space representations

The results of Theorem 7.3 can be used to analyze synchronization in systems described with a state space formalism

$$\begin{cases} \dot{x}_{k,j} &= f_{k,j}(x_{k,j}, v_{k,j}), \\ y_{k,j} &= h_k(x_{k,j}) \end{cases} \tag{7.24}$$

where $y_{k,j}, v_{k,j} \in \mathbb{R}^m$, $x_{k,j} \in \mathbb{R}^{p_k}$, for all $k = 1,\dots,N$, and all $j = 1,\dots,n$. Its proof is a straightforward application of Theorem 7.3 and is omitted.

Corollary 7.6. *Assume that the nonlinear operators $H_{k,j}$, $k = 1,\dots,N$, $j = 1,\dots,n$, associated to (7.24) with some initial conditions $x^0_{k,j} \in \mathbb{R}^{p_k}$ are well defined. Consider the closed-loop system defined by (7.24), with inputs as in (7.2) and suppose that the conditions in Theorem 7.3 are satisfied. Then, there exists $\rho, \beta > 0$, such that*

$$\|Y^{\Delta}\|_T \le \rho\|W^{\Delta}\|_T + \beta, \quad \forall T \ge 0, \tag{7.25}$$

where ρ is given as in the statement of Theorem 7.3. If in addition $W^{\Delta} \in L_2$, then the output asymptotically synchronizes.

As opposed to (Scardovi et al., 2010, Corollary 1), the vector field does not need to be identical among different compartments. In particular, the requirement of zero-state reachability, assumed in (Scardovi et al., 2010, Corollary 1) is not required.

7.4 Robust synchronization in networks of Hindmarsh-Rose neurons

7.4.1 The Hindmarsh-Rose model and its input-output representation

The Hindmarsh-Rose (HR) model, first introduced in (Hindmarsh and Rose, 1984), is a qualitative model of neuronal bursting dynamics. That is, its trajectories mimic the behavior of bursting neurons. The HR dynamics is defined by three differential equations

$$\begin{aligned} \dot{x} &= -ax^3 + bx^2 + I + y - z_{x,i} + u_x \\ \dot{y} &= c - dx^2 - y \\ \dot{z} &= r(s(x + \bar{z} + u_z) - z). \end{aligned} \tag{7.26}$$

The first variable x models the membrane voltage, the second y models fast Na^- and K^+ currents through the membrane, and the third z models slow Ca^{2+} currents. I is a parameter that models external currents through the membrane. u_x models other exogenous electrical inputs (heterogeneities, coupling with other cells, noise, etc.), while u_z models the diffusion of Ca^{2+} ions in the cell. $a, b, c, d, r, s, \bar{z}$ are free parameters that change the qualitative behavior of the system by inducing bifurcations in the underlying dynamics. In particular, r is a small parameter ($r \ll 1$) that lets the time scales of the (x, y) and z subsystems be sharply separated. From a dynamical point of view, the first two variables account for the excitable spike generation mechanism, while the third plays the role of a slowly varying adaptation variable. In particular, the (x, y)-subsystem exhibits a bistable dynamics, in which a stable limit cycle (corresponding to spiking) and a stable fixed point (corresponding to resting) co-exist. Their regions of attraction are separated by the stable manifold of a saddle point (Hindmarsh and Rose, 1984). A slow adaptation dynamics for z let the (x, y) subsystem slowly switch between the resting and spiking attractors, which corresponds to a bursting behavior. The isolated dynamics of x or y does not correspond to any biologically relevant behavior when considered separately. It is then natural to consider the (x, y)-subsystem as single bi-dimensional biological species $X := (x, y)^T$, that interacts in an input-output fashion with the (slow) z species. Letting $y_X := x$ be the output of the X species, and $y_z := z$ be the output of the z species, the HR neurons, with arbitrary initial conditions (x_0, y_0, z_0), can equivalently be modeled as the interconnection of the input/output operators H_X and H_z, modeling the X and z species, respectively, defined by $H_X : v_X \mapsto y_X$ and $H_z : v_z \mapsto y_z$, where

$$\begin{cases} \dot{X} &= F(X) + Bv_X \\ y_X &= x \\ X(0) &= X_0 := (x_0, y_0)^T \end{cases} \tag{7.27}$$

$$\begin{cases} \dot{z} &= r(s(\bar{z} + v_z) - z) \\ y_z &= z \\ z(0) &= z_0 \end{cases} \tag{7.28}$$

with $F(X) := \begin{pmatrix} -ax^3 + bx^2 + y \\ c - dx^2 - y \end{pmatrix}$, $B := \begin{pmatrix} 1 \\ 0 \end{pmatrix}$, $v_X := I + w_X - z$ and $v_z := w_z + x$ are the inputs to the X and z species, and w_X and w_z are the external current and the

external calcium diffusion, respectively. This configuration corresponds to a compartmental input-output interconnection matrix, as defined in (7.3),

$$\Sigma_{HR} := \begin{pmatrix} 0 & -1 \\ 1 & 0 \end{pmatrix}. \tag{7.29}$$

In order to apply Corollary 7.6 to the synchronization of the family of operators (7.27)-(7.28) according to the methodology developed in the previous sections, we have to check that the operators are well defined and study their mutual co-coercivity.

Since the operator associated to the slow z species is defined by the one-dimensional linear system $\dot{z} = r(s(\overline{z}+v_z)-z)$ with input v_z and output z, it is well defined (Van der Schaft, 1999). Moreover, it follows directly from Example 7.1 that an ensemble of input-output operators (7.28) with arbitrary initial conditions defines a family of mutually co-coercive operators with

$$\gamma_z := 1/s. \tag{7.30}$$

The following propositions establish that the operators associated to the X species are well defined, and form a family of mutually co-coercive operators. Their proofs are respectively given in Sections 7.5.5 and 7.5.6.

Proposition 7.7. *For all initial conditions $X_0 \in \mathbb{R}^2$, the operator H_X defined in (7.27) is well defined.*

Proposition 7.8. *For all $X_{10}, X_{20} \in \mathbb{R}^2$, the input-output operators associated to (7.27) with initial conditions X_{10} and X_{20} are mutually relaxed co-coercive with co-coercivity constant $\gamma_X := -\frac{d^2}{2} - b^2$.*

7.4.2 Network of Hindmarsh-Rose neurons

In the following we consider the diffusive interconnection of $n \in \mathbb{N}_{\geq 2}$ HR neuronal compartment (7.27)-(7.28). The initial conditions specifying the input-output behavior of each compartment are assumed to be arbitrary. We let λ_X and λ_z be the algebraic connectivity associated to the X and z species, respectively. The dissipativity matrix $E_{\tilde{\gamma}}$, as defined in (7.4), is then given by

$$E_{\tilde{\gamma}} = \begin{bmatrix} \tilde{\gamma}_X & -1 \\ 1 & \tilde{\gamma}_z \end{bmatrix}, \tag{7.31}$$

where $\tilde{\gamma}_X = \gamma_X + \lambda_X$ and $\tilde{\gamma}_z = \gamma_z + \lambda_z$. From Lemma 7.4 or Lemma 7.5 $E_{\tilde{\gamma}}$, is diagonally stable provided $\lambda_X > -\gamma_X$. Moreover, in the case of zero inputs, the boundedness of the trajectories of each subsystem follows directly from (Oud and Tyukin, 2004, Proposition 1). Hence, from (7.30), Proposition 7.7, and Proposition 7.8q2, all the conditions of Corollary 7.6 are satisfied, provided that

$$\lambda_X > \frac{d^2}{2} + b^2. \tag{7.32}$$

At the light of these considerations, we are able to provide analytical results on the robust synchronization of a network of HR neurons, as stated in the following proposition.

Proposition 7.9. *Consider a network of $n \in \mathbb{N}_{\geq 2}$ HR neurons (7.27)-(7.28). Let W_X^Δ and W_z^Δ be the incremental input of the X and z species, respectively, and W^Δ the resulting incremental input of the network, as defined in Section 7.1. Let Y_X^Δ and Y_z^Δ be the synchronization errors (7.9) associated to the X and z species respectively, and Y^Δ the resulting network synchronization error. Suppose that (7.32) is satisfied. Then there exists $\beta \geq 0$, such that, for all*

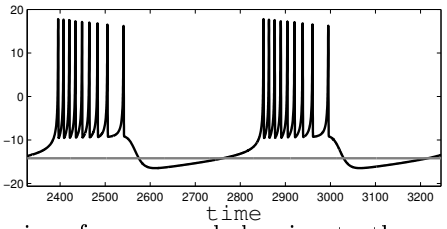

FIGURE 7.2: Typical behavior of a neuron belonging to the *active* population (black) and *silent* population (grey), before the diffusive coupling between the two populations is switched on.

$T \geq 0$,

$$\|Y^{\Delta}\|_T \leq \rho_{HR}\|W^{\Delta}\|_T + \beta, \tag{7.33}$$

where

$$\rho_{HR} := \frac{1}{\min(\tilde{\gamma}_X, \tilde{\gamma}_z)}. \tag{7.34}$$

We point out that, as opposed to (Scardovi et al., 2010), our approach does not require to check the zero-state reachability of the HR model.

7.4.3 Numerical simulation

To illustrate the results, we run numerical simulations on a biologically meaningful interconnection topology. The parameters used in the simulation are as follows: $a = 0.01, b = 0.3, c = 0.1, d = 0.5, r = 0.001, s = 4, \bar{z} = 7$. We have considered the interaction of two distinct neuronal populations. Each populations is composed by qualitatively identical neurons. The first population contains the *active* neurons, *i.e.* with an endogenous rhythmic activity. The second population is composed of silent neurons, that is neurons that are endogenously at rest. The two different behaviors are obtained by fixing different values of w_z, which models the extracellular calcium concentration. A low value ($w_z = 2$) corresponds to the active population, while silent neurons are characterized by a higher value ($w_z = 4$). Moreover, each neuron is affected by an heterogeneous electrical input w_X. Figure 7.2 illustrates the typical behavior of two neurons belonging to each of these populations.

We suppose that the electrical coupling between neurons belonging to the same population is absent. On the contrary, each active neuron is connected to all the silent neurons, and vice-versa, with the same coupling strength K_X. This kind of interconnection represents a simplification of the interaction between different brain neuronal subpopulations. Indeed, for neurons in the sub-thalamic zone, most of the synapses of a neuron belonging to some specific area project outside the interested area (Sato et al., 2000). On the contrary, neurons that are located inside the same area, share the same physical medium. In this way, the natural diffusion in the cellular surrounding of the ions generating the currents in the neuron membrane constitutes a further type of diffusive coupling (Rubin, 2007). In the HR neuron, this can be modeled by a diffusive coupling in the z species, describing the dynamics of Ca^{2+} ions concentration in the cell. We thus suppose that each neuron belonging to a given population is coupled to all the other neurons of this population through diffusive coupling in the z species with homogeneous coupling strength K_z. If the two species have the same number $M \in \mathbb{N}_{>0}$ of neurons, the Laplacian matrices associated to the interconnection topologies among the X and z species are given by

$$L_X = -\begin{bmatrix} 0_{M\times M} & 1_{M\times M} \\ 1_{M\times M} & 0_{M\times M} \end{bmatrix} + MI_N, \tag{7.35}$$

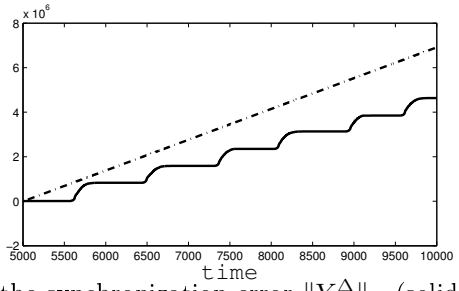

FIGURE 7.3: Evolution of the synchronization error $\|Y^{\Delta}\|_T$ (solid line) and of the predicted bound $\rho\|W^{\Delta}\|_T$ (dashed line) after the diffusive coupling between the active and silent populations is activated. The bias has been removed for clarity.

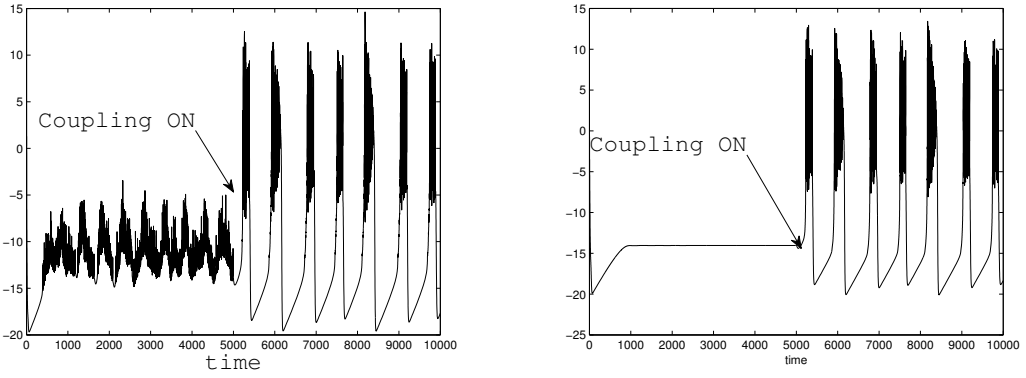

FIGURE 7.4: Mean membrane voltage of the active (left) and silent (right) population before and after the coupling between the two populations is switched on. After the coupling is activated, the system shows a global bursting oscillation even though no interconnections are present inside each neuronal population.

and

$$L_z = -\begin{bmatrix} 1_{M\times M} & 0_{M\times M} \\ 0_{M\times M} & 1_{M\times M} \end{bmatrix} + MI_N. \tag{7.36}$$

The interconnection between the X species corresponds to a complete bipartite graph. If K_X is the coupling strength, the algebraic connectivity is given by $\lambda_X = MK_X$ (Bondy and Murty, 1976, page 5). Since the graph associated to the z species is not connected its algebraic connectivity is zero (Bondy and Murty, 1976). By picking $K_X > \left(\frac{d^2}{2} + b^2\right)/M$ and $K_z \geq 0$, all the assumption of Proposition 7.9 are satisfied. In the simulation we have picked $M = 10$, $K_X = \left(\frac{d^2}{2} + b^2 + 0.5\right)/M$ and $K_z = 0.25/M$. With this choice we get, from Lemma 7.4 or Lemma 7.5, $\rho_{HR} = 4$. Figure 7.3 shows the evolution of the synchronization error. When the coupling is switched on at time $t = 5000$, The theoretical integral bound predicted by Theorem 7.3 is satisfied. The prediction of a robust synchronous behavior is associated to important counterintuitive phenomena. Neurons belonging to the active population are not synchronized before the coupling with the silent population is not present, due to heterogeneities (Figure 7.4, left). Even though they are not directly coupled, they become synchronized once they start to interact with the silent neuronal population. At the same time, the silent neuronal population starts to show global oscillations at the same frequency (Figure 7.4, right). This kind of mutually induced oscillations is typical of the interaction between excitatory and inhibitory neuronal populations (Holgado et al., 2010).

7.5 Proofs

7.5.1 Proof of Proposition 7.2

Integrating both sides of (7.12) and considering (7.13), we get

$$\begin{aligned} -V(x_i^0 - x_j^0) &\leq V(x_i^0(T) - x_j^0(T)) - V(x_i^0 - x_j^0) \\ &\leq -\gamma\|y_i - y_j\|^2 + \langle u_i - u_j, y_i - y_j\rangle_T \\ &\quad + C, \end{aligned}$$

showing the two associated input-output operators are mutually relaxed co-coercive with co-coercivity constant γ and bias $\beta_{1,2} = V(x_i^0 - x_j^0) + C$. □

7.5.2 Proof of Theorem 7.3

The proof is a direct adaptation of that of (Scardovi et al., 2010, Theorem 1). Let the input to the species k be given by $V_k(t) = U_k(t) - L_k Y_k(t)$, that is U_k contains both exogenous disturbances and input-output compartmental coupling. Let the biases appearing in the mutual relaxed co-coercive relation (7.10) associated to the species k be $\beta_{ij}^{(k)}$, $i, j = 1, \ldots, n$, $k = 1, \ldots, N$. With simple computations[3], (Scardovi et al., 2010, Lemma 1) generalizes to the mutual relaxed co-coercivity case in the form

$$\gamma_k \|Y_k^\Delta\|_T^2 \leq \langle Y_k^\Delta, V_k^\Delta\rangle_T + \beta_k, \ k = 1, \ldots, N,$$

for all $T \geq 0$ and all $V_k \in L_{2e}^{nm}$, where

$$\beta_k := n \max_{i=1,\ldots,n} \beta_{ii}^{(k)}. \tag{7.37}$$

It then follows from[4] (Scardovi et al., 2010, Equation (23)) that, for all $k = 1, \ldots, N$,

$$\tilde{\gamma}_k \|Y_k^\Delta\|_T^2 \leq \langle Y_k^\Delta, U_k^\Delta\rangle_T + \beta_k. \tag{7.38}$$

Equation (7.38) shows how the presence of the diffusive coupling increases the incremental co-coercivity of the closed-loop system. Writing $U_k(t) = W_k(t) + \sum_{i=1}^N \sigma_{k,i} Y_i(t)$, (7.38) gives for all $k = 1, \ldots, N$ and all $T \geq 0$,

$$\tilde{\gamma}_k \|Y_k^\Delta\|_T^2 \leq \langle Y_k^\Delta, W_k^\Delta\rangle_T + \langle Y_k^\Delta, \sum_{i=1}^N \sigma_{k,i} Y_i^\Delta\rangle_T + \beta_k,$$

or, equivalently,

$$\langle Y_k^\Delta, W_k^\Delta + \sum_{i=1}^N \sigma_{k,i} Y_i^\Delta - \tilde{\gamma}_k Y_k^\Delta\rangle_T + \beta_k \geq 0, \ k = 1, \ldots, N. \tag{7.39}$$

Recalling the definition of the dissipativity matrix $E_{\tilde{\gamma}} := \Sigma - \mathrm{diag}(\tilde{\gamma}_1, \ldots, \tilde{\gamma}_N)$, (7.39) can also be written as

$$\langle Y^\Delta, W^\Delta + (E_{\tilde{\gamma}} \otimes I_n) Y^\Delta\rangle_T + \sum_{k=1}^N \beta_k \geq 0. \tag{7.40}$$

[3] Just add the bias in each line in the proof of (Scardovi et al., 2010, Lemma 1).

[4] Again, just add the bias in each line of (Scardovi et al., 2010, Equations (19-23))

Suppose that $E_{\tilde{\gamma}}$ is diagonally stable, that is there exists positive constants d_i, $i = 1, \ldots, N$, such that $DE_{\tilde{\gamma}} + E_{\tilde{\gamma}}^T D < 0$. Then, by defining $\beta' := \sum_{k=1}^N d_k \beta_k$

$$\begin{aligned} & \langle (D \otimes I_n) Y^\Delta, W^\Delta + (E_{\tilde{\gamma}} \otimes I_n) Y^\Delta \rangle_T + \beta' \\ = & \sum_{k=1}^N d_k \langle Y_k^\Delta, W_k^\Delta + \sum_{i=1}^N \sigma_{k,i} Y_i^\Delta - \tilde{\gamma}_k Y_k^\Delta \rangle_T + \sum_{k=1}^N d_k \beta_k \\ \geq & \ 0, \end{aligned} \tag{7.41}$$

where the last inequality comes from (7.39) and the positiveness of d_i, $i = 1, \ldots, N$. Let $\underline{d} := \min(\text{spect}(-DE_{\tilde{\gamma}} - E_{\tilde{\gamma}}^T D)) > 0$. Noting that, for all matrix A, $\text{spect}(A \otimes I_n) = \{\text{spect}(A)\}^n$, it follows from (7.41) that

$$\begin{aligned} & \langle (D \otimes I_n) Y^\Delta, W^\Delta \rangle_T + \beta' \\ \geq & -\langle (D \otimes I_n) Y^\Delta, (E_{\tilde{\gamma}} \otimes I_n) Y^\Delta \rangle \\ \geq & \ \underline{d} \|Y^\Delta\|^2. \end{aligned} \tag{7.42}$$

and, by defining $\overline{d} := \max_{i=1,\ldots,N} d_i > 0$, it also holds that

$$\begin{aligned} & \langle (D \otimes I_n) Y^\Delta, W^\Delta \rangle_T \\ \leq & \ \langle (D \otimes I_n) Y^\Delta, W^\Delta \rangle_T \\ & + \frac{1}{2} \| \frac{\overline{d}}{\sqrt{\underline{d}}} W^\Delta - \frac{\sqrt{\underline{d}}}{\overline{d}} (D \otimes I_n) Y^\Delta \|_T^2 \\ = & \ \frac{1}{2} \frac{\overline{d}^2}{\underline{d}} \|W^\Delta\|_T^2 + \frac{1}{2} \frac{\underline{d}}{\overline{d}^2} \|(D \otimes I_n) Y^\Delta\|_T^2 \\ \leq & \ \frac{1}{2} \frac{\overline{d}^2}{\underline{d}} \|W^\Delta\|_T^2 + \frac{\underline{d}}{2} \|Y^\Delta\|. \end{aligned} \tag{7.43}$$

Plugging (7.43) into (7.42) we obtain

$$\begin{aligned} \|Y^\Delta\|_T^2 & \leq \frac{\overline{d}^2}{\underline{d}^2} \|W^\Delta\|_T^2 + 2 \frac{\beta'}{\underline{d}} \\ & \leq \left(\frac{\overline{d}}{\underline{d}} \|W^\Delta\|_T + \sqrt{2 \frac{\beta'}{\underline{d}}} \right)^2, \end{aligned}$$

that is

$$\|Y^\Delta\|_T \leq \rho \|W^\Delta\| + \beta, \tag{7.44}$$

where

$$\rho := \frac{\overline{d}}{\underline{d}}, \tag{7.45}$$

and $\beta := \sqrt{2 \frac{\beta'}{\underline{d}}}$.

□

7.5.3 Proof of Lemma 7.4

The proof of Lemma 7.4 is directly inspired to that of (Arcak and Sontag, 2006, Theorem 1). For notational purposes, let, for all $i = 1, \ldots, N$,

$$\eta_i := \frac{1}{\tilde{\gamma}_i}. \tag{7.46}$$

Let

$$D_\eta := \mathrm{diag}(\eta_1, \ldots, \eta_N), \tag{7.47}$$

and

$$\begin{aligned} A_0 &:= D_\eta E_{\tilde{\gamma}} \\ &= \begin{bmatrix} -1 & 0 & \ldots & 0 & -\eta_1 \\ \eta_2 & -1 & \ddots & & 0 \\ 0 & \eta_3 & -1 & \ddots & \vdots \\ \vdots & \ddots & \ddots & \ddots & 0 \\ 0 & \ldots & 0 & \eta_N & -1 \end{bmatrix}. \end{aligned} \tag{7.48}$$

Moreover define

$$\Delta := \mathrm{diag}\left(1, -\frac{\eta_2}{r}, \frac{\eta_2\eta_3}{r^2}, \ldots, \frac{\eta_2 \cdot \ldots \cdot \eta_N}{r^{N-1}}\right), \tag{7.49}$$

and

$$\begin{aligned} D &:= \Delta^{-2} D_\eta \\ &=: \mathrm{diag}(d_1, \ldots, d_N). \end{aligned} \tag{7.50}$$

Note that

$$\begin{aligned} \overline{d} &:= \max_{i=1,\ldots,N} d_i \\ &\leq \max_{i=1,\ldots,N} \eta_i \\ &\quad \max\left\{1, \left(\frac{r}{\eta_2}\right)^2, \left(\frac{r^2}{\eta_2\eta_3}\right)^2, \ldots, \left(\frac{r^{N-1}}{\eta_2 \ldots \eta_N}\right)^2\right\}. \end{aligned} \tag{7.51}$$

Moreover, by (7.48),(7.49), and (7.50), we can write

$$DE_{\tilde{\gamma}} + E_{\tilde{\gamma}}^T D = \Delta^{-1}\left(\Delta^{-1} A_0 \Delta + \Delta A_0 \Delta^{-1}\right)\Delta^{-1}. \tag{7.52}$$

Note that

$$-\Delta^{-1} A_0 \Delta = \begin{bmatrix} 1 & 0 & \ldots & 0 & (-1)^{N+1} r \\ r & 1 & \ddots & & 0 \\ 0 & r & 1 & \ddots & \vdots \\ \vdots & \ddots & \ddots & \ddots & 0 \\ 0 & \ldots & 0 & r & 1 \end{bmatrix}, \tag{7.53}$$

that is $-\Delta^{-1}A_0\Delta$ exhibits a circular structure when N is odd, and skew-circulant when N is even. From (Davis, 1979) it then follows that $-\Delta^{-1}A_0\Delta$ is diagonalizable with eigenvalues $\alpha_k = 1 + re^{\mathrm{i}(2\pi/N)k}$, $k = 1, \ldots, N$, if N is odd, and $\alpha_k = 1 + re^{\mathrm{i}(\pi/N + (2\pi/N)k}$, $k = 1, \ldots, N$, if N is even. The eigenvalues of its symmetric part $\frac{1}{2}(-\Delta^{-1}A_0\Delta - \Delta A_0 \Delta^{-1})$ are given by the real

parts of the α_k. In both the odd and even case, it holds that $\min_{k=1,\dots,N} \mathrm{Re}\alpha_k = 1 - r\cos(\pi/N)$. Recalling (7.52), it then follows that

$$\begin{aligned} \underline{d} &:= \min\left\{\mathrm{spect}(-DE_{\tilde{\gamma}} - E_{\tilde{\gamma}}^T D)\right\} \\ &\geq 2\left(1 - r\cos\left(\frac{\pi}{N}\right)\right) \\ &\quad \min\left\{1, \left(\frac{r}{\eta_2}\right)^2, \left(\frac{r^2}{\eta_2\eta_3}\right)^2, \dots, \left(\frac{r^{N-1}}{\eta_2\dots\eta_N}\right)^2\right\}. \end{aligned} \tag{7.54}$$

Invoking (7.19),(7.46),(7.51) and (7.54), the lemma follows. □

7.5.4 Proof of Lemma 7.5

The result follows immediately from (7.19) and by noticing that $\frac{1}{2}(E_{\tilde{\gamma}} + E_{\tilde{\gamma}}^T) = -\mathrm{diag}(\tilde{\gamma}_1, \dots, \tilde{\gamma}_N)$. □

7.5.5 Proof of Proposition 7.7

The proof is inspired to (Oud and Tyukin, 2004, Appendix A). The operator H_X can be equivalently defined as

$$H_X : \quad \left\{ \begin{array}{lcl} \dot{X} & = & F(X) + B(v_x - z') \\ \dot{z}' & = & \epsilon(s(x + \overline{z}) - z'),\ \epsilon = 0, \\ y_X & = & x \\ X(0) & = & X_0 \\ z'(0) & = & 0 \end{array} \right. \tag{7.55}$$

Given $c_1, c_2, c_3 > 0$, consider the function $V(x, y, z') = \frac{1}{2}c_1x^2 + \frac{1}{2}c_2y^2 + \frac{1}{2}z'^2$. With the same computation as (Oud and Tyukin, 2004, Appendix A), it follows that along the trajectories of (7.55)

$$\dot{V} \leq -(x - d_1)^2 + C + c_1 x v_x, \tag{7.56}$$

where $C > 0$ and $d_1 \in \mathbb{R}$. Integrating (7.56), and recalling that $z(0) = 0$, we get, for all $T \geq 0$,

$$\begin{aligned} \|x - d_1\|^2 &\leq c_1\langle x, v_x\rangle_T + CT + \frac{1}{2}c_1x(0)^2 + \frac{1}{2}c_2y(0)^2 \\ &= c_1\langle x - d_1, v_x\rangle_T + \langle d_1, v_x\rangle_T + CT \\ &\quad + \frac{1}{2}c_1x(0)^2 + \frac{1}{2}c_2y(0)^2 \\ &\leq c_1\langle x - d_1, v_x\rangle_T + c_1\langle d_1, v_x\rangle_T + CT + \\ &\quad \frac{1}{2}c_1x(0)^2 + \frac{1}{2}c_2y(0)^2 + \\ &\quad \|c_1v_x - (x - d_1)\|_T^2 \\ &= \frac{1}{2}c_1^2\|v_x\|_T^2 + \frac{1}{2}\|x - d_1\|_T^2 + c_1\langle d_1, v_x\rangle_T + \\ &\quad CT + \frac{1}{2}c_1x(0)^2 + \frac{1}{2}c_2y(0)^2. \end{aligned} \tag{7.57}$$

Since the constant $d_1 \in L_{2e}$, (7.57) implies that $x - d_1 \in L_{2e}$ whenever $v_x \in L_{2e}$. The proposition follows noticing that, since L_{2e} is a linear space and $d_1 \in L_{2e}$, $x - d_1 \in L_{2e}$ if and only if $x \in L_{2e}$. □

7.5.6 Proof of Proposition 7.8

The proof is inspired to that of (Oud and Tyukin, 2004, Proposition 3). Given two input functions $v_{x,1}, v_{x,2} \in L_{2e}$, let $X_1(\cdot)$ and $X_2(\cdot)$ be the corresponding evolutions of (7.27) with initial conditions X_{10} and X_{20}, respectively, and $y_1(\cdot)$ and $y_2(\cdot)$ the corresponding outputs (from Proposition 7.7 in L_{2e} as well]). Consider the following function $V(X_1 - X_2) := \frac{1}{2}(x_1 - x_2)^2 + \frac{1}{2d^2}(y_1 - y_2)^2$. The derivative of V along the trajectories of (7.27) can be expressed as

$$\begin{aligned}
&\dot{V} = \\
&-(x_1 - x_2)^2 \left(\frac{x_1^2}{2} + \frac{x_2^2}{2} + \frac{(x_1 + x_2)^2}{2} - b(x_1 + x_2)\right) + \\
&(x_1 - x_2)(v_{x,1} - v_{x,2}) + (y_1 - y_2)(x_1 - x_2) - \\
&\frac{1}{d}(x_1 - x_2)(x_1 + x_2)(y_1 - y_2) - \frac{1}{d^2}(y_1 - y_2)^2.
\end{aligned} \tag{7.58}$$

Following the same computation as (Oud and Tyukin, 2004, Equations (2.20)-(2.21)), it also holds that

$$\begin{aligned}
\dot{V} \leq &-(x_1 - x_2)^2 \left(\frac{1}{2}(x_1 - b)^2 + \frac{1}{2}(x_2 - b)^2 - \frac{d^2}{2} - b^2\right) + \\
&(x_1 - x_2)(v_{x,1} - v_{x,2}).
\end{aligned} \tag{7.59}$$

Let

$$\gamma_X := -\frac{d^2}{2} - b^2, \tag{7.60}$$

then from (7.59) it follows that

$$\begin{aligned}
\dot{V} \quad \leq \quad &-\gamma_X (x_1 - x_2)^2 + (x_1 - x_2)(v_{x,1} - v_{x,2}) + \\
&(x_1 - x_2)(v_{x,1} - v_{x,2}).
\end{aligned} \tag{7.61}$$

Integrating (7.61) along the trajectories of (7.27) the proposition follows. □

Conclusion and perspectives

Summary

Motivated by a medical problem, in this dissertation we have investigated synchronization and desynchronization phenomena in mathematical models of neuronal populations.

Parkinson's disease and the control of neuronal synchronization. We have first recalled the prominent role of neuronal synchronization in generating PD symptoms, and the weaknesses of the present open-loop DBS in eliminating this pathological state. We have then formulated in Chapter 1 a possible closed-loop DBS control goal, and made of it the main objective of Part I. The goal was to investigate how a proportional mean-field feedback could bring a pathologically synchronous neuronal population to either a desynchronized state or to a silent inhibited state.

Mathematical modeling of closed-loop DBS. With the aim of formulating analytical results, we have looked for a simple mathematical representation of this control problem. More precisely, we have derived in Chapter 2 a simplified model of a neuronal population under the effect of its mean-field proportional feedback. This model captures the rhythmic neuronal oscillation and respects basic input/output constraints.

Existence of synchronously oscillating solutions. We have characterized the pathological states in terms of oscillating phase-locked solutions. The existence of such states has been shown to be generically incompatible with any nonzero proportional mean-field feedback, thus supporting the proposed control strategy.

Robustness of the pathological states. Even though oscillating phase-locking mathematically disappears under mean-field feedback, we have proved in Chapter 3 that the pathological states can persist as practically phase-locked solutions and provide necessary conditions for desynchronization via mean-field feedback.

Neuronal inhibition. Under some simplifying assumptions, we have rigorously described in Chapter 4 how the presence of mean-field feedback can actually achieve a first therapeutic objective, that is neuronal inhibition, characterized as an almost globally asymptotically stable fixed point of the phase dynamics. The energy efficiency of the proposed control scheme in achieving this goal has also been rigorously addressed.

Neuronal desynchronization. In Chapter 5, we have approached the problem of desynchronizing an ensemble of phase oscillators. We have proposed a simple definition of desynchronization, and characterized it mathematically. We have then derived sufficient conditions to achieve effective desynchronization via proportional mean-field feedback for a generic interconnection topology and registration/stimulation setup.

In conclusion Part I let us derive a number of mathematical results supporting the efficiency of proportional mean-field feedback DBS in eliminating PD pathological synchronous oscillations, by either inhibiting or desynchronizing the neuronal population.

Part II was then motivated by the need of extending the analysis in Part I to more realistic neuron models. We have approached this problem by looking for modeling principles that are amenable to a comprehensive mathematical analysis and yet offer sufficient fidelity in reproducing neurons behavior.

Hybrid modeling of calcium-gated neurons. In modeling dopaminergic neurons via hybrid dynamical systems of the Izhikevich type, we have highlighted in Chapter 6 a weakness of the Izhikevich model in reproducing a robust pacemaking and ADPs activity. Based on the mathematical analysis of a calcium-gated Hodgkin-Huxley model, we have explained the origins of this deficiency rigorously and we have derived a novel hybrid model to overcome it.

Input-Output modeling. We have provided in Chapter 7 a theoretical extension of some recent works analyzing synchronization in large scale interconnected systems via a purely input-output approach. This extension allowed us to tolerate some heterogeneities between the units. This approach is of interest since it does not require any detailed state-space representation of the neuronal dynamics, and since it permits to naturally study the effects of exogenous inputs via rigorous control theoretical tools. We have showed that the Hindmarsh-Rose neuron model can effortlessly be modeled in this framework, and we have derived some robust synchronization results in a heterogeneous network of such models, thus providing a first extension of the robustness results derived in Chapter 3.

Limitations

Event though some of the theoretical results presented in this dissertation support a closed-loop DBS strategy, the underlying analysis relies on harsh approximations.

Neurons modeling. In its simplicity the oscillators model employed in Part I ignores many important properties of real neurons, as briefly highlighted in Section 1.4.2. More importantly for PD, it does not account for the heterogeneous behavior exhibited by neurons in different BG areas. See, *e.g.*, (Rubin and Terman, 2004).

Synaptic coupling modeling. The assumption of diffusive coupling between neurons ignores the complexity of real synaptic interactions. It does not account, for instance, for gain (the post-synaptic action potential can be larger than the pre-synaptic one) and threshold (only sufficiently large pre-synaptic inputs are able to generate a post-synaptic response) effects typical of chemical synapses. See for instance (Destexhe et al., 1998).

DBS electrode neurons interaction. We have partially accounted for the heterogeneous way in which neurons interact with the DBS electrode by allowing arbitrary input and output gain in our model. Yet, the details of the real neurons-electrode interaction and the way in which the electrical signal diffuse in brain tissues have been completely neglected.

Functional structure of BG. The BG network is characterized by multiple intra- and inter-nucleus interaction loops and projections. The resulting interconnection structure is quite complex and tightly related to the functional role of the BG (Bolam et al., 2000). Even though the proposed model could include any interconnection topology, and both excitatory and inhibitory coupling, analytical results can be derived only for simple, or at least symmetric coupling topologies, which is very simplistic compared to the complexity of the BG network.

Artifacts. We have worked under the optimistic assumption that neurons local field potential can be measured with arbitrary precision, independently of the injected input. This is unrealistic in the medical practice, where prominent artifacts coming from the DBS signal hide the neurons activity. New technology might, however, help to overcome this limitation (Giannicola et al., 2010; Priori et al., 2002; Rosa et al., 2010).

Open questions

The mathematical analysis derived throughout the thesis has highlighted a number of open questions, both in mathematics and control theory.

Global phase-locking robustness analysis. The phase-locking robustness analysis developed in Chapter 3 is local. We firmly believe that under some non-degeneracy assumptions, namely that all the fixed points are isolated and hyperbolic, this analysis can be made global with a small effort by exploiting some recent results on almost global ISS on compact Riemannian manifolds (Angeli and Praly, 2011).

Neuronal inhibition with respect to time-varying inputs. The same result (Angeli and Praly, 2011) does not apply straightforwardly to the neuronal inhibition problem faced in Chapter 4 due to the presence of non-isolated equilibria. One can envision, however, an extension of this type of results to deal with the presence of exponentially unstable manifolds of equilibria, as a generalization of exponentially unstable fixed points. This result would then be applicable to the neuronal inhibition problem, at least in the case of an odd number of oscillators, when the set of non-isolated equilibria is a normally hyperbolic unstable manifold.

Almost global convergence in the presence of degenerate sets of equilibria. In the case of an even number of oscillators, the set of non-isolated fixed points in the neuronal inhibition problem is not globally a manifold, due to the presence of degenerate equilibria. We were not able to prove Conjecture 4.1 in Chapter 4, since, to the best of our knowledge, no global stability and robustness analysis tools have yet been developed to deal with this case in a systematic way.

Neuronal inhibition in the presence of non all-to-all interconnection. The oscillations inhibition analysis has been developed under the assumption of an homogeneous interconnection and registration/stimulation setup. Similarly to what has been done in recent years for the Kuramoto system (Sarlette, 2009), it would be interesting to understand which other coupling topologies and feedback gains ensure the same convergence properties.

Tools to prove (practical) desynchronization. The proof of the desynchronizability of the Kuramoto system via mean-field feedback in Chapter 5 relies at present on elementary trigonometry. These computations do not generalize to phase-dynamics with non-sinusoidal coupling. New tools have then to be developed. We have seen that the proposed definition of desynchronization admits a topological characterization (complete instability) that is in opposition with that of synchronization (asymptotic stability). It would be interesting to investigate whether the stability tools usually exploited in synchronization analysis (Lyapunov, gradient dynamics, ISS, etc.) admit a counterpart for the rigorous analysis of desynchronization and the synthesis of desynchronizing controllers. The existence of an increasing incremental Lyapunov function could, for instance, straightforwardly be used to prove desynchronization.

Non diffusive input-output coupling. The nonlinear operators-based synchronization theory developed in Chapter 7 relies on the harsh constraint that neuronal coupling is of diffusive type only, which is not realistic. Neuron coupling via synapses has indeed a more impulsive nature, and does not directly depend on the neurons states difference, as imposed by diffusive coupling. It is thus of interested to provide a general theoretical extension to the theory in order to deal with more general types of couplings, such as the impulsive one.

Perspectives

We present here some possible research directions that naturally arise from the work presented in this manuscript.

Experimental test of proportional mean-field feedback DBS. We have recently been in contact with the medical and engineering research group of Prof. Rossi at University of Milan, performing DBS implantation on humans. Prof. Rossi's group has also a recognized expertise in the development of technologies permitting the simultaneous recording and stimulation via the DBS electrode (Giannicola et al., 2010; Priori et al., 2002; Rosa et al., 2010). Preliminary discussions suggest that clinical tests on humans of the effects of a proportional feedback DBS might be feasible.

Inhibition and desynchronization in the input-output framework. Similar to what we have done for oscillators, the input-output synchronization analysis can be extended to include the effects of a mean-field feedback. This would permit an input-output control theoretical investigation on the possibility of inhibiting or desynchronizing an originally synchronized nonlinear operators population.

Experimental input-output identification. We believe that the input-output approach developed in Chapter 7 can find an efficient application in an experimental framework. The characterization of the input-output properties of a given neuron type would indeed only require the electrical measurement of the response of the neuron to a set of prototypical inputs, as opposed to the present state-space characterization that needs a detailed study of many other electro-physiological properties. The obtained input-output characterization can be used to build large scale networks of interconnected non-linear operators, whose theoretically predicted behavior could readily be compared to real neurons networks.

Mathematical analysis of calcium-gated synchronization. In its simple form, the reduced model derived in Chapter 6 captures the dynamics behind the behavior of dopaminergic and other calcium-gated neurons, like STN and thalamic neurons. It might thus permit a systematic analytical study of the synchronous oscillatory phenomena observed in the BG in PD conditions, of the effects induced by a high frequency DBS, and of the possible directions that can be undertaken to ameliorate this cure.

Link between our reduced model and antisynergistic ionic currents. The chief feature of the novel reduced model of Chapter 6 can be directly related to the antisynergistic cooperation of potassium and calcium currents. Its distinct feature with respect to the Izhikevich model stems indeed from the presence in the associated detailed model of depolarizing and hyperpolarizing currents which can be simultaneously activated in a same timescale, several times slower than the timescale of the current which generates the action potential. These observations suggest the existence of a qualitative link between the proposed reduced mathematical model and the antisynergistic cooperation of two particular ion currents, at least in the specific case of the dopaminergic neuron. A speculative idea is that a similar link can actually be established in any neuron exhibiting sufficiently pronounced calcium currents.

Bibliography

Acebrón, J. A., Bonilla, L. L., Vicente, C. J. P., Ritort, F., Spigler, R., 2005. The Kuramoto model: A simple paradigm for synchronization phenomena. Reviews of modern physics 77, 137–185.

Aeyels, D., De Smet, F., 2010. Emergence and evolution of multiple clusters of attracting agents. Phys. D 239 (12), 1026–1037.

Aeyels, D., Rogge, J. A., 2004. Existence of partial entrainment and stability of phase locking behavior of coupled oscillators. Progress of Theoretical Physics 112 (6), 921–942.

Amini, B., Clark, J. W., Canavier, C. C., 1999. Calcium dynamics underlying pacemaker-like and burst firing oscillations in midbrain dopaminergic neurons: A computational study. Journal of Neurophysiology 82 (5), 2249–2261.

Angeli, D., Kountouriotis, P. A., August 2011. Decentralized random control of refrigerator appliances. In: Proc. 18th. IFAC World Congress. Milano, Italy, pp. 12144–12149.

Angeli, D., Praly, L., July 2011. Stability robustness in the presence of exponentially unstable isolated equilibria. IEEE Trans. on Automat. Contr. 56 (7), 1582–1592.

Arcak, M., Sontag, E. D., 2006. Diagonal stability of a class of cyclic systems and its connection with the secant criterion. Automatica 42, 1531–1537.

Arcak, M., Sontag, E. D., 2008. A passivity-based stability criterion for a class of biochemical reaction networks. Mathematical biosciences and engineering 5 (1), 1–19.

Aronson, D. G., Ermentrout, G. B., Kopell, N., 1990. Amplitude response of coupled oscillators. Physica D 41 (3), 403–449.

Assisi, C. G., Jirsa, V. K., Kelso, J. A. S., 2005. Synchrony and clustering in heterogeneous networks with global coupling and parameter dispersion. Phys. Rev. Lett. 94 (1).

Azouz, R., Jensen, M. S., Yaari, Y., 1996. Ionic basis of spike after-depolarization and burst generation in adult rat hippocampal CA1 pyramidal cells. The Journal of Physiology 492 (1), 211–223.

Bar-Gad, I., Morris, G., Bergman, H., 2003. Information processing, dimensionality reduction and reinforcement learning in the basal ganglia. Progress in Neurobiology 71 (6), 439 – 473.

Barbeau, A., 1974. The clinical physiology of side effects in long-term L-dopa therapy. Adv. Neurol. 5, 347–365.

Benabid, A., Pollack, P., Gao, D., Hoffman, D., Limousin, P., Gay, E., Payen, I., Benazzouz, A., 1996. Chronic electrical stimulation of the ventralis intermedium nucleus of the thalamus as a treatment of movement disorders. J. Neurosurg. 84, 203–214.

Benabid, A. L., Pollak, P., Gervason, C., Hoffmann, D., Gao, D. M., Hommel, M., Perret, J. E., de Rougemont, J., 1991. Long-term suppression of tremor by chronic stimulation of the ventral intermediate thalamic nucleus. The Lancet 337, 403–406.

Benazzouz, A., Gao, D. M., Ni, Z. G., Piallat, B., Bouali-Benazzouz, R., Benabid, A. L., 2000. Effect of high-frequency stimulation of the subthalamic nucleus on the neuronal activities of the substantia nigra pars reticulata and ventrolateral nucleus of the thalamus in the rat. Neuroscience 99 (2), 289 – 295.

Beurrier, C., Congar, P., Bioulac, B., Hammond, C., 1999. Subthalamic nucleus neurons switch from single-spike activity to burst-firing mode. The Journal of Neuroscience 19 (2), 599–609.

Bhatia, N. P., Szegö, G. P., 1970. Stability theory of dynamical systems. Die Grundlehren der mathematischen Wissenschaften, Band 161. Springer-Verlag, New York.

Billingsley, P., 1995. Probability and Measure, 3rd Edition. Probability and Mathematical Statistics. John Wiley and Sons, Inc., New York, NY.

Blekhman, I., Fradkov, A., Nijmeijer, H., Pogromsky, A., 1997. On self synchronization and controlled synchronization. Syst. & Contr. Letters 31, 299–305.

Bliss, G., 1947. Lectures on the calculus of variations. Chicago Univ. Press.

Bolam, J. P., Hanley, J. J., Booth, P. A. C., Bevan, M. D., 2000. Synaptic organisation of the basal ganglia. J. Anat. 196 (4), 527–542.

Bondy, J. A., Murty, U. S. R., 1976. Graph Theory with Applications. North-Holland.

Boraud, T., Brown, P., Goldberg, J. A., Graybiel, A. M., Magill, P. J., 2005. Oscillations in the basal ganglia: the good, the bad, and the unexpected. In: Bolam, J. P., Ingham, C. A., Magill, P. J., Bures, J., Kopin, I., McEwen, B., Pribram, K., Rosenblatt, J., Weiskranz, L. (Eds.), The Basal Ganglia VIII. Vol. 56 of Advances in Behavioral Biology. Springer US, pp. 1–24.

Brown, E., Holmes, P., Moehlis, J., 2003. Globally coupled oscillator networks. In: Sreenivasan, K., Kaplan, E., Marsden, J. (Eds.), Perspectives and Problems in Nonlinear Science: A Celebratory Volume in Honor of Larry Sirovich. New York.

Brown, J. T., Randall, A. D., 2009. Activity-dependent depression of the spike after-depolarization generates long-lasting intrinsic plasticity in hippocampal CA3 pyramidal neurons. The Journal of Physiology 587 (6), 1265–1281.

Brown, P., Mazzone, P., Oliviero, A., Altibrandi, M. G., Pilato, F., Tonali, P. A., Lazzaro, V. D., 2004. Effects of stimulation of the subthalamic area on oscillatory pallidal activity in Parkinson's disease. Experimental Neurology 188 (2), 480 – 490.

Brown, P., Oliviero, A., Mazzone, P., Insola, A., Tonali, P., Di Lazzaro, V., 2001. Dopamine dependency of oscillations between subthalamic nucleus and pallidum in Parkinson's disease. The Journal of Neuroscience 21 (3), 1033–1038.

Brown, P., Williams, D., 2005. Basal ganglia local field potential activity: Character and functional significance in the human. Clinical Neurophysiology 116 (11), 2510 – 2519.

Byrnes, C., Isidori, A., Willems, J. C., 1991. Passivity, feedback equivalence, and the global stabilization of minimum phase nonlinear systems. IEEE Trans. on Automat. Contr. 36 (11), 1228–1240.

Cassidy, M., Mazzone, P., Oliviero, A., Insola, A., Tonali, P., Lazzaro, V. D., Brown, P., 2002. Movement-related changes in synchronization in the human basal ganglia. Brain 125 (6), 1235–1246.

Chen, G., 2003. Chaotification via feedback: the discrete case. In: Lecture Notes in Control and Information Sciences. Vol. 292. Springer.

Chen, G., Yang, L., 2003. Chaotifying a continuous-time system near a stable limit cycle. Chaos, Solitons and Fractals 15 (2), 245–253.

Chen, S., Yaari, Y., 2008. Spike Ca2+ influx upmodulates the spike afterdepolarization and bursting via intracellular inhibition of KV7/M channels. The Journal of Physiology 586 (5), 1351–1363.

Chopra, N., Spong, M. W., 2009. On exponential synchronization of Kuramoto oscillators. IEEE Trans. on Automat. Contr. 54 (2), 353–357.

Coombes, S., Bressloff, P. C. (Eds.), 2005. Bursting: The Genesis of Rhythm in the Nervous System. World Scientific.

Cotzias, G. C., Papavasiliou, P. S., Gellene, R., 1969. L-dopa in Parkinson's syndrome. New England J. Med. 281 (5), 272.

Courtemanche, R., Fujii, N., Graybiel, A. M., 2003. Synchronous, focally modulated β-band oscillations characterize local field potential activity in the striatum of awake behaving monkeys. The Journal of Neuroscience 23 (37), 11741–11752.

Cui, G., Okamoto, T., Morikawa, H., 2004. Spontaneous opening of T-Type Ca2+ channels contributes to the irregular firing of dopamine neurons in neonatal rats. The Journal of Neuroscience 24 (49), 11079–11087.

Cumin, D., Unsworth, C., 2007. Generalising the Kuramoto model for the study of neuronal synchronisation in the brain. Physica D 226 (2), 181–196.

Daniels, B., 2005. Synchronization of globally coupled nonlinear oscillators: the rich behavior of the Kuramoto model. Ohio Wesleyan Physics Dept., Essay, 7–20.

Danzl, P., Hespanha, J., Moehlis, J., 2009. Event-based minimum-time control of oscillatory neuron models. Biol. Cybern. 101, 387–399.

Davis, P. J., 1979. Circulant Matrices. Wiley, New York.

De Smet, F., Aeyels, D., 2009. Clustering in a network of non-identical and mutually interacting agents. Proceedings of the Royal Society A: Mathematical, Physical and Engineering Science 465 (2103), 745–768.

Demidovich, B., 1967. Lectures on the mathematical stability theory (Russian). Nauka, Moscow.

Destexhe, A., Mainen, Z., Sejnowski, T., 1998. Kinetic models of synaptic transmission, 2nd Edition. MIT Press, Cambridge, MA, USA, pp. 1–25.

Dörfler, F., Bullo, F., 2011. Synchronization and transient stability in power networks and non-uniform Kuramoto oscillators. Trans. on Automat. Contr. (submitted).

Doyle, L. M. F., Kühn, A. A., Hariz, M., Kupsch, A., Schneider, G.-H., Brown, P., 2005. Levodopa-induced modulation of subthalamic beta oscillations during self-paced movements in patients with Parkinson's disease. European Journal of Neuroscience 21 (5), 1403–1412.

Drion, G., Massotte, L., Sepulchre, R., Seutin, V., 05 2011a. How modeling can reconcile apparently discrepant experimental results: The case of pacemaking in dopaminergic neurons. PLoS Comput Biol 7 (5), e1002050.

Drion, G., Sepulchre, R., Seutin, V., 2011b. Mitochondrion- and endoplasmic reticulum-induced SK channel disregulation as a potential origin of the selective neurodegeneration in Parkinson's disease. Genetics and Systems Biology. Springer, to appear.

Ermentrout, G. B., 1990. Oscillator death in populations of "all to all" coupled nonlinear oscillators. Phys. D 41 (2), 219–231.

Ermentrout, G. B., 2002. Simulating, analyzing, and animating dynamical systems: a guide to XPPAUT for researchers and students. SIAM Press, Philadelphia, PA, USA.

Ermentrout, G. B., 2004. XPP/XPPAUT homepage. Available at http://www.math.pitt.edu/~bard/xpp/xpp.html.

Ermentrout, G. B., Kopell, N., 1990. Oscillator death in systems of coupled neural oscillators. SIAM J. Appl. Math. 50 (1), 125–146.

Ermentrout, G. B., Terman, D. H., 2010. Mathematical Foundations of Neuroscience. Interdisciplinary Applied Mathematics. Springer.

Fenichel, N., 1979. Geometric singular perturbation theory. J. Diff. Eq. 31, 53–98.

Filali, M., Hutchison, W. D., Palter, V. N., Lozano, A. M., Dostrovsky, J. O., 2004. Stimulation-induced inhibition of neuronal firing in human subthalamic nucleus. Exp. Brain Res. 156, 274–278.

FitzHugh, R., 1961. Impulses and physiological states in theoretical models of nerve membrane. Biophysical J. 1, 445–466.

Foehring, R. C., Zhang, X. F., Lee, J., Callaway, J. C., 2009. Endogenous calcium buffering capacity of substantia nigral dopamine neurons. Journal of Neurophysiology 102 (4), 2326–2333.

Fradkov, A. L., 2007. Cybernetical physics. From control of chaos to quantum control. Springer: Complexity. Springer-Verlag, Berlin Heidelberg.

Fries, P., 2001. A mechanism for cognitive dynamics: neuronal communication through neuronal coherence. Trends in Cognitive Science 9, 474–480.

Gao, Y., Chau, K., 2002. Chaotification of permanent-magnet synchronous motor drives using time-delay feedback. In: IEEE Annual Conf. of Industrial Electronics Soc. pp. 762–766.

Giannicola, G., Marceglia, S., Rossi, L., Mrakic-Sposta, S., Rampini, P., Tamma, F., Cogiamanian, F., Barbieri, S., Priori, A., 2010. The effects of levodopa and ongoing deep brain stimulation on subthalamic beta oscillations in parkinson's disease. Experimental Neurology 226 (1), 120 – 127.

Godsil, C., Royle, C., 2001. Algebraic graph theory. Springer Graduate Text in Mathematics.

Goebel, R., Sanfelice, R., Teel, A., 2009. Hybrid dynamical systems. Control Systems Magazine, IEEE 29 (2), 28–93.

Golubitsky, M., Guillemin, V., 1973. Stable mappings and their singularities. Springer-Verlag, New York, graduate Texts in Mathematics, Vol. 14.

Guckenheimer, J., 1975. Isochrons and phaseless sets. J. Math. Biol. 1 (3), 259–273.

Guckenheimer, J., 1995. Phase portraits of planar vector fields: computer proofs. Experiment. Math. 4 (2), 153–165.

Guckenheimer, J., Holmes, P., 2002. Nonlinear oscillations, dynamical systems, and bifurcations of vector fields, 7th Edition. Vol. 42 of Applied Mathematical Sciences. Springer, New-York.

Guzman, J. N., Sánchez-Padilla, J., Chan, C. S., Surmeier, D. J., 2009. Robust pacemaking in substantia nigra dopaminergic neurons. The Journal of Neuroscience 29 (35), 11011–11019.

Hale, J., 1969. Ordinary differential equations. Interscience. John Wiley, New York.

Hallworth, N. E., Wilson, C. J., Bevan, M. D., 2003. Apamin-sensitive small conductance calcium-activated potassium channels, through their selective coupling to voltage-gated calcium channels, are critical determinants of the precision, pace, and pattern of action potential generation in rat subthalamic nucleus neurons in vitro. The Journal of Neuroscience 23 (20), 7525–7542.

Hamadeh, A., Stan, G. B., Goncalves, J., 2008. Robust synchronisation in networks of cyclic feedback systems. In: Proc. 47th. IEEE Conf. Decision Contr.

Hammond, C., Ammari, R., Bioulac, B., Garcia, L., 2008. Latest view on the mechanism of action of deep brain stimulation. Movement Disorders 23 (15), 2111–2121.

Hammond, C., Bergman, H., Brown, P., 2007. Pathological synchronization in Parkinson's disease: networks, models and treatments. Trends in Neurosciences 30 (7), 357 – 364, July INMED/TINS special issue–Physiogenic and pathogenic oscillations: the beauty and the beast.

Hao, B., Yua, H., Jinga, Y., Zhanga, S., 2009. On synchronizability and heterogeneity in unweighted networks. Physica A 338 (9), 1939–1945.

Hauptmann, C., Popovych, O., Tass, P. A., 2005a. Delayed feedback control of synchronization in locally coupled neuronal networks. Neurocomputing 65, 759–767.

Hauptmann, C., Popovych, O., Tass, P. A., 2005b. Effectively desynchronizing deep brain stimulation based on a coordinated delayed feedback stimulation via several sites: a computational study. Biol. Cybern. 93, 463–470.

Hauptmann, C., Popovych, O., Tass, P. A., 2005c. Multisite coordinated delayed feedback for an effective desynchronization of neuronal networks. Stochastics and Dynamics 5 (2), 307–319.

Hellwig, B., Schelter, B., Guschlbauer, B., Timmer, J., Lucking, C. H., 2003. Dynamic synchronisation of central oscillators in essential tremor. Clinical Neurophysiology 114 (8), 1462–1467.

Hille, B., 1984. Ionic channels of excitable membranes. Sinauer Associates Inc, Sunderland, MA.

Hindmarsh, J. L., Rose, R. M., 1984. A model of neuronal bursting using three coupled first-order differential equations. In: Proc. Roy. Soc. Lond. Vol. B 221. pp. 87–102.

Hirsch, M., Pugh, C., Shub, M., 1977. Invariant Manifolds. Lecture Notes in Mathematics. Springer-Verlag, Berlin, Germany.

Hirsch, M. W., Smale, S., 1974. Differential equations, dynamical systems, and linear algebra. Pure and applied mathematics. Harcourt Brace Jovanovich, Accademic Press, Inc.

Hodgkin, A., Huxley, A., 1952. A quantitative description of membrane current and its application to conduction and excitation in nerve. J. Physiol 117, 500–544.

Holgado, A., Terry, J., Bogacz, R., 2010. Conditions for the generation of beta oscillations in the subthalamic nucleus-globus pallidus network. J. of Neuroscience 30 (37), 12340.

Hoppensteadt, F. C., Izhikevich, E. M., 1997. Weakly connected neural networks. Vol. 126 of Applied Mathematical Sciences. Springer-Verlag, New York.

Horn, R. A., Johnson, C. R., 1985. Matrix Analysis. Cambridge University Press.

Isidori, A., 1999. Nonlinear control systems II. Springer Verlag, London, England .

Izhikevich, E. M., 2003. A simple model of spiking neurons. IEEE Trans. on Neural Networks 14 (6), 1569–1572.

Izhikevich, E. M., 2007. Dynamical Systems in Neuroscience: The Geometry of Excitability and Bursting. MIT Press.

Izhikevich, E. M., 2010. Hybrid spiking models. Phil. Trans. R. Soc. A 368, 5061–5070.

Jadbabaie, A., Motee, N., Barahona, M., 2004. On the stability of the Kuramoto model of coupled nonlinear oscillators. Proc. American Control Conf., 4296–4301.

Jankovic, J., Cardoso, F., Grossman, R. G., Hamilton, W. J., 1995. Outcome after stereotactic thalamotomy for Parkinsonian, essential, and other types of tremor.

Jones, C. K. R., 1995. Geometric singular perturbation theory. In: Dynamical systems. Springer Lecture Notes in Math. 1609. Springer, Berlin, pp. 44–120.

Kepler, T., Abbott, L., Marder, E., 1992. Reduction of conductance-based neuron models. Biological Cybernetics 66, 381–387.

Khalil, H., 2001. Nonlinear systems. Prentice Hall, 3rd ed., New York.

Ko, T.-W., Ermentrout, G. B., 2009. Phase-response curves of coupled oscillators. Phys. Rev. E (3) 79 (1), 016211, 6.

Kopell, N., Ermentrout, G. B., 2002. Mechanisms of phase-locking and frequency control in pairs of coupled neural oscillators. In: Handbook of dynamical systems, Vol. 2. North-Holland, Amsterdam, pp. 3–54.

Krantz, S., Parks, H., 2002. A primer of real analytic functions, 2nd Edition. Birkhäuser, Boston, MA, USA.

Kringelbach, M. L., Jenkinson, N., Owen, S. L., Aziz, T. Z., 2007. Translational principles of deep brain stimulation. Nat. Rev. Neurosci. 8 (8), 623–635.

Krupa, M., Szmolyan, P., 2001a. Extending geometrical singular perturbation theory to non-hyperbolic points - folds and canards points in two dimensions. SIAM J. Math. Analysis 33 (2), 286–314.

Krupa, M., Szmolyan, P., 2001b. Extending slow manifolds near transcritical and pitchfork singularities. Nonlinearity 14, 1473–1491.

Krupa, M., Szmolyan, P., 2001c. Relaxation oscillation and canard explosion. J. Differential Equations 174 (2), 312–368.

Kühn, A. A., Kupsch, A., Schneider, G.-H., Brown, P., 2006. Reduction in subthalamic 8-35 Hz oscillatory activity correlates with clinical improvement in Parkinson's disease. European Journal of Neuroscience 23 (7), 1956–1960.

Kumar, R., Lozano, A. M., Sime, E., Lang, A. E., 2003. Long-term follow-up of thalamic deep brain stimulation for essential and Parkinsonian tremor. Neurology 61, 1601–1604.

Kuramoto, Y., 1984. Chemical oscillations, waves, and turbulence. Springer, Berlin.

Lee, J., 2006. Introduction to smooth manifolds. Graduate Texts in Mathematics. Springer-Verlag, Berlin, Germany.

Legatt, A. D., Arezzo, J., Jr., H. G. V., 1980. Averaged multiple unit activity as an estimate of phasic changes in local neuronal activity: effects of volume-conducted potentials. Journal of Neuroscience Methods 2 (2), 203 – 217.

Lohmiller, W., Slotine, J. J., 1998. On contraction analysis for non-linear systems. Automatica 34 (6), 683–696.

Lopez-Azcarate, J., Tainta, M., Rodriguez-Oroz, M. C., Valencia, M., Gonzalez, R., Guridi, J., Iriarte, J., Obeso, J. A., Artieda, J., Alegre, M., 2010. Coupling between beta and high-frequency activity in the human subthalamic nucleus may be a pathophysiological mechanism in Parkinson's disease. J. Neurosci. 30 (19), 6667–6677.

Loría, A., Panteley, E., 2005. Cascade nonlinear time-varying systems: analysis and design. In: Lamnabhi-Lagarrigue, F., Loría, A., Panteley, E. (Eds.), Advanced topics in control systems theory. Lecture Notes in Control and Information Sciences. Springer Verlag.

Luo, M., Wu, Y., Peng, J., 2009. Washout filter aided mean field feedback desynchronization in an ensemble of globally coupled neural oscillators. Biol. Cybern. 101, 241–246.

Lygeros, J., Johansson, K., Simic, S., Zhang, J., Sastry, S., 2003. Dynamical properties of hybrid automata. IEEE Transactions on Automatic Control 48 (1), 2–17.

Maistrenko, Y. L., Popovych, O. V., Tass, P. A., 2005. Desynchronization and chaos in the Kuramoto model. Lect. Notes Phys. 671, 285–306.

Malkin, I. J., 1958. Theory of stability of motion. Tech. rep., U.S. Atomic energy commission.

Marsden, J. F., Limousin-Dowsey, P., Ashby, P., Pollak, P., Brown, P., 2001. Subthalamic nucleus, sensorimotor cortex and muscle interrelationships in Parkinson's disease. Brain 124 (2), 378–388.

McIntyre, C., Savasta, M., Kerkerian-Le Goff, L., Vitek, J. L., 2004. Uncovering the mechanism(s) of action of deep brain stimulation: activation, inhibition, or both. Clinical Neurophysiology 115, 1239–1248.

Molineux, M. L., Fernandez, F. R., Mehaffey, W. H., Turner, R. W., 2005. A-Type and T-Type currents interact to produce a novel spike latency-voltage relationship in cerebellar stellate cells. The Journal of Neuroscience 25 (47), 10863–10873.

Motter, A. E., Zhou, C., Kurths, J., 2005. Network synchronization, diffusion, and the paradox of heterogeneity. Phys. Rev. E 71 (1), 016116.

Moylan, P., Hill, D., 1978. Stability criteria for large-scale systems. IEEE Trans. on Automat. Contr. 23 (2), 143–149.

Muenter, M. D., Tyce, G. M., 1971. L-dopa therapy of Parkinson's disease: plasma L-dopa concentration, therapeutic response, and side effects. Mayo Clin. Proc. 46 (4), 231–9.

Nemytskii, V. V., Stepanov, V. V., 1960. Qualitative theory of differential equations. Princeton Mathematical Series, No. 22. Princeton University Press.

Nijmeijer, H., Rodriguez-Angeles, A., 2003. Synchronization of mechanical systems. Vol. 46. World Scientific Series on Nonlinear Science, Series A.

Nini, A., Feingold, A., Slovin, H., Bergman, H., 1995. Neurons in the globus pallidus do not show correlated activity in the normal monkey, but phase-locked oscillations appear in the MPTP model of Parkinsonism. J. Neurophysiol. 74 (4), 1800–1805.

Ogata, K., 2001. Modern control engineering. Prentice Hall.

Olanow, B. M., 2001. Surgical therapies for Parkinson's disease. A physician's perspective. Vol. 86 of Advances in Neurology. Lippincott Williams & Wilkins, Philadelphia.

Olfati-Saber, R., Murray, R. M., 2004. Consensus problems in networks of agents with switching topology and time-delays. IEEE Trans. on Automat. Contr. 49 (9), 1520–1533.

Orsi, R., Praly, L., Mareels, I., 2001. Sufficient conditions for the existence of an unbounded solution. Automatica 37 (10), 1609–1617.

Ortega, R., 1991. Passivity properties for stabilization of nonlinear cascaded systems. Automatica 29, 423–424.

Oud, W. T., Tyukin, I., 2004. Sufficient conditions for synchronization in an ensemble of Hindmarsh and Rose neurons: passivity-based approach. IFAC NOLCOS 2004.

Panteley, E., Loría, A., Teel, A., 2001. Relaxed persistency of excitation for uniform asymptotic stability. IEEE Trans. on Automat. Contr. 46 (12), 1874–1886.

Parent, A., Hazrati, L.-N., 1993. Anatomical aspects of information processing in primate basal ganglia. Trends in Neurosciences 16 (3), 111 – 116.

Pavlov, A., Pogromsky, A., van de Wouw, N., Nijmeijer, H., 2004. Convergent dynamics, a tribute to Boris Pavlovich Demidovich. Syst. & Contr. Letters 52, 257–261.

Pavlov, A., van de Wouw, N., Nijmeijer, H., 2006. Uniform output regulation of nonlinear systems: a convergent dynamics approach. Systems and controls: foundations and applications. Birkhauser, Boston.

Pazó, D., Zaks, M., Kurths, J., 2003. Role of unstable periodic orbits in phase and lag synchronization between coupled chaotic oscillators. Chaos 13 (1), 309–318.

Pham, Q., Slotine, J. J., 2007. Stable concurrent synchronization in dynamic system networks. Neural Networks 20 (1), 62–77.

Pikovsky, A., Rosenblum, M., Kurths, J., 2001. Synchronization: a universal concept in nonlinear sciences. Cambridge Nonlinear Science Series, Cambridge, United Kingdom.

Plenz, D., Kital, S. T., 1999. A basal ganglia pacemaker formed by the subthalamic nucleus and external globus pallidus. Nature 400 (6745), 677–682.

Pogromsky, A., Nijmeijer, H., 2001. Cooperative oscillatory behavior of mutually coupled dynamical systems. IEEE Transactions on Circuits and Systems I 48, 152–162.

Popovych, O., Krachkovskyi, V., Tass, P., 2007. Twofold impact of delayed feedback on coupled oscillators. Int. J. Bifurc. Chaos 17 (7), 2517–2530.

Popovych, O. V., Hauptmann, C., Tass, P. A., 2005. Effective desynchronization by nonlinear delayed feedback. Phys. Rev. Lett. 94, 164102.

Popovych, O. V., Hauptmann, C., Tass, P. A., 2006a. Control of neuronal synchrony by nonlinear delayed feedback. Biol. Cybern. 95, 69–85.

Popovych, O. V., Hauptmann, C., Tass, P. A., 2006b. Desynchronization and decoupling of interacting oscillators by nonlinear delayed feedback. Internat. J. Bifur. Chaos 16 (7), 1977–1987.

Popovych, O. V., Tass, P. A., 2010. Synchronization control of interacting oscillatory ensembles by mixed nonlinear delayed feedback. Phys. Rev. E 82 (2), 026204.

Priori, A., Foffani, G., Pesenti, A., Bianchi, A., Chiesa, V., Baselli, G., Caputo, E., Tamma, F., Rampini, P., Egidi, M., Locatelli, M., Barbieri, S., Scarlato †, G., 2002. Movement-related modulation of neural activity in human basal ganglia and its L-dopa dependency: recordings from deep brain stimulation electrodes in patients with Parkinson's disease. Neurological Sciences 23, 101–102.

Priori, A., Foffani, G., Pesenti, A., Tamma, F., Bianchi, A. M., Pellegrini, M., Locatelli, M., Moxon, K. A., Villani, R. M., 2004. Rhythm-specific pharmacological modulation of subthalamic activity in Parkinson's disease. Experimental Neurology 189 (2), 369 – 379.

Pyragas, K., Popovich, O. V., Tass, P. A., 2008. Controlling synchrony in oscillatory networks with a separate stimulation-registration setup. Euro. Phys. Letters 80 (4).

Rekling, J. C., Feldman, J. L., 1997. Calcium-dependent plateau potentials in rostral ambiguus neurons in the newborn mouse brain stem in vitro. Journal of Neurophysiology 78 (5), 2483–2492.

Rodriguez-Oroz, M. C., Obeso, J. A., Lang, A. E., Houeto, J. L., Pollak, P., Rehncrona, S., Kulisevsky, J., Albanese, A., Volkmann, J., Hariz, M. I., Quinn, N. P., Speelman, J. D., Guridi, J., Zamarbide, I., Gironell, A., Molet, J., Pascual-Sedano, B., Pidoux, B., Bonnet, A. M., Agid, Y., Xie, J., Benabid, A. L., Lozano, A. M., Saint-Cyr, J., Romito, L., Contarino, M. F., Scerrati, M., Fraix, V., Van Blercom, N., 2005. Bilateral deep brain stimulation in Parkinson's disease: a multicentre study with 4 years follow-up. Brain 128, 2240–2249.

Rosa, M., Marceglia, S., Servello, D., Foffani, G., Rossi, L., Sassi, M., Mrakic-Sposta, S., Zangaglia, R., Pacchetti, C., Porta, M., Priori, A., 2010. Time dependent subthalamic local field potential changes after DBS surgery in Parkinson's disease. Experimental Neurology 222, 184–190.

Rosenblum, M., Pikovsky, A., 2004a. Delayed feedback control of collective synchrony: an approach to suppression of pathological brain rhythms. Phys. Rev. E 70 (4), 041904.

Rosenblum, M. G., Pikovsky, A. S., 2004b. Controlling synchronization in an ensemble of globally coupled oscillators. Phys. Rev. Lett. 92, 114102.

Rosenblum, M. G., Tukhlina, N., Pikovsky, A., Cimponeriu, L., 2006. Delayed feedback suppression of collective rhythmic activity in a neuronal ensemble. Int. J. Bifurcation Chaos 16 (7), 1989–1999.

Rubin, J. E., 2007. Burst synchronization. Scholarpedia 2 (10), 1666.

Rubin, J. E., Terman, D., 2004. High frequency stimulation of the subthalamic nucleus eliminates pathological thalamic rhythmicity in a computational model. Journal of Computational Neuroscience 16, 211–235.

Rutishauser, U., Ross, I. B., Mamelak, A. N., Schuman, E. M., 2010. Human memory strength is predicted by theta-frequency phase-locking of single neurons. Nature 464, 903–907.

Sanes, J. N., Donoghue, J. P., 1993. Coherent oscillations in monkey motor cortex and hand muscle EMG show task-dependent modulation. J. Physiol. 501, 225–241.

Sarlette, A., 2009. Geometry and symmetries in coordination control. Ph.D. thesis, University of Liège, Belgium.

Sarma, S. V., Cheng, M., Williams, Z., Hu, R., Eskandar, E., Brown, E. N., 2010. Comparing healthy and Parkinsonian neuronal activity in sub-thalamic nucleus using point process models. IEEE Trans. Biomed. Eng. 57 (6), 1297–1305.

Sato, F., Parent, M., Levesque, M., Parent, A., 2000. Axonal branching pattern of neurons of the subthalamic nucleus in primates. J. Comp. Neurol. 424 (1), 142–152.

Scardovi, L., Arcak, M., Sontag, E. D., 2010. Synchronization of interconnected systems with applications to biochemical networks: an Input-Output approach. IEEE Trans. on Automat. Contr. 55, 1367–1379.

Scardovi, L., Sarlette, A., Sepulchre, R., 2007. Synchronization and balancing on the N-torus. Syst. & Contr. Letters 56 (5), 335–341.

Schiff, S. J., 2010. Towards model-based control of Parkinson's disease. Philos Transact. A Math. Phys. 368 (1918), 2269–2308.

Schuurman, P. R., Bosch, D. A., Merkus, M. P., Speelman, J. D., 2008. Long-term follow-up of thalamic stimulation versus thalamotomy for tremor suppression. Mov. Disord. 23 (8), 1146–53.

Sepulchre, R., Paley, D., Leonard, N. E., 2008. Stabilization of planar collective motion with limited communication. IEEE Trans. on Automat. Contr. 53 (3), 706–719.

Sepulchre, R., Paley, D. A., Leonard, N. E., May 2007. Stabilization of planar collective motion: all-to-all communication. IEEE Trans. on Automat. Contr. 52 (5), 811–824.

Seydel, R., 2010. Practical bifurcation and stability analysis, 3rd Edition. Vol. 5 of Interdisciplinary Applied Mathematics. Springer-Verlag, New York.

Sijbrand, J., 1985. Properties of center manifolds. Transaction of the American Mathematical Society 289 (2), 431–469.

Silberstein, P., Kühn, A. A., Kupsch, A., Trottenberg, T., Krauss, J. K., Wöhrle, J. C., Mazzone, P., Insola, A., Di Lazzaro, V., Oliviero, A., Aziz, T., Brown, P., 2003. Patterning of globus pallidus local field potentials differs between Parkinson's disease and dystonia. Brain 126 (12), 2597–2608.

Skinner, F. K., 2006. Conductance-based models. Scholarpedia 1 (11).

Sochurkova, D., Rektor, I., 2003. Event-related desynchronization/synchronization in the putamen. An SEEG case study. Experimental Brain Research 149, 401–404.

Song, W.-J., Baba, Y., Otsuka, T., Murakami, F., 2000. Characterization of Ca2+ channels in rat subthalamic nucleus neurons. Journal of Neurophysiology 84 (5), 2630–2637.

Sontag, E. D., 1989. Smooth stabilization implies coprime factorization. IEEE Trans. on Automat. Contr. 34 (4), 435–443.

Sontag, E. D., 2006a. Input to state stability: basic concepts and results. Lecture Notes in Mathematics. Springer-Verlag, Berlin, Ch. in Nonlinear and Optimal Control Theory, pp. 163–220, P. Nistri and G. Stefani eds.

Sontag, E. D., 2006b. Passivity gains and the "secant condition" for stability. Syst. & Contr. Letters 55 (3), 177–183.

Sontag, E. D., Wang, Y., 1996. New characterizations of Input-to-State Stability. IEEE Trans. on Automat. Contr. 41, 1283–1294.

Sontag, E. D., Wang, Y., 1999. New characterizations of input-to-state stability. IEEE Trans. on Automat. Contr. 20.

Spong, M., 1996. Motion control of robot manipulators. In: Levine, W. (Ed.), Handbook of Control. CRC Press, pp. 1339–1350.

Stan, G. B., Hamadeh, A., Sepulchre, R., Goncalves, J., 2007. Output synchronization in networks of cyclic biochemical oscillators. In: Proc. American Control Conference. pp. 3973–3978.

Stan, G. B., Sepulchre, R., 2007. Analysis of interconnected oscillators by dissipativity theory. IEEE Trans. on Automat. Contr. 52 (2), 256–270.

Steur, E., Tyukin, I., Nijmeijer, H., 2009. Semi-passivity and synchronization of diffusively coupled neuronal oscillators. Physica D: Nonlinear Phenomena 238 (21), 2119 – 2128.

Strogatz, S., 2001. Nonlinear dynamics and chaos: with applications to physics, biology, chemistry, and engineering. Westview Press.

Strogatz, S. H., 2000. From Kuramoto to Crawford: exploring the onset of synchronization in population of coupled oscillators. Physica D 143, 1–20.

Sydow, O., 2008. Parkinson's disease: recent development in therapies for advanced disease with a focus on deep brain stimulation (DBS) and duodenal levodopa infusion. FEBS Journal 275 (7), 1370–1376.

Tass, P. A., 1999. Phase resetting in medicine and biology: stochastic modelling and data analysis. Springer, Berlin.

Tass, P. A., 2003a. Desynchronization by means of a coordinated reset of neural sub-populations - a novel technique for demand-controlled deep brain stimulation. Prog. Theor. Phys. Suppl. 150, 281–296.

Tass, P. A., 2003b. A model of desynchronizing deep brain stimulation with a demand-controlled coordinated reset of neural subpopulations. Biol. Cybern. 89, 81–88.

Tass, P. A., 2011. Device for the desynchronization of neuronal brain activity. USPTO patent. USPTO Applicaton number: 20060212089 - Class: 607045000.

Tass, P. A., Majtanik, M., 2006. Long-term anti-kindling effects of desynchronizing brain stimulation: a theoretical study. Biol. Cybern. 94 (1), 58–66.

Traub, R. D., 2003. Fast oscillations and epilepsy. Epilepsy Curr. 3 (3), 77–79.

Traub, R. D., Wong, R. K., 1982. Cellular mechanism of neuronal synchronization in epilepsy. Science 216 (4547), 745–747.

Trevors, J. T., Saier Jr, M. H., 2011. Thermodynamic perspectives on genetic instructions, the laws of biology and diseased states. Comptes Rendus Biologies 334 (1), 1 – 5.

Trošt, M., Su, P. C., Barnes, A., Su, S. L., Yen, R.-F., Tseng, H.-M., Ma, Y., Eidelberg, D., 2003. Evolving metabolic changes during the first postoperative year after subthalamotomy. Journal of Neurosurgery 99 (5), 872–878.

Tukhlina, N., Rosenblum, M., 2008. Feedback suppression of neural synchrony in two interacting populations by vanishing stimulation. J. Biol. Phys. 34, 301–314.

Tukhlina, N., Rosenblum, M., Pikovsky, A., Kurths, J., 2007. Feedback suppression of neural synchrony by vanishing stimulation. Physical Review E 75 (1), 011918.

Van der Schaft, A., 2000. An introduction to hybrid dynamical systems. Springer Berlin/Heidelberg.

Van der Schaft, A. J., 1999. $\mathcal{L}_2$-Gain and passivity techniques in nonlinear control, 2nd Edition. Communications and Control Engineering. Springer Verlag, London.

Van Hemmen, J. L., Wreszinski, W. F., 1993. Lyapunov function for the Kuramoto model on nonlinearly coupled oscillators. Jour. of Statistical Physics 72, 145–166.

Vernier, P., Moret, F., Callier, S., Snapyan, M., Wersinger, C., Sidhu, A., 2004. The degeneration of dopamine neurons in Parkinson's disease: insights from embryology and evolution of the mesostriatocortical system. Annals of the New York Academy of Sciences 1035 (1), 231–249.

Vidyasagar, M., 1981. Input-Output Analysis of Large Scale Interconnected Systems. Springer Verlag, Berlin.

Vitek, J., 2005. Neural interfaces workshop. Bethesda, MD, USA.

Volkmann, J., Joliot, M., Mogilner, A., Ioannides, A. A., Lado, F., Fazzini, E., Ribary, U., Llinás, R., 1996. Central motor loop oscillations in Parkinsonian resting tremor revealed by magnetoencephalography. Neurology 46, 1359–1370.

Wang, W., Slotine, J. J., 2004. On partial contraction analysis for coupled nonlinear oscillators. Biological Cybernetics 92 (1), 38–53.

Waroux, O., Massotte, L., Alleva, L., Graulich, A., Thomas, E., Liégeois, J.-F., Scuvée-Moreau, J., Seutin, V., 2005. SK channels control the firing pattern of midbrain dopaminergic neurons in vivo. European Journal of Neuroscience 22 (12), 3111–3121.

Weinberger, M., Mahant, N., Hutchison, W. D., Lozano, A. M., Moro, E., Hodaie, M., Lang, A. E., Dostrovsky, J. O., 2006. Beta oscillatory activity in the subthalamic nucleus and its relation to dopaminergic response in Parkinson's disease. Journal of Neurophysiology 96 (6), 3248–3256.

Wikipedia, 2011. Creative commons attribution-share alike 3.0 unported license (www.wikipedia.org).

Williams, D., Kühn, A., Kupsch, A., Tijssen, M., van Bruggen, G., Speelman, H., Hotton, G., Yarrow, K., Brown, P., 2003. Behavioural cues are associated with modulations of synchronous oscillations in the human subthalamic nucleus. Brain 126 (9), 1975–1985.

Williams, D., Tijssen, M., van Bruggen, G., Bosch, A., Insola, A., Lazzaro, V. D., Mazzone, P., Oliviero, A., Quartarone, A., Speelman, H., Brown, P., 2002. Dopamine-dependent changes in the functional connectivity between basal ganglia and cerebral cortex in humans. Brain 125 (7), 1558–1569.

Winfree, A. T., 1980. The geometry of biological times. Springer, New-York.

Wu, C. W., 2005. Algebraic connectivity of directed graphs. Linear and Multilinear Algebra 53 (3), 203–223.

Zhang, H., Liu, D., Wang, Z., 2009. Controlling chaos: suppression, synchronization and chaotification. Communications and Control Engineering. Springer-Verlag.

Zhu, Z.-T., Munhall, A., Shen, K.-Z., Johnson, S. W., 2004. Calcium-dependent subthreshold oscillations determine bursting activity induced by n-methyl-d-aspartate in rat subthalamic neurons in vitro. European Journal of Neuroscience 19 (5), 1296–1304.